THE STRUCTURAL PERMEABILITY OF CONCRETE
AT CRYOGENIC TEMPERATURES

PHILLIP BRIAN BAMFORTH

Thesis submitted for the degree of
Doctor of Philosophy

THE UNIVERSITY OF ASTON IN BIRMINGHAM

APRIL 1987

THE UNIVERSITY OF ASTON IN BIRMINGHAM

THE STRUCTURAL PERMEABILITY OF CONCRETE
AT CRYOGENIC TEMPERATURES

by

PHILLIP BRIAN BAMFORTH

Thesis submitted for the degree of Doctor of Philosophy

1987

Summary

The thesis describes a programme of research designed to identify concretes for application at cryogenic temperature, in particular for storage of Liquefied Natural Gas which is maintained at a temperature of -165°C. The programme was undertaken in two stages. Stage 1 involved screening tests on seventeen concrete mixes to investigate the effects of strength grade (and water/cement ratio), air entrainment, aggregate type and cement type. Four mixes were selected on the basis of low temperature strength, residual strength after thermal cycling and permeability at ambient temperature. In Stage 2 the selected mixes were subjected to a comprehensive range of tests to measure those properties which determine the leak tightness of a concrete tank at temperatures down to -165°C. These included gas permeability; tensile strength, strain capacity, thermal expansion coefficient and elastic modulus, which in combination provide a measure of resistance to cracking; and bond to reinforcement, which is one of the determining factors regarding crack size and spacing.

The results demonstrated that the properties of concrete were generally enhanced at cryogenic temperature, with reduced permeability, reduced crack proneness and, by virtue of increased bond to reinforcement, better control of cracking should it occur. Of the concretes tested, a lightweight mix containing sintered PFA aggregate exhibited the best performance at ambient and cryogenic temperature, having appreciably lower permeability and higher crack resistance than normal weight concretes of the same strength grade. The lightweight mix was most sensitive to thermal cycling, but there was limited evidence that this behaviour would not be significant if the concrete was prestressed.

Relationships between various properties have been identified, the most significant being the reduction in gas permeability with increasing strain capacity. The structural implications of the changing properties of the concrete have also been considered.

KEYWORDS

CONCRETE, CRACKING, CRYOGENIC, PERMEABILITY

ACKNOWLEDGEMENTS

C O N T E N T S

- 4 -

TABLES

LIST OF PLATES

LIST OF SYMBOLS

A	Cross-sectional area
a	Dimension of test cube
α	Thermal expansion coefficient
b	Constant in Klinkerbergs equation
c	Function of creep and restraint
D	Thermal diffusivity
E	Elastic Modulus
ε_t	Tensile strain in concrete
ε_r	Recorded (or apparent) strain
ε_{sct}	Strain capacity in direct tension
ε_{scf}	Strain capacity in flexure
ε_{tc}	Temperature correction factor
f	Frequency of occurrence, frequency of vibration
f_c	Compressive strength of concrete
f_t	Direct Tensile strength of concrete
f_f	Flexural strength of concrete (modulus of rupture)
f_b	Bond strength between concrete and reinforcement
f_y	Yield strength of reinforcement
g	Acceleration due to gravity
γ	Surface energy
h	Pressure head
K	Thermal conductivity, permeability
K	Darcy coefficient of permeability, for liquid flow
k_L	Instrinsic coefficient of permeability for liquid flow
k_g	Coefficient of permeability for gas flow
l	Length
m	Moisture content, mass per unit length
η	Viscosity
P	Applied load
p	Pressure, period of vibration
pm	Mean Pressure
Q	Volume flow rate
Q_t	Volume flow rate of test gas
Q_c	Volume flow rate of carrier gas
r	Radius
r_h	Hydraulic radius
ρ	Density

ρ_{crit} Critical steel ratio

s   Specific heat

t   Time

θ Temperature, contact angle

ν Void   content

x   Thickness

x_p Depth of penetration

Y_t Mole fraction

ρ_{crit} Critical steel ratio

s   Specific heat

t   Time

θ Temperature, contact angle

1. INTRODUCTION

1.1 BACKGROUND

Liquefied Natural Gas (LNG) is stored at a temperature of -165°C. This enables large volumes of gas, primarily methane, to be stored in relatively small containments, the volume of the liquid methane occupying only 1/600th of the gaseous volume. For many years double skinned steel tanks were used to contain LNG. The most common systems comprise an inner tank of 9% nickel steel, to maintain ductility at the very low operating temperature, and a carbon steel outer tank. The annular space between the two is filled with insulation, usually powdered perlite, to minimise boil-off. In recent years the use of increasingly larger tanks has created difficulties with the conventional double skinned steel containments, particularly in welding the thick sections required. Combined with the introduction of even more stringent safety regulations, this has led to a new design philosophy and the introduction of composite tanks using prestressed concrete[1,2,3]. A steel liner is used to provide an impermeable gas barrier, whilst the concrete provides structural rigidity. This system permits the use of easily fabricated thin steel plate to form the liner. Some typical LNG tank configurations are shown in Figure 1.1.

In addition to providing structural stability, the prestressed concrete provides a number of benefits when compared with steel tanks. For example, the unzipping mode of failure of a primary steel tank, albeit unlikely with the use of special cryogenic steel, would be avoided with the use of prestressed concrete as a primary containment. This in turn would permit a more rational design of the secondary or outer tank which would no longer have to withstand the possible dynamic load from spilling LNG of up to six times the hydrostatic load[4]. Concrete has also demonstrated its ability to withstand severe fires due to its low conductivity and slow reduction in strength when exposed to elevated temperatures[5]. It will also withstand considerable impact. For example, a 1m thick reinforced concrete wall will resist the impact of a light aircraft travelling at 220m/sec[6].

Aston University

Illustration removed for copyright restrictions

FIGURE 1.1. Typical LNG tank configurations (Ref. 3)

1.2 LNG TANK DESIGN

The design of cryogenic containment structures incorporating prestressed concrete is generally based on the ambient material properties of the concrete. This is considered to be a safe assumption, the mechanical properties of concrete having been shown to be enhanced at low temperature[1]. The strength may increase by as much as 200% when concrete is cooled from ambient to -165°C, whilst the elastic modulus can increase by 50%.

In addition to being structurally sound at cryogenic temperature, concrete has also been used for many years for a range of water retaining structures, such as dams, header tanks and reservoirs. Nevertheless, unlined prestressed concrete has still not been used for LNG containment. The reason for this is related to risk. For the containment of LNG, the continued leak tightness of the structure is the single most important design criterion[7]. The consequence of a major leak could be catastrophic and the probability of such an occurrence must, therefore, be extremely low.

In an unlined concrete tank leak tightness is determined by both the inherent permeability of the concrete and the extent to which flaws occur during construction, commissioning and operation of a tank, i.e. the structural permeability. Whilst a well designed concrete may, in theory, be sufficiently impermeable to contain LNG, concerns over the possibility of cracks, opening of joints and localised areas of high permeability, cause the designer, user and insurer to doubt structural impermeability and demand a liner to prevent leakage.

1.3 STRUCTURAL PERMEABILITY

The ability of structural prestressed concrete to contain LNG must therefore be proven if a liner is to be omitted. If the liner could be omitted, not only would unlined tanks provide a lower cost alternative to current designs but also concrete could be considered as a secondary impermeable barrier in new or existing composite systems.

At present unlined concrete is more likely to be used for secondary leak containment where designers may be urged to provide enhanced

resistance to external accidents. However, advances in construction and materials technology may alleviate some of the fears associated with the use of concrete for primary containment of LNG. Admixtures which impart high levels of workability to low w/c ratio concretes facilitate transportation, placing and compaction with minimum effort[8]. Materials can be selected and construction sequences designed to minimise the risk of early thermal cracking due to heat of hydration[9]. Techniques are available for achieving leak tight construction joints[10]. Such methods have been used for high technology structures such as nuclear pressure vessels, gas tight secondary containments for nuclear reactors and oil production platforms.

So by careful materials selection, mix design and construction procedures, a low permeability structure may be achieved at ambient temperature. For the storage of LNG, this performance must be maintained at cryogenic temperature.

1.4 RELEVANT CONCRETE PROPERTIES

The fact that even mature concrete contains some free water, which will freeze when the temperature is reduced sufficiently, infers that the permeability will reduce at cryogenic temperature.

Regarding defects, cracking is likely to be of major concern. The initial cooldown of a tank, its filling with LNG and any subsequent level changes will all cause thermal stresses. These operations are generally controlled, in order that the level of thermal stress be maintained within acceptable limits. Prestress is also used to limit tension in the concrete. In the event of an accident however, conditions are not controlled. In such circumstances, where temperature differentials of the order of 180°C may exist through the tank wall, cracking cannot be prevented, but can be limited. To minimise cracking, desirable properties of the concrete include a low thermal expansion coefficient and a high tensile strain capacity. A low expansion coefficient will result in smaller strains for a given temperature change, and a high capacity for tensile strain will enable the thermal strains to be sustained more easily.

- 24 -

Reinforcement is, of course, included to limit crack widths in the event that cracking occurs. The efficiency of the reinforcement in this respect is directly related to the concrete-steel bond strength as in conventional r.c. design.

To assess structural permeability, data is therefore required for the following concrete properties at both ambient and cryogenic temperatures:-

- Permeability
- Strain capacity in tension
- Thermal expansion coefficient
- Bond strength to reinforcement.

1.5 DEVELOPMENT OF THE TEST PROGRAMME

Previous test programmes to investigate the performance of concrete down to cryogenic temperatures have, in general, been limited to conventional structural concretes. Variations in mix proportions have been considered, in particular the water-cement ratio, and occasionally cements other than OPC have been included. Air-entrained concrete has often been used, on the assumption that resistance to environmental freeze-thaw conditions might be extended to the extreme temperature changes occurring in cryogenic storage facilities. The influence of moisture content has also been widely studied.

The properties which have been measured most commonly at cryogenic temperature are compressive strength, tensile and flexural strength, elastic modulus and thermal contraction. In relation to structural permeability, properties which are of specific interest are permeability, thermal expansion, strain capacity and bond to reinforcement. The test programme was therefore designed to measure these particular properties of the concrete, and to identify whether one or more types of concrete would yield superior performance with respect to these properties.

With these objectives in mind, the programme was divided into two distinct phases. Phase 1 comprised screening tests on 17 concrete mixes, selected to investigate a range of mix parameters as follows:-

1)   Strength grade, as determined by cement content and water-cement ratio.

2)   Aggregate types; gravel, crushed rock and lightweight.

3)   The use of Pulverised Fuel Ash (PFA) and Ground Granulated Blastfurnace Slag (GGBS) to partially replace OPC.

4)   The use of admixtures, including air entraining agents and superplasticers.

Tests used to rank the performance of these 17 concretes were as follows:

-    Compressive strength at cryogenic temperature and after thermal cycling.

-    Tensile splitting strength at cryogenic temperature and after thermal cycling.

-    Water permeability at ambient temperature.

Based on the results obtained from these screening tests, four concretes were selected for more comprehensive testing to determine the following properties at cryogenic temperature.

(i)   Permeability.

(ii)   Strain capacity in direct tension and in flexure.

(iii) Thermal contraction.

(iv)   Elastic modulus

(v)   Bond strength to reinforcement.

In addition, tests were carried out on each of the four concretes to determine the influence of thermal cycling between ambient and cryogenic temperature on gas permeability and for two of the four concretes the relationship between permeability and pore structure was investigated.

2. LITERATURE ANALYSIS

2.1 INTRODUCTION

The properties of concrete under normal environmental conditions are determined primarily by the constituent materials and the mix proportions, in particular the water-cement ratio. With regard to structural performance, other factors, such as curing and moisture content, are generally of secondary importance (although where durability is a primary design requirement this may not be the case). In relation to the use of concrete for cryogenic applications, however, there are two additional primary factors which influence the in-service properties of the concrete, namely

i)   Temperature
ii) Moisture content.

The way in which these two factors influence the performance of concrete at cryogenic temperature is a clear indication that property changes are related to the formation of ice in both the large capillaries and finer pores in the cement paste, and the subsequent contraction of the ice as the temperature is reduced below its freezing point.

2.2 ICE FORMATION

Work by Yamane et al[11] indicated that between 0°C and -5°C, freezing of the water in the larger pores of about 100 Å was predominant, and that at temperatures between -30°C and -40°C freezing of water in smaller pores of 10 Å was predominant due to the reduced freezing point of the capillary water. Turner[12] has suggested that freezing is initiated in the larger capillaries, which contain some 30% of the free water, at about -3°C to -4°C and continues gradually until all the capillary water is frozen at about -20°C. According to Tognon[13], the water in the finer pores begins to freeze at -30°C and this gradually continues until all the free water has frozen at about -70°C. This progressive ice formation and associated pore filling therefore results in a gradual strength increase over this temperature range.

The continual increase in strength at temperatures below -70°C is attributed by Tognon[13] to 'internal prestressing'. The ice has a higher coefficient of contraction than the other constituents of concrete, i.e. 53 microstrain per °C compared with 10 microstrain per °C[14] (1 microstrain = 10^{-6} strain), and therefore places the concrete under triaxial compression which increases its strength considerably. The magnitude of effective prestress applied by the ice contraction has been determined by Tognon by recording the level of biaxial restraint required to increase the strength of moist concrete to values equal to those measured at low temperature. These results are shown in Figure 2.1. So, for example, to achieve an increase in strength from 25 N/mm^2 under uniaxial conditions at 20°C to 90 N/mm^2 would require either a reduction in temperature to -100°C or biaxial restraint equivalent to a stress of 9 N/mm^2.

At a temperature of -115°C, ice changes from its hexagonal structure (ICE I) to an orthorhombic structure (ICE II). At this stage, the volume of the ice decreases suddenly so that its density increases to 1.15 kg/m^3. There is limited evidence to suggest that this may cause the strength of concrete to decrease slightly[15], although the vast majority of data indicate little change in strength below this temperature. A further phase change takes place at -155°C when ice crystallizes in tetragonal form (ICE III). Again there is no evidence to suggest that this has a significant effect on the strength of the concrete. It should be noted however that these changes occur in pure water. Whilst similar changes are likely to take place in the free water in concrete, the absolute temperatures at which the changes occur are likely to differ significantly from those above due to the complex nature of the pore fluids.

2.3 INFLUENCE OF MOISTURE CONTENT ON STRENGTH

The compressive strength of concrete is the property which has been most widely examined at low temperature, work having been undertaken in Italy[13], Germany[16], Japan[11,17-24], United States[15,25] and Russia[26,27]. This property has therefore been selected to identify the influence of moisture content on low temperature behaviour.

FIGURE 2.1. Equivalent biaxial restraint required to cause a
compressive strength increase comparable to that
achieved by reduced temperature (Ref. 13).

2.3.1 Saturated Concrete

To illustrate the influence of temperature on compressive strength and to show the general consistency of data from different sources, results obtained by Monfore and Lentz[15], Okada and Iguro[20], Goto and Miura[17], Tognon[13] and Yamane et al[11] are included in Figure 2.2 for saturated concrete. The results are presented in terms of both the increase in strength with reducing temperature (Figure 2.2a) and the relationship between cold strength at -50°C, -100°C and -160°C and the strength at 20°C (Figure 2.2b). It will be seen from Figure 2.2a that between 20°C and 0°C the strength is largely unaffacted. Below 0°C, as the free water freezes, there is a gradual increase in strength down to a temperature of about -120°C. The increase is almost linear with reducing temperature, the strength gain being equivalent to about 6 N/mm^2 for each 10°C drop. Below -120°C, the strength is largely unaffected by further reducing the temperature.

The alternative presentation of the data in Figure (2.2b) shows the relationship between the cold strength and the strength at 20°C to be approximately linear. Furthermore, the slope of the curves at each of the temperature levels examined was constant, the curve simply being shifted upwards as the temperature dropped.

2.3.2 Partially Dry Concrete

Many researchers have tested concretes which have been subjected to atmospheric drying, typically at 20°C, 65% RH. This condition, between saturated and oven dry has been defined as partially dry. Relationships based on data obtained by Monfore and Lentz[15], Tognon[13] and Iwata et al[22] are included in Figure 2.3 for partially dry concrete and again indicate close agreement. The increase in strength, as expected, was lower than recorded for saturated concrete but was still of the order of 2 N/mm^2 per 10°C drop in temperature down to -120°C (Figure 2.3a). The linear relationship between cold strength and strength at 20°C was again observed (Figure 2.3b),

- 30 -

(a)

(Data from Refs. 11, 13, 15, 17, 20)

COMPRESSIVE STRENGTH (N/mm^2)

TEMPERATURE $(^{\circ}C)$

(b)

STRENGTH AT CRYOGENIC TEMPERATURE (N/mm^2)

$-165^{\circ}C$
$-100^{\circ}C$
$-50^{\circ}C$

STRENGTH AT $20^{\circ}C$ (N/mm^2)
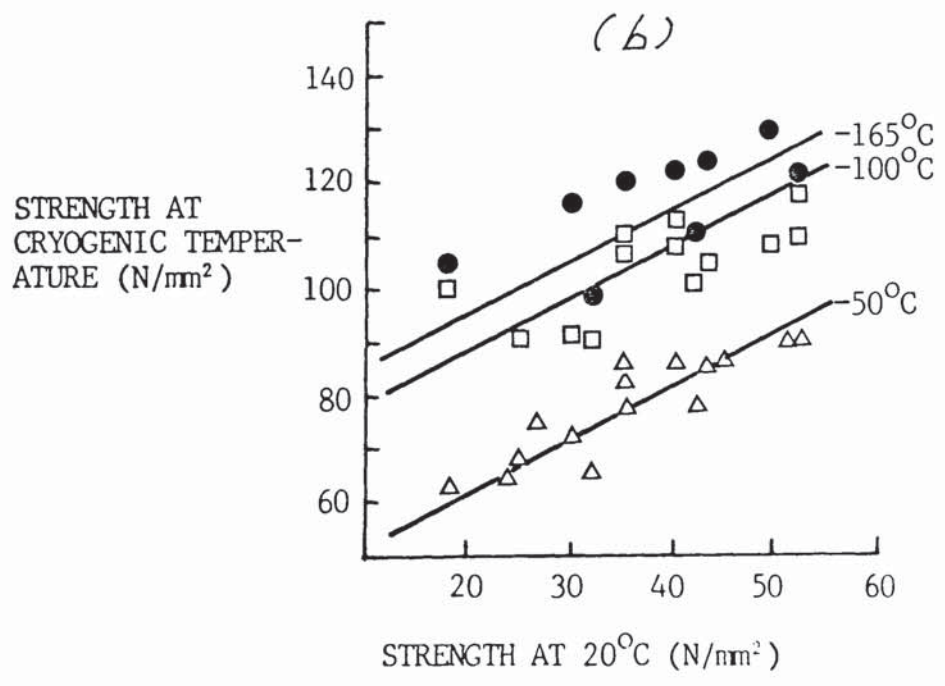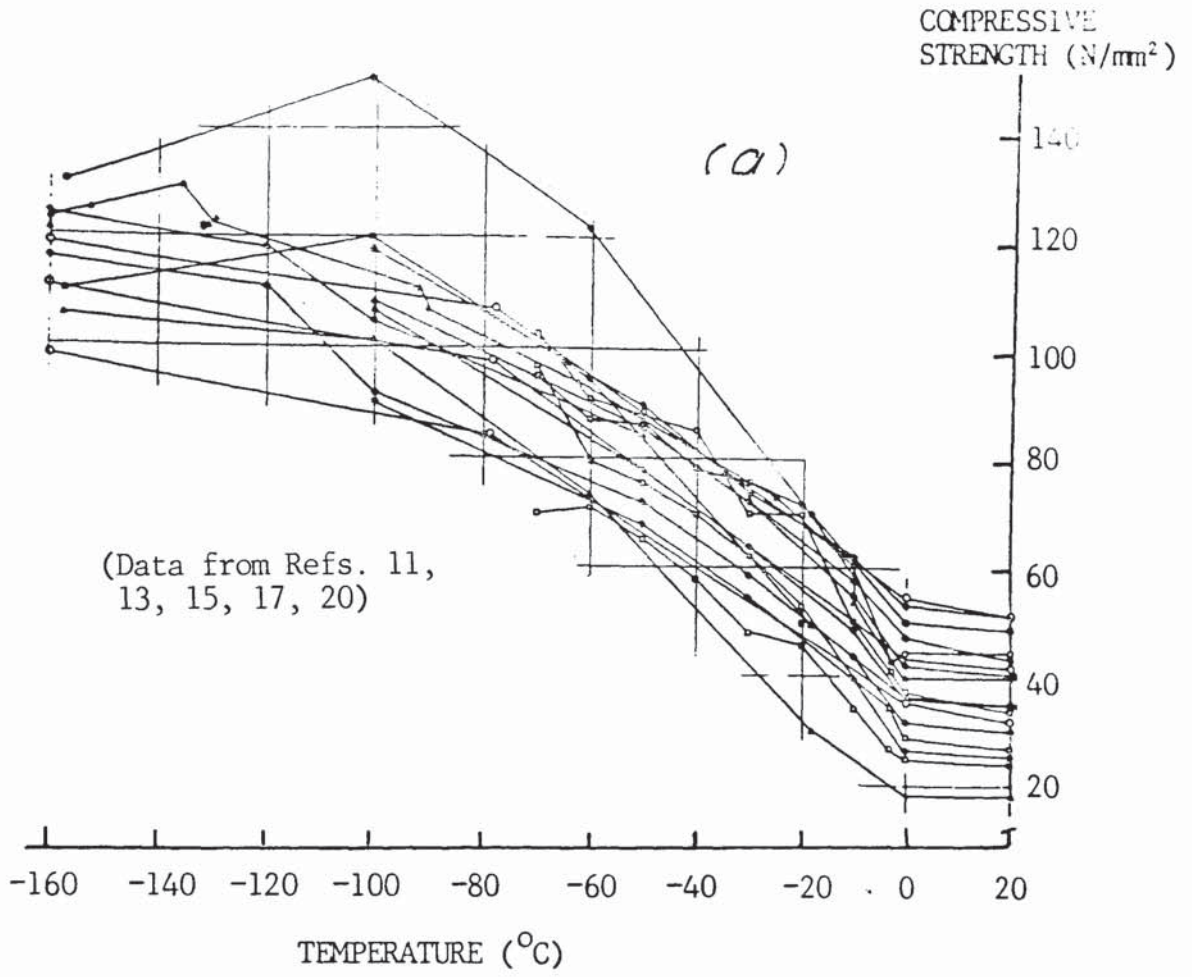
FIGURE 2.2. The influence of temperature on the compressive strength of saturated concrete.
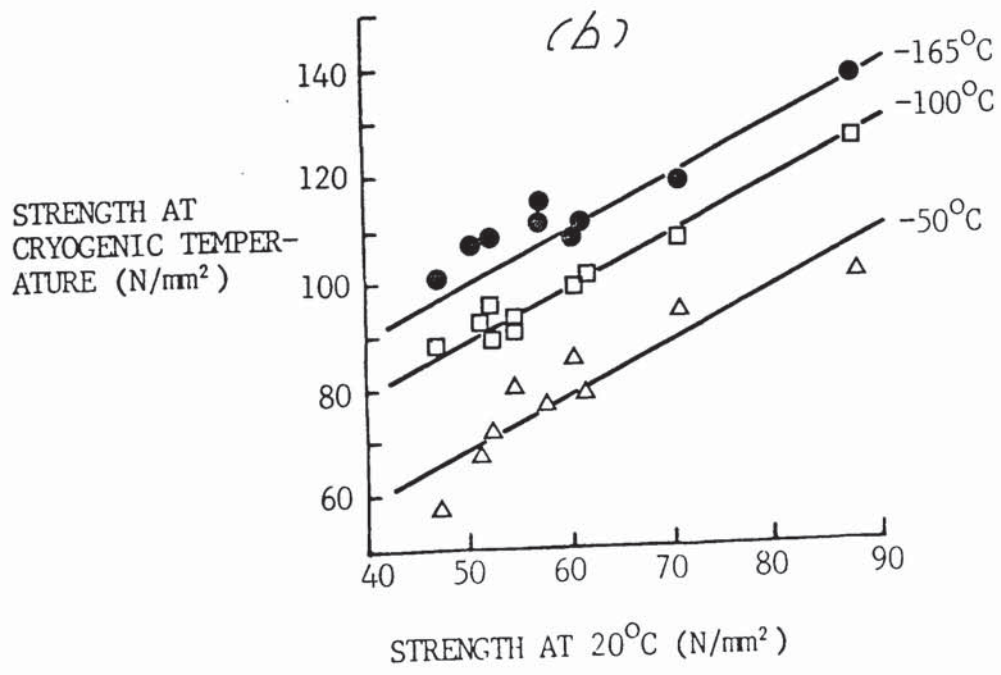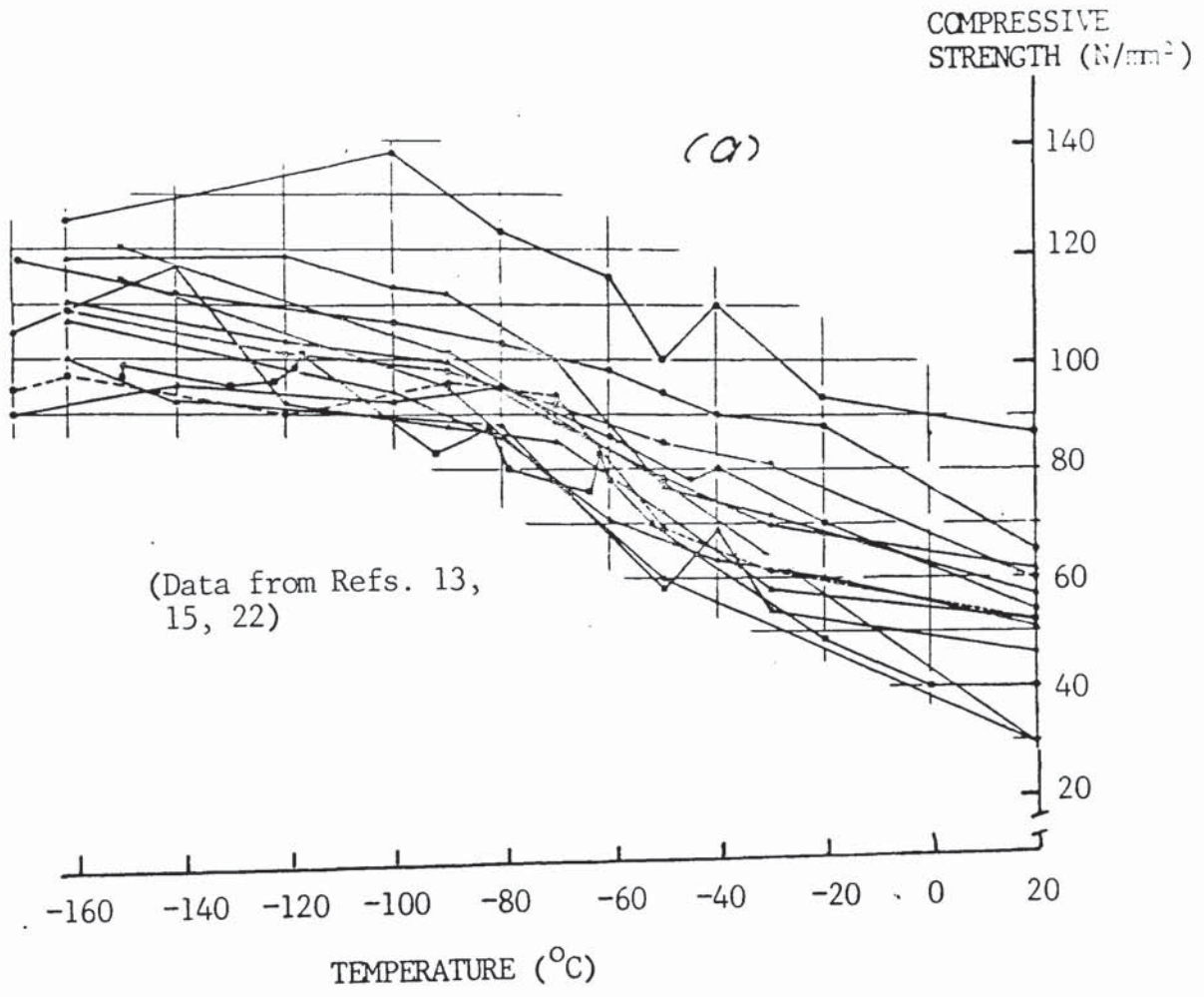
FIGURE 2.3. The influence of temperature on the compressive strength of partially dried concrete.

(Data from Refs. 13, 15, 18)
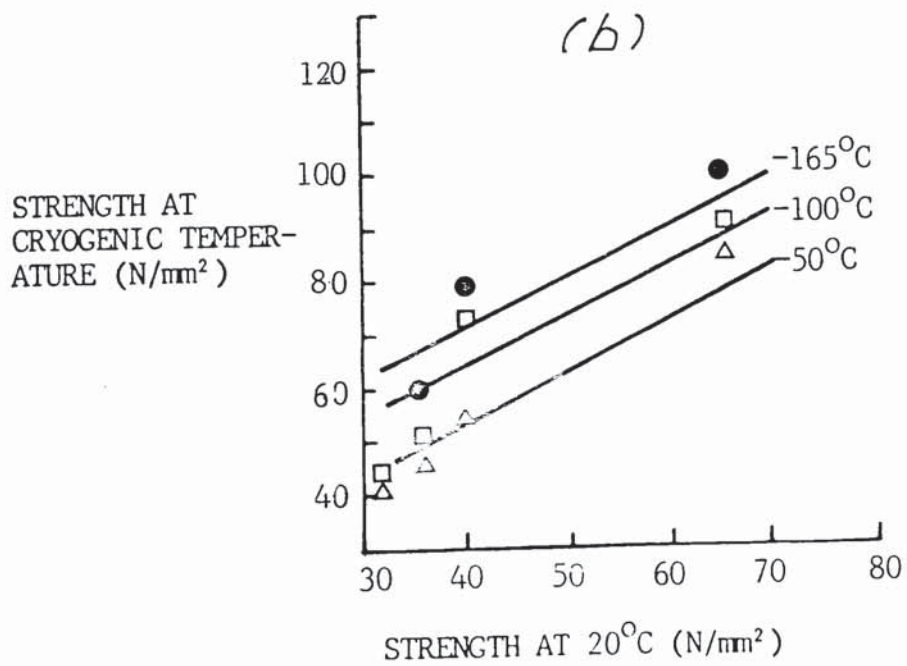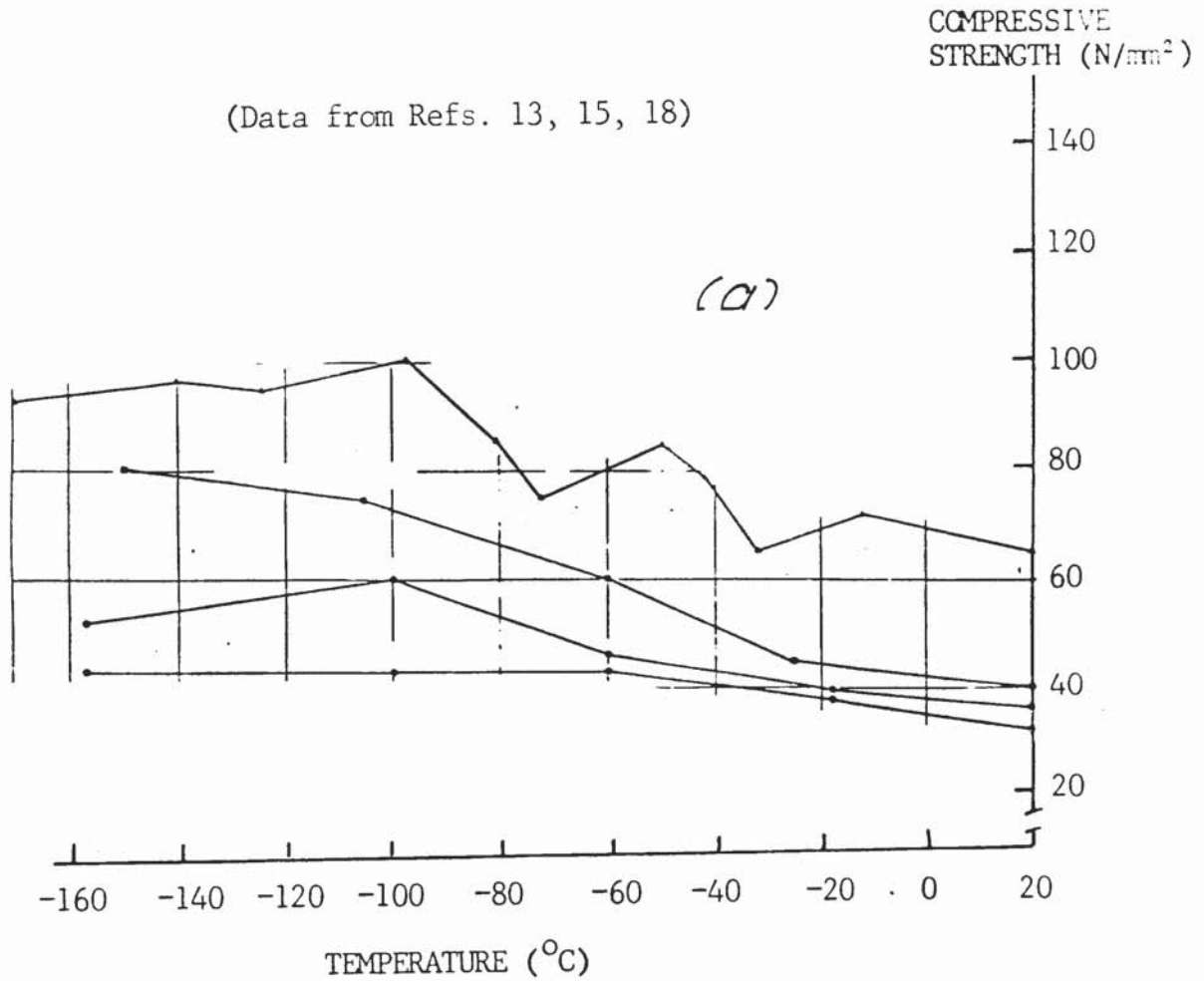
FIGURE 2.4.   The influence of temperature on the compressive
strength of oven dried concrete.

the slope of the curves being the same at each temperature and more importantly, the same as recorded for saturated concrete.

2.3.3 Oven Dried Concrete

Data on oven dried concrete obtained by Tognon[13], Goto and Miura[18] and Monfore and Lentz[15] are included in Figure 2.4. Whilst results are limited, there is sufficient data to indicate a small increase in strength with reducing temperature. The results are more scattered however, perhaps indicating that the extent of moisture loss under oven drying conditions was not consistent between the various researchers. This condition is not, however, typical of insitu concrete which has a moisture content of about 5%[28]. It is interesting to note that the relationship between cold strength and strength at 20°C can again be approximated by a straight line with the same slope derived for saturated and partially dried concrete (Figure 2.4b).

2.3.4 Estimating Cold Strength

Based on the above data, a simple equation has been derived for estimating the cold strength of concrete within the range 0°C to -120°C. Above 0°C there is no significant effect of temperature for the normal operating range and similarly, below -120°C, there is no appreciable change in strength as temperature is reduced. Within the range 0°C to -120°C the cold strength can be related to the ambient strength at 20°C, the percentage moisture content by weight of concrete, m, and the temperature θ , by the equation,

$$f_{c(\theta)} = f_{c(20)} - \frac{\theta . m}{12} \qquad (2.1)$$

Values of strength predicted using equation 2.1 are illustrated in Figure 2.5 together with a summary of the data presented in Figures 2.2, 2.3 and 2.4 for concretes at different moisture contents. Other relationships have been derived by Goto and
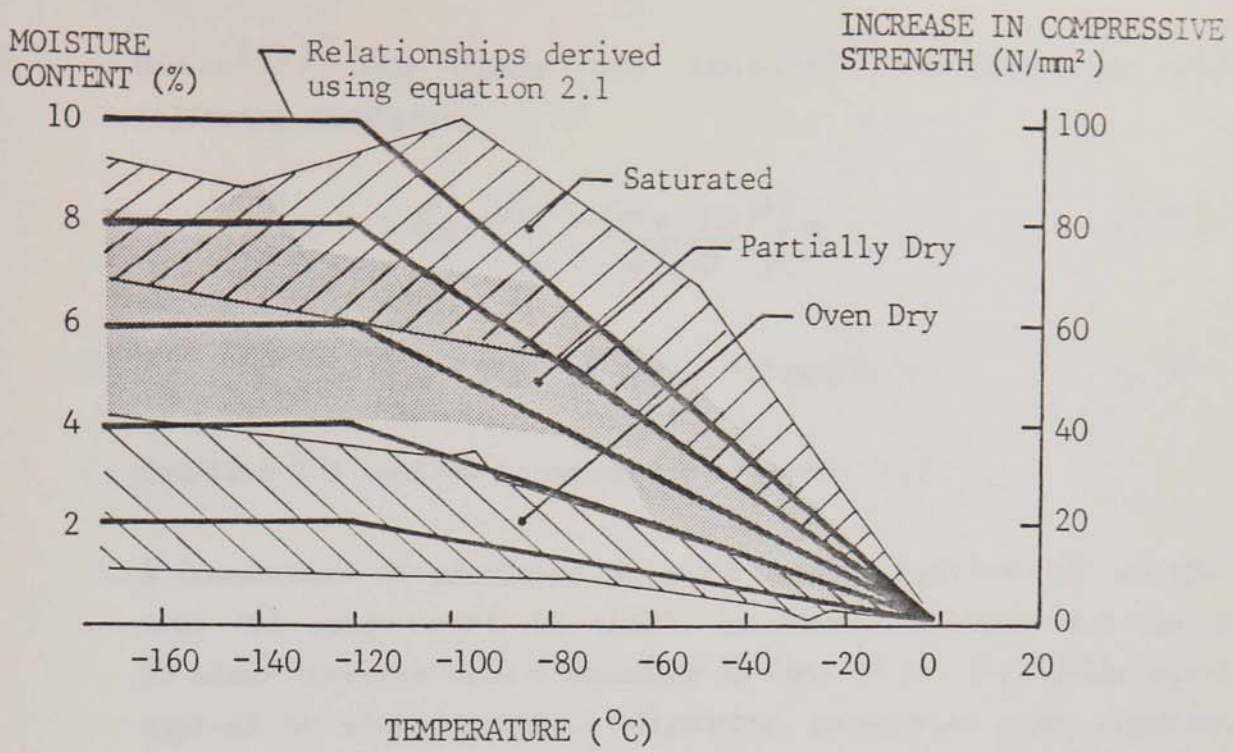
FIGURE 2.5. A comparison between the predicted increase in com-
pressive strength at cryogenic temperature and
experimental data for concretes at different moisture
contents.

$$f_{c(\theta)} = f_{c(20)} + 5.4 - 0.864\theta - 0.00276\theta^2$$
$$(Ref. 20.)$$

$$f_{c(\theta)} = f_{c(20)} + \left\{12 - \frac{1}{2700}(\theta + 180)^2\right\}m$$
$$(Ref. 14.)$$

$$f_{c(\theta)} = f_{c(20)} - \frac{\theta m}{12}$$
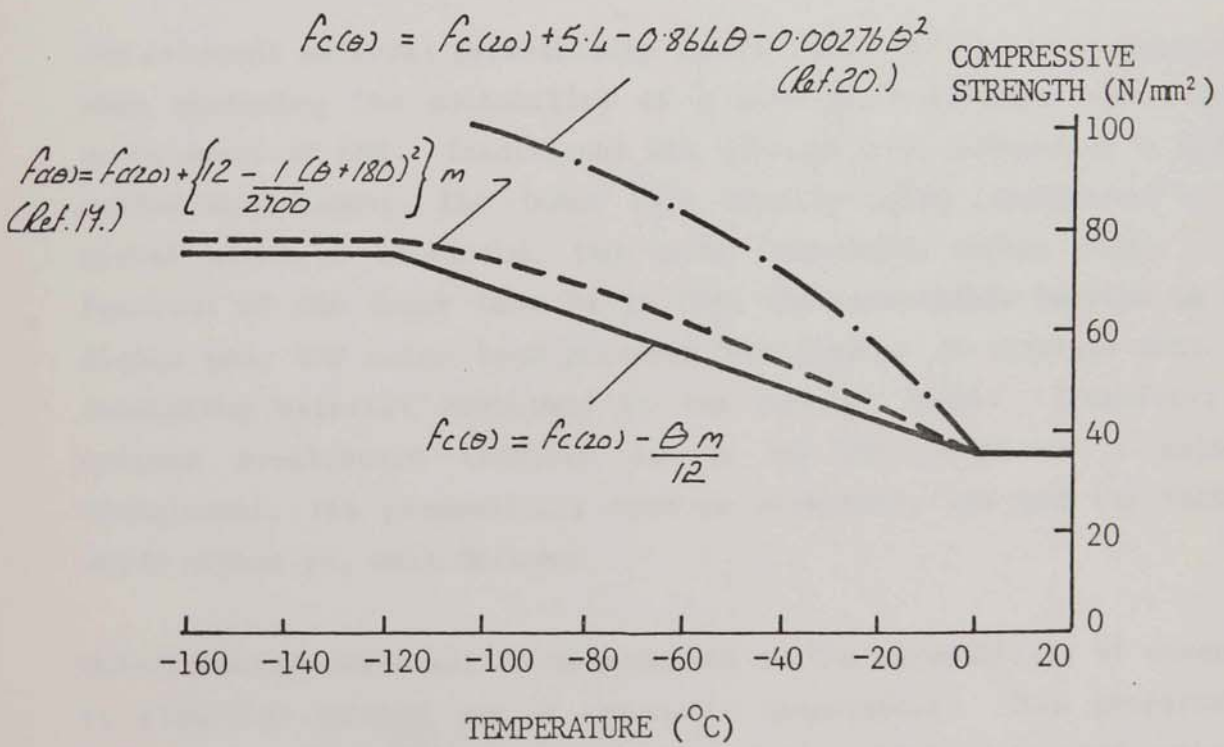
FIGURE 2.6. A comparison between predicted compressive strengths
obtained using different empirical equations.

Muira[17] and Okada and Iguro[20], defined by the following equations.

$$f_{c(\theta)} = f_{c(20)} + \left(12 - \frac{(\theta + 180)^2}{2700}\right) m. \qquad (2.2)$$

$$f_{c(\theta)} = f_{c(20)} + 5.4 - 0.864\theta - 0.00276\theta^2 \qquad (2.3)$$

Equation 2.3 applies to saturated concrete only.

A comparison of predicted strength using equations 2.1 and 2.2 over the range +20°C to -160°C is shown in Figure 2.6 for a 35 N/mm^2 concrete with a moisture content of 5%, the latter being typical of site concrete. Strengths determined using equation 2.2 are in excess of the authors predicted values by up to 10%. However, both equations clearly illustrate the significance of moisture content on the property change with temperature.

2.4 PERMEABILITY

The inherent material permeability is the first factor to be considered when assessing the suitability of a particular material for primary containment of LNG. Traditional LNG storage tanks consist of a double walled containment, the inner tank usually being constructed of 9% nickel steel or aluminium, the outer comprising carbon steel. The function of the inner tank is to form the impermeable barrier to the liquid gas, the outer tank prevents the ingress of moisture into the insulating material contained in the annular space. Therefore, if unlined prestressed concrete is to be considered as a primary containment, its permeability must be acceptably low and the factors which affect it, well defined.

Unfortunately, very little data exists on the permeability of concrete to liquefied natural gas at cryogenic temperature. This property is least adequately covered in the literature, although limited work has been carried out by the US Institute of Gas Technology[29] on the permeability of concrete to both liquid and gaseous methane at temperatures down to -143°C, and by Imperial College of Science and Technology on permeability of concrete to liquid nitrogen at

-196°C[30,31]. The reason for the lack of experimentation in this area is believed to be due not only to the fact that a metallic barrier is generally used to contain the LNG, but also because of the problems associated with the accurate measurement of concrete permeability to LNG and gaseous methane at cryogenic temperatures.

There are, however, extensive data on the permeability of concrete to both liquids and gases at room temperature. One of the most comprehensive investigations into the water permeability of concrete was carried out by Glanville as long ago as 1926[32]. More recent studies have been carried by Murata[33] and Goto and Roy[34] and many other workers. Gas permeability results have been reported by Huart[35], Loughborough[36] and Graiffer et al[37], amongst others. The factors which influence permeability have been well defined and can be divided into four main areas,

i)   Constituent materials and mix proportions
ii)   Degree of compaction
iii)   Curing regime and extent of cement hydration
iv)   Moisture content

and these are described in the following sections.

2.4.1 Effect of Constituent Materials and Mix Proportions

For normal dense aggregate, the range of values of measured water permeability coefficient are of the same order as measured for mature cement pastes i.e. 1×10^{-9} m/sec to 2.5×10^{-14} m/sec[38]. The aggregate is, however, a discontinuous phase and, therefore, has a less significant effect on the permeability of concrete than that of the continuous cement paste phase. Changes in aggregate type therefore tend to have only a marginal effect on concrete permeability.

There is no evidence to suggest that changes in the nature of OPC appreciably influence the permeability of concrete. However, results obtained by the US Bureau of Reclamation have indicated that the use of pulverised fuel ash (PFA) to replace 30% of OPC may cause a reduction in permeability of about one order of

- 37 -

magnitude[39]. More recently, tests using ground granulated blastfurnace slag (GGBS) have identified that this material may also provide benefits in terms of reduced permeability in structural concrete[40]. However, the benefit of reduced permeability with both PFA and GGBS is dependent on adequate curing.

Early work by Powers et al[41] illustrated the importance of w/c ratio on the permeability of cement paste. A variation in w/c ratio from 0.4 to 0.7 caused an increase in permeability of about two orders of magnitude. Powers also found that there was a critical w/c ratio of about 0.4 above which it was impossible to achieve a discontinuous capillary state in the cement paste and that, below this value of w/c, the permeability was markedly reduced. Similarly, Huart found that a reduction in cement content from 600 kg/m^3 to 200 kg/m^3 with an associated change in w/c ratio increased the gas permeability by a factor of 35[35]. More recent tests indicate that the influence of w/c ratio is less marked than that observed by Powers. A summary of results is included in Figure 2.7, which includes data from References 32-34 and 42-46. Whilst the results are scattered, the relative change in permeability within each test programme, over the range of w/c ratios reported by Powers, is the order of only 10 times. This is illustrated more clearly in Figure 2.8, in which the results have been presented in relation to a datum value of a w/c of 0.45. The difference in the results may be due to the change in cement properties since Powers early work. Also, much of the recent research used concretes rather than cement pastes.

Both water-reducing and air-entraining admixtures can be used to reduce the permeability of concrete. Water reducing admixtures can be used either to enable a reduction in w/c ratio, with the associated reduction in permeability, or to improve workability and hence enable more complete compaction. Air entraining agents (AEA) can effectively improve the cement paste permeability by enabling a small reduction in w/c and also by uniformly distributing discrete voids in the cement paste. This improvement in permeability using an AEA is usually small
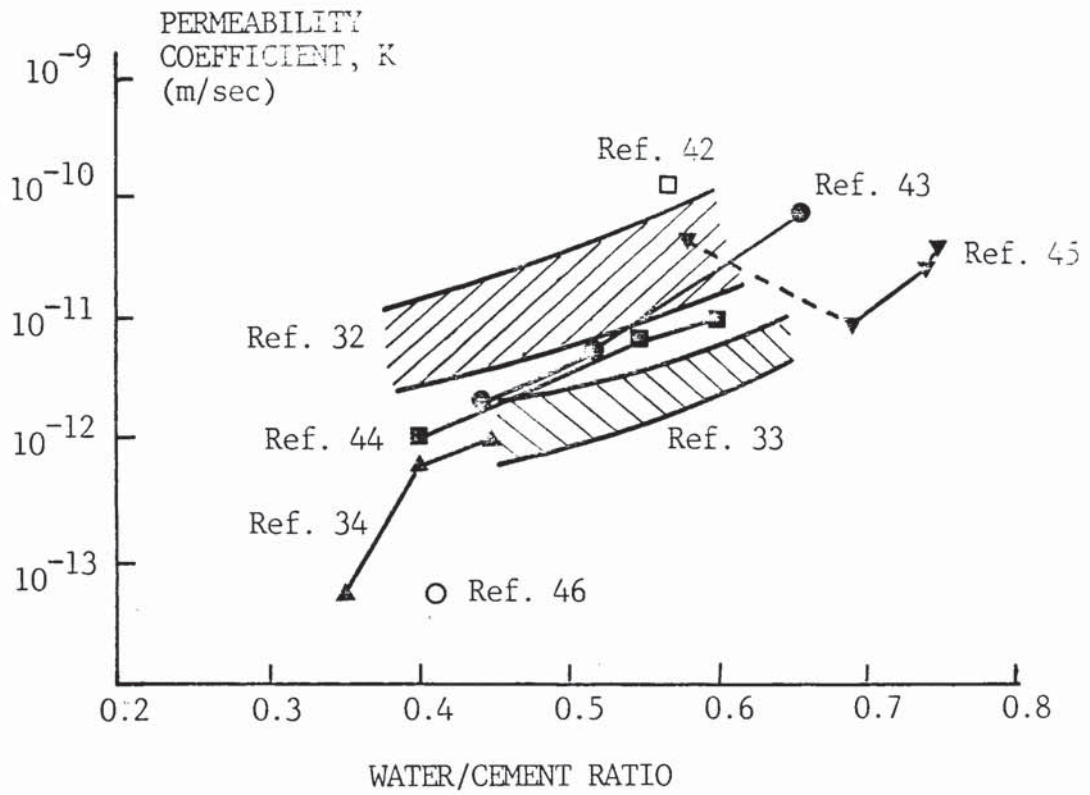
FIGURE 2.7. A summary of experimental data showing water permeability coefficients related to water/cement ratio.
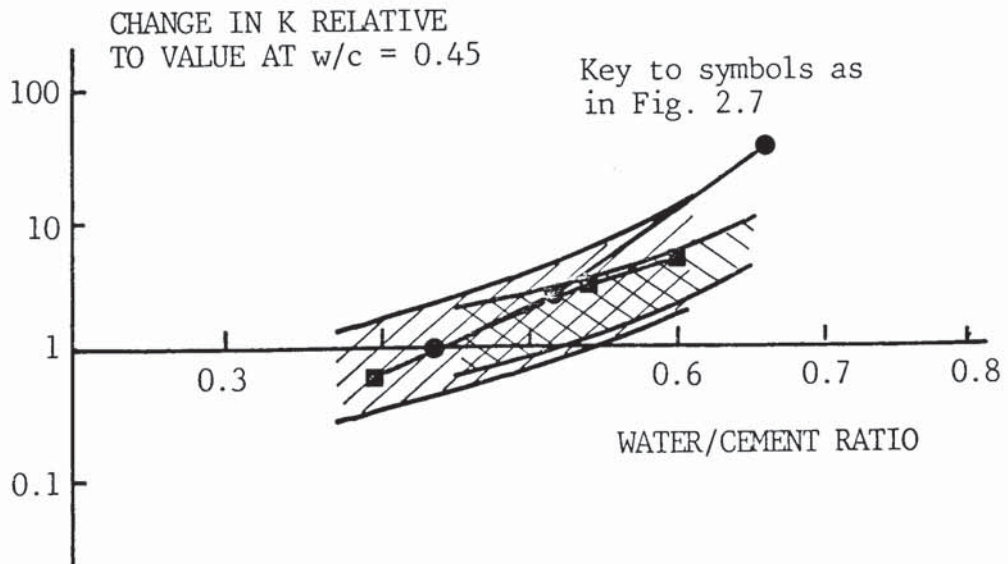
FIGURE 2.8. The relative change in water permeability coefficient with water/cement ratio.

compared with the effects of moisture content or water/cement ratio[33], but can be as high as two orders of magnitude[37].

2.4.2 Degree of Compaction

To achieve its optimum performance concrete must be thoroughly compacted. An increase in permeability of several orders of magnitude can easily result from inadequate compaction[32]. However, over compaction can often result in the top surface zone having a higher w/c ratio than the bulk of the pour due to upward migration of water as the concrete settles. This results in a surface zone with increased permeability but is generally only a major problem in concretes which have been poorly designed. In general, concrete cast on site would be expected to be less resistant to water and gas penetration than concrete produced in the laboratory, due not only to a better quality control of the material which can be achieved in the laboratory, but also to better compaction.

2.4.3 Curing

Previous tests have been carried out by Taylor Woodrow on the effects of different curing regimes on the permeability of concrete in relation to the durability of offshore structures[47]. Standard water curing, fog curing and air curing (no cure) have all been investigated. The results showed a reduction in the permeability of water cured concretes of 3 orders of magnitude or more, illustrating the importance of adequately curing concrete on site.

In addition, the permeability of air cured concrete was found to be reduced significantly whilst being tested using water due to renewed hydration of the cement. This occurred at whatever age the concrete was tested, even 35 years[48].

2.4.4 Moisture

Moisture content is a very important factor controlling the gas

permeability of concrete not only by blocking the pores in the
concrete, but also by allowing further hydration to take place,
as described above. Increases of the evaporable moisture content
of concrete from zero (oven dried) to 100% (saturated) have been
found to reduce the gas permeability by a factor of as much as
two orders of magnitude[37].

2.4.5 Temperature

As indicated previously, very little data exists on the
permeability of concrete to liquefied methane or natural gas at
cryogenic temperatures. The Institute of Gas Technology[29]
carried out short term tests on one mix only. Variations in the
permeability of concrete to methane gas were recorded at
different degrees of saturation, oven-dry, dried at 50% relative
humidity and fully saturated. The permeability at both room
temperature and down to $-143^{o}C$ reduced as the moisture content
increased to the extent that, under fully saturated conditions,
the concrete was found to be impervious to methane gas even under
a pressure of 0.276 N/mm^2 (40 p.s.i.). Values of gas
permeability coefficient for oven dried concrete and specimens
stored at 50% RH were of the order of 1.3 x 10^{-13} and 1.1 x 10^{-15}
m^2[a] respectively, the former being very permeable even
under a pressure of only 0.97 x 10^{-3} N/mm^2 (0.14 p.s.i.). These
results are shown in Figure 2.9.

It is therefore apparent that the moisture content plays an
equally important role in determining the permeability of
concrete at both cryogenic and room temperature. The effect of
cooling to $-143^{o}C$ was to reduce the permeability coefficient by
a factor of 3. This relatively small reduction is believed to be
due to the general contraction of the pore sizes within the
cement paste combined with the formation of ice.

(a)   The gas permeability coefficient is expressed in units of m^2. This
differs from the Darcy coefficient for non-compressible liquids for
which the units are m/sec. Permeability coefficients are discussed in
greater detail in Section 4.2.
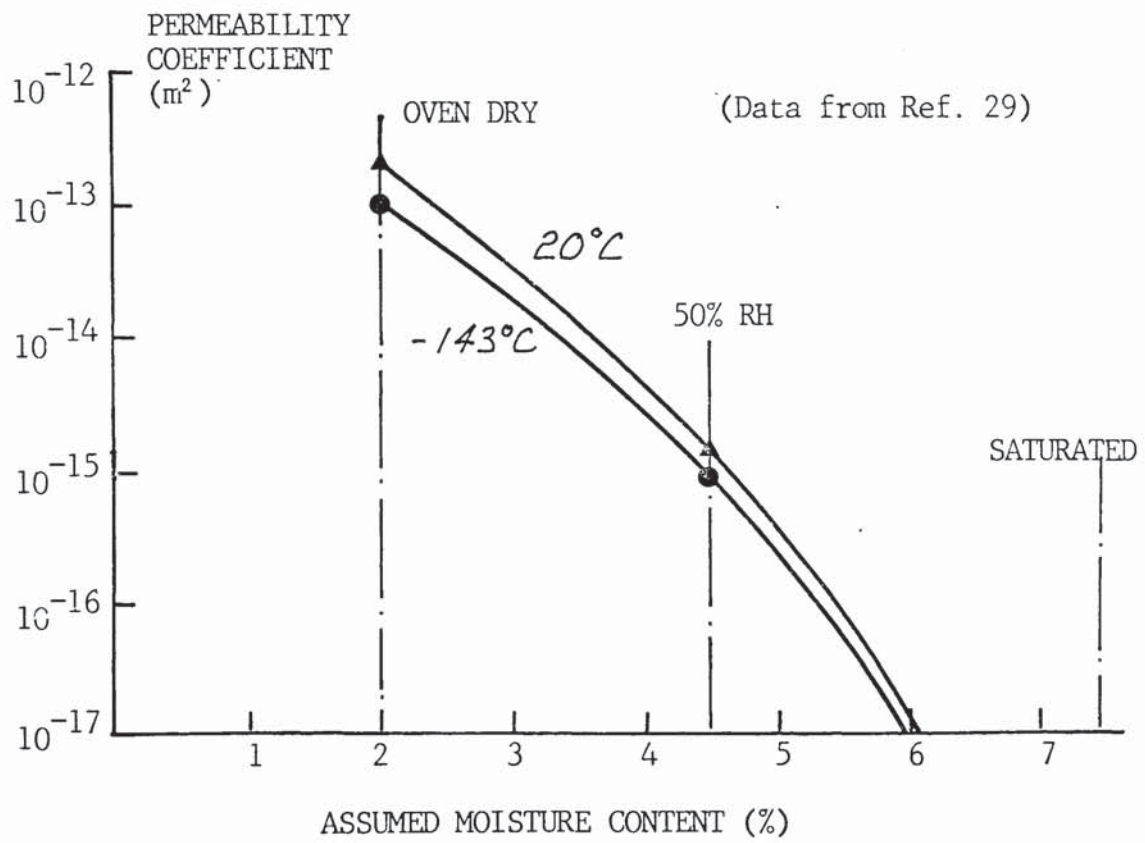
FIGURE 2.9.   The influence of temperature and moisture content on gas permeability coefficient.

In a preliminary study undertaken by Imperial College[30] the work was of a qualitative nature and no specific values of permeability were reported. However, the results did indicate that within the limits of the testing technique, concrete could be made impermeable to nitrogen at temperatures down to -196°C. This involved the use of surface treatments and polymer impregnation. However, the tests were only short term, generally of the order of minutes, and no definite conclusions could be drawn from the work other than to say that certain types of surface treatment were effective in reducing concrete permeability to nitrogen at -196°C, in the short term.

More recent tests at Imperial College[31] have provided quantitative data on the permeability of concrete to liquid nitrogen with permeability coefficients of the order of 10^{-10} m/sec. However, by the very nature of the tests it was impossible to identify the influence of temperature.

2.5 TENSILE & FLEXURAL PROPERTIES

2.5.1 Tensile Splitting Test

Extensive measurements of the tensile strength of concrete have been undertaken in Japan, US and Spain at temperatures down to -157°C. Data obtained by Iwata et al[22], Okada and Iguro[20], Yamane et al[11] Monfore and Lentz[15] and Elices et al[49] are included in Figure 2.10. The majority of data are for saturated concrete but limited results for partially dry[15,22] and oven dry[22] concrete were also recorded. In each case, the tensile strength increased with reducing temperature but the relationship was less well defined than that observed for compressive strength.

2.5.1.1 Saturated concrete

Results for saturated concrete measured by Monfore and Lentz[15] showed a maximum increase in strength of the order of 150% at a temperature of about -60°C. As the temperature dropped below -60°C there was a
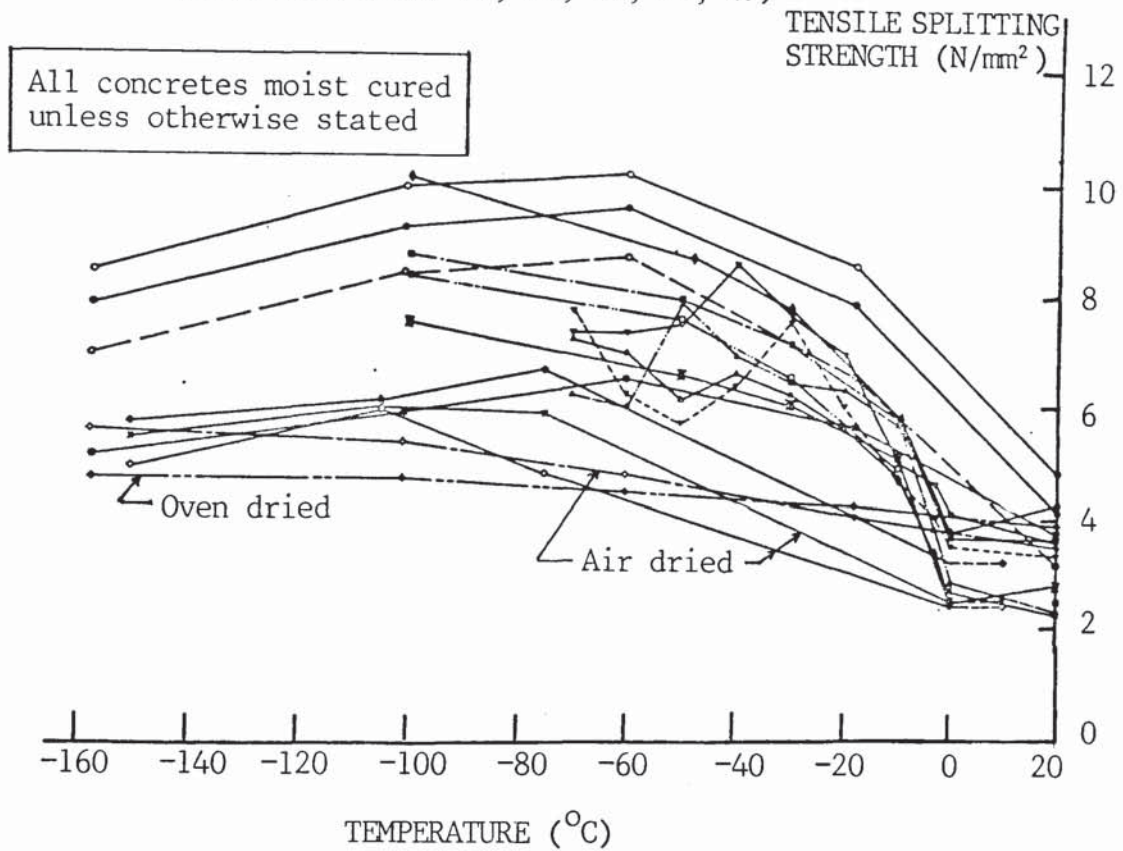
FIGURE 2.10. The influence of temperature on tensile strength.

reduction from the peak value such that at -157°C, the increase in strength above that at 20°C was about 100%. A similar effect was observed by Iwata[22], although the general level of the peak strength increase was lower. Okada and Iguro[20], however, recorded a steady increase in strength down to -100°C (no results were obtained below this temperature) whilst Yamane et al[11] indicated that the peak strength was achieved at a temperature of -40°C with no further change down to -70°C. Elices et al [49] carried out tests at 20°C and -196°C and recorded an increase in strength of 188% at the lower temperature.

2.5.1.2 Partially dried and oven dried concrete

For partially dried and oven dried concretes the increase in tensile strength with reduced temperature was, in the case of data from Montfore and Lentz[15], considerably less than recorded for saturated concrete, but did indicate a gradual and continuous increase as the temperature reduced down to -157°C. Iwata et al[22] however, found that there was little difference in the behaviour of water cured and air dried specimens down to -150°C. Elices recorded an increase of 50% for concrete with a moisture content of 2%[49].

2.5.1.3 Estimating cold strength

Whilst the tensile strength of concrete is clearly influenced by both the temperature and the moisture content in a similar way to compressive strength, the data available is not sufficiently consistent to enable a general predictive equation to be derived based on these factors. This may be due to the fact that the tensile strength is more sensitive to small changes in moisture content and possible disruption due to the progressive ice formation. Unfortunately, specific values for

moisture content have not been reported and hence, this cannot be confirmed.

It should be noted that the change in the tensile strength of concrete will have a significant effect on the design of reinforcement for crack control and must therefore be considered in this respect. This is discussed in greater detail in Section 9.3.2. To enable the tensile strength to be estimated, relationships between tensile and compressive strength are illustrated in Figure 2.11. Equations describing the relationship have been derived by Okada[20] (equation 2.4) and Goto[18] (equation 2.5) and are as follows:

$$f_t = (0.063 f_c + 2.4)\ N/mm^2 \qquad (2.4)$$

$$f_t = 0.214\ f_c^{3/4}\ N/mm^2 \qquad (2.5)$$

where f_t represents tensile splitting strength and f_c represents compressive strength, both measured using cylinders with a 2:1 aspect ratio. In the UK, where compressive strength is measured using 150mm cubes, these equations have to be modified by multiplying the value of f_c for cylinders by 1.25[50]. The revised equations are,

$$\text{equ (2.4)} \qquad f_t = 0.0504 f_c + 2.4 \qquad (2.6)$$

$$\text{equ (2.5)} \qquad f_t = 0.181 f_c^{3/4} \qquad (2.7)$$

Predicting tensile strength values using each of these equations for concretes with cold compressive strengths typically within the range 60 - 100 N/mm^2 will result in values which differ by about 2 N/mm^2, the higher values being achieved using equation 2.6. For design purposes,
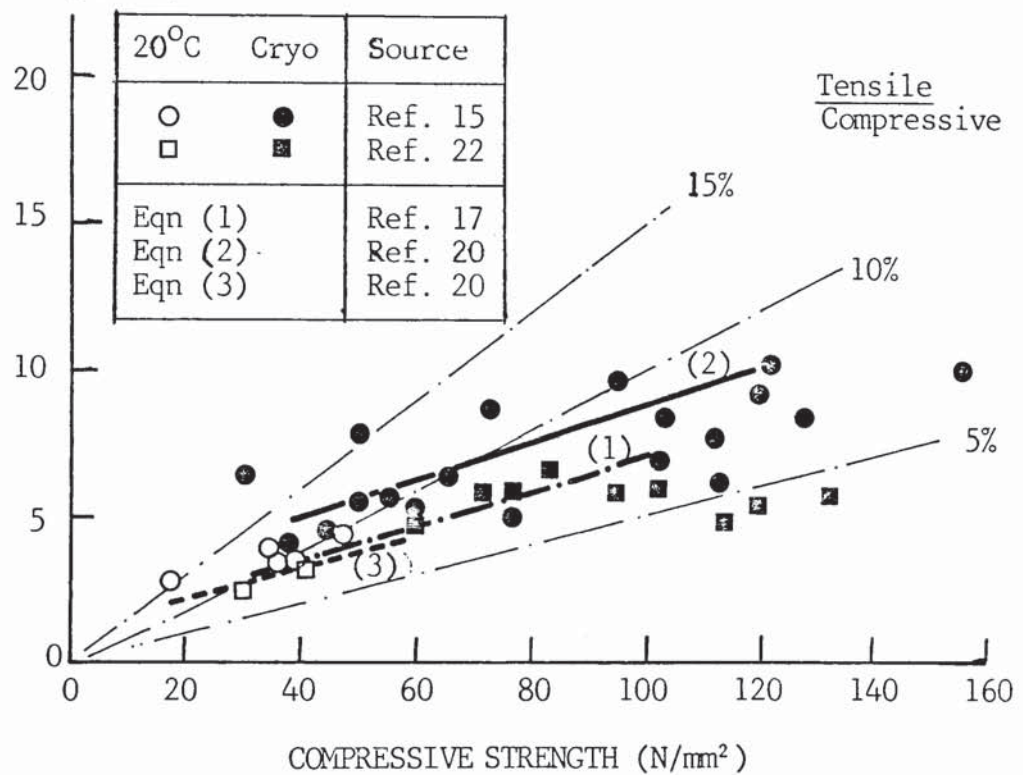
FIGURE 2.11.   The relationship between tensile and compressive
strength at temperatures down to -196°C.

when a value is being estimated in relation to the design
of reinforcement, the upper value is recommended; when
the value is being estimated in relation to the load
bearing capacity of concrete in tension the low value
from equation 2.7 should be used.

2.5.2 Flexural Strength (Modulus of Rupture)

2.5.2.1 Effect of temperature

The recorded variation in flexural strength with
temperature is illustrated in Figure 2.12. Results have
been obtained by Tognon[13], Yamane et al[11],
Okada et al[19] and Iwata et al[22]. As observed
for tensile strength, there was considerable variation in
the results of the different researchers which may again
have been due to variations in moisture content, although
the majority of tests were undertaken using concrete
which had been either water cured or fog cured at 100% RH
for some considerable time.

Not only was there a range in the magnitude of values of
flexural strength, but also a variation in the form of
the strength/temperature relationship. Tognon[13],
who undertook by far the most comprehensive series of
tests, found that the strength increased to a peak value
at a temperature of -50°C to -60°C, reduced as the
temperature dropped further to a value of about -90°C,
and then recovered again as the temperature reduced to
-180°C. This phenomenon was observed for a range of
concretes with different aggregate types (including
limestone, granite, silica, phorphyry, basalt) and with
both OPC and pozzolanic cement. A similar form of
strength/temperature relationship was also recorded by
Yamane et al[11] with the initial peak strength
occurring at a slightly higher temperature of -30°C.
The tests were only carried out down to -70°C, however,
and the lower value beyond which Tognon had observed
a recovery in strength was not reached. Values of

- 48 -

(Data from Refs. 11, 13, 19, 22)

All concretes water cured unless otherwise stated

FLEXURAL STRENGTH (N/mm²)

— Air Dried
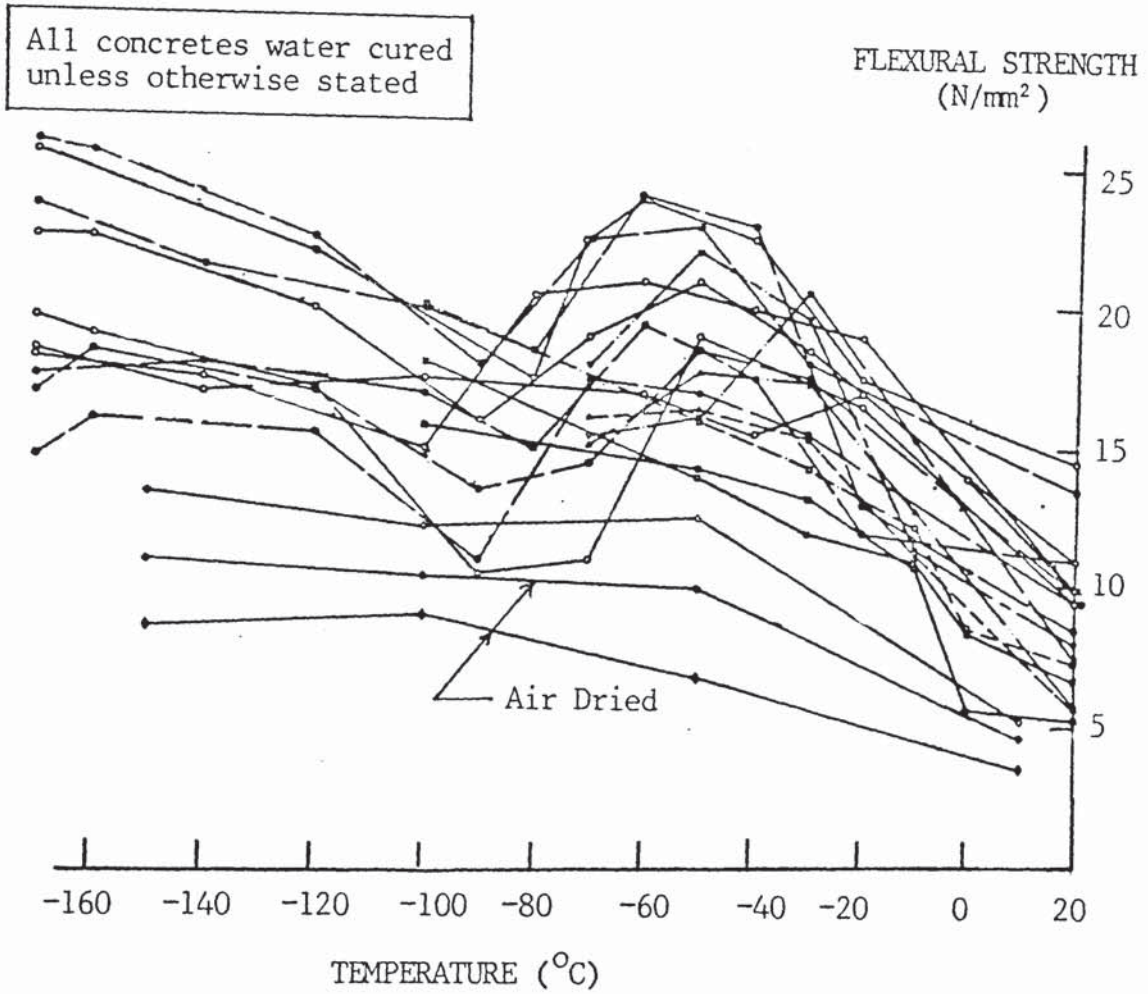
TEMPERATURE (°C)

FIGURE 2.12.   The influence of temperature on flexural strength.

flexural strength reported by Yamane et al were presented
in terms of the percentage change from the value at
20°C. Absolute values were not given and were
therefore estimated using values of tensile splitting
strength and the relationship between flexural and
tensile splitting strength derived from results of Okada
et al[19].

The influence of temperature on flexural strength
observed by Okada et al[19] and Iwata et al[22]
was considerably different to that described above.
Whilst the initial increase in strength was observed, in
one case this continued at a reduced rate as the
temperature reduced down to -100°C[19], and in the
other[22], increased down to -50°C with no
appreciable change thereafter. In the latter case,
similar behaviour was observed for water cured and air
dried concrete, although the magnitude of strength
increase was, as expected, lower for air dried
specimens.

The difference in concrete behaviour indicated by the two
sets of results is difficult to explain, the only
significant difference in test conditions being the age
of the specimens. Tognon[13] and Yamane et
al[11] carried out tests on concrete at an age of 5 -
6 months, whilst Iwata et al[22] and Okada[19]
undertook tests on concrete at an age of only 28 days.
This would explain the higher strengths recorded for the
older concrete, but does not indicate why the strength
change with reducing temperature has maximum and minimum
values at -50°C and -90°C, respectively. This is
clearly an area which requires further investigation.

2.5.2.2 Estimating cold strength

The relationship between flexural and compressive
strength is shown in Figure 2.13. Again there was a
considerable scatter of results making it difficult to

- 50 -

$$f_f = 0.1041 f_c + 6.5$$
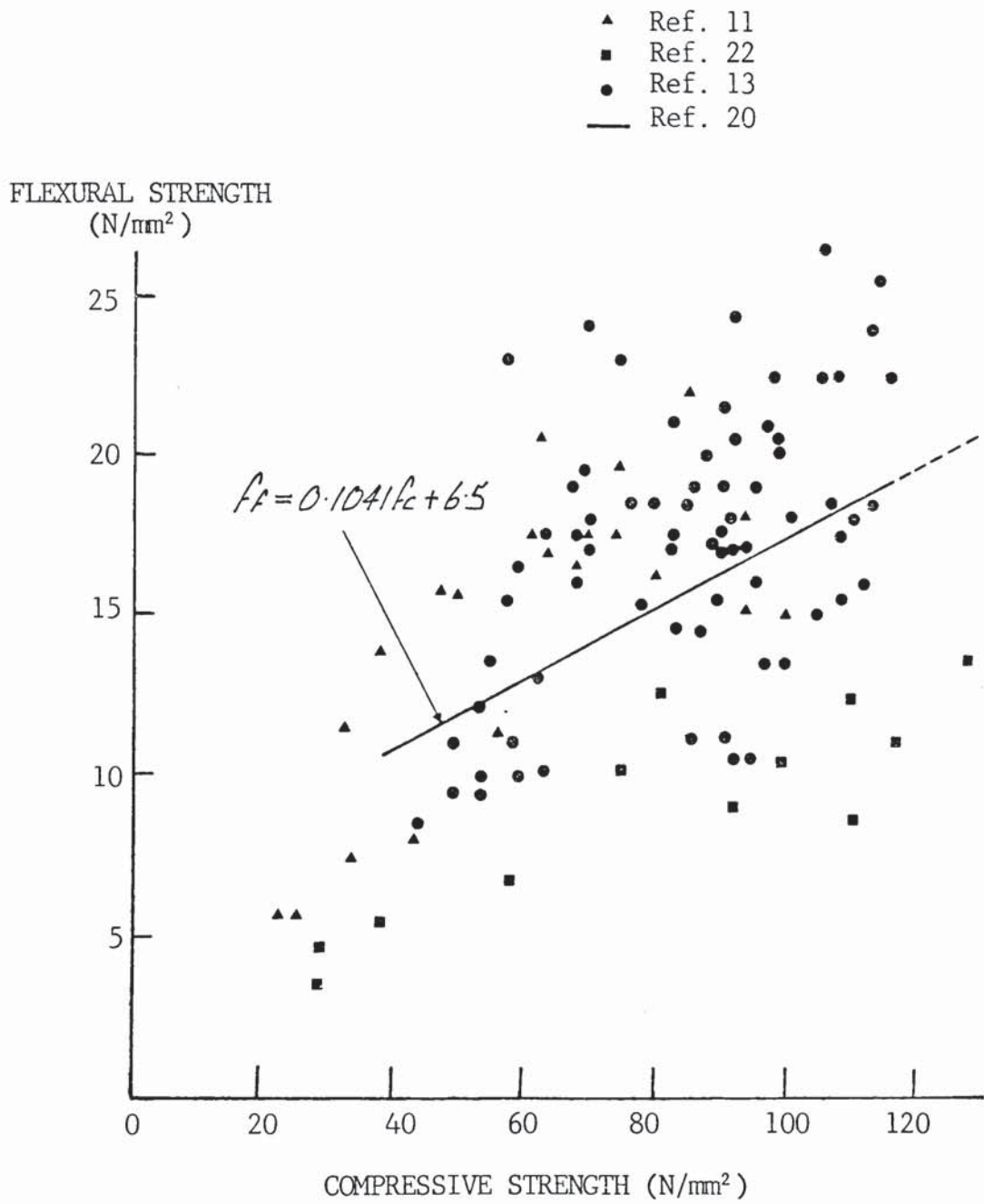
FIGURE 2.13. The relationship between flexural strength and compressive strength.

derive a general equation. However, Okada et al[19] have determined a linear relationship between flexural and compressive strength over the range -10°C to -100°C of the form.

$$f_f = 0.1041 f_c + 6.5 \qquad (2.8)$$

In view of the scatter of results this would appear to be a reasonable approximation for the data included in Figure 2.13.

2.6 THERMAL PROPERTIES

2.6.1 Thermal Expansion Coefficient

Of the strains induced in the wall or base of an LNG tank, by far the most significant are those resulting from changes in temperature. For example, during cooldown from 20°C to -165°C, the concrete may contract by as much as 1500 microstrain (this is equivalent to 90 mm movement for a 60 m diameter tank), compared with strains of the order of 300 microstrain due to a prestress of 10 N/mm². Further, if concrete contracts at a different rate to the reinforcing and prestressing steel, internal stresses and changes in prestress may occur during the cooldown process. It is therefore important that the thermal contraction of concrete is known with some degree of accuracy, in order to be able to design prestressed concrete tanks with predictable performance. Various factors which influence the thermal contraction of concrete have been investigated including constituent materials, mix proportions, curing regime and moisture content, age at test and rate of cooldown. However, whilst individual researchers have been able to observe the effects of these parameters, the variation between the results of the different workers has made it difficult to determine general trends in behaviour.

A summary of results from five sources is shown in Figure 2.14. Data obtained by Monfore and Lentz[15], Tognon[13] and Yamane [11] are generally in close agreement; the total
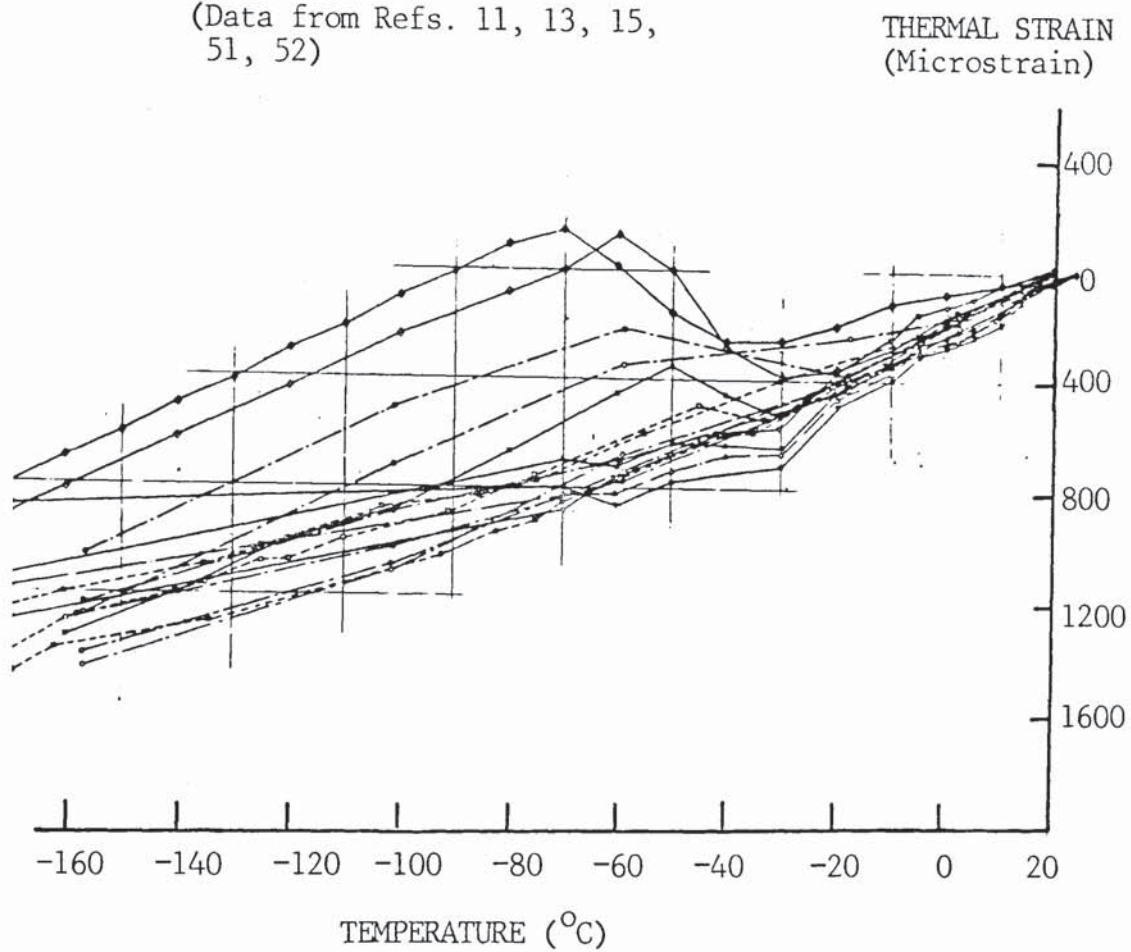
FIGURE 2.14. Temperature-strain relationships for concrete in the range 20°C to -165°C.

contraction measured over the range +20°C to -170°C was about 1300 ± 200 microstrain, i.e. a variation of ± 15% from the mean. These results covered a range of mix proportions and moisture contents. For example, Monfore and Lentz examined concretes with cement contents from 237 to 415 kg/m^3 and moisture contents from saturated to oven dried. Tognon also examined a range of moisture conditions but for one mix only, whilst Yamane et al examined a range of mix proportions (227 to 353 kg/m^3 cement content) under a single saturated moisture condition.

Data obtained by both Marachel[51] and Rostasy et al[52] indicated a significant difference in the thermal contraction of concrete, especially within the temperature range -30° to -70°C, when a nett expansion was observed in each case. This phenomenon was most prominent, as recorded by Rostasy, for water saturated concrete cooled at the rate of 60°C per hour. Rostasy also carried out tests using mortars and cement pastes and was able to identify the influence of moisture content in terms of both the initial w/c ratio and the pore water content. This is shown in Figure 2.15 for saturated and oven dried specimens with w/c ratios of 0.8, 0.5 and 0.3. It is clear that increasing the w/c ratio increased the extent of the discontinuity as did increasing the moisture content at test. This led Rostasy to conclude that the expansion was a result of ice formation in the finer pores accompanied by an internal pressure increase. It is interesting to note that for saturated specimens with the same w/c ratio, the thermal deformation was very similar for both mortar and concrete. This was so with the use of both OPC and blastfurnace slag cement, although in the latter case the expansion which occurred was 2- 3 times higher than recorded for OPC specimens. This was attributed by Rostasy to the larger proportion of finer pores measured for b.f.s. cement paste and hence, a larger proportion of evaporable water creating internal pressure when forming ice. Marachel[51], observing a similar expansion over the range -18° to -50°C, put forward a similar argument to explain this behaviour. In addition, he also identified that in concretes with a high cement content (500 kg/m^3) and a low w/c ratio (0.36), the expansion phenomenon did not occur despite curing at 98% R.H. He suggested

----- Ordinary Portland Cement
——— Slag Cement

1,2	Saturated Mortar, w/c = 0.8
3,5	Saturated Mortar, w/c = 0.5
4,6	Saturated Concrete, w/c = 0.5
7,10	Saturated Cement Paste, w/c = 0.3
8,9	Dry Mortar, w/c = 0.5

(From Ref. 52)
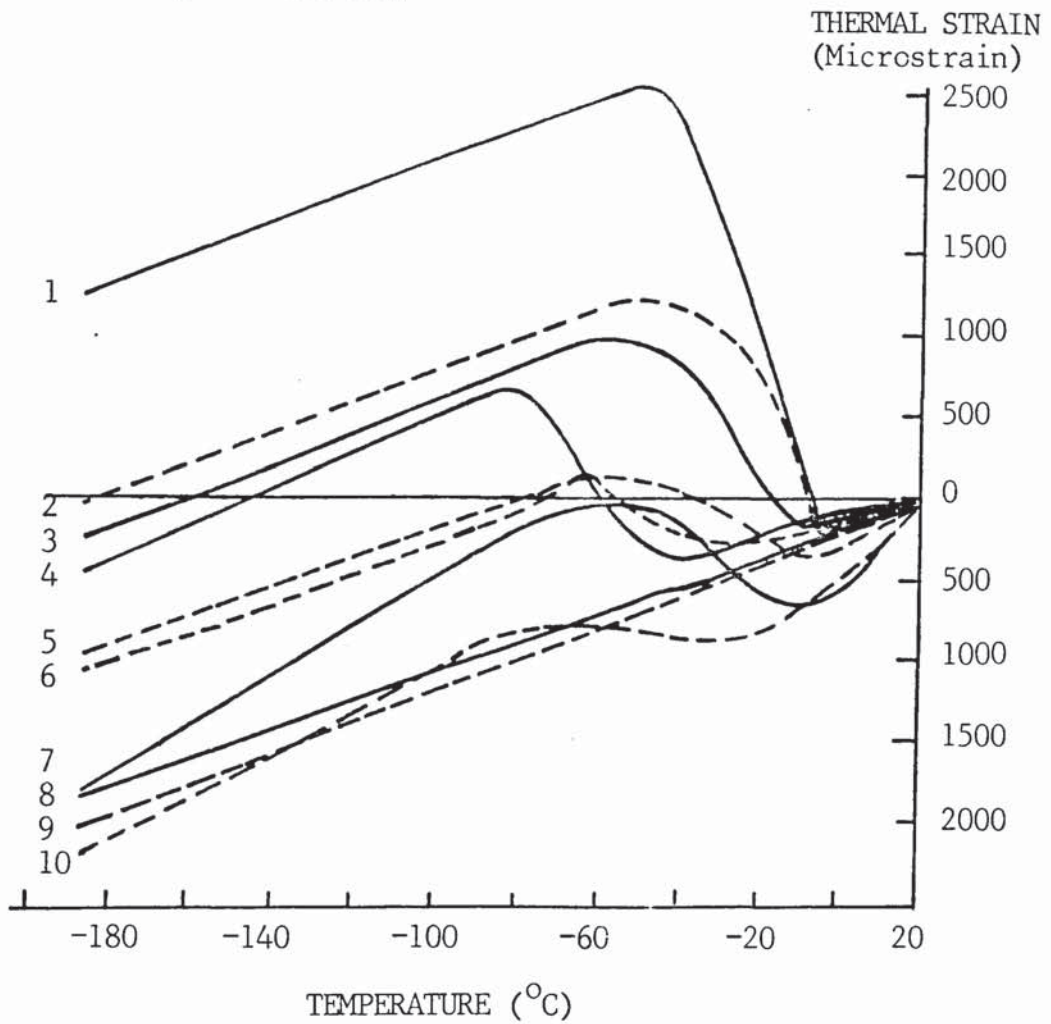
FIGURE 2.15. The influence of initial water/cement ratio and
moisture content on thermal contraction of cement
paste, mortars and concretes.

that this was due to the lack of evaporable water, the majority having been used for hydration. This may also have been due to the formation of a discontinuous capillary system as described by Powers[41], for concretes with a w/c less than 0.4. This would result in a very low permeability matrix preventing the ingress of atmospheric moisture in the curing environment to replace that used for hydration.

Having highlighted the influence of moisture content, reinspection of the results obtained by Monfore and Lentz[15], Tognon[13] and Yamane et al[11] indicated that similar behaviour had occurred but to a far lesser extent. For example, Tognon had recorded a nett expansion over the temperature range -35° to -45°C, but only of the order of 50 microstrain. The fundamental difference between those concretes exhibiting apparently uniform contraction and those with a discontinuity is therefore clearly attributable to the moisture content in relation to the void space in the concrete.

Concretes tested by Monfore and Lentz were air entrained, whilst Tognon generally examined air dried concrete with no air entrainment. Marachel and Rostasy both tested non air-entrained, moist concretes. This makes the findings of Marachel for low w/c concrete particularly relevant, indicating that the use of low w/c can be as effective as air entrainment for minimising freezing effects. This provides an alternative approach to the design of concrete for low temperature application.

The data for non air entrained concrete is important in confirming the influence of ice on the behaviour of concrete. In particular, it stresses the need to avoid internal pressure generated by the expansion of water to ice. The resulting expansion of concrete, which occurs between -20°C and -50°C, can be up to 800 microstrain; this would hardly be compatible with the contraction of about 400 microstrain for reinforcing and prestressing steel which would occur over the same temperature range.

2.6.2 Thermal Conductivity

It is unlikely that concrete will ever be used to provide heat insulation for an LNG tank, values of conductivity being some two orders of magnitude higher than those of typical insulating materials. However, the thermal conductivity is important in relation to the rate of thermal stress development during initial cooldown and any subsequent temperature excursions. A high conductivity concrete will enable steady state conditions to be established more rapidly and may reduce the magnitude of thermal gradients.

Measurements of thermal conductivity have been undertaken by Monfore and Lentz[53,54], Iwata et al[22] and Yoshiwa and Iwata[21]. By far the most comprehensive programme was carried out by Monfore and Lentz who examined a range of concrete mixes under three moisture conditions defined as moist, dried at 50% R.H. and oven dried. The results are shown in Figure 2.16. For moist concrete with dense aggregates, the thermal conductivity increased linearly with reducing temperature over the range +25° to -157°C by about 60%. Partially dry concrete exhibited a smaller increase, about 20% over the same range, and oven dried concrete was virtually unaffected by temperature. It was apparent, therefore, that the increase in thermal conductivity with reducing temperature was primarily a function of the ice in the system. Further tests by Monfore and Lentz on cement paste and aggregates led to the conclusion that the conductivity of concrete was primarily influenced by the conductivity of the aggregate at comparable moisture content and temperature, and that w/c and degree of hydration had virtually no effect.

Tests undertaken by Iwata et al[22] and Yoshiwa and Iwata[21] on moist and air dried concrete confirmed the influence of moisture content on conductivity. The data are also included in Figure 2.16. For moist concrete the increase in conductivity was less than recorded previously, being of the order of 30% over the range +40°C to -170°C. The results for air dried concrete were, however, in very close agreement with
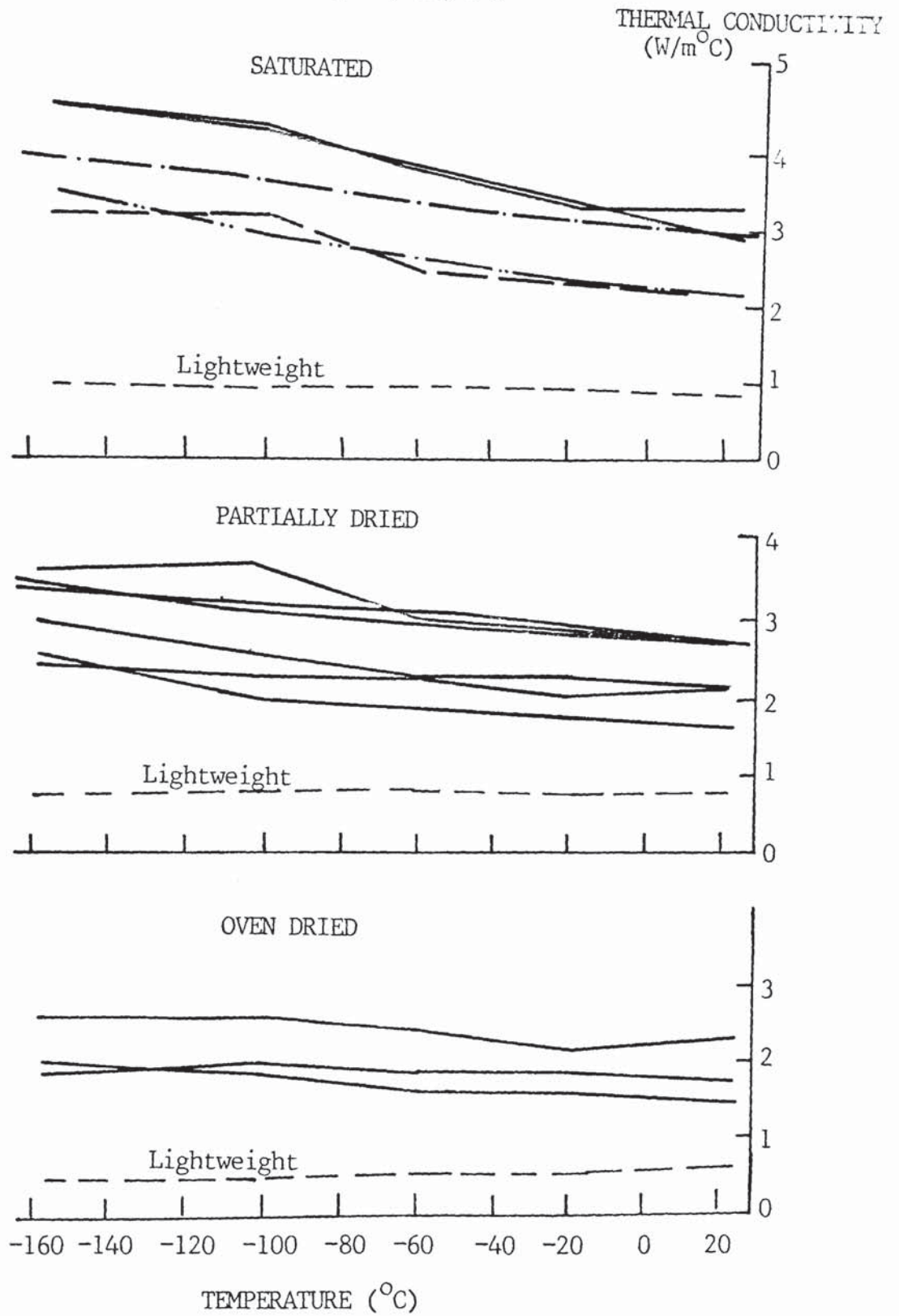
FIGURE 2.16. The influence of temperature on thermal conductivity.

the data of Monfore and Lentz for concrete dried at 50% R.H. and using a similar gravel aggregate.

Based on the limited data, an equation has been developed which relates the conductivity of the concrete K_θ at temperature θ, to the conductivity at room temperature, K_{20} and the moisture content of the concrete, m expressed as percentage by weight of concrete.

$$K_\theta = K_{20} \left(1 - \frac{0.63(\theta - 20)m}{1000} \right) \qquad (2.9)$$

It may be difficult to incorporate the changing conductivity into a transient heat flow calculation. However, when predicting thermal gradients, the worst case will generally occur when the conductivity is lowest. To achieve a conservative estimate of thermal gradients, it is therefore recommended that values used in the analysis be those recorded under ambient conditions.

Unlike normal dense aggregate concrete, lightweight concrete was found by Monfore and Lentz to be unaffected by temperature, regardless of its moisture content. The reason for this is not altogether clear but may be due to the fact that, even when fog cured, there is still an appreciable volume of air in the lightweight aggregate which would offset the influence of the changing state of ice during cooldown.

2.6.3 Specific Heat

Under steady state conditions, heat flow can be calculated directly from the thermal conductivity of the concrete. However, under transient conditions, knowledge of the variation of the specific heat of the concrete is required to enable thermal gradients to be established.

The only data identified relating to the specific heat of concrete was reported by Iwata et al[22]. The results are given in Figure 2.17. For both water cured and air dried concrete a reduction in specific heat of about 60% was recorded.
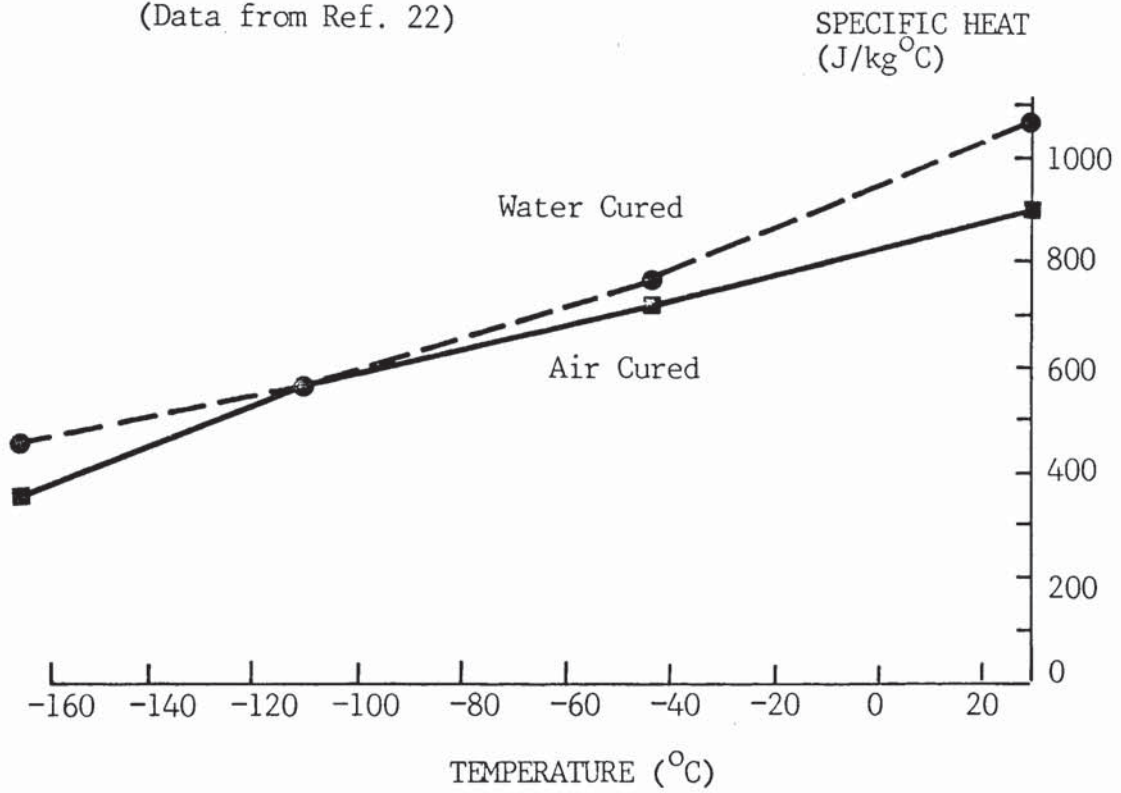
FIGURE 2.17. The influence of temperature on specific heat.

There was a small difference between the two concretes probably
due to the additional water in the moist specimen.

The influence of temperature in reducing specific heat is of
significance and should be taken into account when analysing
transient conditions. In the absence of more comprehensive data,
a relationship between the specific heat, S , and temperature θ ,
has been derived from the results of Iwata, of the form,

$$S_\theta = S_{20} \left(1 + \frac{0.31(\theta - 20)}{100} \right) \qquad (2.10)$$

The specific heat is not significantly affected by changes in mix
proportions and constituent materials and this relationship is
therefore likely to hold true for a range of concretes.

2.6.4 Thermal Diffusivity

The thermal diffusivity is used to calculate heat flow under
transient conditions and is related to the conductivity by the
equation:-

$$D_\theta = \frac{K_\theta}{S_\theta . \rho} \qquad (2.11)$$

where
K_θ is the thermal conductivity in W/m^{o}C
S_θ is the specific heat in J/kg^{o}C
ρ is the density in kg/m^3

It has been seen that whilst the conductivity increases with
reducing temperature, the specific heat reduces. This will
therefore, have a compound effect on diffusivity. Substituting
for K_θ and S_θ in equation 2.11, this now becomes

$$D_\theta = \frac{K_{20} \left(1 - \frac{0.63(\theta-20)m}{1000} \right)}{S_{20} \left(1 + \frac{0.31(\theta-20)}{100} \right)} . \frac{1}{\rho}$$

but $\dfrac{K_{20}}{\rho . S_{20}} = D_{20}$

$$\therefore \quad \frac{D_\theta}{D_{20}} = \frac{\left(1 - \frac{0.63(\theta-20)m}{1000} \right)}{\left(1 + \frac{0.31(\theta-20)}{100} \right)} \qquad (2.12)$$

Moisture Content

DIFFUSIVITY AT TEMP θ
────────────────────
DIFFUSIVITY AT 20°C
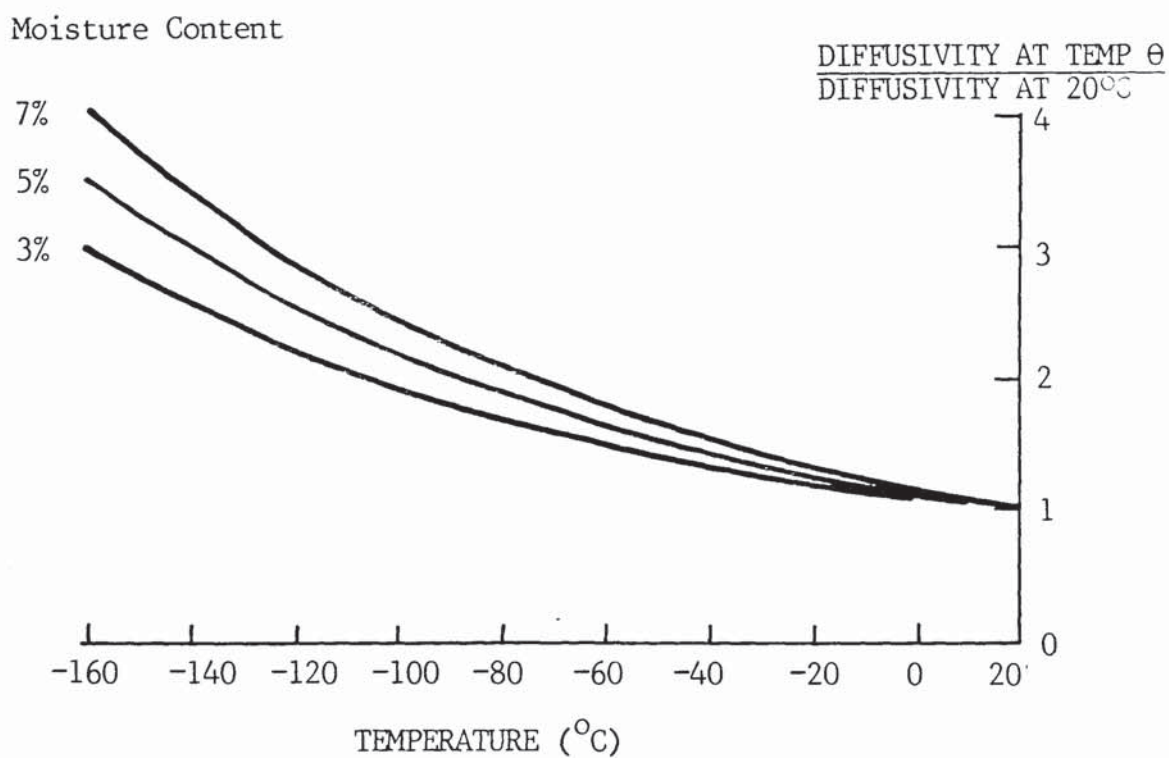
FIGURE 2.18. The change in thermal diffusivity with temperature
derived from reported changes in thermal conducti-
vity and specific heat.

This relationship between   and temperature   is illustrated
in Figure 2.18, for concrete with moisture contents of 3, 5 and
7%. It can be seen that at -160°C, the diffusivity can be 3 to
4 times the value at 20°C. This should certainly be taken into
account when predicting the development of thermal gradients.

2.7 ELASTIC MODULUS

2.7.1 Effect of Temperature

Values of elastic modulus have been measured by Monfore and Lentz
[15], Yamane et al[11], Marachel[55], Okada and Iguro
[20], Wozniak et al[56] and Iwata et al[22]. In each
case, there was found to be a general tendency for the modulus of
moist concrete to increase with reducing temperature, as shown in
Figure 2.19. However, unlike the strength characteristics which
resulted in typical increases of up to 200%, the influence of
temperature on elastic modulus was much less significant.
Recorded increases were generally of the order of 50%, the
majority of which occurred within the temperature range -20°C to
-120°C. The increase in modulus at temperatures below -120°C was
small. The influence of temperature within the range +20°C to
-20°C was erratic with changes in modulus varying from 20%,
recorded by Monfore and Lentz[15], to -24% recorded by Yamane
et al[11]. The reason for this is not clear. No change would
be expected within the range 20°C to 0°C and assuming the modulus
to be related to strength, an increase would have been expected
from 0°C to -20°C.

Untypical behaviour was also recorded for concretes examined by
Marachel[55] and Yamane[11] which exhibited peak values
at -50°C. In the latter case, this was recorded for only one of
four mixes examined. Marachel attributed this to changes in
internal stresses due to the expansion of progressive ice
formation in the finer pores over the temperature range -18°C to
-50°C. This behaviour was similar to the variation in flexural
strength with temperature recorded by Tognon[13] and Yamane
et al[11] and it is interesting to note that the test
specimens were in each case cured for periods of the order of 6

(Data from Refs. 11, 15, 20, 22, 55, 56)

ELASTIC MODULUS (kN/mm²)
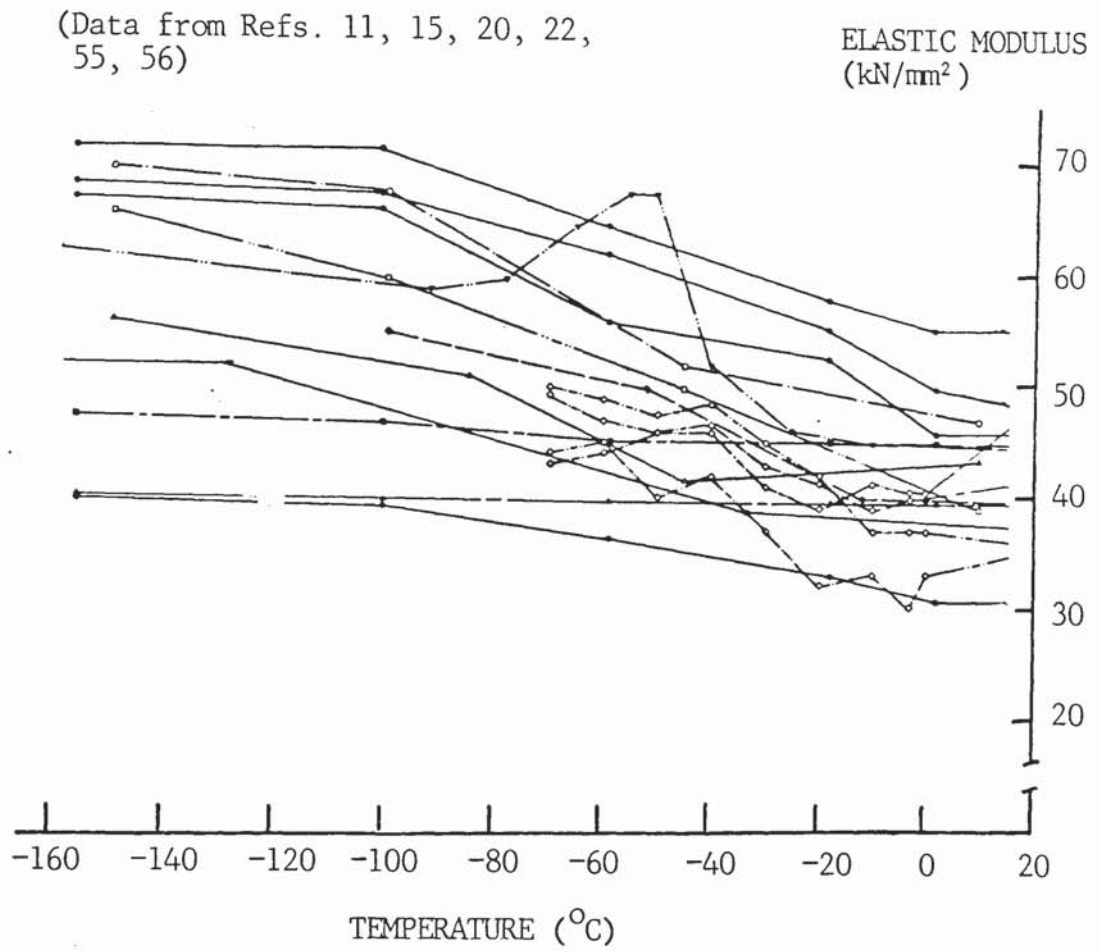
FIGURE 2.19. The influence of temperature on elastic modulus.

months prior to testing. In all other cases, specimens were cured for a maximum period of 28 days after which time they were either tested immediately or stored in air or sealed containers prior to testing at a later date.

On the basis of the flexural strength results, it was considered that the age of the concrete at test defined its behaviour at low temperature. In the light of the additional modulus results, it now seems clear that it is not simply the age of the concrete but the duration of fog or water curing which is the important factor. The mechanism suggested by Marachel to explain the peak values at -50°C (i.e. ice formation in the finer pores) would be most effective in a moist concrete which has a high proportion of finer pores. This will be the case for well cured concretes in which the hydration of the cement has proceeded to a greater extent.

The influence of moisture has been recorded by both Monfore and Lentz[15], for concretes dried at 50% relative humidity and oven dried, and Iwata et al[22] for air dried concrete. For oven dried concrete there appeared to be no increase in modulus with reduced temperature[15]. The behaviour of air dried concrete was inconsistent, with recorded increases in modulus from only 7% to as high as 93%. The latter value was not typical however, being in excess of values recorded for moist concrete.

2.7.2 Estimating Elastic Modulus

The relationship between elastic modulus and compressive strength is shown in Figure 2.20. Whilst the results are generally scattered, the data obtained from the individual test programmes indicate a linear relationship between modulus and strength. An equation relating the modulus , E, and compressive cylinder strength , f_c, has been derived by Okada and Iguro[20] over the range -10°C to -100°C, of the form

$$E = 0.3 f_c + 13.6 \quad kN/mm^2 \qquad (2.13)$$

To relate E to cube strength the equation becomes,
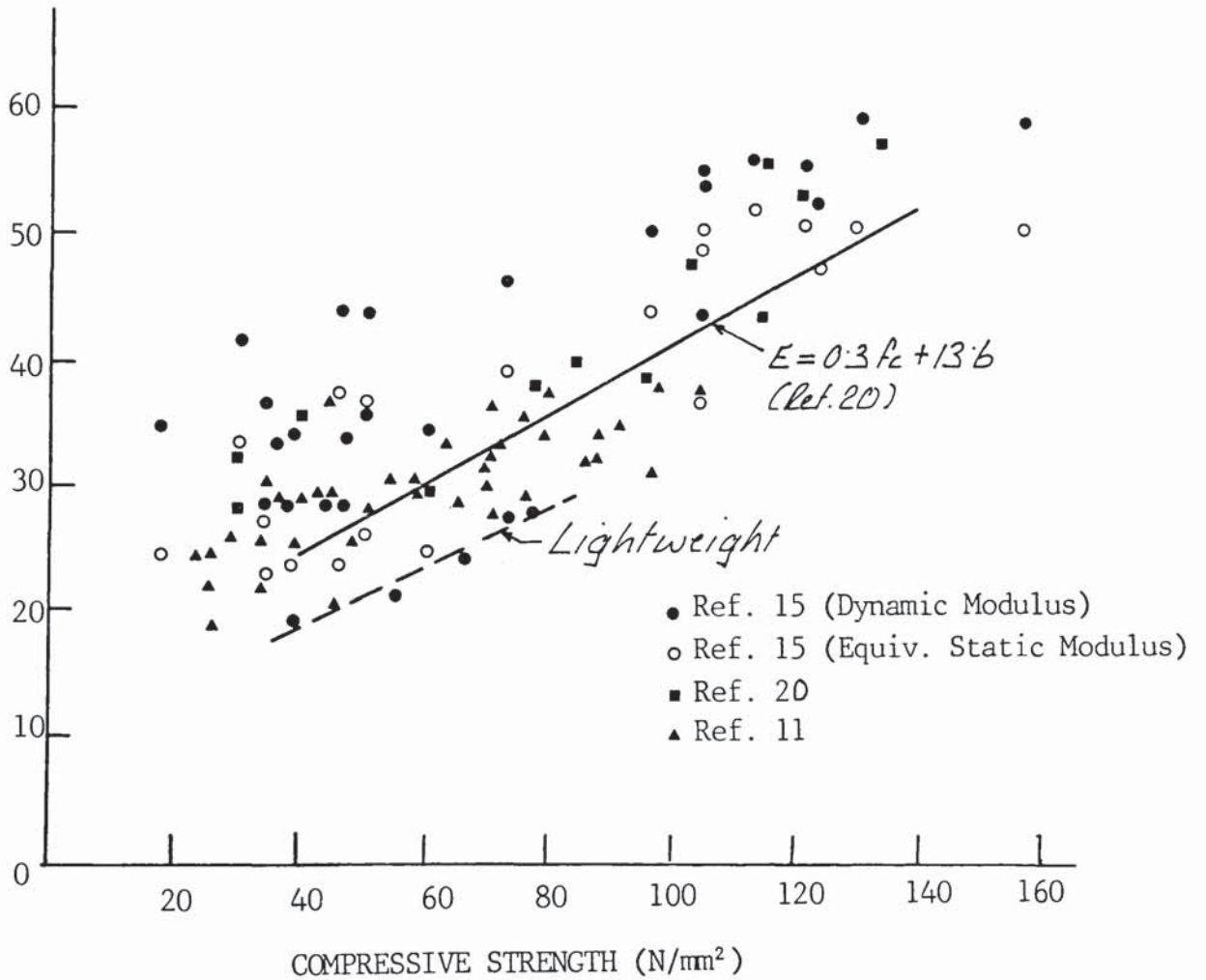
FIGURE 2.20. The relationship between elastic modulus and compressive strength at temperatures down to -165°C.

$$E = 0.24 f_c + 13.6 \quad \text{kN/mm}^2 \tag{2.14}$$

This equation does not initially appear to represent data from other sources. For example, Monfore and Lentz [15] recorded values of modulus which were 10 - 15 kN/mm² higher than reported by Okada for a given compressive strength, whilst results obtained by Yamane et al[11] and Iwata et al[22] were in relatively close agreement. The difference can be attributed however, to the different methods of testing employed. Monfore and Lentz measured the dynamic modulus using the resonance frequency method whilst the other researchers determined Youngs Modulus by stress-strain measurement. According to the British Code for Concrete CP 110, 1972[57] the values of moduli can be related by the equation,

$$E_s = 1.25 E_D - 19 \tag{2.15}$$

Where E_s and E_D are expressed in kN/mm². Adjusting the data of Monfore and Lentz using this equation brings the values of elasticity into much closer agreement with the results obtained using the static test. It is therefore recommended that equation (2.14) be used for the determination of elastic modulus.

2.8 BOND STRENGTH TO REINFORCEMENT

The bond strength of both plain and deformed reinforcement to concrete has been measured by Yamane et al[11] using bars mounted horizontally in 150 mm cubes. The influence of temperature for water cured concretes is shown in Figure 2.21. Tests were generally undertaken down to a temperature of -70°C and over this range, a gradual increase in bond strength was observed. For deformed bars, the bond strength was increased by about 100% from a typical value at 20°C of 8 N/mm². For plain round bars, the proportional increase in bond was significantly higher, up to 400% in the case of concretes with higher levels of air entrainment and w/c ratio. Yamane et al attributed the improved performance of air entrained concrete to the reduced bleed characteristics and hence, the smaller amount of water under the horizontally embedded steel. This effect was not observed for deformed bars which tend to rely largely on mechanical bond rather

- 67 -

Ref. 11 ·
○ ▲ ▼ ▢   WET D. 16mm BARS
● ▲ ▼ ■ ◆   WET Ø 19mm BARS
◇   AIR DRY Ø 19mm BARS
Ref. 17
×

BOND STRENGTH
(N/mm²)
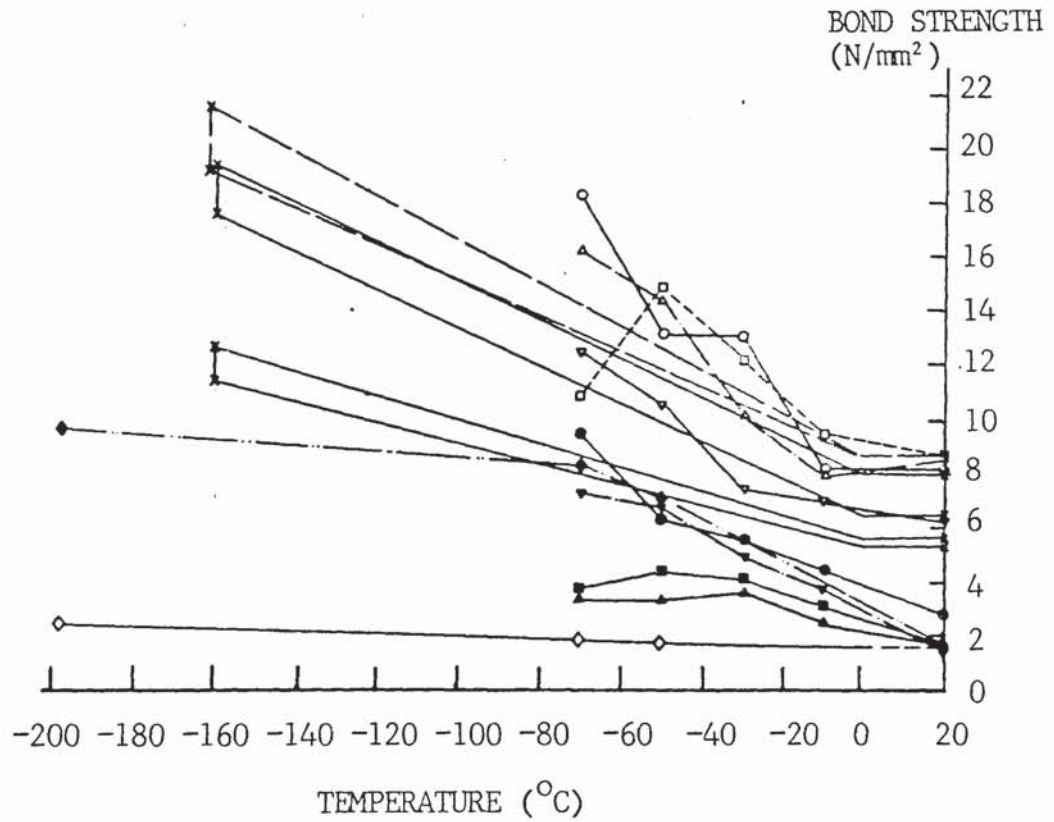
TEMPERATURE (°C)

FIGURE 2.21.   The influence of temperature on bond strength of
concrete to reinforcement.

MIX No	1	2	3	4
DEFORMED BARS	o	▽	△	□
PLAIN BARS	●	▼	▲	■
MOIST CONCRETE		⊙		
AIR DRIED CONCRETE		◇		

(From Ref. 11)
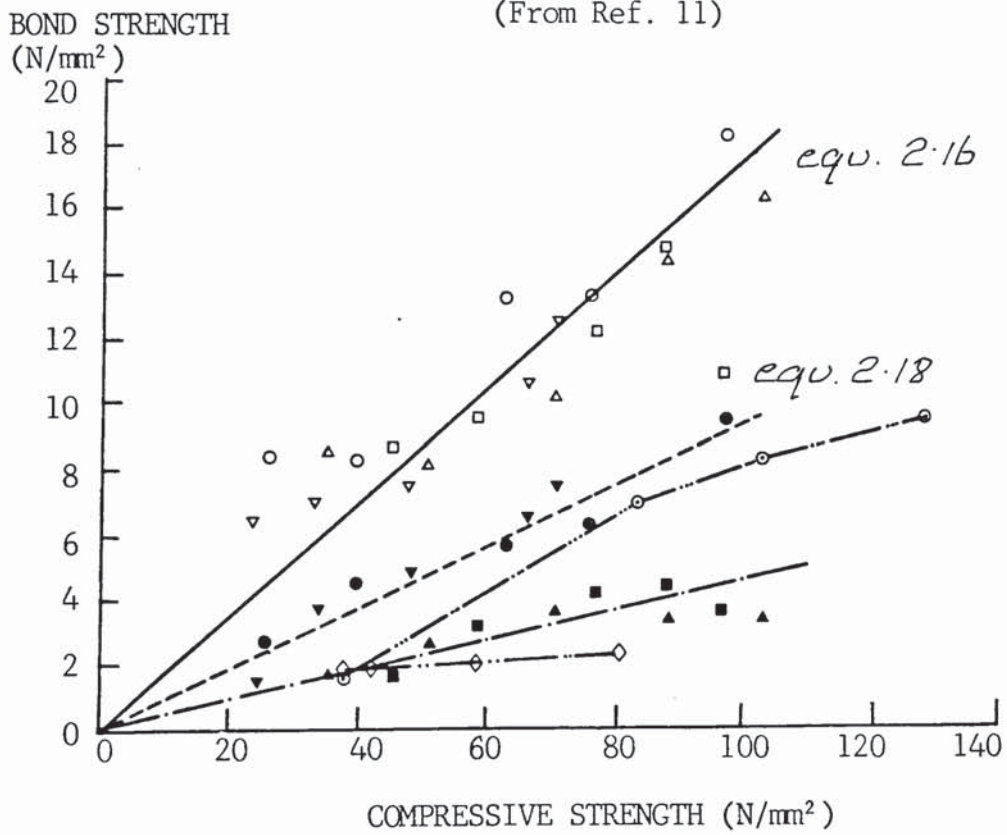
FIGURE 2.22. The relationship between bond strength and compressive strength.

than adhesion. These results apply to water cured moist concrete. Additional data recorded by Yamane et al showed that, for air dried concrete with a low moisture content, the increase in bond was considerably lower for plain round bars. No tests were undertaken to determine the influence of moisture content using deformed bars, but a similar effect could be expected. The results obtained by Yamane[11] have been confirmed by Goto and Miura[17], who also recorded increases in bond strength in excess of 100% at a temperature of -160°C. These results are also shown in Figure 2.21.

The relationship between bond strength and compressive strength is shown in Figure 2.22. For deformed bars, the bond strength f_b was found to be proportional to compressive strength f_c and related by the equation:-

$$f_b = 0.177 f_c \tag{2.16}$$

This applies to moist concrete and is independent of concrete mix proportions, air content, etc. The compressive strengths were however measured using 2:1 cylinders, and equation 2.16 must therefore be adjusted if bond strength is to be based on the B.S. cube using the factor f_c (cylinder) x 1.25 = f_c. (cube). Hence equation 2.16 becomes

$$f_b = 0.142 f_c \tag{2.17}$$

The equivalent relationship for plain round bars in moist concrete appears to be dependent on mix proportions and air content, as described previously. For a cohesive concrete with low bleed characteristics (i.e. assuming uniform bond around the bar), the bond strength can be defined by the equation

$$f_b = 0.095 f_c \text{(cylinder)} \tag{2.18}$$

or

$$f_b = 0.076 f_c \text{(cube)} \tag{2.19}$$

There is insufficient data to adequately describe the influence of moisture content on bond, although it is clear that for plain round

bars, there is a smaller increase in bond strength at low temperature
when the moisture content of the concrete is low.

2.9 INFLUENCE OF THERMAL CYCLING

Under normal service conditions a storage tank for LNG would not be
subject to freeze thaw cycles. Once the tank is cooled down and put
into service, it would not be expected to return to above freezing
unless taken out of service for maintenance or inspection. The most
severe cyclic conditions is likely to be one in which the temperature
at the top of a tank, which is being continually filled and emptied
(e.g. at a receiving terminal), will fluctuate in the range -162°C to
perhaps -90°C. Tests have, however, been undertaken to establish the
effects of freeze thaw cycling and observe the performance of concrete
under these particularly arduous conditions.

2.9.1 Compressive Strength

The compressive strength of concretes subjected to up to 12 cold
cycles within the temperature range +20°C to -196°C have been
measured by Tognon[13], Iwata et al[22], Rostasy et
al[52] and Yamane et al[11]. A summary of the results is
shown in Figure 2.23 which illustrates the residual strength in
terms of the percentage of the strength at 20°C against number
of cold cycles. It will be seen that the influence of cycling
varied considerably. At one extreme the strength was found to
increase even after ten cycles, whilst at the other extreme the
strength was reduced by 70% after only four cycles. Inspection
of the mixes tested and the experimental conditions indicated
that three factors were of prime importance in relation to the
freeze thaw resistance of concrete, the strength being most
adversely affected for the following conditions:-

i)   High moisture content of the concrete
ii) Low air content of the concrete
iii) High rate of cooldown

In general, concretes cured in moist conditions, i.e. underwater
or at 100% R.H., are most severely affected by freeze thaw

- 71 -

Ref. 13	⊙	POZ CEMENT
	⊡	O.P.C.
Ref. 22	▲	
	△	
	●	
	○	
Ref. 16	■	O.P.C./ SLAG
	□	O.P.C./ SLAG
	◆	O.P.C. MORTAR
	◇	SLAG CEMENT MORTAR
Ref. 11	▼	

PERCENT OF STRENGTH
BEFORE THERMAL CYCLING

N - LOW AIR CONTENT
R - RAPID COOLDOWN
W - HIGH MOISTURE CONTENT

NUMBER OF CYCLES
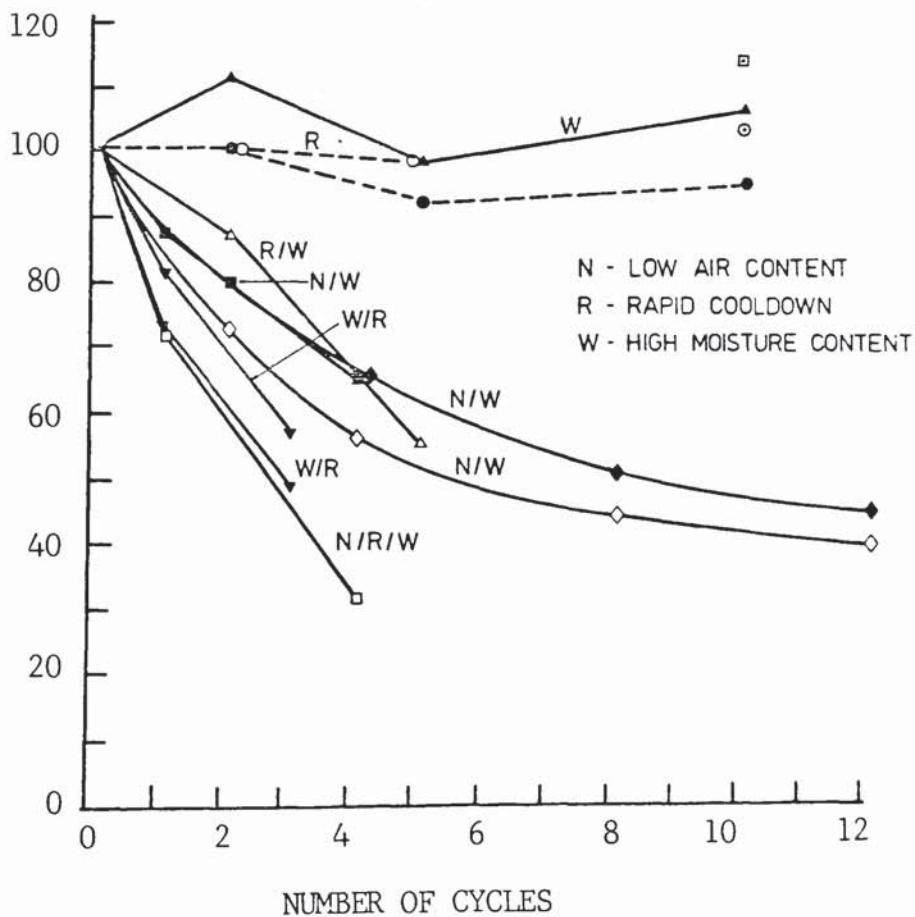
FIGURE 2.23. The influence of thermal cycling in the range 20°C
to −196°C on compressive strength.

cycling due to their high moisture content and the fatigue effects of the expansion and contraction of ice. However, for the most severely damaged concretes, the high moisture content was associated with either a rapid rate of cooldown, a lack of air entrainment or a combination of both. At moderate rates of cooling (e.g. 10°C per hour) and with sufficient air entrainment (e.g. 3% minimum), cold cycling need not have an adverse effect even after 10 cycles[22].

Similarly, rapid cooldown (i.e. immersion in liquid nitrogen at -196°C) may not adversely affect the strength if the concrete is air entrained and has a low moisture content[22], although data for this condition is only available for up to 5 cycles. Also concretes with no air entrainment may not be damaged if the moisture content and rate of cooling are low[13].

Iwata et al[22], testing water cured concrete cooled instantaneously to -196°C, recorded a strength reduction of 45% after only 5 cycles. A similar reduction was recorded by Rostasy et al [52] for water cured concretes and mortars with no air entrainment and cooled at a rate of 60°C per hour; Yamane et al (11) recorded a 50% reduction after only 3 cycles for air-entrained, moist concrete cooled instantaneously to -196°C. The most severe damage was recorded by Rostasy et al for non air-entrained, moist concrete cooled rapidly to -196°C, with the strength being reduced by 70% after only 4 cycles.

It would therefore appear that for serious damage to result from cold cycling, two of the three conditions described above must be met.

2.9.2 Tensile Strength

The tensile and flexural strength of concretes subjected to up to 10 cold cycles within the range +20°C to -196°C have been measured by Tognon[13], Iwata et al[22] and Rostasy et al[52]. A summary of the results is shown in Figure 2.24 which illustrates the residual tensile strength in terms of the percentage of the strength at 20°C against the number of cold

Ref. 13	⊙ POZ CEMENT
	▫ O P.C
Ref. 22	▲
	△
	●
	○
Ref. 16	■ O.P.C./ SLAG
	□ O.P.C./ SLAG
	◆ MORTAR
	◇ SLAG CEMENT MORTAR

PERCENT OF STRENGTH
BEFORE THERMAL CYCLING

N - LOW AIR CONTENT
W - HIGH MOISTURE CONTENT
R - RAPID COOLDOWN

NUMBER OF CYCLES
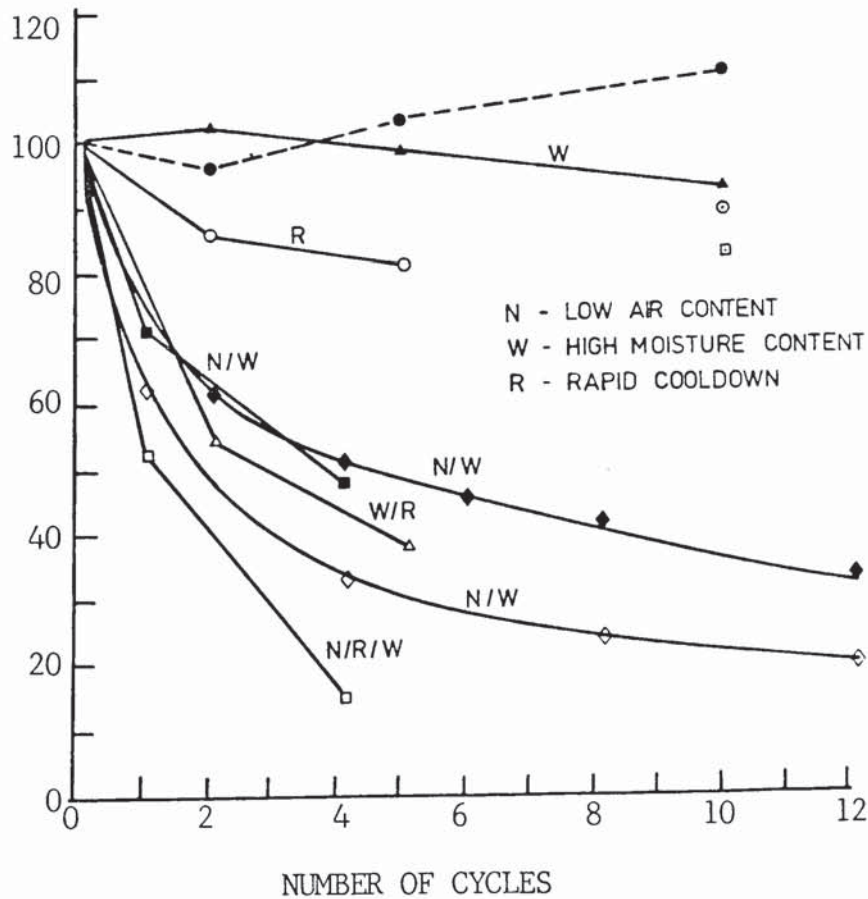
FIGURE 2.24. The influence of thermal cycling in the range $20^{\circ}C$ to $-196^{\circ}C$ on tensile splitting strength.

cycles. Again, a considerable variation in results was obtained varying from a flexural strength increase of 10% after 10 cycles to a reduction in tensile splitting strength of 85% after only 4 cycles. The factors which influenced the degree of strength loss were similar to those identified from compressive strength data, although, where damage was observed, the extent of the tensile strength loss was greater. For example, in the most extreme case of rapid cooldown for a non air-entrained moist concrete, the tensile strength was reduced by 85% after 4 cycles compared with a 70% reduction in compressive strength.

2.9.3 Thermal Contraction

Hysteresis curves for concretes and mortars subjected to cooling and warming cycles have been measured by Tognon[13] and Rostasy et al[52]. A summary of the results is given in Figure 2.25. For fog-cured mortars cycled between +20°C and -150°C, Tognon observed a residual expansion of 340 microstrain after 3 cycles. For fog cured mortars between +20° and -55°C, the residual strain increased linearly to a value of 340 microstrain after 5 cycles.

Storing concrete at 90% R.H. reduced the residual expansion to less than 50 microstrain after 3 cycles and oven drying eliminated the hysteresis effect altogether. These were for short term tests, however. For concretes cured at 85% R.H. and subjected to 10 cycles in the range +20° to -196°C over a period of 1 year, the residual strain was of the order of 150 microstrain contraction. However, some drying of the specimens would have occurred during this period (for non-cycled specimens stored at 20°C at 85% R.H. this was found to be about 300 microstrain). The cycled specimens when compared with drying control specimens, therefore, indicate a potential residual expansion. The magnitude of the residual expansion cannot, however, be determined precisely as the rate of drying will have been influenced by the thermal cycling.

Tests undertaken by Rostasy[52] indicated a considerably greater hysteresis effect, although the results were obtained for

- 75 -

RESIDUAL STRAIN
(Microstrain)
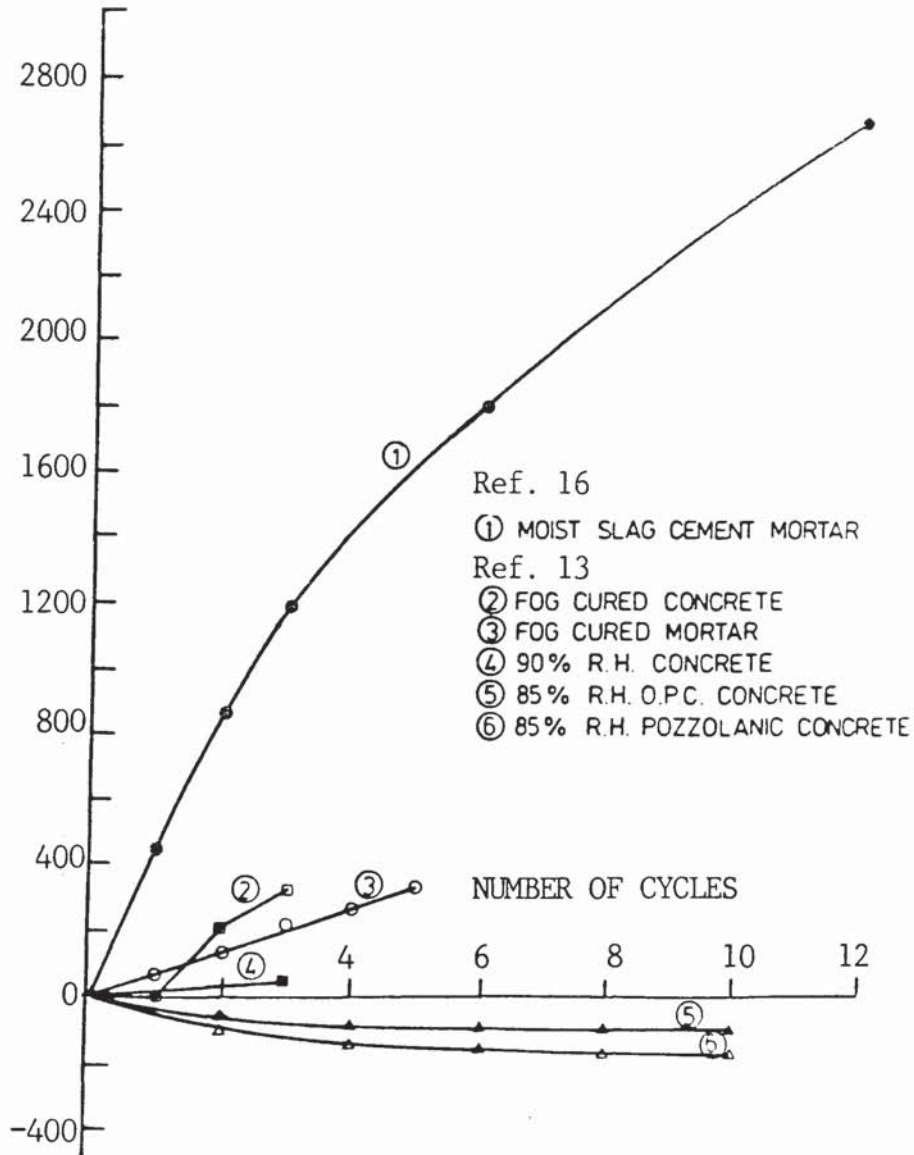
FIGURE 2.25. The residual strain after thermal cycling between
20°C and -196°C.

a moist mortar using blastfurnace slag cement and cooled at a
rate of 150°C per hour. The residual expansion was of the
order of 1600 microstrain after 5 cycles and 2700 microstrain
after 12 cycles. The reason for the considerable difference in
the results compared with those of Tognon is not altogether
clear. Both mortars have high moisture contents and neither are
reported as having air entrainment. The mortar tested by Rostasy
did contain blastfurnace slag cement which was shown to have a
higher proportion of finer pores than OPC paste and hence, be
more susceptible to internal bursting stresses during cooldown.
It is unlikely, however, that this factor alone would cause such
dissimilar behaviour. The more rapid rate of cooldown used by
Rostasy (150°C per hour) may have been an additional
contributory factor. This was certainly significant in relation
to the strength loss after cold cycling. Without additional
data, however, it is impossible to define the precise cause.

2.9.4 General Discussion

Three prime factors have been identified as affecting the
residual properties of concrete after thermal cycling. These
are:-

i)   Moisture content of the concrete
ii) Air content of the concrete
iii) Rate of cooldown.

In primary containments for LNG, the rate of cooldown will be
controlled and air entrainment will most certainly be used in the
light of existing results. The third factor, moisture content,
is less easily controlled. In a thick section, say 500mm, drying
will take some considerable time and the moisture content of
structural concrete is likely to be relatively high. However, it
is unlikely that the concrete will be saturated.

In any event, it is improbable that the concrete will ever be
subjected to cold cycling to the extent examined (i.e. +20°C
to -196°), a more probable cycle being in the range -162°C to
-90°C as discussed previously. Cycling in this range would not

be expected to cause the same extent of damage. Rostasy has
investigated the extent of cold cycling down to temperatures of
-30°C, -70°C and -170°C. The strength loss resulting from
12 cycles between +20°C and -170°C was no worse than that
which occurred for 12 cycles between +20° and -70°C, as shown
in Figure 2.26. This indicates that the disruptive forces
resulting from ice formation occur at temperatures down to
-70°C but are no worse at lower temperatures. Varying the
temperatures within the range -70° to -162°C is, therefore,
unlikely to cause additional disruption. To support this
argument, Tognon, whilst not presenting specific results,
observed that for cooling and warming between -50° and -90°C,
no hysteresis effect occurred.
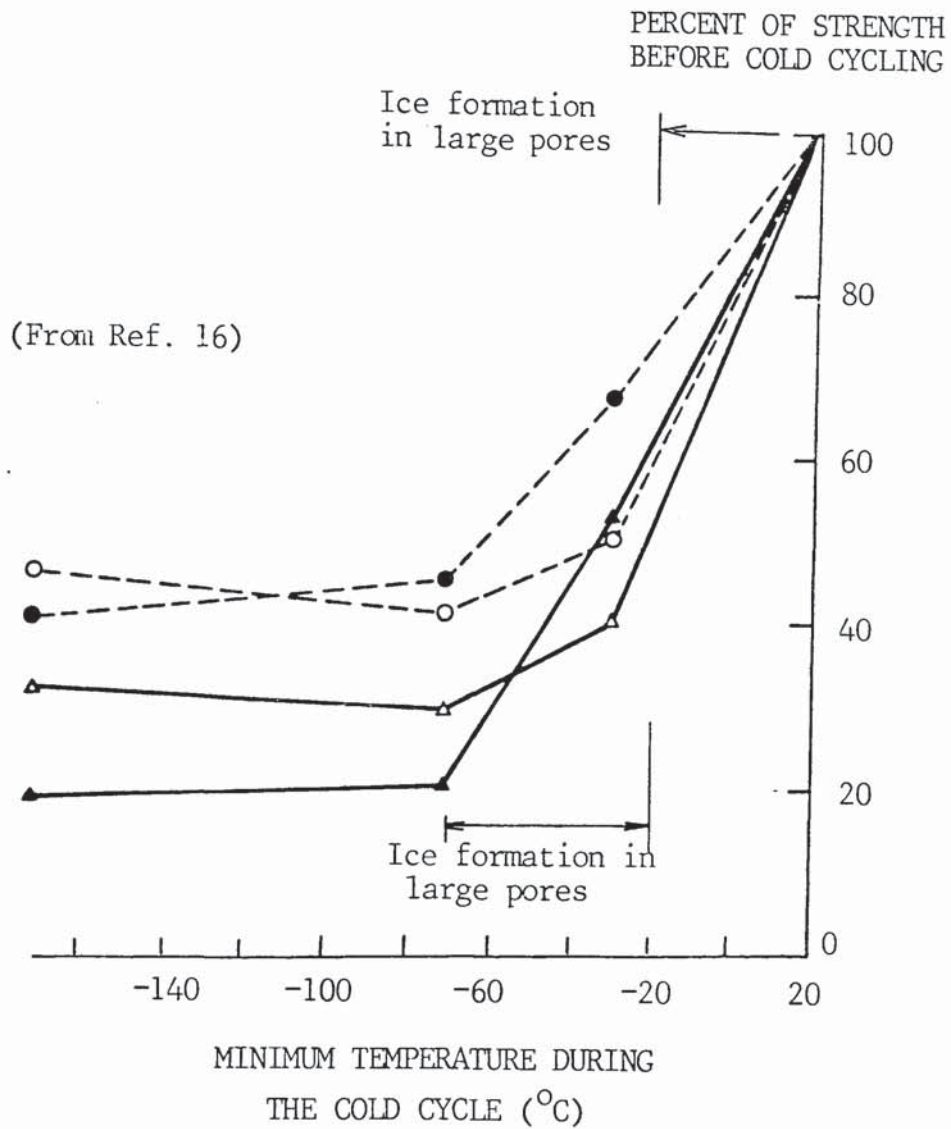
FIGURE 2.26. The influence of temperature range on residual
strength after 12 thermal cycles.

3.   SCREENING TEST PROGRAMME

3.1 SELECTION OF CONCRETE MIX PARAMETERS

Concretes for study in the screening test programme were not selected soley on the basis of proven or expected good performance at cryogenic temperatures. Other properties, which have been shown to influence construction and subsequent performance under normal environmental conditions, were also considered.

3.1.1 Strength Grade

It has been demonstrated that concretes with low water-cement ratio (w/c) are less likely to be disrupted by ice formation during cooldown[52]. Also, low w/c concretes have been shown to exhibit low permeability, particularly at values of w/c below about 0.4 (see Section 2.4.1). Six mixes were designed to encompass a wide strength range. These have been designated mixes S1 to S6 (See Table 3.1) and include typical structural concretes with values of w/c in the range 0.4 to 0.55, as well as mixes with very high (0.84) and very low (0.32) w/c ratios. The latter was achieved by the use of a superplasticiser to reduce the water demand.

3.1.2 Air Entrainment

The use of air entraining agents (AEA) is common in concretes which are to be exposed to freeze-thaw conditions. AEA's have also been shown to provide resistance to degradation under conditions of extreme thermal cycling to cryogenic temperatures (see Section 2.8.6). The use of an AEA has therefore been included in the screening test programme. Three doseage levels were used, $x\frac{1}{2}$, standard and x2. The mixes have been designated AE1 to AE3.

3.1.3 Aggregate Type

During cooldown, disruption may occur not only due to the formation of ice, but also due to the differential thermal

contraction of the aggregate and cement paste. Studies of strength loss resulting from exposure to elevated temperature have identified that the extent to which damage occurs is a function of both modulus of elasticity, $\mathcal{E}_a$, and thermal expansion coefficient, α_a, of the aggregate. In general aggregates have a much lower thermal expansion coefficient than cement paste, and a much higher modulus of elasticity. Hence the magnitude of thermal stress developed is a function of $\dfrac{\alpha_c}{\alpha_a} \cdot \dfrac{\mathcal{E}_a}{\mathcal{E}_c}$.

Three aggregates have been selected for screening tests, a gravel, a crushed dolerite, and a lightweight aggregate (sintered PFA). These provide a range of values of both modulus and thermal expansion coefficient[58]. The two crushed dolerite mixes have been designated A1 and A2 and the two lightweight mixes A3 and A4. The gravel mixes are S1 and AE2, from 3.1.1 and 3.1.2 above.

3.1.4 Cement Type

The use of pulverised fuel ash (PFA) and ground granulated blastfurnace slag (GGBS) is becoming increasingly common in large civil engineering structures[59]. In addition to providing economies in materials costs, a number of technical benefits can also be achieved. These include:

i) improved placing characteristics i.e. better flow, improved pumpability, easier compaction,

ii) delayed setting time, minimising the occurrence of cold joints in large pours,

iii) reduced heat of hydration, reducing the risk of thermal cracking during the early age heat cycle,

iv) enhanced in-situ strength in the long term,

v) reduced permeability if properly cured.

Concretes containing either PFA or GGBS to partially replace OPC have therefore been investigated. The two PFA mixes have been designated C1 and C2, the two GGBS mixes, C3 and C4.

3.2 CONCRETE MIX DETAILS

Based on the above criteria, a total of 17 No. concrete mixes were selected. Two control mixes were designed to achieve a grade 35N concrete, using OPC and gravel aggregate, one containing a standard dose of air entraining agent. General details of the 17 No. mixes are given in Table 3.1. Specific mix proportions are given in Table 3.2.

3.3 EXPERIMENTAL DETAILS

The following tests were carried out in order to rank the performance of the 17 No. concretes investigated.

1) Cube crushing strength at 20°C, at -165°C and after thermal cycling in the range 20 to -165 to 20°C.

2) Tensile splitting strength at 20°C, at -165°C and after thermal cycling in the range 20 to -165 to -20°C.

3) Water permeability at 20°C.

3.3.1 Manufacture of Test Specimens

Each mix comprised 14 No. 100mm cubes for strength measurement and 2 No. cylindrical specimens, 100mm diameter by 50mm thick, for the measurement of water permeability. Batching, mixing and casting the specimens were carried out in general accordance with BS 1881. However, the method of curing was modified to be more representative of that which occurs insitu. Instead of storing the specimens underwater at 20°C, as specified in BS 1881[50], the specimens were sealed in plastic bags immediately after being stripped from their moulds at an age of 24 hours. The sealed bags were then stored in a constant temperature room at 20°C until the specimens were removed for testing. This method of 'sealed' curing simulates the condition in which the only water available for curing is that which is introduced at the mixing stage, this being the condition that exists in the bulk of a thick structural member.

MIX NO.	DESCRIPTION	STRENGTH GRADE	AIR ENTRAINMENT	AGGREGATE TYPE	CEMENT TYPE
	STRENGTH GRADE				
S1	Non air entrained control	35	–	Gravel	OPC
S2	Low grade, with reduced cement content	10	–	Gravel	OPC
S3	High grade, with increased cement content	50	–	Gravel	OPC
S4	High grave, as S1, with reduced w/c using SP	50	–	Gravel	OPC
S5	Very high grade, with increased cement and reduced w/c	85	–	Gravel	OPC
S6	Very high grade, with increased cement and reduced w/c	85	–	Gravel	OPC
	AIR CONTENT (Control Mix S1)				
AE1	½ x Std dose AEA and modified mix to maintain strength	35	½ x Std dose	Gravel	OPC
AE2	1 x Std dose AEA and modified mix to maintain strength	35	1 x Std dose	Gravel	OPC
AE3	2 x Std dose AEA and modified mix to maintain strength	35	2 x Std dose	Gravel	OPC
	AGGREGATE TYPE (Gravel Control Mixes S1 and AE2)				
A1	Crushed Dolerite, non AE	35	–	Dolerite	OPC
A2	Crushed Dolerite, 1 x Std dose AEA	35	1 x Std dose	Dolerite	OPC
A3	Lytag, non AE	35	–	Lytag	OPC
A4	Lytag, 1 x Std Dose AE	35	1 x Std dose	Lytag	OPC
	CEMENT TYPE (OPC Control Mixes S1 and AE2)				
C1	OPC/PFA, non AE	35	–	Gravel	OPC/PFA
C2	OPC/PFA, 1 x Std Dose AEA	35	1 x Std dose	Gravel	OPC/PFA
C3	OPC/GGBFS, non AE	35	–	Gravel	OPC/GGBFS
C4	OPC/GGBFS, 1 x Std Dose AEA	35	1 x Std dose	Gravel	OPC/GGBFS

TABLE 3.1. General details of the 17 candidate mixes selected for screening tests.

MIX NO.	OPC (kg/m³)	PFA[1] OR GGBFS[2] (kg/m³)	20mm AGG. (kg/m³)	10mm AGG. (kg/m³)	SAND (kg/m³)	WATER (1/m³)	AEA OR SP	AIR CONTENT (%)	SLUMP (mm)	W/C
S1	355	–	760	300	740	185	–	1.0	60	0.51
S2	215	–	795	315	815	180	–	1.3	60	0.84
S3	420	–	770	305	685	180	–	1.2	75	0.43
S4	370	–	770	305	750	165	SP1	1.5	90	0.45
S5	455	–	800	355	620	165	SP1	0.9	100	0.36
S6	475	–	805	355	625	155	SP1	0.9	90	0.32
AE1	405	–	770	305	670	185	½ AEA	1.7	70	0.46
AE2	440	–	790	310	600	170	1 AEA	3.5	70	0.39
AE3	500	–	755	300	530	160	2 AEA	7.2	85	0.32
A1	365	–	820[3]	375[3]	655	200	–	0.5	80	0.55
A2	400	–	845[3]	385[3]	560	185	1 AEA	2.4	75	0.46
A3	410	–	–	695[4]	560	220	1 AEA	6.0	75	0.54
A4	480	–	–	695[4]	505	205	1 AEA	9.4	85	0.43
C1	280	120[1]	730	290	700	185	–	0.9	85	0.46
C2	355	150[1]	730	290	605	185	1 AEA	1.0	85	0.37
C3	110	255[2]	760	300	735	180	–	0.9	95	0.49
C4	130	300[2]	765	295	580	175	1 AEA	4.8	85	0.41

(1) PFA
(2) GGBFS
(3) Crushed Dolerite
(4) Lytag, sintered PFA, 12mm

TABLE 3.2. Concrete mix proportions for the 17 candidate mixes.

3.3.2 Compressive Strength

Six cubes were tested in compression for each mix, 2 No. control cubes at ambient temperature, 2 No. cubes at cryogenic temperature and 2 No. cubes after thermal cycling. As far as possible, cubes were tested according to BS 1881[50], using a Denison Loading Machine. Some changes to the standard testing procedure were required, however, to accommodate the low temperature specimens which were placed in special stainless steel rigs prior to testing, as shown in Figure 3.1(a). The rigs were used to prevent the cold concrete specimens coming into direct contact with the warm platens of the loading machine and, in the case of the splitting test specimens, to avoid unnecessary handling when locating the specimens in the loading machine. The specimens were cooled down at a rate of 60°C per hour in an insulated cabinet, then removed and allowed to warm up in the laboratory air. Cooling was achieved by spraying liquid nitrogen, which has a boiling point of -196°C into the cabinet, at a controlled rate. Cycled and control specimens were also tested in restraining rigs. The former were not contained in rigs during the cold cycle but installed immediately prior to testing as were the cubes tested at ambient temperature.

The cryogenic specimens were cooled to -180°C and then removed from the cold cabinet and tested in the Denison. During testing, two 100mm cube stainless steel spacers were placed between the rig and the plattens of the loading machine, to take the whole of the temperature gradient between the cryogenic specimens and the loading machine as shown in Figure 3.1. To be consistent, this condition was also maintained for cycled and control specimens tested at ambient temperature. There was a period of up to 5 minutes between the removal of the specimens from the cold cabinet and failure in the test machine. During this time, measures were taken to reduce the heat flow into the specimen by using expanded polystyrene insulation placed around the test cubes. Some heat flow was expected and to compensate for this the specimens were cooled to -180°C, this being some 15°C below the required test temperature. Furthermore, analysis of

Modified rig
for tensile
splitting tests $\longrightarrow$

Restraining Rig with Spring
Washers

Test Specimen (100mm Cube)

Spacer Block

Insulated Box

Loading Machine Platens
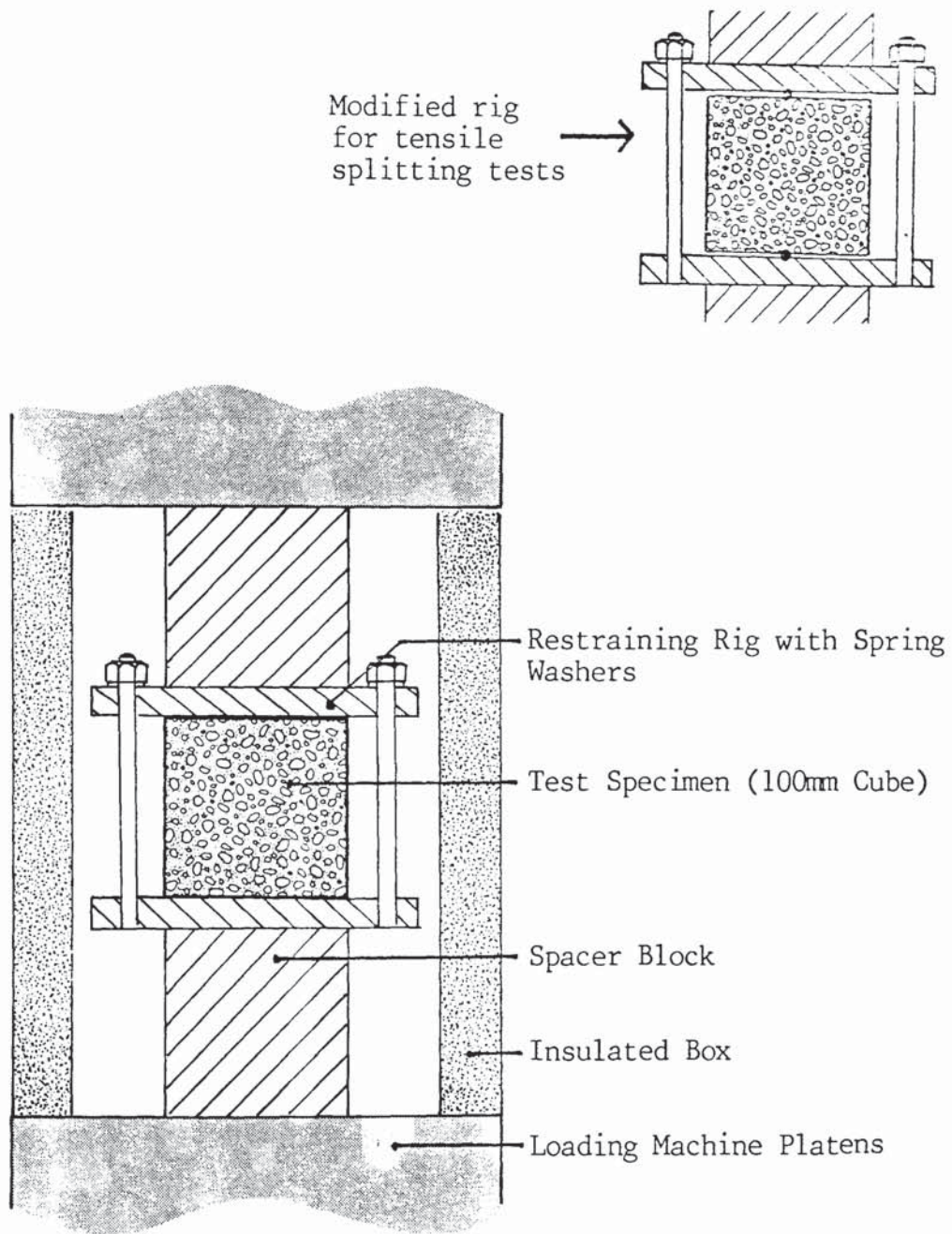
FIGURE 3.1. Arrangement for compressive and tensile testing of
pre-cooled cubes located in restraining rigs.

published data had shown that, at temperatures below -120°C, the variation in strength was small, compared with changes which had already taken place.

To ensure that the heat flow was not excessive, three instrumented test cubes were run through the test procedure and the temperatures at the centre and the surface of each cube were monitored using embedded thermocouples. The results are shown in Figure 3.2. The maximum temperature achieved during these trials was -135°C. For the purpose of screening tests this was felt to be acceptable.

3.3.3 Tensile Splitting Strength

Tensile strengths were measured by splitting concrete cubes. The specimens were stored, cooled and tested under similar conditions to the compressive test specimens. The restraining rigs were slightly modified, however, as shown in Figure 3.1(b). The test differed from a conventional splitting test in as much as the spacers at the top and bottom of the cube, through which the line loads were applied, were stainless steel rods. At ambient temperature 'soft' timber spacers are normally used, hence the load is spread over a small area. There was concern, however, that a soft spacer would change its properties at low temperature and that this would invalidate comparisons between tensile splitting strength over the range of test temperatures. The stainless steel rods were therefore chosen, as their hardness and stiffness would be similar at ambient and cryogenic temperature. It was recognised, however, that this may influence the absolute values of tensile splitting strength. The tensile strength was calculated using the equation

$$f_t = \frac{2P}{\pi a^2} \qquad (3.1)$$

where

f_t = tensile stress

P = maximum load applied

a = side of cube
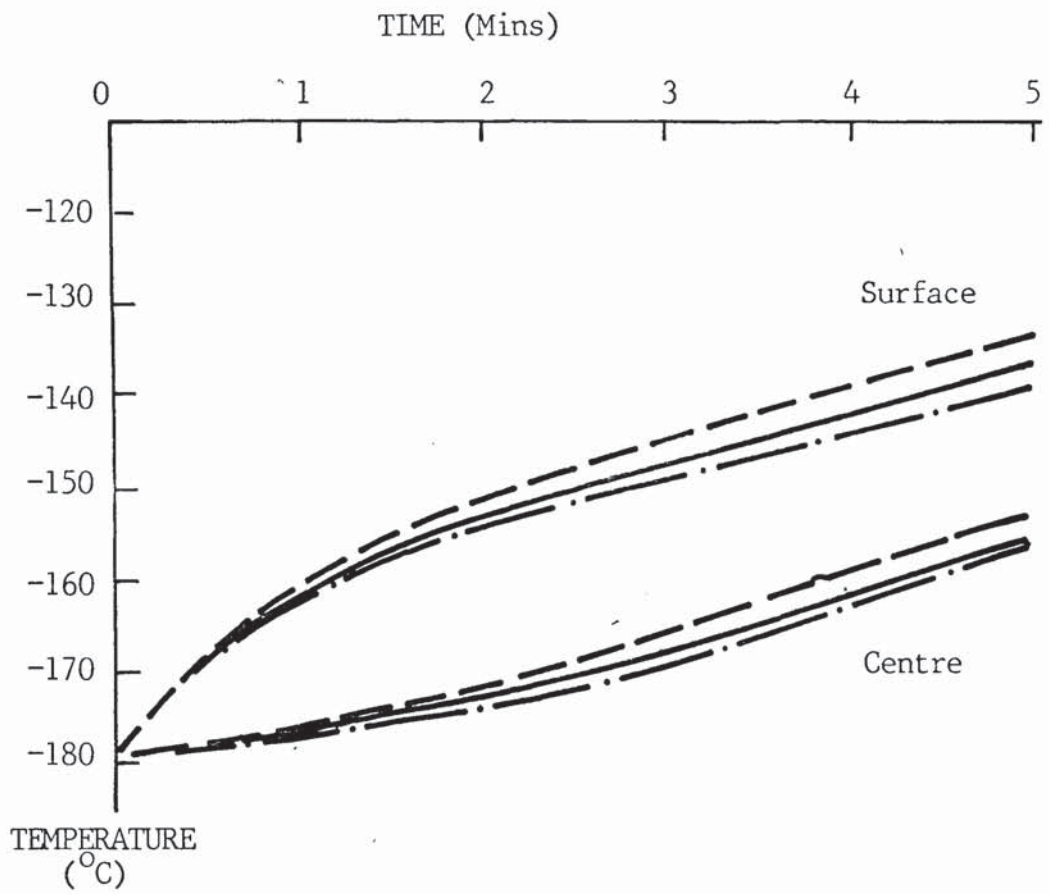
FIGURE 3.2. Heating curves recorded for three trial cubes during compressive strength testing.

3.3.4 Water Permeability

The water permeability of concrete discs at ambient temperature, was determined by using a rig developed within Taylor Woodrow Research Laboratories, as shown in Figure 3.3 and Plate 3.1. The 100mm dia. test specimens were prepared by placing them in brass moulds 110mm in diameter and filling the 5mm annular space with epoxy resin to form a tapered resin sleeve. After the resin had cured for 24 hours, the specimens were taken out of the moulds and put into the cylindrical brass test rig. A rubber 'O' ring was used to form a watertight seal. The brass rig was then bolted between the top steel plate (with the perspex observation disc) and the bottom plate, and a pressure equivalent to 100m head of water was applied over the bottom plate. As soon as the sample was fully saturated, determined by visual observation of the top surface, a reading was taken to calculate the rate of flow through the specimen. This was achieved by connecting a 4mm diameter pipe to the top of the rig and measuring the rise of water over a period of 10 minutes. A second reading was taken 24 hours after application of pressure.

For high permeability concretes, a period of only 1 minute was sufficient to obtain a reading. In the case of very low permeability concrete, complete penetration was not always achieved within 24 hours. In such cases the specimens were maintained under pressure for a period of 7 days. If complete penetration had still not occurred, the specimens were then removed from their rigs and split to expose the penetration front. A permeability coefficient was then calculated from the average penetration depth. The equations used to calculate the coefficient of permeability [60] are as follows:-

a) By Flow (Darcy)

$$K = \frac{Q \, x}{A \, h} \qquad (3.2)$$

b) By penetration (Valenta)

$$K = \frac{x_p^2 \, V}{2 \, h \, t} \qquad (3.3)$$

To Calibrated Tube

Clamp

M.S. Top Ring
Perspex Cover

Concrete Specimen
'O' Rings
Resin
Brass Sleeve
'O' Ring
M.S. Bottom Plate

Water Inlet
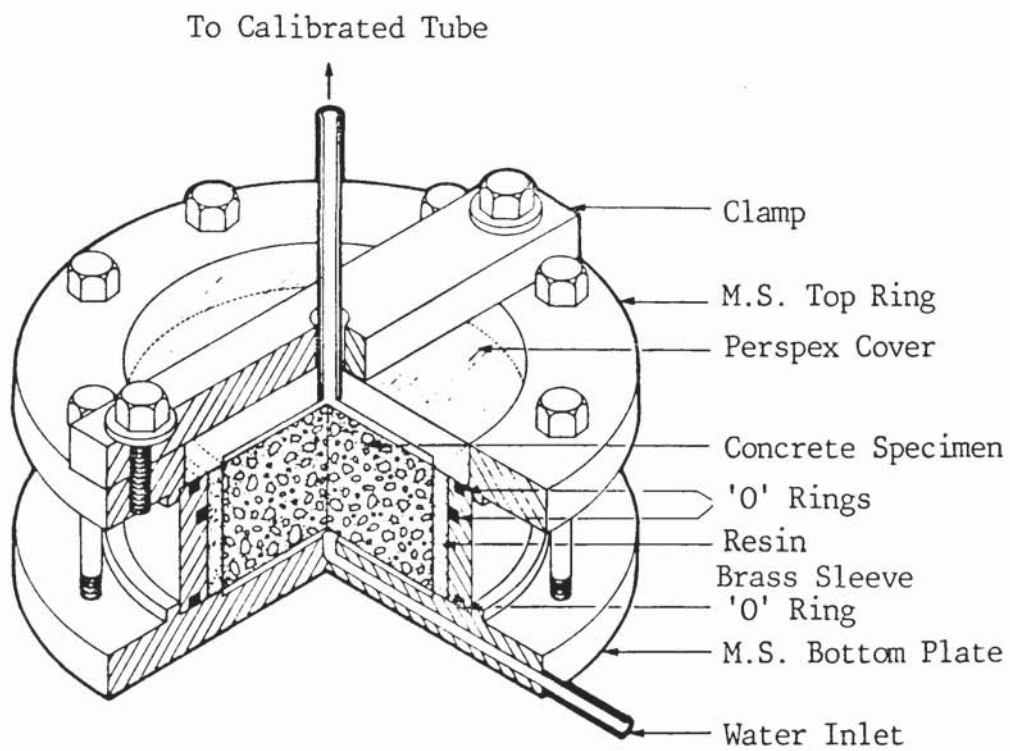
FIGURE 3.3. Water permeability test rig.

PLATE 3.1. Water permeability test rigs.

Where K = coefficient of permeability (m/s)

       Q = volume flow rate (m^3/s)

       x = specimen thickness in the direction of flow (m)

       h = head of water (m)

       x_p = depth of penetration (m)

       V = volume of voids filled by water in the penetrated zone (determined by measuring weight gain)

       t = time to penetrate to depth, x_p (s).

3.4 TEST RESULTS

Values of compressive cube strength and tensile splitting strength are given in Table 3.3. Values of water permeability obtained 24 hours after the start of the test (or by observation of penetration depth at a later age if complete penetration was not achieved) are given in Table 3.4. It should be noted that as the water permeability test proceeds the flow rate decreases. In order to compare results the values must therefore be quoted at a specific time. This will be discussed in more detail in Section 3.4.2.

3.4.1 Compressive and Tensile Strength

The results are summarized in Table 3.5 which shows the average value at each condition. As expected, the compressive strength of all concretes tested increased considerably when cooled down to about -165°C. The relationship between the control strength at 20°C and the cold strength is illustrated in Figure 3.4. It can be seen that the results generally agree closely with curves derived using equation 2.1 for concretes with a moisture content in the range 4-6%, this being typical of site cured concrete. It is also significant that, despite the range of concretes examined, the same relationship could generally be applied to each mix. This indicates that the approximate cold strength can be predicted using equation 2.1 (see Section 2.3.4) regardless of the mix proportions or constituent materials.

Three types of concrete appeared to have cold strengths marginally higher than the rest. These were concretes containing crushed rock aggregate (mixes A1 and A2), lightweight aggregate

MIX	CUBE SIZE	COMPRESSIVE STRENGTH						TENSILE SPLITTING STRENGTH					
		Ambient		Cryogenic		Residual		Ambient		Cryogenic		Residual	
		Failure Load kN	N/mm²	Failure Load kN	N/mm²	Failure Load kN	N/mm²	Failure Load kN	N/mm²	Failure Load kN	N/mm²	Failure Load kN	N/mm²
S1	100mm	520	52.0	1120	112.0	520	52.0	24.0	1.48	82.5	5.25	20.0	1.27
		510	51.0	1110	111.0	560	56.0	18.0	1.11	115.0	7.32	28.0	1.78
S2	4 ins	170	16.5	380	36.8	165	16.0	17.0	1.05	70.0	4.32	12.5	0.77
		170	16.5	770	74.5	165	16.0	17.5	1.08	72.5	4.47	13.0	0.80
S3	100mm	595	59.5	1030	103.0	605	60.5	46.0	2.93	90.0	5.73	42.0	2.67
		630	63.0	1100	110.0	580	58.0	30.0	1.91	77.5	4.93	38.0	2.42
S4	4 ins	590	57.2	1090	105.6	655	63.5	45.0	2.78	107.5	6.63	37.5	2.31
		660	63.9	1050	101.7	640	62.0	42.5	2.62	107.5	6.63	45.0	2.78
S5	100mm	970	97.0	1720	172.0	975	97.5	62.5	3.98	107.5	6.84	52.3	3.34
		970	97.0	1600	160.0	980	98.0	42.5	2.70	114.0	7.26	57.5	3.66
S6	100mm	1020	102.0	1840	184.0	980	98.0	62.0	3.94	122.5	7.80	52.0	3.31
		985	98.5	1580	158.0	960	96.0	60.0	3.82	125.0	7.96	59.0	3.76
AE1	4 ins	480	46.5	1000	96.9	550	53.3	34.5	2.13	107.5	6.63	22.5	1.39
		450	43.6	1030	99.8	440	42.6	22.5	1.39	72.0	4.44	38.0	2.35
AE2	100mm	540	54.0	1000	100.0	525	52.5	30.0	1.91	90.0	5.73	25.0	1.59
		460	46.0	1100	110.0	600	60.0	27.0	1.72	52.5	3.34	33.0	2.10
AE3	100mm	415	41.5	910	91.0	515	51.5	30.0	1.91	67.5	4.30	26.5	1.69
		480	48.0	1000	100.0	520	52.0	30.0	1.91	87.5	5.57	17.5	1.11
A1	100mm	485	48.5	1210	121.0	470	47.0	38.0	2.42	80.0	5.09	26.5	1.69
		485	48.5	1160	116.0	445	44.5	33.5	2.11	70.0	4.46	30.0	1.91
A2	4 ins	575	55.7	1240	120.1	560	54.3	34.0	2.10	92.5	8.70	35.0	2.16
		580	56.2	1240	120.1	520	50.4	45.0	2.78	92.0	5.67	43.0	2.65
A3	4 ins	480	46.5	1135	109.9	475	46.0	37.5	2.31	87.0	5.36	29.5	1.82
		530	51.3	1130	109.5	505	43.9	35.0	2.16	96.0	5.86	34.5	2.13
A4	100mm	418	41.8	1200	120.0	500	50.0	33.5	2.13	75.5	4.81	32.5	2.07
		400	40.0	1150	115.0	435	43.5	32.5	2.07	88.0	5.09	30.0	1.91
C1	4 ins	443	42.9	1030	99.8	460	44.6	30.0	1.85	105.0	6.48	24.0	1.48
		440	42.6	1085	105.1	475	46.0	22.5	1.89	92.5	5.90	35.0	2.16
C2	100mm	530	53.0	1040	104.0	545	54.5	25.0	1.59	108.0	6.88	35.0	2.23
		570	57.0	1000	100.0	560	56.0	30.0	1.91	82.5	5.25	21.0	1.33
C3	4 ins	370	35.8	790	76.5	323	31.3	27.5	1.70	60.0	3.70	16.0	0.99
		350	33.9	715	69.3	325	31.3	21.0	1.30	57.5	3.55	13.0	0.80
C4	4 ins	375	36.3	860	83.3	345	33.4	19.0	1.17	76.5	4.72	27.0	1.67
		390	37.8	740	71.7	343	33.2	18.0	1.11	60.0	3.70	20.0	1.23

TABLE 3.3. Individual results from compressive strength and tensile splitting strength tests.

TABLE 3.4 — Individual results from water permeability tests.

MIX	Thickness (mm)	Diameter (mm)	CSA (mm²)	Rise in 4mm Dia. Pipe (mm)	Penetration Depth (mm)	Time (S)	Flow Rate at 24 Hrs (10^{-10} m³/s)	Permeability Coefficient (x 10^{-11} m/s)
S1	52	102	8170	83	–	600	17.38	11.06
	52	102	8170	66	–	600	13.82	8.80
S2	47	102	8170	150	–	60	314.10	180.73
	48	103	8330	135	–	90	188.50	108.62
S3	49	102	8170	8	–	600	1.68	1.01
	52	102	8170	11	–	600	2.53	1.61
S4	46	102	8170	30	–	600	6.28	3.54
	50	102	8170	8	–	600	1.68	1.03
S5	52	102	8170	–	31	7 days	–	0.048
	51	102	8170	–	28	7 days	–	0.040
S6	52	102	8170	–	23	7 days	–	0.027
	50	102	8170	–	21	7 days	–	0.021
AE1	50	102	8170	18	–	600	3.77	2.31
	52	102	8170	19	–	600	3.98	2.53
AE2	52	102	8170	23	–	600	4.82	3.07
	52	102	8170	35	–	600	7.34	4.67
AE3	47	104	8500	20	–	900	2.78	1.54
	52	102	8170	17	–	600	3.56	2.27
A1	52	102	8170	75	–	600	15.71	10.00
	52	102	8170	106	–	600	22.23	14.17
A2	52	102	8170	40	–	600	8.37	5.33
	52	102	8170	42	–	600	8.80	5.60
A3	52	102	8170	–	23	8 dys 5 hrs	–	0.048
	51	102	8170	–	20	8 dys 5 hrs	–	0.034
A4	52	102	8170	–	10	7 days	–	0.010
	52	102	8170	–	43	90 days	–	0.014
C1	51	103	8330	24	–	600	5.03	3.08
	52	102	8170	24	–	600	5.03	3.20
C2	52	102	8170	28	–	600	5.87	3.73
	52	102	8170	17	–	600	3.56	2.23
C3	52	102	8170	60	–	600	12.57	8.00
	52	100	7860	145	–	600	30.37	20.10
C4	52	102	8170	60	–	600	12.57	8.00
	52	102	8170	75	–	600	15.71	10.00

TABLE 3.4. Individual results from water permeability tests.

MIX	Compressive Strength (N/mm²) At 20°C	At -165°C	Residual	Tensile Strength (N/mm²) At 20°C	At -165°C	Residual	Permeability Coefficient (x 10^{-11} m/s)
S1	51.5	111.5	54.0	1.30	6.29	1.53	9.87
S2	16.5	55.7	16.0	1.06	4.40	0.79	140.11
S3	61.3	106.5	59.3	2.42	5.33	2.55	1.28
S4	60.6	103.7	62.8	2.70	6.63	2.55	1.91
S5	97.0	172.0	97.8	3.34	7.05	3.50	0.044
S6	100.3	191.0	97.0	3.88	7.88	3.54	0.024
AE1	45.1	98.4	48.0	1.76	5.54	1.87	2.41
AE2	50.0	105.0	56.2	1.82	4.54	1.85	3.79
AE3	44.8	95.5	51.8	1.91	4.94	1.40	1.87
A1	48.5	118.5	45.8	2.27	4.78	1.80	11.90
A2	56.0	120.1	52.4	2.44	5.69	2.41	5.46
A3	48.9	109.5	47.5	2.24	5.61	1.98	0.040
A4	40.9	117.5	46.8	2.10	4.95	1.99	0.012
C1	42.3	102.5	45.3	1.62	6.09	1.82	3.14
C2	55.0	102.0	55.3	1.75	6.07	1.78	2.88
C3	34.9	72.9	31.4	1.50	3.63	0.90	12.68
C4	37.0	77.5	33.3	1.14	4.21	1.45	8.94

TABLE 3.5. Average values of compressive strength, tensile splitting strength and water permeability.
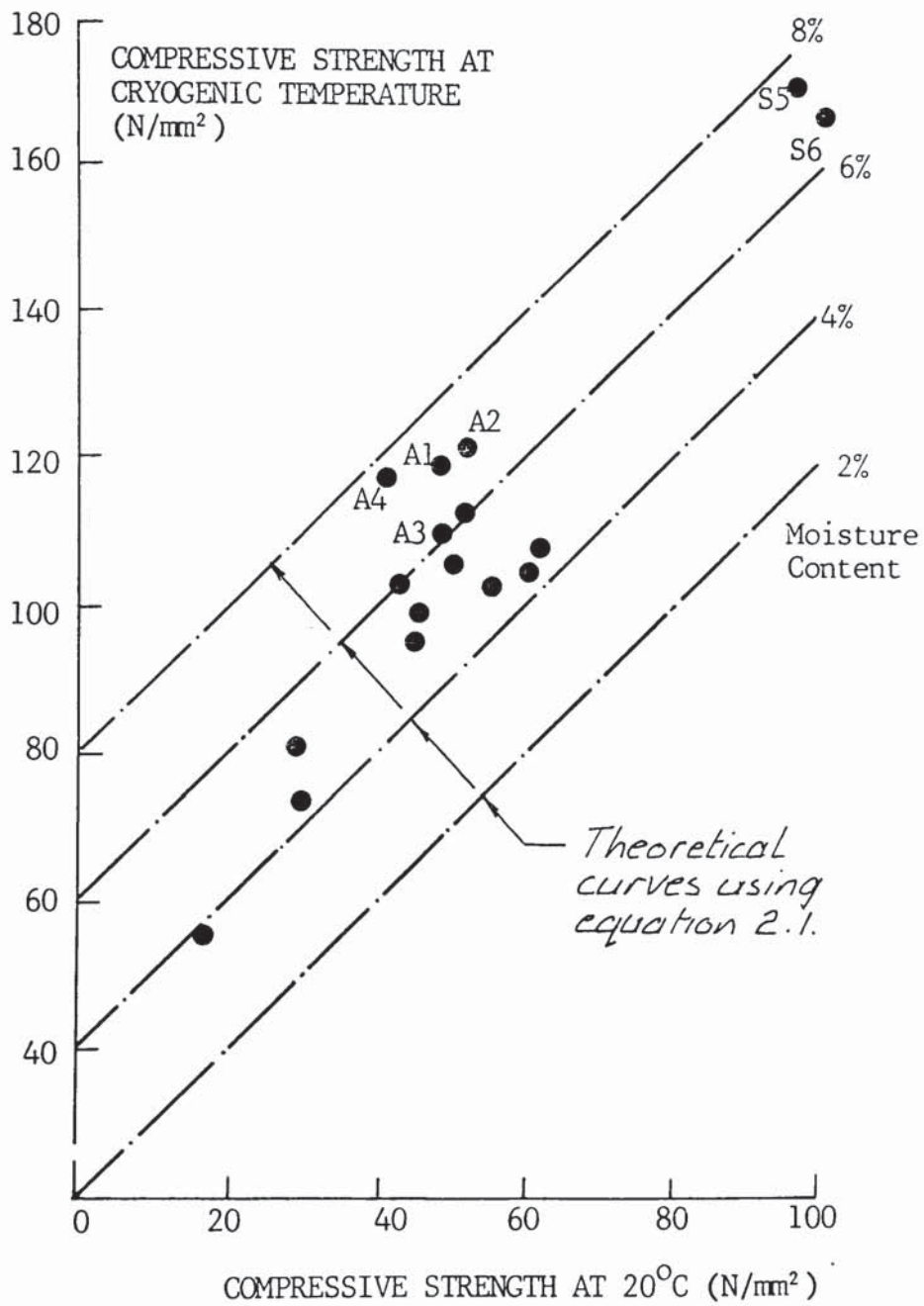
FIGURE 3.4. The relationship between compressive strength at 20°C and −165°C.

(mixes A3 and A4) and the very high strength grade 85 mixes (S5 and S6). In the case of mixes A1 to A4 the initial water content required to achieve the workability was higher than for the gravel aggregate mixes and this may account for the additional strength increment. The reason for the higher increase in strength of mixes S5 and S6 is less clear as both mixes were designed with low water contents, achieved by the use of a superplasticiser.

One result was appreciably lower than the remainder. In the case of mix S3 the result was believed to be suspect. The cold strength appeared to have reduced from 61.3 N/mm^2 at 20°C to 55 N/mm^2 at low temperature. The test was therefore repeated with the two spare cubes and in this case a cold strength of 106.5 N/mm^2 was recorded. The original result was therefore excluded from the analysis.

The residual compressive strength after cold cycling is shown in Figure 3.5, related to the control strength. It would appear that the compressive strength was unaffected to any appreciable extent with no one concrete differing significantly from any other. This is most likely due to the partially dry condition achieved by sealed curing. These results agree closely with the results of Tognon[13] for concretes cycled 10 times between +20°C and -196°C, which are also shown in Figure 3.5.

A considerable increase in tensile splitting strength was also observed at low temperature; in some cases the increase was up to 400% as shown in Figure 3.6, which illustrates the relationship between the control strength and the strength at -165°C. This increase in tensile strength was generally higher than recorded for compressive strength. This is compatible with the hypothesis by Tognon[13] that at very low tempertures the contraction of the ice effectively prestresses the concrete, resulting in a state of triaxial compression. For failure to occur in tension, not only must the tensile strength of the concrete be exceeded, but also the precompression. It may be for this reason that the scatter of results for tensile strength was appreciably greater
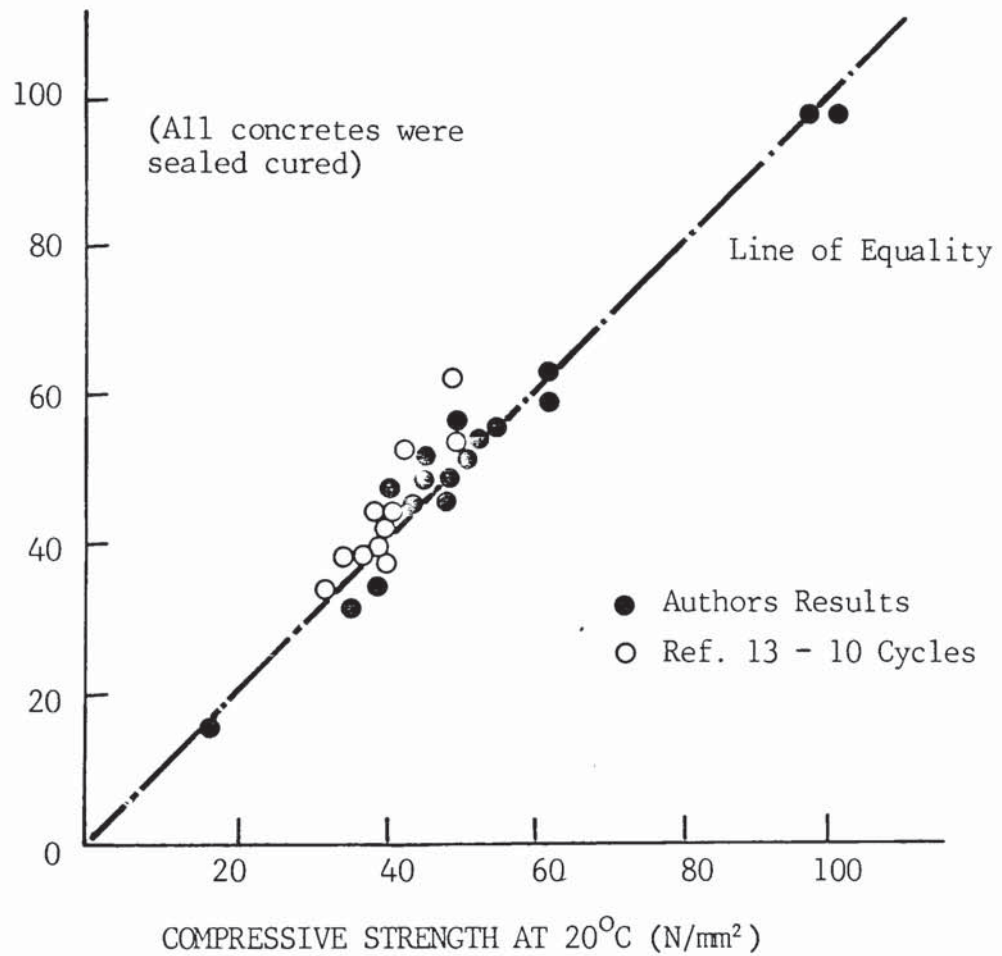
FIGURE 3.5. The relationship between compressive strength at 20°C and the residual compressive strength after thermal cycling in the range 20°C to −165°C.

TENSILE SPLITTING STRENGTH
AT CRYOGENIC TEMPERATURE
(N/mm^2)
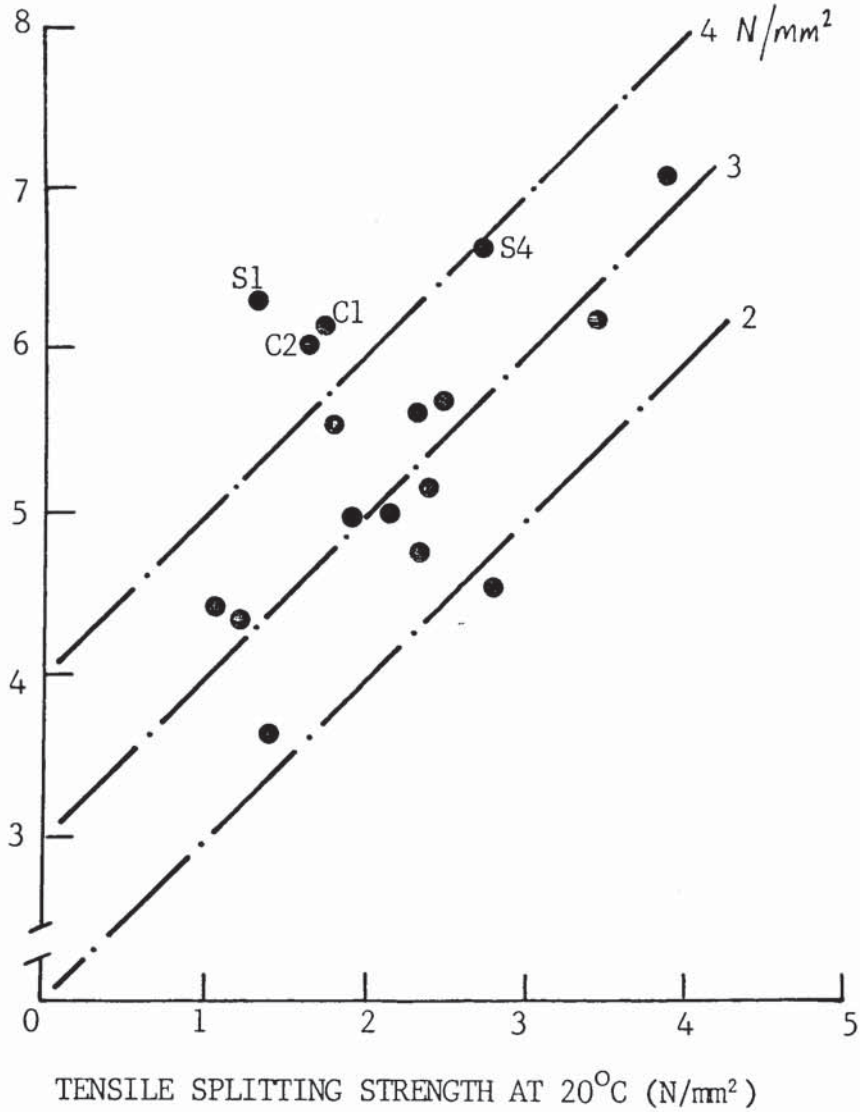
FIGURE 3.6. The relationship between tensile splitting strength
at $20^{\circ}C$ and $-165^{\circ}C$

than recorded in compression. The temperature control during the test was solely reliant on the insulation placed around the test specimen during loading and it was accepted that the actual temperature at failure could vary from specimen to specimen by several degrees. In compression, this was not believed to be significant as published results indicated only marginal changes in compressive strength below about -120°C. In tension however, their is limited evidence to suggest that significant changes in strength may occur at temperatures below -120°C. Hence, the lack of a more reliable method of temperature control may have introduced at least part of the variation.

Another possible cause of variation was the use of the stainless steel rods used for application of the point loads. Under normal ambient conditions the point loads are applied through a relatively soft material (e.g. timber) hence the load is spread over a small area. For low temperature testing, the change in properties of this material was of concern. Hence stainless steel rods were chosen, which would have similar hardness and stiffness at ambient and cryogenic temperature, enabling direct comparison of the results.

With regard to variation it should be noted that those concretes which merited particular attention resulting from their behaviour in compression (i.e. concrete with crushed rock or lightweight aggregate and the grade 85 mixes) conformed with the general trend in behaviour in tension. This suggests that the scatter may have been due simply to random variation and that care should be taken when drawing conclusions from individual results. Concretes exhibiting the most significant increase in tensile strength were mixes S1, C1, C2 and S4. Mix S1 was a non-air entrained gravel concrete; mix C1 was a similar concrete with PFA replacing 30% of the OPC, mix C2 was an air-entrained PFA concrete, and mix S4 was a superplasticised flowing concrete. In no case has any particular reason been identified to explain why the performance should have been better than any other concrete, again indicating random scatter of the results.

The effect of cold cycling on the tensile splitting strength is illustrated in Figure 3.7 which shows the strength before and after the thermal cycle. It is apparent that for many of the concretes tested, the tensile strength was adversely affected by thermal cycling. It is not surprising, however, that defects were detected by tensile strength measurement which were not observed by compressive strength tests. Any internal cracking, either at the aggregate-cement paste interface or through the cement matrix may close up under compressive loading, depending on their orientation. Under a tensile stress however, these cracks would tend to propogate, and hence influence the concrete behaviour more significantly.

The concrete which appeared to be most adversely affected by the cold cycle was mix AE2. No reason has been identified why this particular mix should have suffered most severely. Indeed, being air-entrained it would have been expected to provide more resistance to thermal cycling than the non air-entrained mixes.

The relationship between tensile and compressive strength is shown in Figure 3.8. At room temperature the results indicate that the tensile strength is generally 3 to 5% of the compressive cube strength[28]. When testing in accordance with BS 1881[50], the tensile strength would normally be expected to be 5 to 7% of the cube strength and it is believed that the testing technique is to blame for the lower ratio. As discussed previously, point loads applied to the specimens are normally via a 'soft' material, e.g. timber. The rigid stainless steel rods used in the current tests are believed to have concentrated the stress, hence reducing the load required to cause a splitting failure.

At cryogenic temperature the tensile splitting strength increased to a value generally within the range 4 to 6% of the compressive strength. This relative increase in tensile strength can again be attributed to the suggested prestress imposed by contracting ice. This would tend to increase the tensile strength, the applied stress having to overcome precompression, but partially offset the increase in compressive strength.

TENSILE SPLITTING STRENGTH
AFTER THERMAL CYCLING
(N/mm^2)

TENSILE SPLITTING STRENGTH AT 20°C (N/mm^2)
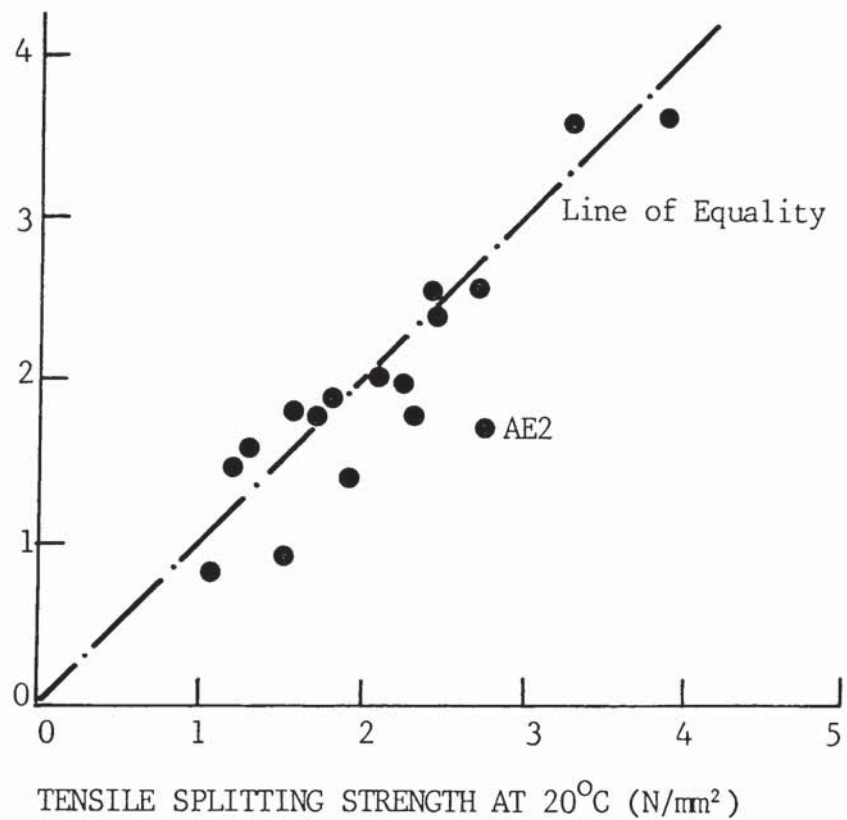
FIGURE 3.7. The relationship between tensile splitting strength at 20°C and the residual tensile strength after thermal cycling in the range 20°C to -165°C.
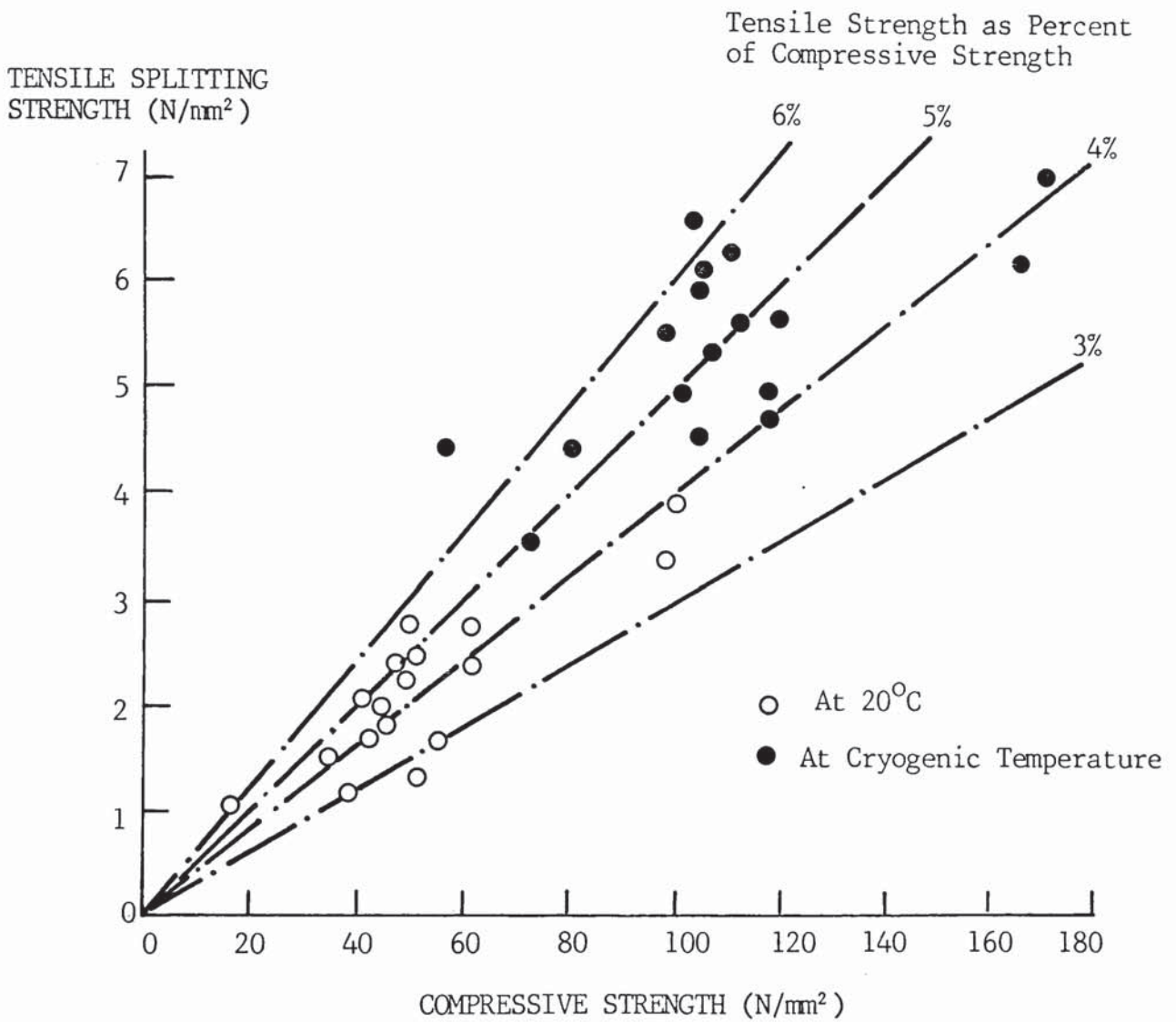
FIGURE 3.8.   The relationship between tensile splitting strength
and compressive strength at ambient and cryogenic
temperature.

3.4.2 Water Permeability

The results are summarized in Table 3.5 together with strength data. Permeability coefficients represent average values obtained for each mix. In general permeability coefficients fell within the range 1.5×10^{-10} to 1.5×10^{-11} m/sec. Notable exceptions to this were mixes S2, S5, S6, A3 and A4.

Mix S2 was a low grade concrete with an abnormally high w/c ratio of 0.84; the permeability coefficient was high also. Mixes S5 and S6 were very high grade concretes (85N) with very low w/c ratios (0.36 and 0.32); the permeability coefficients were low also. Mixes A3 and A4 were lightweight concretes. The reason for the very low permeabilities was not immediately obvious but it is believed that this was the result of a combination of factors including:

(i)   The high cement contents required to achieve concrete of structural quality with lightweight aggregate.

(ii)   Absorption of mix water into the aggregate resulting in an effectively lower w/c ratio paste.

(iii)   Internal curing provided by water absorbed into the aggregate particles, resulting in a greater degree of hydration, and hence a less permeable cement paste phase.

(iv)   A possible reaction between the sintered PFA aggregate and the cement, resulting in chemical bonding between the aggregate and cement paste, and hence less likelihood of potential leak paths at aggregate/cement paste boundaries.

(v)   The spherical shape and low modulus of elasticity of the aggregate minimising the occurence of microcracking.

The relative contributions of each of the above factors has not been established, being outside the scope of the study. However, this is clearly an area where further research would be beneficial.

It has been identified in previous research that the w/c ratio has a significant influence on permeability[41]. The relationship between permeability coefficient and w/c has

therefore been plotted in Figure 3.9. For the dense aggregate concretes which are non air-entrained and contain OPC a relationship clearly exists. The effect of air entrainment can also be seen. Whilst the air-entrained concretes were, in all cases, less permeable than the control mixes with no air entrainment, it is clear that the reduction was due not to the air itself, but primarily due to the reduced w/c ratio. The results indicate that at a given w/c ratio, air entrainment may cause an increase in permeability. Similar findings have been reported by Murata[33], the effect of air entrainment being to increase the water permeability in concretes with w/c ratio less than 0.6. At higher w/c ratios Murata found that air entrainment reduced permeability. The use of both PFA and GGBS also resulted in an increase in permeability at a given w/c ratio.

The lightweight concretes deviated significantly from the general relationship having much lower permeability coefficients than could be attributed simply to w/c ratio. Possible reasons for this have been discussed above.

In practice, concretes are specified by strength. The relationship between permeability and cube strength is illustrated in Figure 3.10. Again a relationship clearly exists with the permeability reducing logarithmically as the strength increases. The effects of air entrainment, PFA and GGBS appear more beneficial when considered on a strength basis. Increasing the air content (whilst adjusting the mix proportions to maintain strength) tends to result in reduced permeability. Similarly the use of PFA and GGBS tend to yield lower permeability than OPC concrete, when designed to achieve equal strength.

Again, the most significant deviation from the general relationship occurred with lightweight mixes A3 and A4 which achieved considerably lower permeability in relation to their strength.
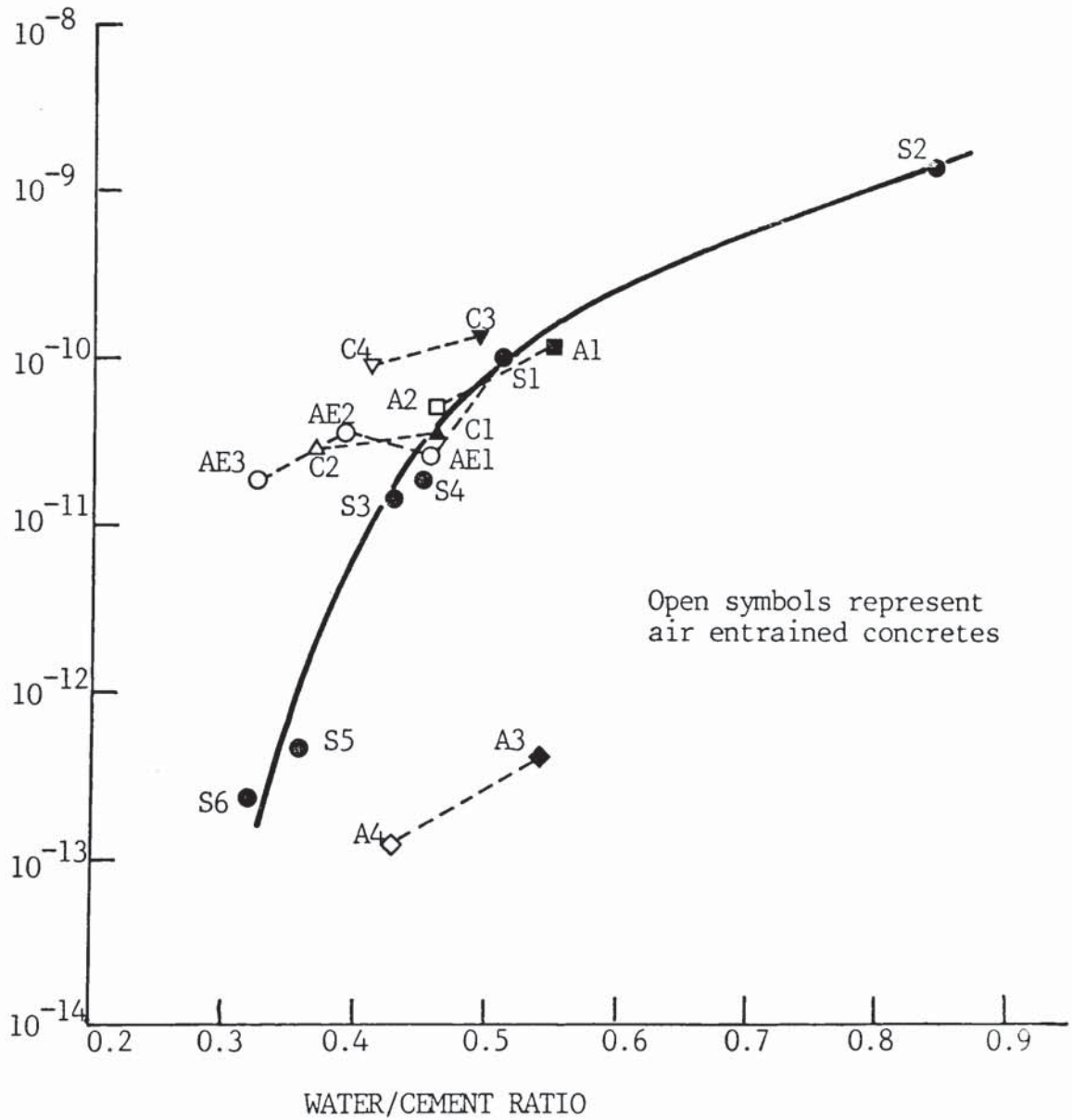
FIGURE 3.9. The relationship between water permeability coefficient and water/cement ratio.
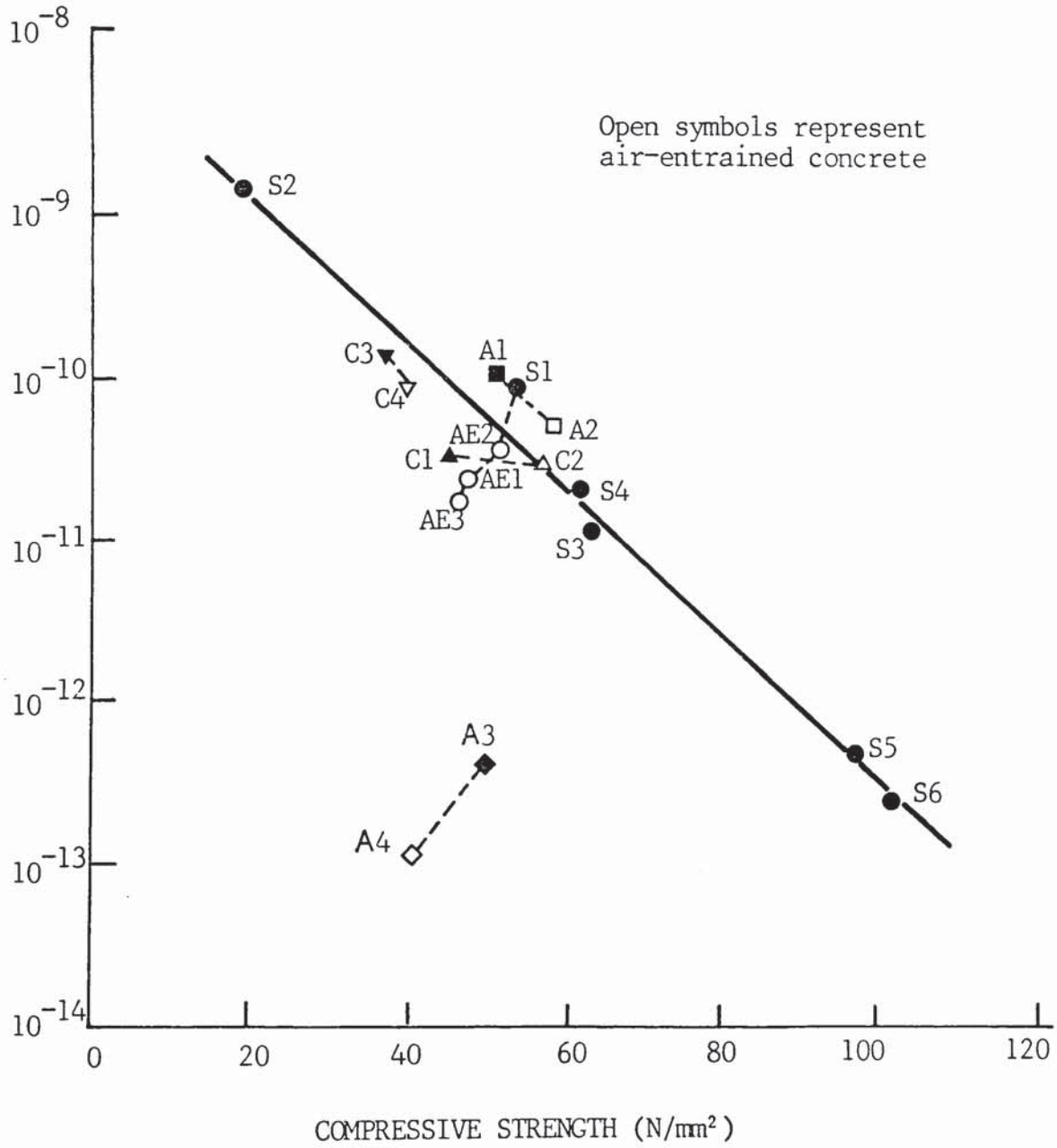
FIGURE 3.10. The relationship between water permeability coefficient and compressive strength.

3.5 SELECTION OF MIXES FOR THE MAIN TEST PROGRAMME

It was proposed at the outset of the programme to select four concretes on the following basis:-

i) Increase in strength at cryogenic temperature comparable with published data.

ii) Greatest resistance to thermal cycling, i.e. minimum strength loss.

iii) Lowest water permeability.

In every case the increase in both compressive and tensile strength was acceptable. Mix selection has therefore been based on residual strength and permeability alone.

To obtain an initial short list, concretes were eliminated which exhibited a compressive or tensile strength loss of 10% or more after thermal cycling. This is a somewhat arbitrary value but at least provided a starting point for the analysis. Using this criterion the following concretes were eliminated:-

S2, AE3, A1, A3, C3, C4

The remaining 11 mixes were then considered in relation to their water permeability. Three of these clearly exhibited much lower values than the majority of concretes tested, namely mixes S5, S6 and A4. Mix A3 also had a very low permeability but had already been eliminated. Mixes S5 and S6 were very similar and hence only one of these, mix S6, was selected for more detailed study. Mix A4, the air entrained lightweight mix was also selected, not only because of its low permeability, but also because at ambient temperature, other important properties related to crack resistance, such as strain capacity and thermal expansion coefficient, have been shown to be superior to dense aggregate concrete[9].

Of the remaining 8 concretes, there was very little difference in performance. Permeability coefficients all fell within the range 1.31 to 9.93 x 10^{-11} m/sec, with none of the mixes exhibiting a significant

change in strength due to thermal cycling. The two additional mixes for inclusion in the main test programme were therefore selected on the following basis:

i)   Mix AE2 represents the type of structural concrete which is currently likely to be used for cryogenic applications, a grade 35 air entrained concrete. Much of the published data has been obtained for a concrete of this type. As the permeability coefficient of 3.87×10^{-11} m/sec was at the lower end of the range for the remaining 8 mixes, this was therefore selected as a control concrete against which to compare the other 3 concretes.

ii) Mix C1 contains PFA as 30% of the total cementitious material (OPC + PFA). As discussed in Section 3.1.4, PFA can impart a number of technical benefits in both the fresh, hardening and hardened concrete and it is now commonly used in large civil engineering structures (e.g. nuclear power stations, offshore oil production platforms). In view of this, and the relatively low permeability coefficient (3.14×10^{-11} m/sec), mix C1 was therefore selected to complete the set of 4 concretes for comprehensive testing.

The four mixes selected as the basis for further investigation in the main test programme were therefore as follows:

Mix AE2 — Air entrained, gravel aggregate, OPC, grade 35.

Mix S6   — Non air entrained, gravel aggregate, OPC, grade 85.

Mix A4   — Air entrained, lightweight aggregate, OPC, grade 35.

Mix C1   — Non air entrained, gravel aggregate, OPC/PFA, grade 35.

4. PERMEABILITY AND POROSITY

4.1 INTRODUCTION

The objective of this phase of the programme was to investigate, for the four concretes selected from the screening tests, the following:-

(i)   Gas permeability and its change with reducing temperature.

(ii) The residual permeability after thermal cycling and the influence of rate of cool down.

(iii) The relationship between permeability and pore structure.

During the course of the work it was also possible to investigate the relationship between water and gas permeability.

4.2 PERMEABILITY COEFFICIENTS

The results obtained from water permeability tests described in Section 3.3.4 were presented in terms of the Darcy coefficient of permeability in units of m/sec. The Darcy coefficient is derived for a specific fluid, flowing through a specific porous medium. For this reason it is impossible to specify a Darcy permeability coefficient for the flow of gas through concrete. Being compressible, the density of the gas varies with pressure, hence whilst the mass flow rate through a concrete specimen will be constant along the direction of flow, the volume flow rate (used to derive the Darcy permeability coefficient) will vary. Also, the pressure gradient through concrete, subjected to gas pressure on one face, may not be linear. In the Darcy flow equation for non-compressible fluids the pressure gradient is assumed to be uniform.

For gas flow it is therefore, necessary to derive an alternative flow equation. For a compressible fluid the general equation governing flow through a porous medium[61] is:

$$Q = \frac{k A (P_1^2 - P_2^2)}{2P}$$ (4.1)

where Q = volume flow rate

   A = cross sectional area

   P_1 = upstream pressure

   P_2 = downstream pressure

   P = pressure at which Q is measured

In the above expression k is called the 'permeability'. Multiplying the permeability by the specimen thickness, x, gives the 'permeability coefficient' $k.x.$, which is dependent on both pore structure and the nature of the gas. Multiplying the permeability coefficient by the viscosity, η , gives the specific permeability, $k.x.\eta$, which should depend only on the pore structure, and be independent of the nature of the gas. If the specific permeability $k.x.\eta$ is designated, k_g , then the substitution can be made in equation 4.1 as follows:

$$Q = \frac{k_g A}{x \eta} \cdot \frac{P_1^2 - P_2^2}{2P} \tag{4.2}$$

The dimensions of k_g are L^2. In SI, the units are m^2.

For non-compressible fluids a similar specific permeability can be derived using the equation

$$Q = \frac{k_l A (P_1 - P_2)}{x \cdot \eta} \tag{4.3}$$

where k_l is again in units of m^2. This can be compared with the Darcy equation (3.2).

$$Q = \frac{A K h}{x} = \frac{A K (P_1 - P_2)}{x \rho g}, \text{ where } P_1 - P_2 = h \rho g$$

Hence, $\dfrac{A.k (P_1 - P_2)}{x \eta} = \dfrac{A K (P_1 - P_2)}{x \rho g}$

$$k = \frac{K.\eta}{\rho.g} \tag{4.4}$$

For water, η = 0.01 poise = 10^{-3} Nsec/m^2

ρ = 1000 kg/m^3

g = 9.81 m/sec^2

Hence, $$k_l = \frac{K \cdot 10^{-3}}{1000 \times 9.81} = 1.02 \times 10^{-7} K$$

The specific permeability, k_l , in units of m^2, determined using water is, therefore, approximately equal to the Darcy coefficient, K in units of m/sec, multiplied by a factor of 10^{-7}, i.e. 10^{-11} m/sec = 10^{-18} m^2.

4.3 EXPERIMENTAL DETAILS

4.3.1 Concrete Mixes

The mix proportions for the four selected concretes are given in Table 4.1. To enable the concretes to be more readily identified, the mix designations have been changed as follows;

Mix Details	Original Designation	New Designation
Air entrained Gravel Aggregate OPC Grade 35	AE2	AEC – Air Entrained Control
Non air entrained Gravel Aggregate OPC Grade 85	S6	HS – High Strength
Air entrained Lightweight Aggregate OPC Grade 35	A4	LW – Lightweight

Mix Details	Original Designation	New Designation
Non air entrained Gravel Aggregate OPC/PFA Grade 35	C1	PFA - Pulverised Fuel Ash

Mixes AEC and HS have exactly the same mix proportions as mixes AE2 and S6 respectively. Mixes A4 and C1 were modified slightly, however, to increase the strength. Mix LW has an increased cement content of 505 kg/m^3 compared with 480 kg/m^3 in mix A4. The coarse aggregate content has also been marginally increased and the sand content marginally reduced. The cement content of mix PFA was also greater than mix C1, with the sand content being reduced to compensate.

4.3.2 Test Specimens

Two sets of test specimens were prepared. For low temperature testing, cylindrical specimens 100mm in diameter and 75mm long were cast. It was originally proposed to test each of the four mixes so as to assess the influence of curing conditions (sealed and water cured) and moisture content (as cured and air dried at 65% relative humidity). A total of 12 specimens were, therefore, cast from each mix, three for testing after each combination of curing and drying.

The water cured specimens were stripped after 24 hours storage at 20°C and immersed in water at 20°C for a further 27 days. They were then removed from the tank and divided into two equal sets. One set was sealed in heavy duty polythene bags, the other being stored in air at 20°C and 65% relative humidity. The sealed cured specimens were also removed from their moulds at 24 hours. They were then sealed in heavy duty polythene bags and stored at 20°C. At 28 days, half the specimens were removed from the bags and exposed to drying at 20°C and 65% relative humidity.

	AEC	HS	LW	PFA
OPC	440	475	505	335
PFA	–	–	–	115
Gravel (20-5mm)	1100	1160	–	1100
Lytag (12mm)	–	–	780*	–
Sand (Zone 2)	600	625	495	563
Water	170	155	205**	185
Melment L10	–	7 litres	–	–
Sika AEA	0.31 litres	–	0.18 litres	–
W/C	0.39	0.33	0.41	0.41
Slump (mm)	75	80	70	70
Air Content (%)	4.8	1.3	6.4	0.8
28 Day Compressive Cube Strength (MPa)	51.9	90.3	49.5	57.0

* Saturated surface dry value with 12% moisture content

** Free water content, excluding water absorbed into the aggregate

TABLE 4.1. Concrete mix details for concretes selected for the main test programme.
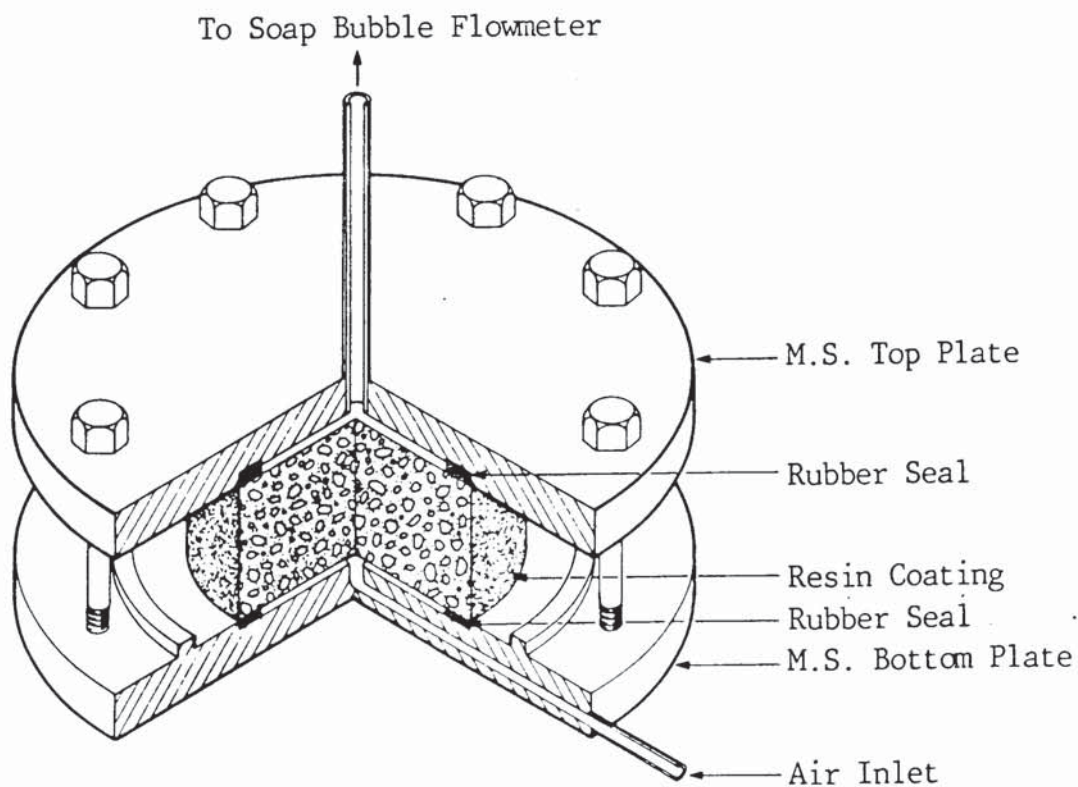
FIGURE 4.1. Gas permeability test rig.

For additional water permeability tests and to measure the effect
of thermal cycling on gas permeability, standard test specimens
were employed. These comprised 100mm diameter by 50mm thick
discs, cut from 100mm diameter by 200mm long cylinders. For each
concrete 3 No. cylinders were cast together with 6 No. 100mm
cubes for control purposes. The cylinders were stored in their
covered moulds for a period of 24 hours in a constant temperature
room at 20°C. They were then stripped from the moulds,
individually sealed in heavy duty polythene bags and stored in
the a room maintained at 20°C, 65% RH until the time of
testing. One week before testing, the cylinders were removed
from the plastic bags, and cut using a diamond saw into three
50mm thick slices, having removed the 25mm thick layer from the
top and bottom. The slices were stored for 24 hours at 20°C,
65% RH to allow the surface moisture, absorbed during the cutting
process, to dry out. They were then replaced in their plastic
bags and stored at 20°C until installation in the permeability
cells.

4.3.3 Gas Permeability at Ambient Temperature

The test rig used to measure gas permeability at ambient
temperature is basically similar to the water permeability rig
described in Section 3.3.4 with a modified top plate. The
composite steel/perspex top plate was replaced with a solid steel
plate as shown in Figure 4.1. To prevent gas leakage through the
curved face of the cylindrical specimen, two coats of epoxy resin
were brush applied with a 24 hour delay between coats. Before
application of the second coat, the first coat was roughened with
emery cloth. The specimen was not tested until the top coat had
cured for at least 24 hours.

The effectiveness of the resin in preventing gas leakage from the
curved surface of the specimen was established by measuring flow
rates through a specimen before and after the application of one
or two coats. The results were compared with a flow analysis
carried out using the electrical analogy[62], with flow lines
through the specimen being derived using Teledeltos conducting
paper. This is a standard method for predicting seepage of water

through soils. Actual and theoretical flow rates are given in Table 4.2. The flow rate in the uncoated specimen was estimated to be about 25% of the sealed specimen. This has been calculated from the flow net shown in Figure 4.2 derived using the Teledeltos paper. Following flow lines from the upstream to the downstream face illustrates that only gas within the central area of the upstream face (defined by a circle with half the radius of the exposed surface) is collected from the downstream face. The remainder is lost through the curved surface of the specimen. Hence by simple calculation, the volume of gas collected at the downstream face would be expected to equal about one quarter of the inflow. An effective surface sealer could therefore be defined as a material which increases the outflow through the downstream face by a factor of four. The results obtained using a single coat of epoxy resin increased the flow by a factor of 3.27 indicating that some gas loss was still occurring. However, after a second coat the flow increased by a factor of 4.32 over the uncoated specimen, indicating that gas leakage had been eliminated. Leakage at the rubber seals was checked visually using soapy water. No leakage was observed.

Having prepared the specimen, it was located in the test rig. Sealing between the specimen and the top and bottom platens was achieved using rubber seals to accommodate the roughness of the concrete surface. Nitrogen, at a pressure of 1.03 MPa (150 psi), was applied through the rig to the bottom face of the specimen and the flow rate of gas through the concrete was measured using a soap bubble flow meter. Three rigs were used to enable three specimens to be tested simultaneously.

Having applied the pressure, the flow was maintained for a period of 10 minutes before a reading was taken. Ten successive readings then taken, each measuring the time to achieve $2cm^3$ flow. When the flow rate at a pressure of 1.03 MPa was too fast for a bubble to be formed in the flowmeter, the tests were repeated using a reduced pressure of 0.69 MPa (100 p.s.i.). Using equation 4.2 this would theoretically reduce the rate of flow by 52%.

	TIMES FOR 2cc FLOW (Secs)	AVERAGE FLOW RATE (cc/min)	RELATIVE FLOW RATES	PREDICTED RELATIVE FLOW RATES
No Coat	19.5 18.6 18.6 18.1 17.8 18.2	6.5	1.00	1.00
One Coat	6.2 6.2 5.2 5.5 5.5 5.2	21.3	3.27	4.00
Two Coats	5.2 4.2 4.0 4.0 4.2 4.0	28.1	4.32	4.00

TABLE 4.2.   Measured and calculated flow rates through a gas permeability test specimen used to establish the efficiency of resin coating as a gas tight seal.
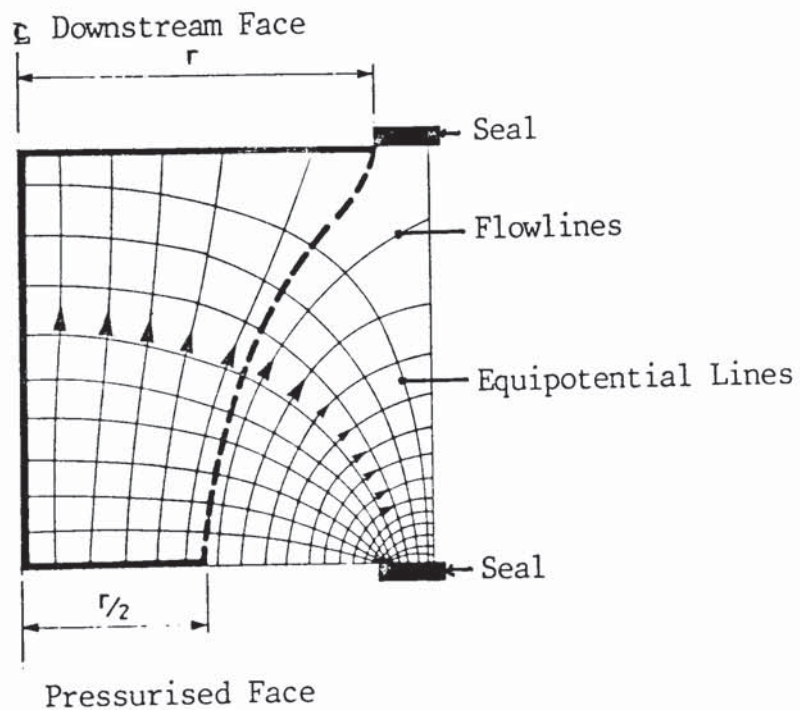
FIGURE 4.2.   Flow net through an uncoated gas permeability test specimen.

4.3.4 Gas Permeability at Low Temperature

To monitor the change in gas permeability with reducing temperature, a new experimental system was designed. Accurate flow measurement is essential for the determination of permeability, and this is especially so for the high grade, low permeability concretes required for containment structures. To determine the required precision of flow measurement for the low temperature test, calculations have been carried out to identify the acceptable level of permeability for an LNG storage tank wall (see Section 9.2). To prevent penetration of liquefied methane through a 500mm thick wall of a typical $100,000m^3$ tank within an assumed 30 year design life, requires the specific permeability of the concrete to be no greater than 7×10^{-21} m^2 at the bottom of the wall where the hydrostatic pressure is greatest. This value was derived for liquid flow. For gas flow, the value of specific permeability is generally between 10 and 100 times greater (see Section 4.4.5). Hence, if the required maximum specific liquid permeability is $7 \times 10^{-21}m^2$, the equivalent value for gas is likely to be within the range $7 \times 10^{-20}m^2$ to $7 \times 10^{-19}m^2$. For the design of the experiment, the lower value was assumed.

To measure flow rates through concrete with this low level of permeability, requires a high degree of precision. For a 100mm diameter by 75mm thick specimen, the theoretical time taken to achieve $1cm^3$ flow under an applied pressure of 1 bar, determined by equation 4.2, is given in Table 4.3 for different specific gas permeability coefficients. These figures take no account of possible reductions in permeability with temperature. At the very low permeability levels, requiring measurements over several days, changes in environmental conditions, (e.g. laboratory temperature and barometric pressure), would make the accurate measurement of very low flow rates difficult. An alternative method for measuring gas permeability for high quality concretes was therefore devised. This involved the use of methane as the test gas and nitrogen as a carrier gas on the downstream face to collect the methane which had permeated through the concrete. This technique has been used previously by Chen and Katz at ambient temperature (63).

GAS PERMEABILITY COEFFICIENT (m^2)	TIME
10^{-17}	5 mins
10^{-18}	55 mins
10^{-19}	9 hours
10^{-20}	90 hours

TABLE 4.3.   Calculated times for 1 cm³ flow at 1 bar pressure, through concretes with a range of permeability coefficients.

4.3.4.1 Permeability Cell

Tests were carried out using the experimental system illustrated in Figure 4.3. The permeability cell, shown in Figure 4.4, comprised a cylindrical stainless steel chamber with bolt on end plates. Working drawings are included in Appendix 1. The internal surface of the cylinder was tapered, the diameter reducing from 106mm at one end to 102mm at the other, over a length of 160mm. Concrete specimens were 100mm diameter.

The seal between the concrete and the stainless steel was made using an epoxy resin, Araldite AY11. This was selected after extensive discussions with material suppliers to identify materials which were compatible with concrete, and which would operate at cryogenic temperatures (see Appendix 2). The efficiency of the seal was further increased by the taper, the pressure being applied at the wide end of the tube, and at low temperature by the thermal contraction of the steel cylinder onto the concrete as the permeability cell was cooled down. Raco cryogenic seals were used between the cylinder and the end plates.

4.3.4.2 Cryogenic Enclosure

To enable the specimens to be cooled down to cryogenic temperatures, the three permeability cells were located in a cryogenic cabinet. Cooling was achieved by controlled injection of liquid nitrogen (LN_2) to achieve a specified rate of cooldown within the cabinet. The temperature in the cabinet was monitored using a thermocouple located adjacent to the permeability cells. This was linked to a temperature controller with a ramping facility, which in turn activated a solenoid valve in the LN_2 supply line. This enabled either a
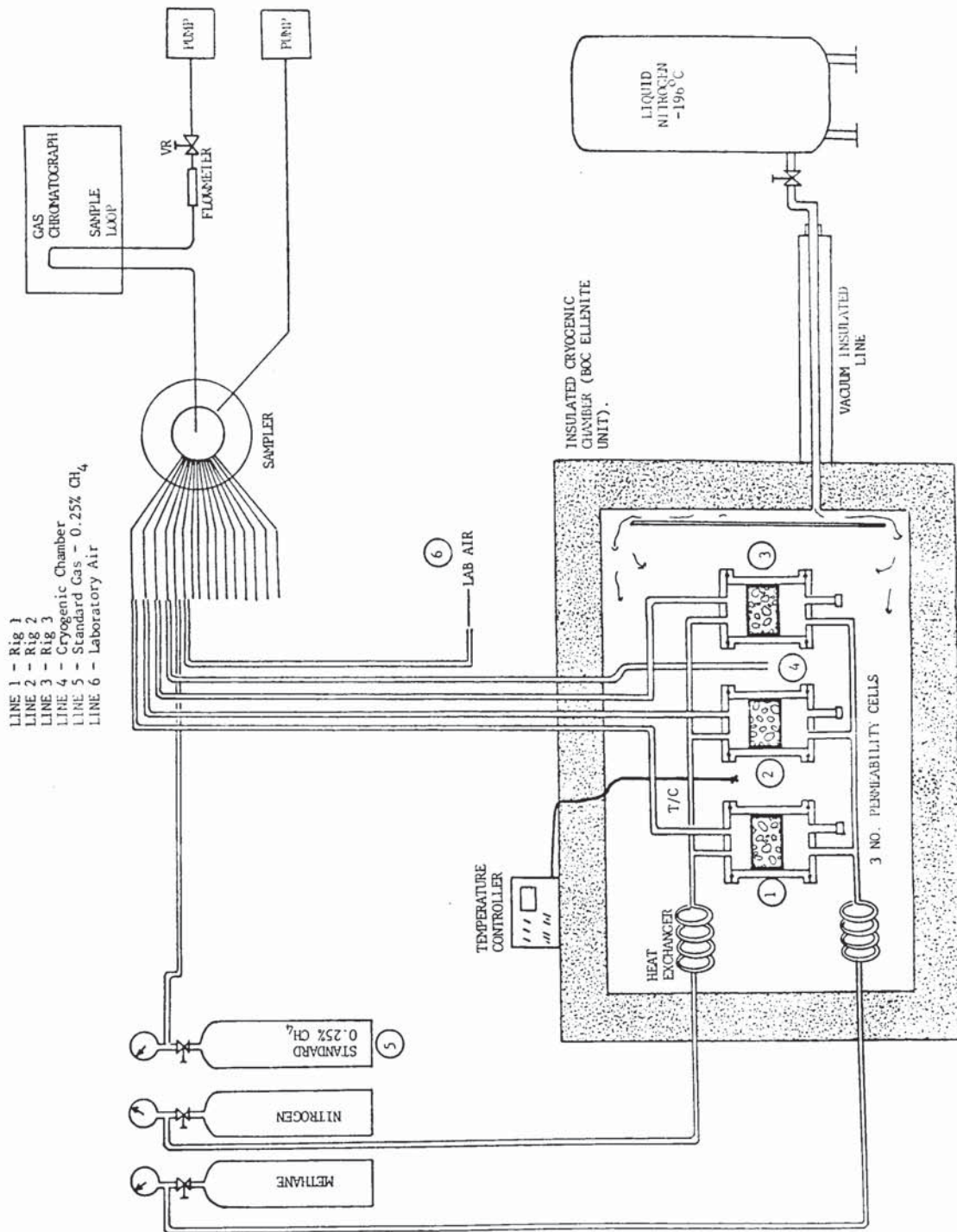
FIGURE 4.3. Experimental system for the measurement of gas permeability down to cryogenic temperatures.

Raco Cryogenic Seal

75mm

Concrete Specimen

Tapered Tube
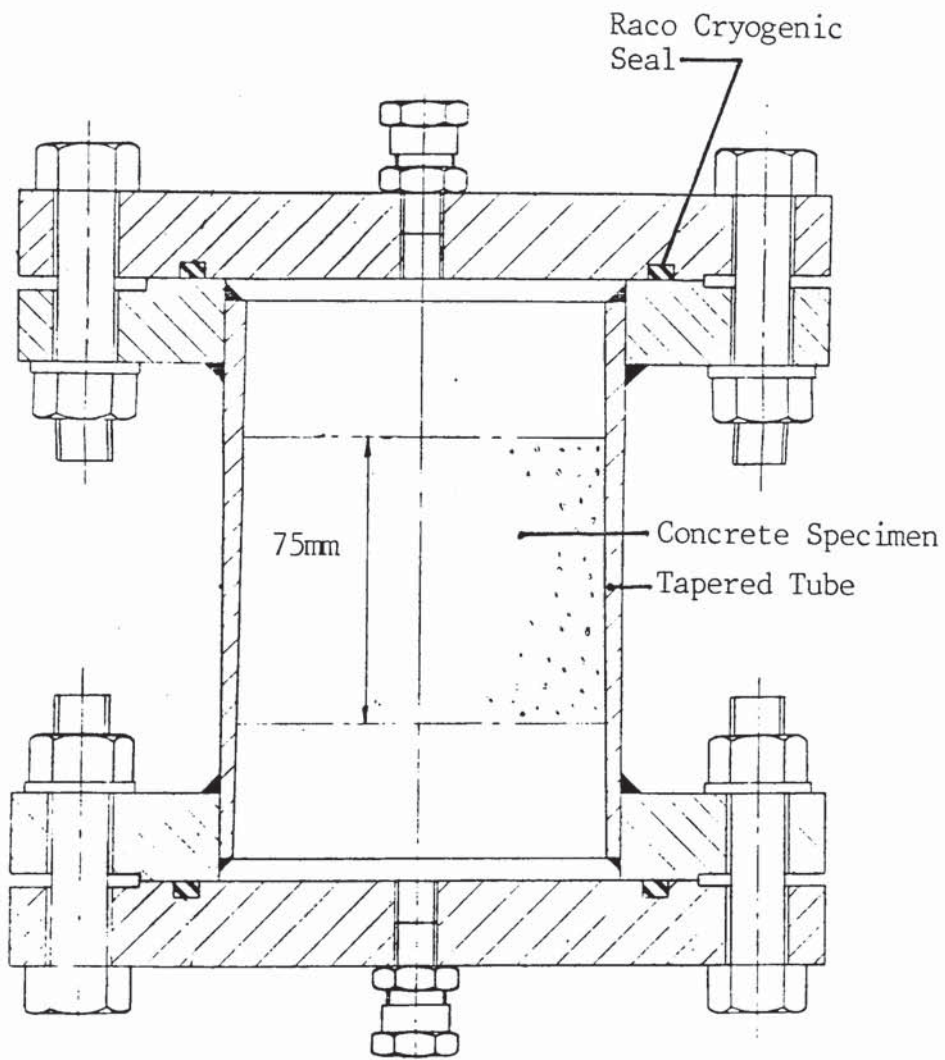
FIGURE 4.4.   Details of the stainless steel permeability test
cell for cryogenic testing.

constant temperature to be maintained in the cabinet (within ± 5°C) or the temperature to be decreased at a preprogrammed rate. A fan in the cabinet was used to minimise the temperature variation by circulating the cold gas. In addition, baffles were used at the gas inlet port, to protect the contents of the chamber from being sprayed directly with LN$_2$, and to disperse the gas around the chamber.

4.3.4.3 Direct Flow Measurement

At the higher levels of permeability (i.e. $10^{-18}m^2$) direct flow measurement was achieved using a simple soap bubble flowmeter. The test gas was supplied at a pressure of 3.5 bar from a standard nitrogen gas bottle using a pressure regulator. To cool the test gas to the temperature of the cabinet a 1.5m long length of coiled copper pipe was used to form a heat exchanger. A similar device was used to reheat the gas to ambient temperature upstream of the flowmeter.

Nitrogen was used as the test gas for two specific reasons. Firstly, nitrogen is inert and could be used without introducing the additional hazards associated with the use of methane. And secondly, higher pressures could be applied to nitrogen at the low test temperatures whilst maintaining a gaseous state. For methane, the boiling point is increased with pressure[64] as shown below.

Pressure	Boiling Point °C
Atmospheric	-162
1.0 bar	-153
3.5 bar	-140
10.0 bar	-123

Using methane, a low pressure would therefore be necessary to avoid condensation of the gas. This in turn would reduce flow rates and make measurement more difficult.

4.3.4.4 Measurement Using Carrier Gas

For the detection of flow at permeability coefficients beyond the precision of the direct flow test, the alternative method of flow measurement was used. Methane was used as the test gas at an applied pressure of 1 bar. As shown in Section 4.3.4.3 above, the boiling point of methane at a pressure of 1 bar, is $-153°C$. Cryogenic testing was therefore carried out at temperatures down to $-145°C$ only, to ensure that condensation would not occur. The downstream face of the specimen was purged with nitrogen at a rate of 15 cm^3/min. The nitrogen carrier gas was sampled periodically and analysed using a Perkin Elmer gas chromatograph (GC) to determine the quantity of methane collected, enabling the flow rate of methane through the concrete to be derived.

The experimental apparatus is illustrated in Figure 4.3. In addition to analysing the carrier gas from each of the three permeability cells, samples of gas were also collected from,

a)   a standard gas bottle with 0.25% CH_4 in nitrogen for continuous calibration,

b)   the cryogenic chamber, to identify methane leaks from the pressurised end of the system,

c)   the laboratory atmosphere, to identify methane leaks outside the cryogenic chamber.

It should be noted that considerable difficulties were experienced with this method of measurement, primarily due to leaks which developed at low temperature, and this part of the test programme was terminated after testing only 5 specimens.

4.3.4.5 Leak Tests

To check the efficiency of the end plate seals, preliminary tests were carried out prior to the installation of concrete specimens into the rigs. With the top and bottom plates fixed, an inlet flow rate of about $4cm^3/min$ was established from a nitrogen cylinder and the outlet flow monitored. Leakage from the system was to be assessed by comparing the inlet and outlet flow. Measurements were taken over a period of 6 hours using Hastings Mass Flowmeters on the inlet and outlet streams. The results are shown in Table 4.4. At the start of the test, the recorded outlet flow was about 30% less than the recorded inlet flow. Three possible reasons were considered for this difference between inlet and outlet flow:-

(1)   Errors in the flowmeters.
(2)   Time lag due to the system filling.
(3)   Leakage from the system.

To establish the accuracy of the flow measurement, tests were carried out in which the two mass flowmeters, one calibrated for nitrogen and the other calibrated for oxygen, were installed in series with a soap bubble flow meter. Nitrogen gas was then used to compare the three flow meters at flow rates up to 4.4 cm^3/min. The results are shown in Figure 4.5. At low flow rates the mass flow meters tended to overestimate the flow, the error reducing as the flow rate increased. At $4cm^3/min$

TIME (Hours)	INLET PRESSURE (cm Hg)	INLET FLOW (cm³/min)	OUTLET FLOW (cm³/min)	OUTLET FLOW AS PROPORTION OF INLET FLOW
1	10.4	4.15	2.77	0.67
2	10.4	4.15	2.76	0.67
3	10.4	4.15	3.13	0.75
4	10.4	4.15	4.13	0.99
5	10.3	4.15	3.77	0.91
6	11.0	4.20	4.30	1.02
7	11.0	4.20	–	–
8	11.0	3.97	4.13	1.04

TABLE 4.4. Inlet and outlet flow rates recorded during ambient leak testing.

SET FLOW RATE (cm³/min)	MEASURED FLOW RATE IN SAMPLE LINE (cm³/min)		
	Cell 1	Cell 2	Cell 3
2.32	2.45	2.47	2.40
3.00	3.16	3.16	3.08

TABLE 4.5. Measured flow rates compared with the 'set' value to establish the degree of control and the likelihood of leakage.

(MASS FLOWMETERS)
FLOW RATE
(cm^3/min)

N$_2$ Flowmeter

O$_2$ Flowmeter
(corrected for N$_2$ flow)

O$_2$ Flowmeter
(uncorrected)

Line of Equality

FLOW RATE (cm^3/min)
(SOAP BUBBLE METER)
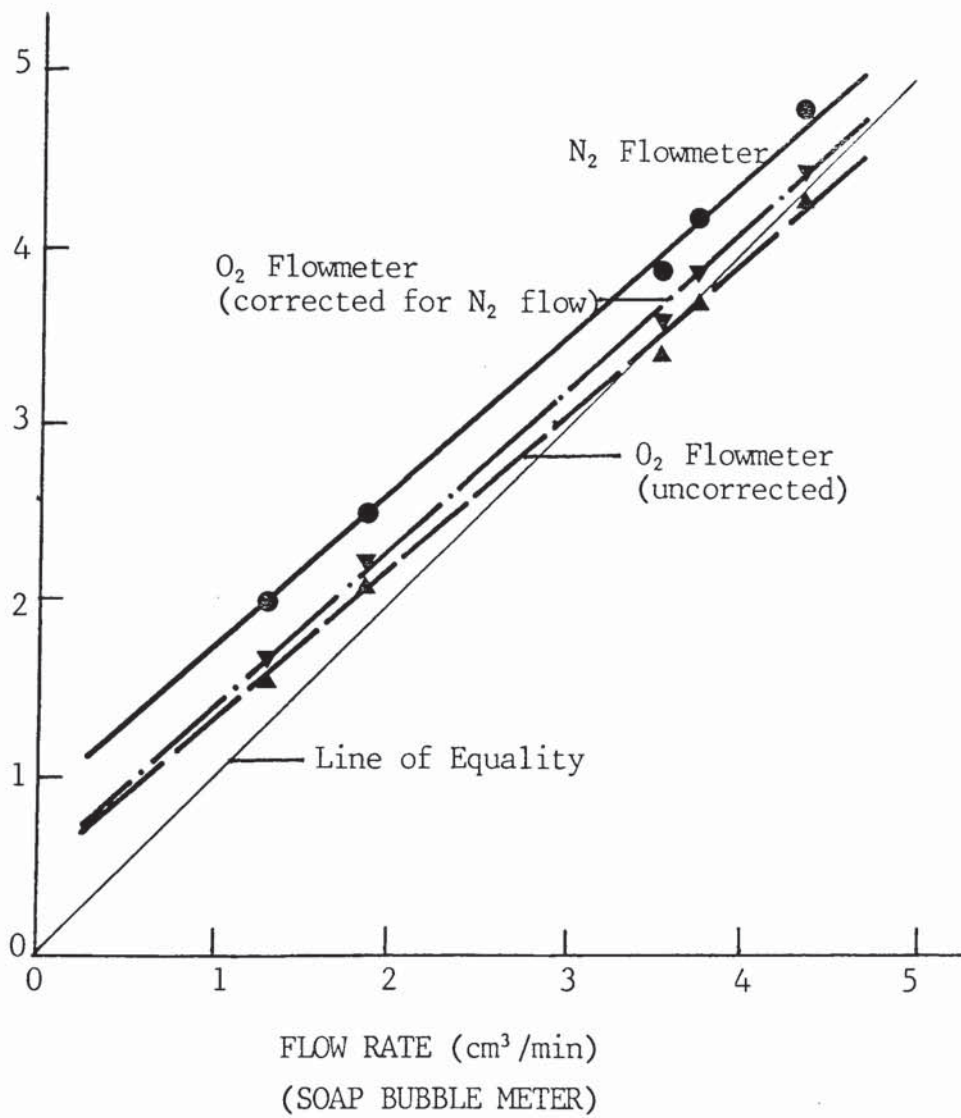
FIGURE 4.5. Results of calibration tests on mass flow meters.

there was less than 10% difference between the three readings. Surprisingly, the mass flowmeter calibrated for oxygen indicated a value closer to the soap bubble flow meter reading, than did the mass flow meter calibrated for nitrogen. However, as the indicated flow was similar for all three devices, errors in flow meter readings were not considered to have contributed significantly to the difference between flow into and out of the system.

The possibility of a time lag due to the mass of gas in the chamber increasing was, therefore, investigated as it was noted that as the end plate seal test proceeded, the outlet flow progressively increased until, after a period of 4 hours, the two values were almost identical. The increasing ratio of outlet to inlet flow with time is illustrated in Figure 4.6. The reason for the time taken for the inlet and outlet flow to become equal was believed to be due to the relatively large volume of the permeability chamber (approximately 1,250 cm^2 plus the associated pipework) in relation to the flow rate, combined with the resistance to flow offered by the downstream mass flowmeters.

Using Boyles Law (PV = constant) and the results obtained during the leak test, this hypothesis was confirmed. During the test, the difference between inlet and outlet flow varied between about 1.5cm^3/min at the start of the test and zero, after a period of about 4 hours. During this time the average difference can be assumed to be approximately 0.75 cm^3/min. Hence, over a 4 hour period the nett volume increase (at atmospheric pressure) was 180 cm^3. The applied pressure to achieve the flow rate was 11 cm of mercury, hence the pressure in the chamber (assuming negligible losses due to flow) was approximately 15% above atmospheric. The volume of
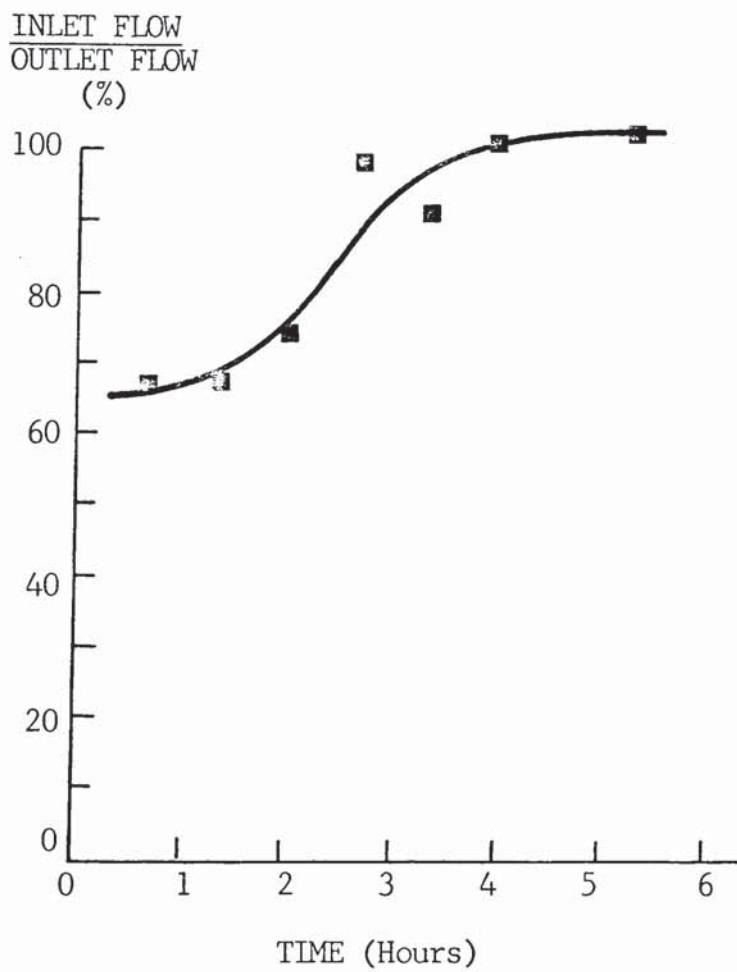
FIGURE 4.6.   Changes in the relative inlet and outlet flow rates during leak testing of the gas permeability system at ambient temperature.

the chamber was 1,250cm^3, hence at the increased pressure, the equivalent atmospheric volume of additional gas which could be accommodated was 0.15 x 1,250 = 188 cm^3. This figure is very close to the estimated nett inflow, supporting the hypothesis that the initial difference between inlet and outlet flow was not leakage, but simply the relatively large volume of the chamber accommodating an increased atmospheric volume of gas at the increased pressure.

Additional tests were carried out to support this theory in which inlet and outlet measurements were taken with the outlet flow either completely blocked with a shut-off valve, or fully open, using a soap bubble flow-meter to detect flow.

With the valve closed, and hence no outlet flow, an inlet flow of 1.5cm^3/min was established at a pressure of 10cm Hg. With the valve open, the inlet flow increased to 3.20cm^3/min and the recorded outlet flow was 3.18cm^3/min.

Similar tests were carried out with the gas chromatograph sampler in the line. In this case, the initial outlet flow was reduced to 0.21cm^3/sec from an inlet flow value of 2.9cm^3/sec. This difference was again believed to be due to the relatively low flow rates in relation to the volume of the permeability cells and the restriction to flow offered by the GC sampler.

In view of the time dependent variations in flow rate resulting from the pressure build-up in the permeability cells and the observed flow restrictions caused by both the flowmeters and the GC sampler, it was decided to modify the system to control the outlet flow independently using vacuum pumps. The inlet and outlet

flow would, therefore, be maintained independently at the same rate. Flow tests were carried out using this system and the results are shown in Table 4.5. Each sample line was recorded independently, the other lines being pumped through the exhaust. In every case, the measured output from the GC was marginally higher than the adjusted flow rate, by about 5%. This difference was considered acceptable in view of the anticipated orders of magnitude variations in concrete permeability.

Having established that leakage was minimal and that steady flow rates could be established at ambient temperature, low temperature tests were carried out. The first trial involved pumping methane into the system at a pressure of 0.14 N/mm^2 (20 psi), the cells being blocked using stainless steel plugs. After an initial inflow of gas it was expected that the flow would progressively approach zero. This was achieved at ambient temperature and the temperature was then reduced at a rate of 20°C per hour. Stability was maintained at temperatures down to -75°C, when there was a sudden increase in the flow of methane into the system indicating that one or more leaks had developed. The flow was immediately shut off, the system allowed to return to ambient temperature and all the connections were tightened. Whilst for safety reasons the leakage of methane was undesirable, with regard to the experiment the leakage of methane into the cryogenic cabinet would only be of significance if the gas could be drawn back into the nitrogen carrier gas lines which run at sub-atmospheric pressure, thus bypassing the test specimen. To test whether this was likely to occur, a further series of tests were carried out using air as the test gas with a nitrogen/oxygen ratio of 3.8. The carrier gas was helium and the gas in the cabinet, by test, had an N_2/O_2 ratio of about 40. If leakage occurred through the resin seal around the specimen, this would be indicated by an increase of both N_2 and O_2

in the ratio 3.8:1. Leakage into the purge gas from the cabinet would be detected by a disproportionately large increase in N_2. The test was run with the air at a pressure of 0.14 N/mm^2 (20psi), the cabinet being cooled at 20°C per hour. In addition to monitoring the N_2 and O_2 content in the helium purge gas from each of the three rigs, gas from the cryogenic cabinet and the laboratory was also sampled. The results are shown in Figure 4.7. Within two hours N_2 and O_2 were detected in the carrier gas from all three rigs (graphs 1-3), the ratio being consistent with air leakage through the resin seal (graph 4). However, the leakage rate was equivalent to flow through a concrete specimen with a gas permeability coefficient of the order of 3 x $10^{-22}m^2$. This is two orders of magnitude lower than the expected value for good quality structural concrete and, therefore, acceptable. As cooling continued, the leakage rate increased slowly in all three rigs until at -40°C the leakage rate had about doubled to an equivalent permeability coefficient of 6 x $10^{-22}m^2$.

Below -40°C, however, the leakage rate increased significantly in rig 3 (graph 3). In this case, however, the N_2/O_2 ratio also increased dramatically indicating the leakage of nitrogen from the cabinet directly into the carrier gas line (graph 4). From -40°C to -120°C the N_2/O_2 ratio recorded in rig 3 (graph 3) was very erratic, some variation was observed in rig 2, and rig 1 remained stable. The test was stopped at -120°C and further checks on all connections were made. However, identification of the specific location of leaks was only possible at ambient temperature and even though these could then be made good, there could be no guarantee that leaks would not again occur on further cooling. It was, therefore, decided to proceed with the tests on the concrete samples, and to take sufficient measurements to enable a reasonable estimate of concrete permeability to be made. A discussion of these results is given in Section 4.4.1.
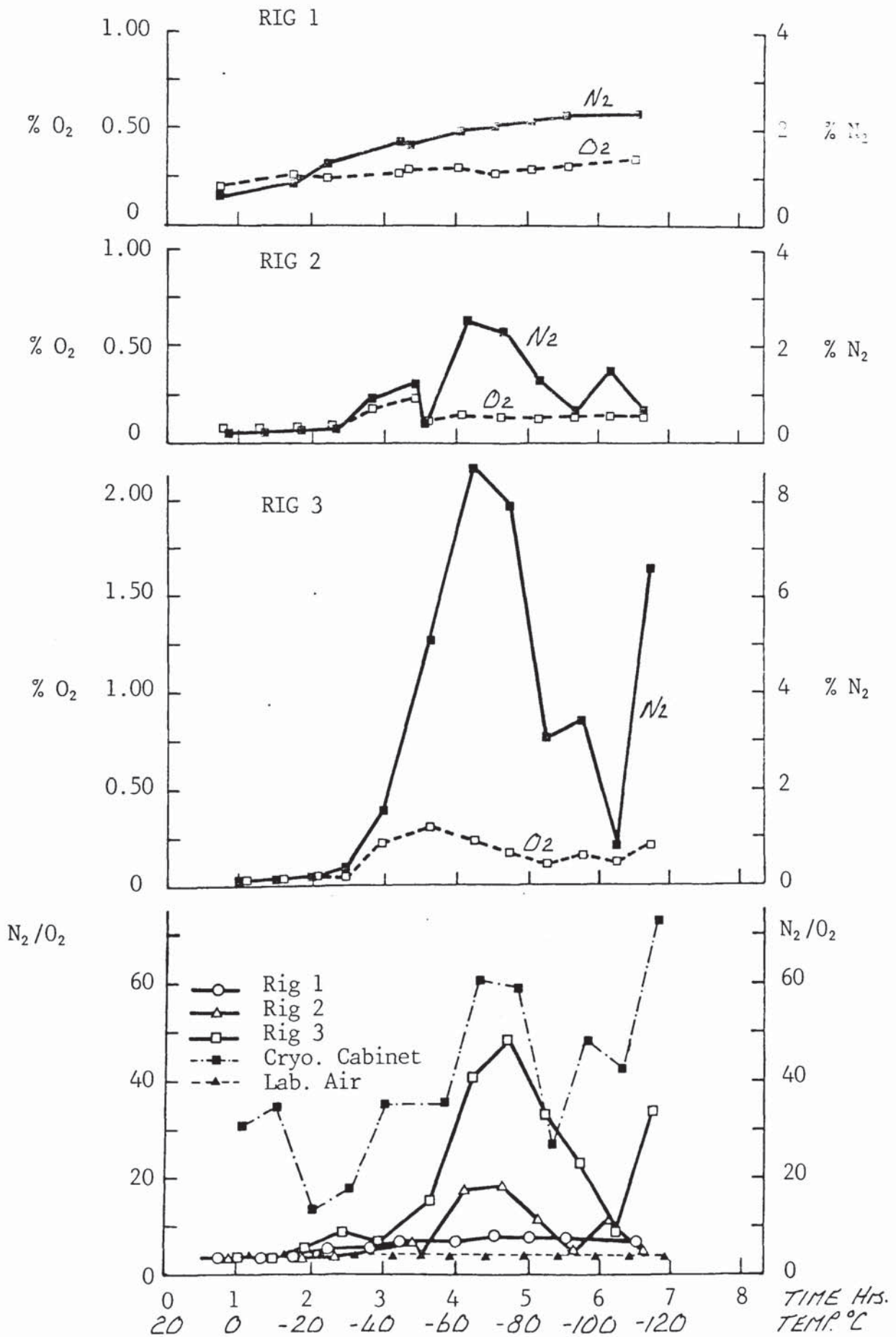
FIGURE 4.7. Results of tests to identify the source of leaks at low temperature.

4.3.4.6 Calculation of Permeability Using the Carrier Gas
Method

For conditions of direct flow the specific permeability
coefficient is calculated by rearranging equation 4.2 as
follows;

$$k = \frac{2Q x \eta P}{A(P_1^2 - P_2^2)} \tag{4.5}$$

Using the carrier gas method Q is not measured directly
but is derived from analysis of the quantity of
permeating gas (in this case methane) collected by the
nitrogen carrier gas. The flow rate of the methane test
gas through the concrete specimen Q_t is calculated by
multiplying the flow rate of the nitrogen carrier gas
Q_c by the mole fraction of methane collected by the
nitrogen Y_t .

Hence, $Q_t = Q_c Y_t$

Equation (4.5) is, therefore, modified as follows:

$$k = \frac{2 Q_c Y_t x \eta P}{A(P_1^2 - P_2^2)} \tag{4.6}$$

For the low temperature test, the equation must be
modified further. The flow of methane occurs at low
temperature and is collected by nitrogen at low
temperature, but the flow of nitrogen is measured at
20°C. The value of Q_c must, therefore, be modified
to take into account the lower volume flow rate at the
absolute test temperature in the permeability cell.

Hence, $Q_{t(cell)} = Q_{c(cell)} Y_t$

But, $Q_{c(cell)} = Q_{(atmos)} \dfrac{\theta_{(cell)}}{\theta_{(atmos)}}$

- 132 -

By substitution, equation (4.5) now becomes

$$k = \frac{2 \, Q_{c(atmos)} \, y_t \, x \, P \, \eta}{A \, (P_1^2 - P_2^2)} \cdot \frac{\theta_{(cell)}}{\theta_{(atmos)}} \qquad (4.7)$$

4.3.5 Thermal Cycling

To establish the residual permeability after thermal cycling, tests were carried out on 18 month old concrete. The specimens were cut from the 100mm diameter by 200mm long cylinders which had been stored in sealed plastic bags as described in Section 4.3.1. To establish the influence of thermal cycling on the residual properties, measurements were made of gas permeability at 20°C. This test, described in Section 4.3.3, was selected because the gas permeability measurements could be repeated on the same specimen before and after thermal cycling. Tests with water[32] have been shown to change the permeability of the concrete as the test proceeds and repeat tests would not therefore provide data on the influence of thermal cycling alone. Water permeability tests were carried out, however, for comparison with the previous tests and to identify whether there was a relationship between the permeabilities to gas and water. The procedure for the water permeability tests is described in Section 3.3.4.

To establish the influence of rate of thermal cycling, two rates of cooling were used. Slow cooling, at a rate of 4°C per hour down to -165°C, was achieved by placing the specimens in a cryogenic chamber, similar to that used for the low temperature permeability cells (see Section 4.3.3). Liquid nitrogen was supplied at a rate controlled by a solenoid valve and temperature ramping unit to cool the chamber at the predetermined rate.

Rapid cooling was achieved by immersing the specimens in liquid nitrogen at a temperature of -196°C. The specimens remained immersed until the boil-off of liquid nitrogen had reduced to the level prior to immersion, indicating that no further heat was being removed from the specimen. This generally occurred within a period of about 15 to 20 minutes.

- 133 -

The allocation of tests specimens is shown in Table 4.6. Nine test specimens were cut from three cylinders for each mix. The three specimens from each mix were designated 1, 2 and 3, and the slices cut from each specimen a, b and c from the top to the bottom. Hence specimen No. AEC/3c was the bottom slice, cut from specimen No. 3, cast using mix AEC. Of the nine specimens available for each mix, six were selected for gas permeability measurement, the remaining three being tested using water.

Having tested the six specimens from each mix for gas permeability at ambient temperature, the selection of specimens for thermal cycling was made on the basis of these results. From each mix two specimens were selected for slow cycling and two for fast cycling. Within each pair, one specimen was selected which had yielded a gas permeability coefficient at the high end of the range recorded for that particular mix; the other was selected from the low end of the range.

The specimens were then subjected to thermal cycling as described above. After completion of the thermal cycle an additional coating of epoxy resin was applied to the curved surface of the specimen to seal any cracks which may have occurred. After allowing a 24 hour period for the resin to cure the gas permeability was remeasured.

4.3.6 Porosity and Pore Size Distribution

The characteristic distribution of pore sizes in hydrated cement paste, mortar and concrete has been shown to influence both strength and permeability[65]. It was, therefore, decided to use the mercury intrusion technique to determine the porosity and pore size distribution and their relationship with permeability.

Mercury porosimetry provides information on pore radii from an upper radius of 75 μm, to a lower limit of 0.05 μm (75,000 Å and 50 Å respectively). This range covers pore sizes just larger than those for gel pores, but includes the range for capillary pores whose size and number vary considerably with water/cement ratio and maturity. The method works as follows. A non-wetting

MIX	SPECIMEN NO.	WATER PERMEABILITY	GAS PERMEABILITY			PORE STRUCTURE ANALYSIS		
			Ambient	Residual After		Ambient	Residual After	
				Slow Cycle	Rapid Cycle		Slow Cycle	Rapid Cycle
AEC	1a	●				● ●		
	1b		●					
	1c		●	●				
	2a		●		●			
	2b	●						
	2c		●		●			● ●
	3a		●	●			● ●	
	3b		●					
	3c	●						
AW	1a	●	●		●			
	1b		●					
	1c		●		●			
	2a							
	2b	●						
	2c		●	●				
	3a		●	●				
	3b		●					
	3c	●						
LW	1a	●	●			● ●		
	1b		●					
	1c		●					● ●
	2a		●		●			
	2b	●						
	2c		●	●			● ●	
	3a		●	●				
	3b		●		●			
	3c	●						
PFA	1a	●	●		●			
	1b		●		●			
	1c		●	●				
	2a		●					
	2b	●						
	2c		●					
	3a		●					
	3b		●	●				
	3c	●						

TABLE 4.6. Allocation of test specimens for assessment of the influence of thermal cycling.

liquid, i.e. one forming a contact angle with a given solid of greater than 90 degrees, will intrude open pores in a solid only under applied pressure. The pressure required is a function of the contact angle, the surface energy of the liquid and the geometry of the pores. For the case of cylindrical pores, the relation is given by the Washburn equation[66]:

$$P = \frac{2 \, \gamma \, \cos\theta}{r} \qquad (4.8)$$

Where:

P = pressure required to intrude a pore (kg/cm^2)

r = radius of intruded pore (Å)

γ = surface energy of the liquid (dyn/cm)

θ = contact angle between liquid and pore wall (deg).

Mercury is generally used because it has a low vapour pressure, it is relatively chemically inert and it does not wet most surfaces. Therefore, equation[4.8] reduces to [65]:

$$r = \frac{75,000}{P} \qquad (4.9)$$

At a given pressure 'P_1', a volume of mercury will be intruded into all pores of radii not less than r. This volume will be equal to the volume of pores of radius r, in the sample.

By incrementally increasing the pressure, the cumulative pore volume distribution is obtained for smaller pore radii over the working range of 75,000 Å to 50 Å.

Five major sources of error have to be allowed for during the measurement of pore radii[66]:

1) Moisture content of the specimen. Different moisture contents will produce different results, as pores containing water will not be intruded by mercury. All specimens must

be oven dried to a constant weight and then cooled in a dessicator. This in itself may alter the pore structure.

2) Air content of the specimen. Air in the pores will resist mercury intrusion. All specimens must be placed in a vacuum before immersion in mercury.

3) Compressibility of the mercury. A correction has to be applied to allow for compressibility of the mercury as the pressure is increased.

4) Thermal expansion of the mercury. Test specimens and the test equipment must be at a constant temperature during the test.

5) Concrete is a composite material and the recorded pore structure will be determined by the properties of the different phases and any discontinuities between them.

The term 'radius' in equation$^{(4.9)}$ refers to the "pore entry radius" which exists at the surface of the specimen. Although an internal pore may have a larger diameter than the pore connecting it to the surface, it will not be intruded until the pressure is sufficient for intrusion of the smaller pore. Also, if the pore entry radius is less than 50 Å, the larger internal pore will not be intruded. This is offset by the fact that at high pressures, the walls of discrete pores can be ruptured, giving access for mercury to enter these spaces. As a consequence of the above, and the limited intrudable range of 50 Å to 75,000 Å, the measured intruded pore volume will be less than the total pore volume.

Many authors[65-67] report that mercury intrusion measurements on dried cement paste, give a reproducible and apparently satisfactory direct method for the assessment of pore size distribution. This indicates that the assumptions made above concerning the cylindricity of the pores and the pore entry radius, affect the results in a relatively consistent manner.

From the results of a mercury porosimetry test, the pore size distribution can be represented by a cumulative plot of intruded pore volume against pore radius. The differential pore size distribution can also be calculated, using the equation:

$$f(r) = \frac{dV}{dr} \qquad (4.10)$$

Where $f(r)$ = frequency of occurrence of pores of radius r on an
                   equal radius internal distribution curve
       V   = pore volume (cm^3)
       r   = pore radius (Å)

However, because of the wide range of pore sizes involved, this is normally transformed to:

$$f(r) \frac{r}{2.303} = \frac{dV}{d \, Log_{10}r} \qquad (4.11)$$

Therefore, a graph of $\frac{dV}{d \, Log_{10}r}$ against r will give the pore size distribution

For cement paste it has been reported[68,69] that the distribution is affected by both the water/cement ratio and the degree of hydration of the cement. The higher the water/cement ratio the larger will be the grain spacing and hence the larger will be the size and number of capillary pores in the hardened cement for a given maturity. The degree of hydration determines what proportion of the cement has reacted and so also affects the size and number of capillary pores.

Three further pore parameters can be calculated from the results obtained by mercury intrusion porosimetry[68]:-

1.   Surface Area of Intruded Pores

$$St = \sum_{i=1}^{n} \frac{2dV_i}{r_i} \; (m^2/g) \qquad (4.12)$$

- 138 -

2. Hydraulic radius (r_h) of the pore system which is the ratio of total intruded pore volume to the total surface area, is given by:

$$r_h = \frac{V_{max}}{S_t} \quad (\text{Å})$$ (4.13)

Where n   = number of volume steps used

V_{max} = total intruded pore volume at the

maximum pressure, usually 1,500 kg/cm$_2$.

3. Maximum continuous pore radius (r_m), which is defined as the pore radius at which $\frac{dV}{dP}$ has a maximum value.

The surface area and hydraulic radius of the pore system give some measure of the overall distribution of pores between the intruded range of 50 Å to 75,000 Å. The maximum continuous pore radius (MCPR) is more specific. By definition, it gives the pore radius above which very little mercury is intruded, but below which rapid intrusion occurs. This is believed to indicate that pores of this radius are continuous to some extent.

With regard to durability of the hardened cement paste, the size and number of capillary pores will affect factors such as the permeability and gas diffusion. However, below a certain radius, gas and water movement will be so slow as to be negligible in comparison with flow though the larger pores. Mehta[70] considers pores below 660 Å radius do not contribute to water permeability. Therefore, calculating the values of surface area and hydraulic radius of only those pores greater than 660Å radius may give a more relevant measure of pore distribution.

Results for concretes and mortars are complicated by two factors:

1) The aggregate generally has a lower porosity than the cement paste. The measured intruded pore volume will be a superposition of the pore size distributions for cement

paste and aggregate, factored in accordance with the surface available for mercury intrusion.

2) Non-cylindrical microcracks are likely to form at the aggregate paste interface due to a combination of plastic movement (shrinkage, settlement) and stresses generated during oven drying (drying shrinkage, thermal incompatibility etc).

Correcting for the volume of paste replaced by aggregate should enable results for pastes, mortars and concretes to be compared. However, the extent of microcracking will be dependent upon the aggregate type, the amount of aggregate present (aggregate volume concentration or AVC) and the water/cement ratio. Published data shown in Figure 4.8 gives an example of the cumulative pore size distribution for hardened cement paste and mortars of 0.5 water/cement ratio and 28 days curing[68]. The corrected intruded paste volumes are also shown, along with the specific surface area and hydraulic radius.

When mixes of the same aggregate volume concentration are compared, the effects of water/cement ratio and curing are similar to those for hardened cement paste shown in Figure 4.9[65], namely an increase in w/c ratio or a decrease in the length of cure will produce an increase in both the MCPR, and the surface area. For the hydraulic radius, the trend is less obvious.

From the above, it may be expected that good agreement will be found between the pore size distribution of concretes having the following properties:

1) similar aggregate volume concentrations,
2) similar water/cement ratios,
3) similar degree of hydration.

As items (2) and (3) control the size and number of capillary voids in the concrete, the test may be used to indicate variations in the quality of a particular concretes.

Illustration removed for copyright restrictions

FIGURE 4.8. The effect of aggregate volume concentration on
            cumulative pore size distribution. (Ref. 68)

FIGURE 4.9. The effect of water/cement ratio and curing period
on cumulative pore size distribution. (Ref. 65)

For comparison with other properties of concrete such as water permeability, the volume of pores with radii below 660 Å may be disregarded[70]. The volume and distribution of pores greater than 660 Å will indicate the permeability of the concrete. Okpala[68] has shown that good agreement may be obtained between the effective hydraulic radius of pores greater than 650 Å and oil permeability of mortar (Figure 4.10).

In view of the lack of data on mortar and concrete it would be unfair to specify limits of acceptability based on the pore size distribution. However, as stated above, the use of mercury porosimetry can be useful by providing a measure of the change in pore structure for a specific concrete.

Tests have been carried out on mixes AEC and LW only. Two 10 x 10 x 50mm samples were cut from each of three 50mm thick by 100mm diameter discs providing six samples for each of the two mixes. Of the two samples from each core, one was cut from the surface and one from the centre. To establish the influence of thermal cycling on pore structure, porosimetry tests were carried out on specimens taken from uncycled cores, and cores which had been subjected to both the slow and rapid cooling regimes.

4.4 TEST RESULTS AND INTERPRETATION

4.4.1 Effect of Temperature

At the start of the programme it had been proposed that a full factorial test programme be carried out on four selected concretes, subjected to two curing conditions and tested at two moisture contents. Tests were to be carried out using methane in both the gaseous and liquid state. In the latter case, because of the very low flow rates, it was proposed that temperature and pressure be adjusted to generate two phase flow, with the methane entering one face of the concrete as a liquid, and leaving the other face as a gas. This would provide greater accuracy of flow measurement at the downstream face. Unfortunately, the considerable difficulties experienced with the apparatus resulted

FIGURE 4.10.   The effect of pore radius on permeability of con-
crete to oil.   (Ref. 68)

in this part of the test programme being significantly curtailed. Only gas flow measurements were ultimately carried out on a reduced number of specimens.

Details of the specimens which were tested at low temperature are given in Table 4.7. Out of the proposed 16 conditions only 6 were investigated. Fortunately, these included the two extreme moisture conditions; sealed-cured, air-dried concrete; and water-cured concrete with no drying. Whilst the test was sufficiently sensitive to detect the gross differences between these two conditions there were a number of inconsistencies, which render the results suspect in absolute terms. Specific values should therefore be viewed with caution.

The effect of low temperature was monitored in three separate test runs as follows:

Run 1 Rig 1 - Control mix AEC; sealed cured and air dried.
       Rig 2 - Control mix AEC; sealed cured and air dried.
       Rig 3 - Steel blank.
       Test Gas - Nitrogen.
       Temperature Range - +20 to -165°C.
       Permeability determined by direct flow measurement.

Run 2 Rig 1 - Mix LW, sealed cured, as cured.
       Rig 2 - Steel blank.
       Rig 3 - Mix AEC, sealed cured, as cured.
       Test Gas - Methane.
       Temperature Range - +20°C to -145°C.
       Permeability determined by analysis of carrier gas.

Run 3 Rig 1 - Mix LW, water cured, as cured.
       Rig 2 - Mix PFA, water cured, as cured.
       Rig 3 - Mix AEC, water cured, as cured.
       Test Gas - Methane.
       Temperature Range - +20°C to -70°C.
       Permeability determined by analysis of carrier gas.

The results obtained during each test run are illustrated in Figures 4.11, 4.12 and 4.13.

An examination of the results obtained from Run 2, and in particular rig 2 which contained the steel blank, illustrates some of the leakage problems identified during proof testing of the carrier gas system. The CH_4 concentration collected by the purge gas increased with the CH_4 concentration in the cryogenic cabinet, as shown in Figure 4.14. This suggests that at temperatures below -70°C, leaks occurred in both the upstream and downstream ends of the system with the transfer of methane from one end to the other via the cabinet thus bypassing the test specimen. The presentation of data graphically in Figure 4.14 enables the leakage rate through the resin seal to be estimated. The linear relationship between the logarithm of CH_4 concentration in the carrier gas, and CH_4 concentration in the cabinet, meets the vertical axis at a point which represents leakage through the resin seal alone, i.e. when the CH_4 concentration in the cabinet is zero. The calculated equivalent permeability coefficient associated with this CH_4 concentration is $9 \times 10^{-22} m^2$, being very similar to the value derived from the leakage tests described in Section 4.3.4.5. Hence, whilst permeability coefficients determined at temperatures above -70°C are not likely to have been significantly influenced by leakage, values measured at -145°C must represent upper bound values only. Comments on each of the three test runs are as follows.

4.4.1.1 Run 1

In run 1, permeability was measured by flow using a soap bubble flow-meter. No results are given for the cell containing the steel blank as no flow was detected. This indicates that leakage through the resin seal was certainly less than $0.2 cm^3$ per hour, this being the lower limit of detection and equivalent to a permeability coefficient of 10^{-20} m^2. This is consistent with the leakage rates measured during proof testing of the system. Furthermore, as the specimens were of relatively high permeability, being of the order

CURING CONDITION	MOISTURE STATE	CONCRETE MIX			
		AEC	HS	LW	PFA
Sealed	As Cured	✗	✓	✓	✗
	Air Dried	✓✓	✗	✗	✗
Immersed	As Cured	✗	✓	✓	✓
	Air Dried	✗	✗	✗	✗

√ indicates specimens tested

TABLE 4.7.   Specimen allocation for low temperature gas permeability testing.
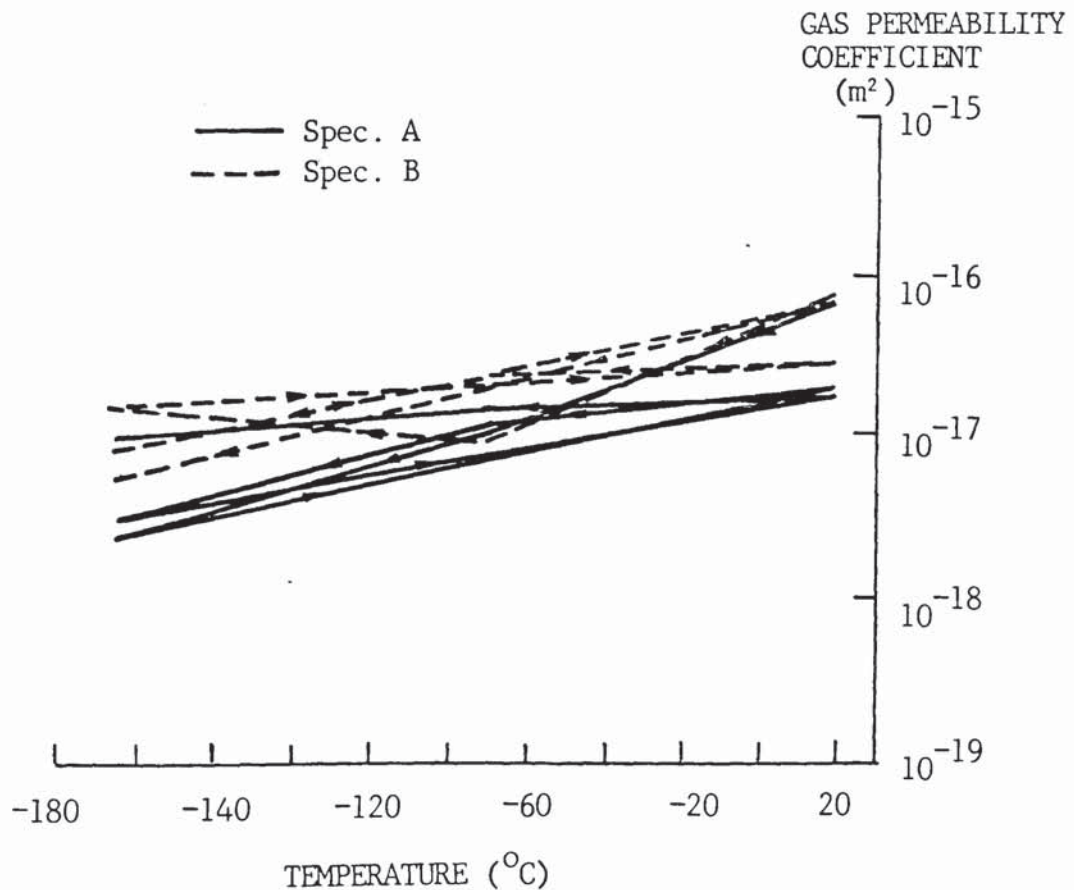
FIGURE 4.11.   Gas permeability coefficients down to -165°C obtained by direct flow measurement using nitrogen (Run 1).
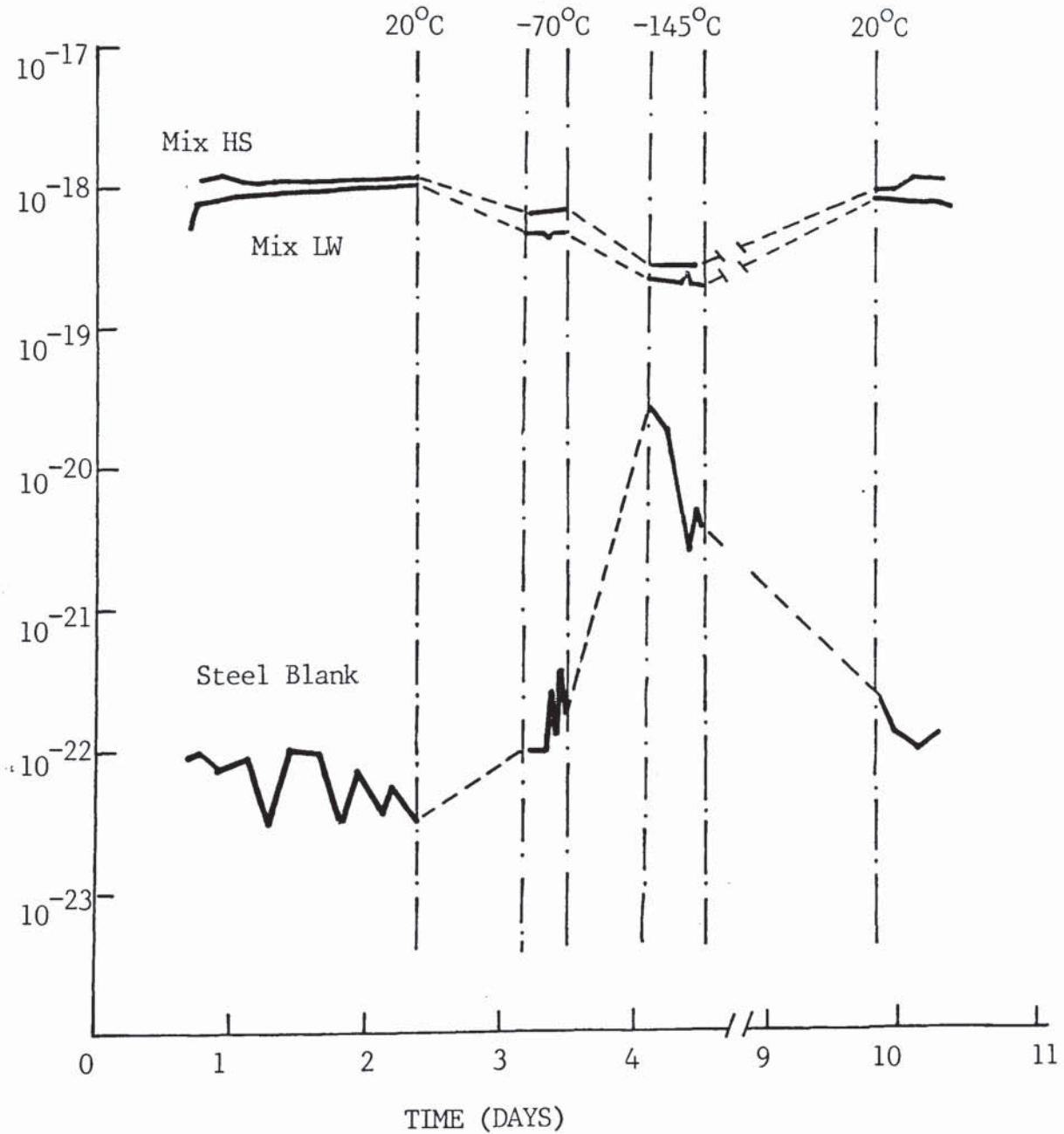
FIGURE 4.12.   Gas permeability coefficients down to -145°C
obtained using the carrier gas method with methane
as the test gas (Run 2).
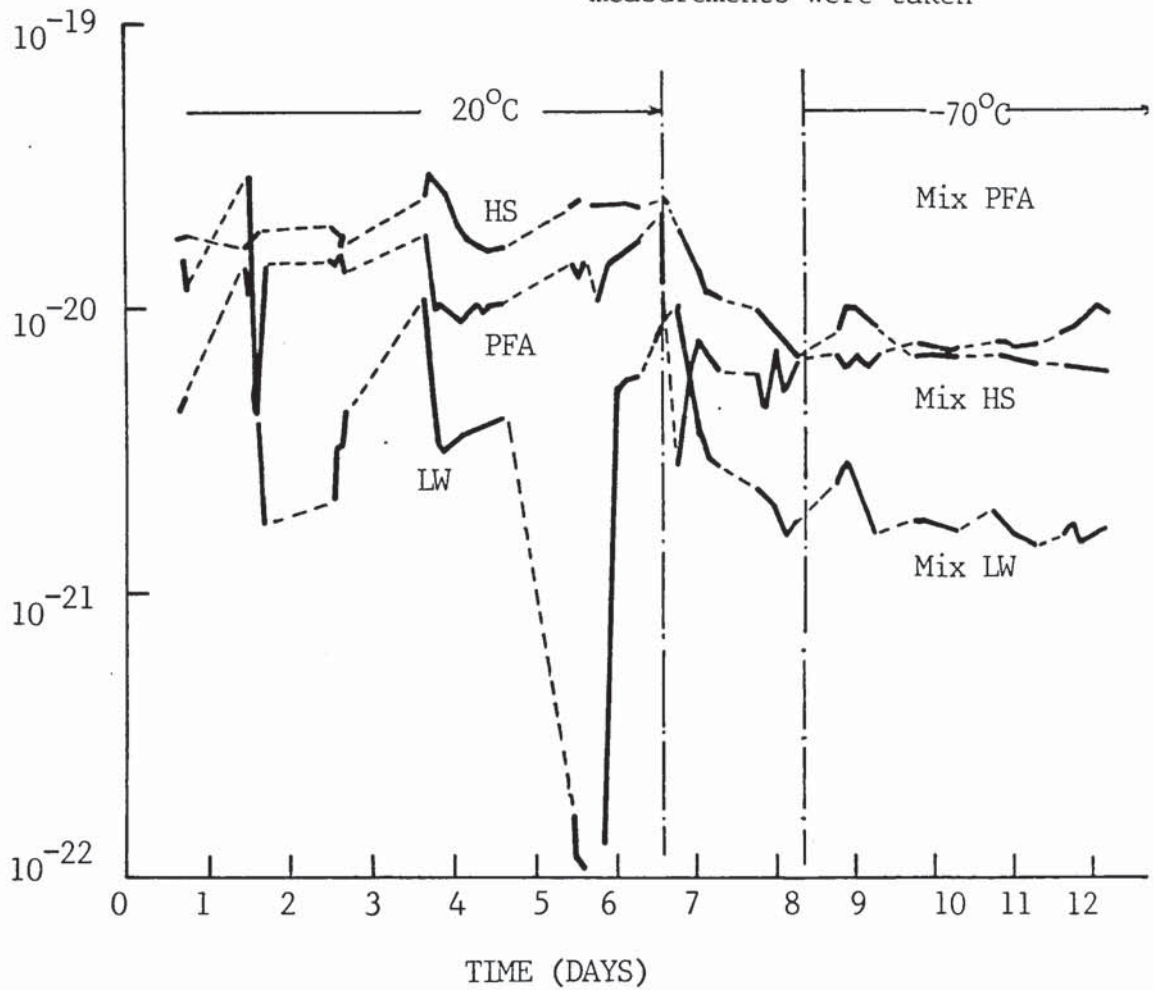
FIGURE 4.13.   Gas permeability coefficients down to -70°C obtained
using the carrier gas method with methane as the
test gas (Run 3).
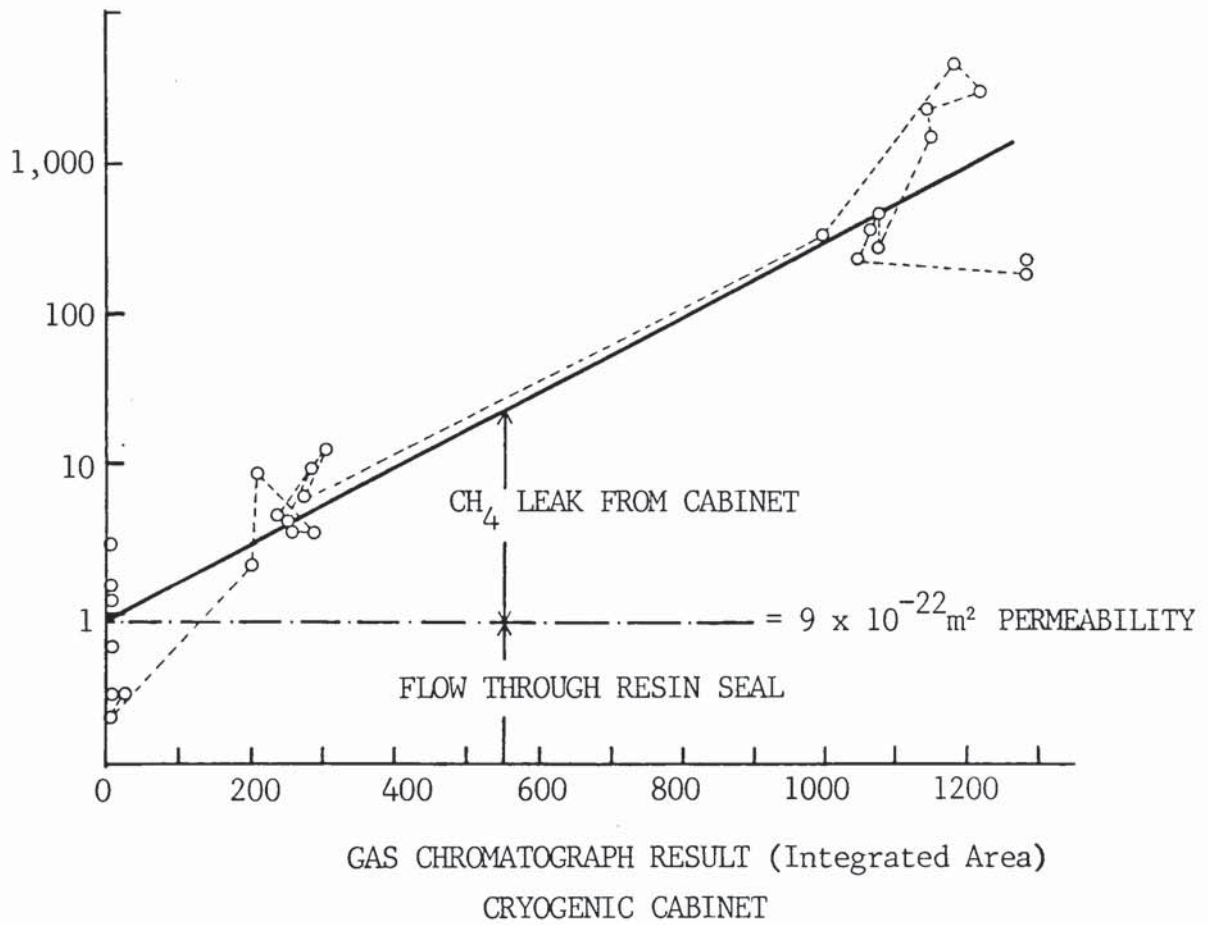
FIGURE 4.14. The methane concentration in the cryogenic cabinet vs the methane leakage into the permeability cell containing a steel blank.

of 3×10^{-17} m^2, leakage will have been of less
significance compared with the high flow rates through
the concrete (10 cm^3/min).

The two specimens were both cycled three times between
20°C and -165°C, and the results are plotted in Figure
4.11. It was interesting to observe that with
progressive cycles, no significant changes were recorded
in permeability. However, the specimens were sealed
cured and air dried prior to testing and so the moisture
content at test will have been very low. Hence, damage
due to ice formation will have been minimised.

4.4.1.2 Run 2

Two specimens were tested, one from each of mixes HS and
LW, as illustrated in Figure 4.12. Both specimens were
maintained in a sealed cured condition until testing.
Whilst rig 2, which contained the steel blank, exhibited
erratic flow behaviour, the cells containing the two
concrete specimens stabilised very quickly at each test
temperature and maintained constant flow rates for
several hours. Furthermore, after completion of the
test, both specimens returned to their original ambient
permeability, once again exhibiting no signs of
disruption due to the thermal cycle.

4.4.1.3 Run 3

Following the success of run 2, it was decided to test
concrete specimens in each of the three rigs. Samples
were selected for mixes HS, LW and PFA. In this case,
all three specimens had been water cured for 28 days,
followed by storage in sealed conditions. Permeability
coefficients were generally about 100 times lower than
recorded during run 2 with values round 10^{-20}m^2. As
shown in Figure 4.13, readings were taken over a period
of several days at ambient temperature before stability
was achieved. Whist it was expected that these very

low permeability mixes would take a long period to achieve steady state conditions, the variability of results at ambient temperature was surprising. It is possible that moisture vapour from the water cured specimens caused problems with the gas chromatograph, but no specific reason was established.

On cooldown to -70°C the results stabilised, contrary to the proof test results which indicated that at low temperature leakage would be more of a problem. The lowest permeability coefficient was again recorded for mix LW with a value of about $1.5 \times 10^{-21} m^2$ at -70°C and about 4 times lower than mixes HS and PFA, which stabilised at about $6 \times 10^{-21} m^2$.

A summary of permeability coefficients obtained during the low temperature tests is given in Table 4.8. It is interesting to note that reducing the temperature, to as low as -165°C, has a relatively small effect on the specific gas permeability, in general less than an order of magnitude. The change in permeability with reducing temperature for each of the seven specimens is shown in Figure 4.15 together with data published by the US Institute of Gas Technology[29]. The relative change in permeability, related to the value at 20°C is shown in Figure 4.16. Whilst there is clearly a reduction in specific gas permeability with reducing temperature, its effect in relation to other influencing factors, such as mix proportions, curing and moisture content is small. This is not surprising. If it is assumed that the only change in the concrete with reducing temperature is its porosity as water expands to form ice, this change will be small, since the water only expands by 9% to form ice. In concrete the total porosity may be of the order of 20% and part of this will be filled with water. For typical in-situ concrete the moisture content by weight is about 5% i.e. 12% by volume. Hence, the remaining 8% of the voids are empty and it is through these voids that gas may flow. When the water is frozen, its volume will increase by 9%, i.e. from 12% to 13% by volume

GAS PERMEABILITY
COEFFICIENT (m²)
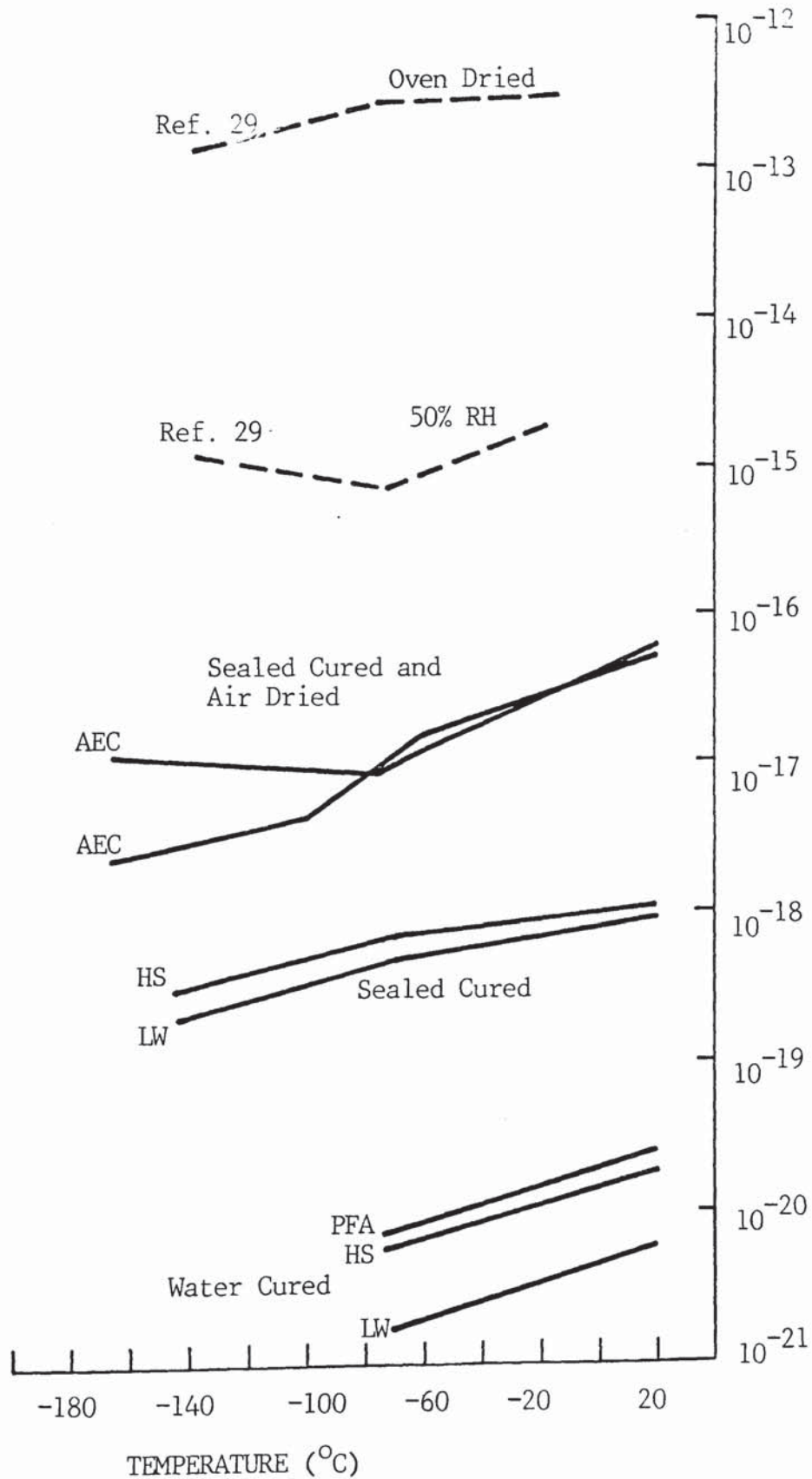
FIGURE 4.15. The influence of temperature on the gas permeability coefficient of concretes subjected to different curing and drying regimes.

MIX	SPECIMEN CONDITION	TEST GAS AND METHOD USE	CYCLE	GAS PERMEABILITY (m^2)			
				20° C	-70°C	-145°C	-165°C
AEC	Sealed cure Air dried	Nitrogen by direct flow	1 2 3	5.03×10^{-17} 1.96×10^{-17} 1.91×10^{-17}	1.02×10^{-17} 1.06×10^{-17} 1.42×10^{-17}		0.23×10^{-17} 0.29×10^{-17} 0.98×10^{-17}
AEC	Sealed cure Air dried	Nitrogen by direct flow	1 2 3	5.50×10^{-17} 2.70×10^{-17} 5.30×10^{-17}	0.85×10^{-17} 2.16×10^{-17} $-$		1.28×10^{-17} 0.88×10^{-17} 0.56×10^{-17}
HS	Sealed cure As cured	Methane by carrier gas	1	1.05×10^{-18}	0.70×10^{-18}	0.30×10^{-18}	
LW	Sealed cure As cured	Methane by carrier gas	1	0.89×10^{-18}	0.50×10^{-18}	0.20×10^{-18}	
HS	Water cured As cured	Methane by carrier gas	1	2.50×10^{-20}	0.60×10^{-20}		
LW	Water cured As cured	Methane by carrier gas	1	0.60×10^{-20}	0.17×10^{-20}		
PFA	Water cured As cured	Methane by carrier gas	1	1.90×10^{-20}	0.80×10^{-20}		

TABLE 4.8.   Summary of low temperature gas permeability results.
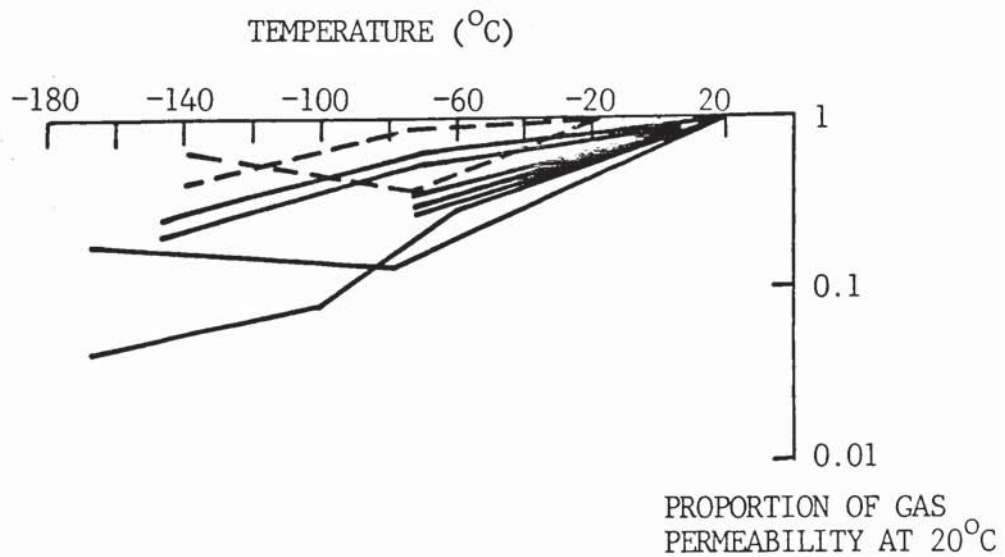
FIGURE 4.16.   Summary of results showing the relative change in gas permeability coefficient with temperature.

- 154 -

of the concrete, difference of only 1%. The open voids still comprise 7%, hence the modest reductions at low temperature are not unexpected.

Despite the experimental problems, the limited results obtained are generally consistent within themselves and when compared both with published data and the earlier water permeability tests (Section 3.4.2). The highest results were obtained for sealed cured, air dried concrete, whilst the lowest values were achieved with water cured concrete. Also the lightweight mix consistently yielded the lowest permeability when compared with other concretes subjected to similar curing conditions. It is therefore likely that the results obtained are a true reflection of the relative performance of the different concretes, the effect of curing and the change in permeability with reducing temperature.

4.4.2 Effect of Thermal Cycling

Gas permeability results obtained at a pressure of 1.03 N/mm^2 are presented in Table 4.9 for each of the 24 no. specimens tested. For each concrete 6 individual specimens were tested prior to thermal cycling, 2 of these specimens were then tested after slow cycling at the rate of 4°C per hour and 2 further specimens were tested after rapid cycling by immersion in liquid nitrogen.

The tests prior to thermal cycling were carried out at a pressure of 1.03 N/mm^2. At this pressure the flow rates were sufficient to enable rapid measurement whilst being slow enough to allow a soap bubble to form in the flow meter. After thermal cycling, however, the permeability of some specimens was such that, at a pressure of 1.03 N/mm^2, the gas flow was too fast for a soap bubble to form. The measurements were therefore repeated at a lower pressure of 0.69 N/mm^2 for all the heat cycled samples. The results obtained at the lower pressure are given in Table 4.10. The relationship between coefficients obtained at the two pressure levels is shown in Figure 4.17 indicating that the permeability coefficient was marginally increased at the lower pressure. The reason for this is discussed in Section 4.4.4.

- 155 -

MIX	SPEC NO	UNCYLED Time For 2cc Flow (sec)	UNCYLED Flow Rate (10^{-6} m³/sec)	UNCYLED Ks (Gas) (10^{-18} m²)	AFTER SLOW CYCLE Time For 2cc Flow (sec)	AFTER SLOW CYCLE Flow Rate (10^{-6} m³/sec)	AFTER SLOW CYCLE Ks (Gas) (10^{-18} m²)	AFTER FAST CYCLE Time For 2cc Flow (sec)	AFTER FAST CYCLE Flow Rate (10^{-6} m³/sec)	AFTER FAST CYCLE Ks (Gas) (10^{-18} m²)
AEC	1b	4.8	0.417	11.44					Too Fast to Form Bubble	
	1c	5.6	0.357	9.81	4.2	0.475	13.05		Too Fast to Form Bubble	
	2a	3.0	0.667	18.31						
	2c	4.4	0.606	12.49	3.1	0.656	18.02			
	3a	3.8	0.526	14.46						
	3b	3.6	0.556	15.26						
HS	1b	9.8	0.204	5.61				1.1	1.850	50.82
	1c	17.8	0.112	3.09						
	2a	70.8	0.028	0.77				3.6	0.550	15.11
	2c	191.4	0.010	0.29	130.2	0.015	0.41			
	3a	57.8	0.035	0.95	24.8	0.081	2.23			
	3b	178.6	0.011	0.31						
LW	1b	141.0	0.014	0.39						
	1c	109.4	0.018	0.50				0.8	2.550	68.67
	2a	128.0	0.016	0.43						
	2c	275.8	0.007	0.20	1.9	1.039	28.54			
	3a	122.2	0.018	0.45	1.5	1.380	37.91			
	3b	69.2	0.029	0.79						
PFA	1b	19.6	0.102	2.80				2.1	0.943	25.90
	1c	9.2	0.217	5.97				4.1	0.494	13.57
	2a	18.4	0.109	2.99	14.1	0.142	3.90		Specimen Cracked	
	2c	15.4	0.130	3.57						
	3a	26.0	0.077	2.11	30.2	0.066	1.81			
	3b	28.0	0.071	1.96						

TABLE 4.9. Gas permeability results at a pressure of 1.03N/mm^2 before and after thermal cycling.

TABLE 4.10.

MIX	SPEC NO	UNCYCLED	AFTER SLOW CYCLE			AFTER FAST CYCLE		
			Time For 2cc Flow (Secs)	Flow Rate (10^{-6} m³/sec)	Ks (Gas) (10^{-18} m²)	Time For 2cc Flow (Secs)	Flow Rate (10^{-6} m³/sec)	Ks (Gas) (10^{-18} m²)
AEC	1b	No readings were taken on uncycled specimens at reduced pressure	13.2	0.152	11.38	2.0	0.985	73.73
	1c					1.4	1.429	106.96
	2a		7.4	0.267	19.99			
	2c							
	3a							
	3b							
HS	1b					3.6	0.556	4.62
	1c							
	2a		Too Slow 23.9	0.042	3.14			
	2c					11.0	0.182	13.62
	3a							
	3b							
LW	1b							
	1c							
	2a		4.6	0.476	35.63	2.1	0.971	72.68
	2c		4.0	0.500	37.43			
	3a							
	3b							
PFA	1b							
	1c		41.7	0.048	3.59	3.7	0.546	40.87
	2a							
	2c		77.4	0.026	1.95	10.0	0.200	14.97
	3a						Specimen Cracked	
	3b							

TABLE 4.10. Gas permeability results obtained during repeat tests at a pressure of 0.69N/mm² after thermal cycling.

GAS PERMEABILITY COEFFICIENT
1.03N/mm² (m²)
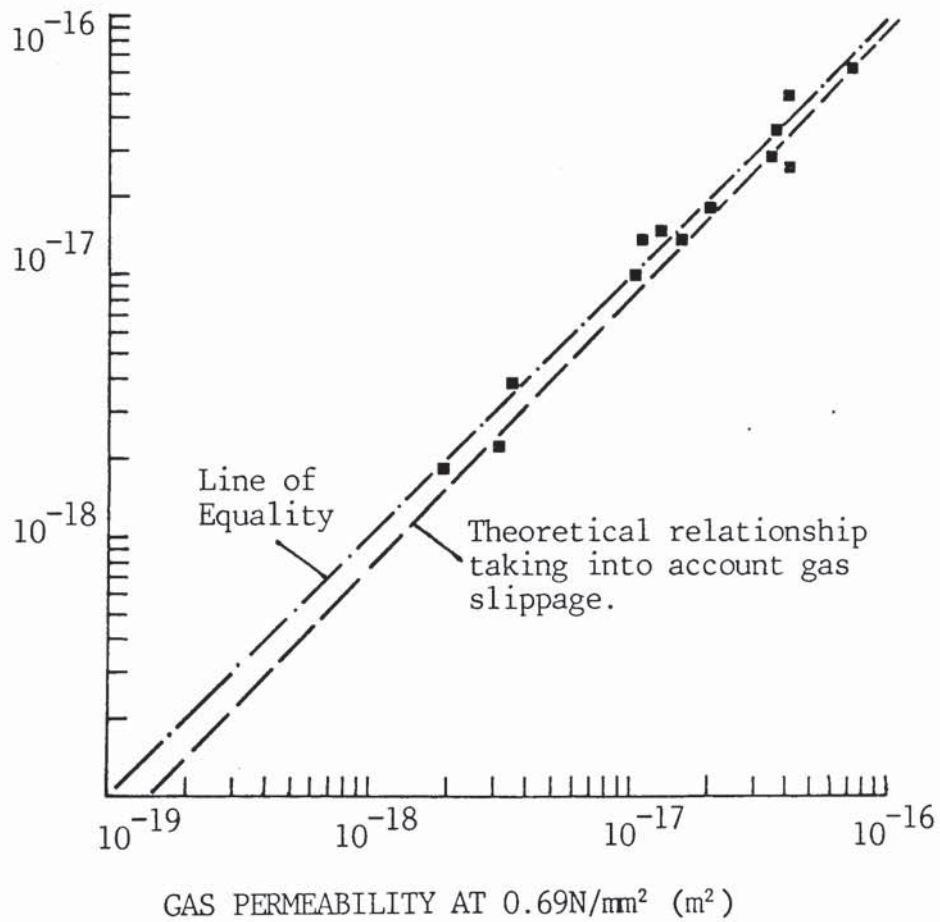
FIGURE 4.17. The relationship between gas permeability coefficients derived at pressures of 1.03N/mm² and 0.69N/mm².

The change in gas permeability resulting from thermal cycling is illustrated in Figure 4.18 which includes the following:-

(1) Individual results obtained before and after thermal cycling.

(2) Mean values of permeability coefficient derived from all specimens tested i.e. 6 no. prior to thermal cycling and 2 no. after either slow or rapid cycling. As the permeability coefficient changes logarithmically, geometric mean values have been determined.

(3) Relative changes in permeability coefficient derived from changes in the geometric mean of specific pairs of specimens, tested before and after thermal cycling.

Permeability coefficients presented in Figure 4.18 have been derived largely from values obtained at the higher pressure of 1.03 N/mm^2, as all the ambient results were obtained at this pressure. Exceptions to this are specimens AEC/2B and AEC/2D after rapid thermal cycling for which the flow rate at the higher pressure was too rapid for a soap bubble to form. For these two specimens therefore, the values obtained at the lower pressure have been used, having been corrected for the pressure difference using equations 4.14 and 4.16.

Examination of the data in Figure 4.18, indicates that the permeability increased as a result of thermal cycling, and more so as the rate of temperature change increased. Three points are of particular interest, however.

(i)   The increase in permeability of the dense aggregate mixes HS, AEC and PFA was only marginal when thermal cycling was slow. Mix HS, the worst affected, increased by a factor of only 2.

(ii) Even after immersion in LN$_2$, the increase in the permeability of mixes HS, AEC and PFA was generally within an order of magnitude. In comparison with changes associated with other factors, e.g. curing, this does not seem excessive, particularly in view of the extreme thermal shock to which the concrete was exposed.
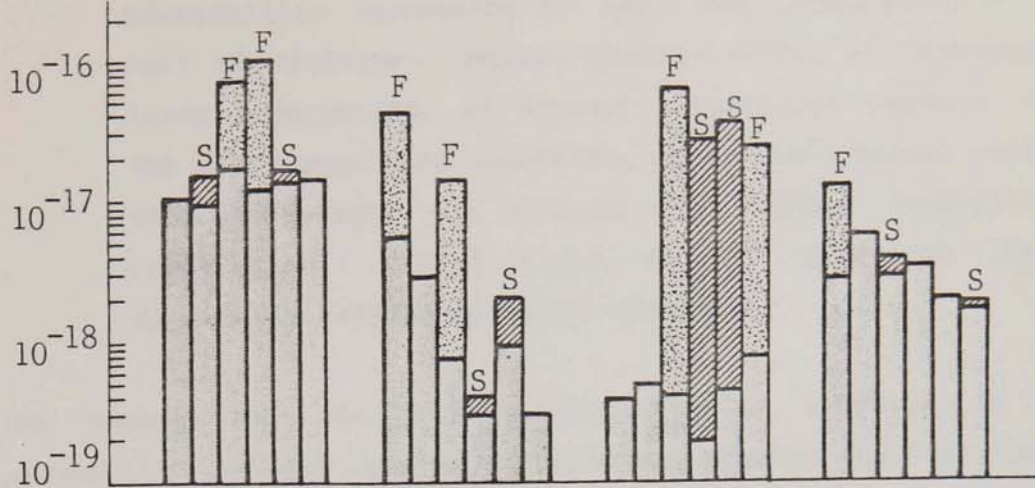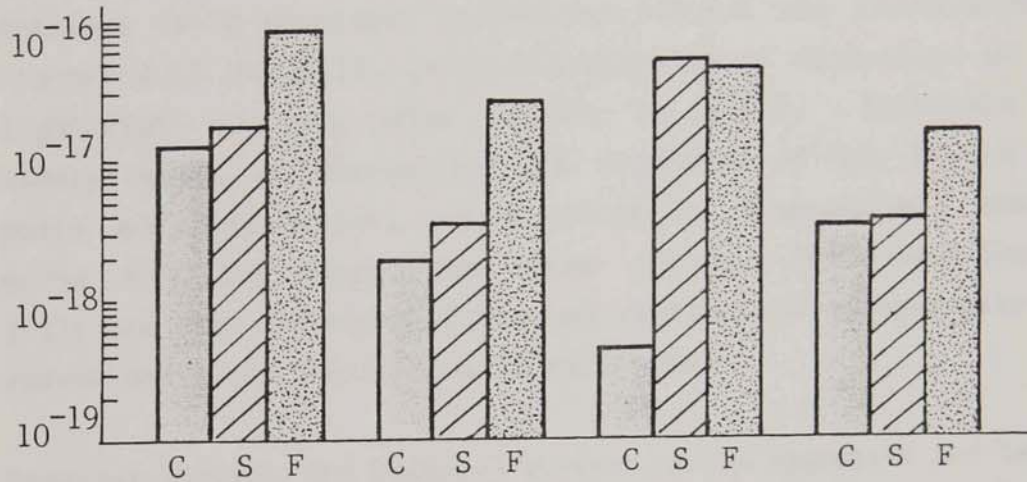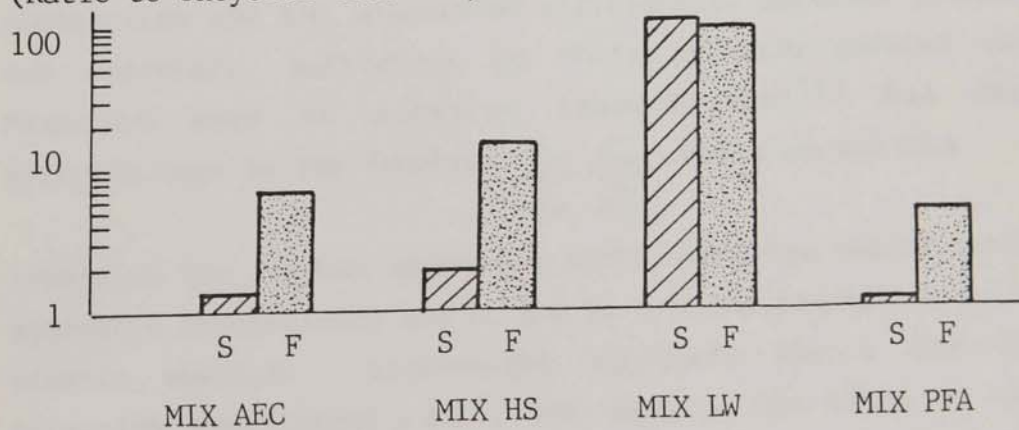
FIGURE 4.18. Gas permeability coefficients obtained before and after thermal cycling.

(iii)   The lightweight concrete, mix LW, was most severely
         affected by thermal cycling, the coefficient of
         permeability increasing by 100 times, regardless of the
         rate of cooldown. Hence, despite having an appreciably
         lower permeability at ambient temperature compared with
         the dense aggregate concretes, after slow thermal cycling
         the lightweight mix yielded the highest permeability
         coefficient.   After rapid cooling there was little
         difference between all four concretes.

The reason for the considerably greater increase in the
permeability of the lightweight concrete compared with the normal
weight mixes has been considered, particularly as the results of
previous tests described in Section 4.4.1.2 and illustrated in
Figures 4.12 and 4.13, gave no indication of disruption of the
lightweight concrete after cooling to -165°C. There are two
likely causes of disruption; the expansion of ice in the gel
pores and capillaries, which occurs in progressively smaller
pores over the temperature range -20 to -70°C (see Section
2.2); and the differential thermal contraction of aggregate and
cement paste and their relative stiffness.

Consider firstly the relative properties of aggregate and cement
paste.   Disruption will occur due to differential thermal
contraction and the associated differential stresses between the
two materials, determined by their relative modulus values.
Previous work at elevated temperatures[71] has related
strength loss to the function $\dfrac{\alpha_c\, E_a}{\alpha_a\, E_c}$ where α_c and α_a

represent the thermal expansion coefficient for cement paste and
aggregate respectively and E_c and E_a are the respective values of
elastic modulus.   Lightweight aggregate has a low thermal
expansion coefficient, α, but also a low value of elastic
modulus compared with dense aggregate. These two factors are
counteracting, the lower value of α_a resulting in higher
differential thermal strains, whilst the lower modulus reduces
the associated stresses.   The nett effect is difficult to
quantify but the influence of low modulus is likely to be
predominant as, in terms of concrete properties, the use of

lightweight aggregate has a more significant effect on elastic modulus than it does on thermal expansion coefficient[72]. This being the case disruption due to differential thermal stresses would be expected to be reduced by the use of lightweight aggregate.

Now consider the likely disruption due to ice formation during cooling. Lightweight concrete has a much higher moisture content by virtue of the porous aggregate. However, the volume of water penetrable voids is also greater. Relative values of water/voids ratio have not been measured. However, the total porosity of the lightweight mix has been determined by mercury porosimetry and compared with results obtained for mix AEC, the air entrained control concrete. These results are discussed in more detail in Section 4.4.3 but average values of total porosity for the two mixes, tested prior to thermal cycling, were 9.8% for mix AEC and 22.6% for mix LW, an absolute difference of 12.8% but a relative difference of almost 100%. The difference in free moisture would be largely due to the water absorbed by the lightweight aggregate. For mix design purposes this is normally assumed to by 12% by weight of dry aggregate, in this case $0.12 \times 720 = 86.4$ litres = $0.0864m^3$ or 8.6% by volume of the concrete.

The extent of damage likely to occur due to the formation of ice would be expected to be determined by the ratio of water content to water penetrable voids. If the above analysis is correct, and total porosity determined by mercury intrusion can be assumed to be equivalent to water penetrable voids, the ratio reduces for Lytag concrete i.e. the increase in porosity compared with normal weight concrete is greater than the increase in moisture content. This being the case, less disruption would be expected. This is not consistent with the considerable increase in permeability. All the pores in concrete are not water penetrable, however. It has been reported that, in water permeability tests, no flow is achieved through pores with a radius less than 650Å.[70]. The average values of porosity obtained for mixes AEC and LW, recalculated to omit pores smaller than 650Å radius are 11.0% and 5.1%, an absolute difference of only 5.9% but again a relative difference of 100%. Using these modified figures, the

- 162 -

increase in water penetrable porosity associated with the use of the lightweight aggregate is less than the increase in water content hence, as observed, disruption is more likely as discussed in Section 4.4.3.

As the permeability of the lightweight concrete increased significantly as a result of thermal cycling, the predominant effect, therefore, must have been the increased ratio of water content to water penetrable voids. The influence of the thermal expansion coefficient and lower modulus of the aggregate, which would tend to minimise the disruption of the lightweight concrete is apparently of secondary importance under conditions of extreme thermal cycling to very low temperatures.

The above analysis applies to concrete in which the expansion due to ice formation can occur unrestrained. In the previous tests, however, in which the residual permeability after thermal cycling was unaffected, the concrete specimens were confined in the stainless steel cell. Furthermore, as the specimens were cooled down, contraction of the cell would impose an effective prestress in the concrete. Hence, ice formation would be unable to cause expansive and disruptive strains. Measurement of the thermal contraction of both unrestrained and prestressed concrete has been undertaken by Elices[73] which has demonstrated that even modest prestress will inhibit the expansion caused by ice formation, supporting the above hypothesis. This is clearly an area which requires further investigation as in most instances the concrete used in cryogenic storage tanks, particularly in primary containments, will be prestressed.

4.4.3 Relationship between Permeability and Pore Structure

Graphical presentations of differential and cumulative pore size distributions for individual test specimens obtained using mercury intrusion porosimetry are given in Figures 4.19 and 4.20, to compare the pore characteristics of mixes AEC and LW. Various pore parameters have been derived from the test. These include total pore volume and the associated surface area and hydraulic radius, the maximum continuous pore radius (MCPR), and the pore
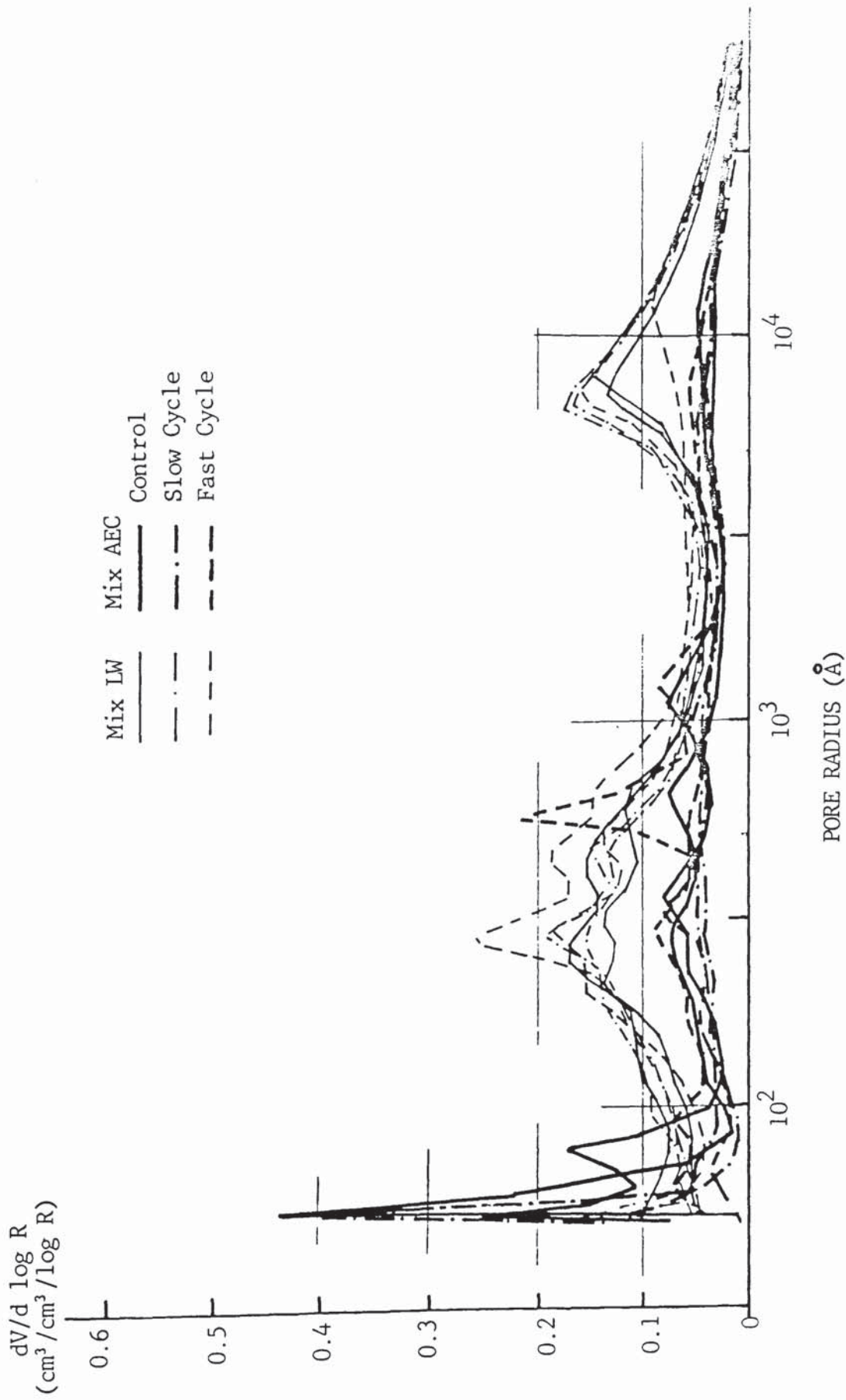
FIGURE 4.19. Differential pore size distributions for Mixes AEC and LW before and after thermal cycling.
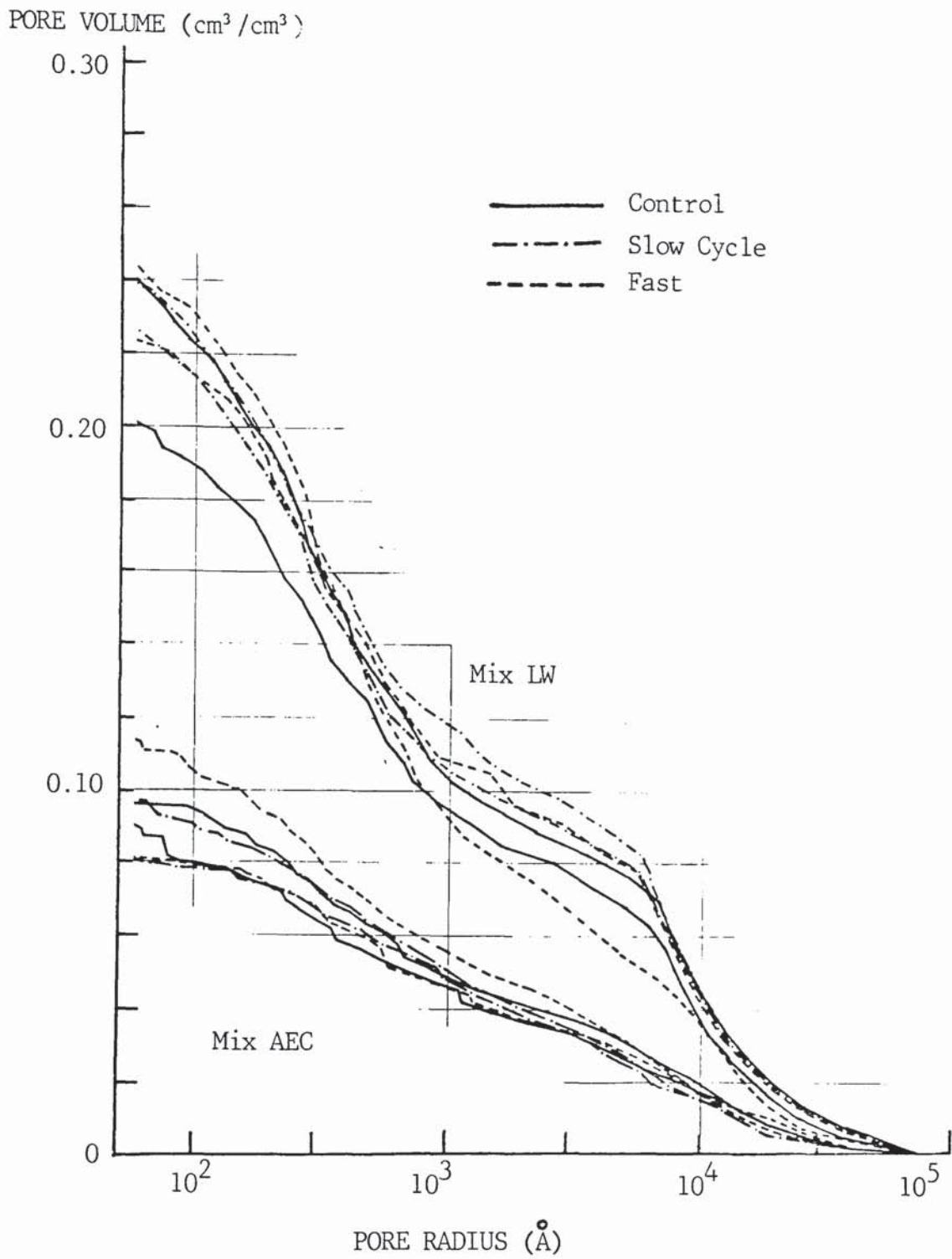
FIGURE 4.20. Cumulative pore size distributions for Mixes AEC and LW before and after thermal cycling.

volume, surface area and hydraulic radius excluding pores less than 660Å radius. These pore parameters are given in Table 4.11.

There are two particular features of the results which are of interest.

(i)   The difference in the pore structures of the two mixes is clearly identified. The lightweight mix has a total pore volume of the order of 20-25%, compared with a value of the order of 10% for the control mix. The difference is largely due to a higher proportion of voids in the lightweight concrete in two ranges; 100-1000Å and above about 5000Å. Within each range, the additional volume of voids present in the lightweight mix is of the order of 7% and 5% respectively.

(ii)   Thermal cycling does not appear to have significantly affected the pore size distribution of either concrete, as determined by mercury intrusion porosimetry. Despite the 100 times increase in gas permeability coefficient for mix LW (after both slow and rapid cooling) and almost ten times increase for mix AEC after rapid cycling, gross changes in the pore parameters were not detected. Small increases in the average pore volume were identified for the cycled specimens however. These average changes in pore volume are presented graphically in Figure 4.21 in relation to the average increase in gas permeability determined previously. Whilst the trend is for increasing gas permeability with increasing pore volume, the scatter of results prohibits a more detailed analysis.

Hence for each individual concrete, thermal cycling resulted in an increase in average porosity, with the tendency for the greatest increase in porosity to be associated with the greatest increase in gas permeability. However, comparing the two concretes (mixes AEC and LW), the lightweight mix has a porosity which is more than double that of the gravel aggregate concrete, but as shown in Table 4.9 has a gas permeability which is, on

MIX	SPEC NO	TEMP CYCLE	PORE VOLUME (cm³/cm³)		HYDRAULIC RADIUS (Å)		SURFACE AREA (m²/g)		MCPR (Å)
			Total	660A	Total	660A	Total	660A	
AEC	1b-M	–	0.099	0.054	192.6	1192.2	5.16	0.46	31,250
	1b-S	–	0.097	0.048	123.6	1282.3	7.83	0.37	31,250
	2c-M	Slow	0.115	0.059	169.2	1237.9	6.81	0.48	21,875
	2c-S	Slow	0.081	0.049	283.4	1253.6	2.87	0.39	21,875
	3a-M	Rapid	0.103	0.055	114.7	1130.6	7.10	0.49	16,875
	3a-S	Rapid	0.091	0.054	135.6	1084.9	6.72	0.50	16,875
LW	1b-M	–	0.247	0.116	146.1	1218.6	16.93	0.95	21,875
	1b-S	–	0.205	0.103	173.0	1380.5	11.82	0.74	31,250
	2c-M	Slow	0.229	0.116	172.4	1340.2	13.28	0.86	31,250
	2c-S	Slow	0.245	0.122	159.9	1538.0	15.33	0.79	31,250
	2a-M	Rapid	0.229	0.118	180.4	1440.9	12.71	0.82	21,875
	2a-S	Rapid	0.250	0.110	158.8	975.0	15.72	1.13	21,875

TABLE 4.11. Concrete pore characteristics before and after thermal cycling.

RATIO TO PERMEABILITY
COEFFICIENT OF
UNCYCLED CONCRETE
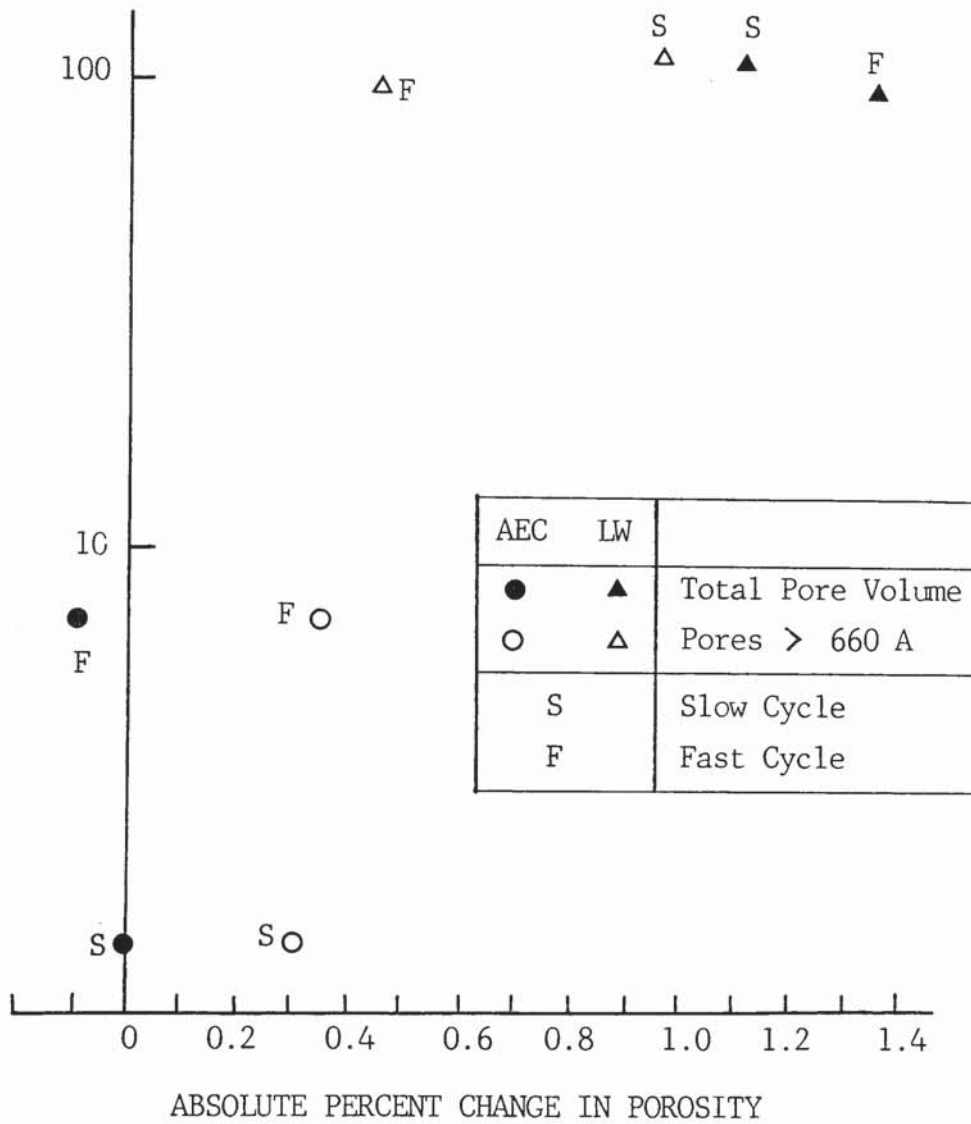
FIGURE 4.21.   The relationship between the change in gas per-
meability coefficient and the change in porosity.

average, about 30 times lower. This clearly indicates that the measurement of porosity, using the mercury porosimeter above, is unlikely to be sufficient to predict, or even crudely estimate the value of gas permeability. Other pore parameters have been considered such as hydraulic radius, surface area and HCPR, for both the total porosity and for pores greater than 660Å radius. Once again, the higher values are associated with the lightweight concrete, despite its lower permeability.

4.4.4 Relationship Between Water and Gas Permeability

Values of water permeability obtained for the four mixes are given in Table 4.12. The low permeability coefficients were derived from penetration measurements using the Valenta equation discussed in Section 4.2. Only two specimens from mix AEC were sufficiently permeable for flow measurement to be achieved within 24 hours of the start of the test. The water permeability coefficients, converted to units of m^2 are given in Table 4.13 together with the gas permeability coefficients for non-cycled specimens presented in Table 4.7. For each cylinder two values of gas permeability and one value of water permeabiity have been determined.   Also included in Table 4.13 are geometric mean values for each mix.

The results are presented graphically in Figure 4.22.   As expected there is a relationship between the two coefficients, but the values are not equal, with the difference increasing as the permeability reduces. For the most permeable concrete, mix AEC, the gas permeability coefficient is 5 to 6 times the water permeability coefficient (13.35×10^{-18} c.f. 2.39×10^{-18}). For mix LW, the least permeable concrete, the difference is of the order of 60 times (0.43×10^{-18} c.f. 0.73×10^{-20}).

The difference between values of permeability obtained using liquid and gas has been investigated previously by Klinkenberg[74].   Tests were carried out using relatively high permeability materials (largely in the range 10^{-15} to 10^{-13} m^2) to support calculations of flow in underground oil and gas reservoirs.   Klinkenberg reported a difference in permeability

MIX	SPECIMEN NO.	PENETRATION		FLOW		THICKNESS (mm)	WEIGHT CHANGE (gms)	WATER PENETRATED VOIDS (%)	PERMEABILITY COEFFICIENT (m/sec)
		Depth (mm)	Time (Days)	Volume (cm³)	Time (min)				
AEC	1a	-	-	0.5	14m30s	50.2	30.3	7.69	3.67×10^{-11}
	2b	50	1.25	-	-	50.0	26.5	6.89	7.80×10^{-11}
	3c	-	-	1.0	25m2s	52.2	23.4	5.96	4.43×10^{-11}
HS	1a	46	12	-	-	51.6	18.9	5.23	5.34×10^{-13}
	2b	35	12	-	-	51.5	14.3	5.20	3.07×10^{-13}
	3c	32	13	-	-	51.0	14.5	5.77	2.63×10^{-13}
LW	1a	7	13	-	-	52.2	8.1	14.73	3.21×10^{-14}
	2b	6	12	-	-	50.0	6.9	14.64	2.54×10^{-14}
	3c	40	25	-	-	53.9	38.3	12.19	45.15×10^{-14}
PFA	1a	46	12	-	-	52.9	17.6	4.87	4.97×10^{-13}
	2b	35	13	-	-	51.5	13.4	4.87	2.66×10^{-13}
	3c	40	13	-	-	51.0	17.7	5.63	4.01×10^{-13}

TABLE 4.12. Water permeability results obtained at a pressure of $1.03 N/mm^2$.

MIX	SPECIMEN NO.	GAS PERMEABILITY COEFFICIENT kg $(10^{-18}m^2)$	WATER PERMEABILITY COEFFICIENT kl $(10^{-18}m^2)$	kg/kl
AEC	1	11.44/9.81	3.74	
	2	18.31/12.49	0.81	
	3	14.46/15.26	4.52	
	Mean	(13.35)	(2.39)	5.6
HS	1	5.61/3.09	5.44×10^{-2}	
	2	0.77/0.29	3.16×10^{-2}	
	3	0.95/0.31	2.68×10^{-2}	
	Mean	(1.02)	(3.58×10^{-2})	28.5
LW	1	0.39/0.50	3.27×10^{-3}	
	2	0.43/0.20	2.59×10^{-3}	
	3	0.45/0.79	46.05×10^{-3}	
	Mean	(0.43)	(7.31×10^{-3})	58.8
PFA	1	2.80/5.97	5.07×10^{-2}	
	2	2.99/3.57	2.71×10^{-2}	
	3	2.11/1.96	4.09×10^{-2}	
	Mean	(3.01)	(3.83×10^{-2})	78.5

TABLE 4.13. Average water permeability and gas permeability coefficients.
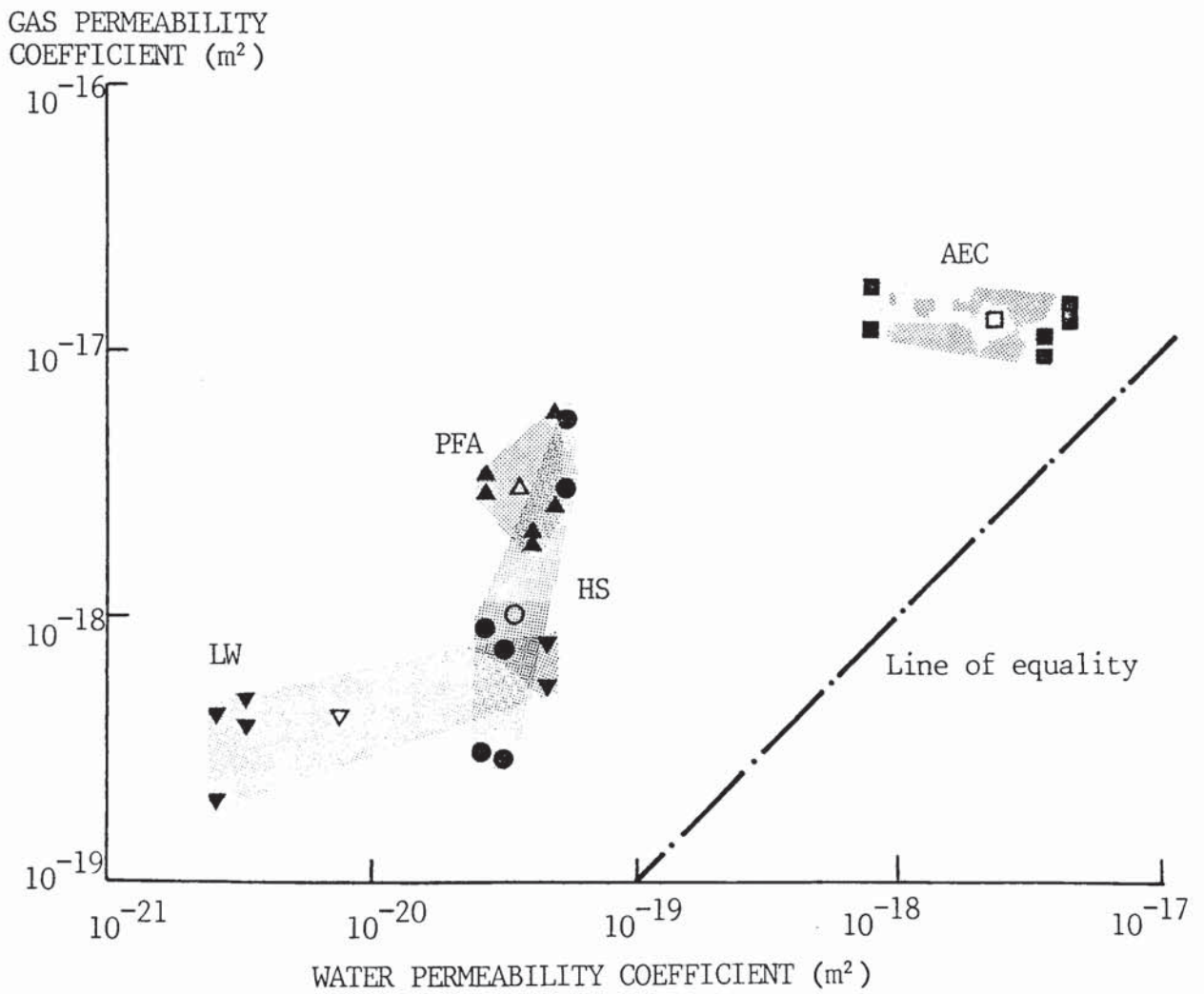
FIGURE 4.22.   The relationship between water permeability and gas
permeability showing individual test results.

coefficient for liquids and gases and stated that '....with highly permeable media, the differences between liquid and air permeability were small, whereas these differences were considerable for media of low permeability'. The difference was explained by the theory of slip in the flow of gas, whereby the gas in the immediate vicinity of the wall has a finite velocity. As a consequence the quantity of gas flowing through a capillary is larger than would be predicted from Poiseulles formula. The gas slippage theory suggests that the flow of gas will be affected by pressure (which in turn influences the mean free path) and Klinkenberg derived an equation relating liquid and gas permeability k_l and k_g to the mean pressure at which the gas is flowing p_m as follows.

$$k_l = \frac{k_g}{1 + \frac{b}{p_m}} \qquad (4.14)$$

where b is a constant for a given gas and a given porous medium. The work by Klinkenburg was extented by an API Special Research Project[75] in which the constant b was derived for oil sands from various sources by the equation

$$b = 0.777 \, k_l^{-0.39} \qquad (4.15)$$

where k_l is measured in millidarcies $= 10^{-15} m^2$.

From these two equations it will be seen that, as stated by Klinkenberg, the difference between k_l and k_g increases as the permeability reduces. The relationship between k_l and k_g , calculated using equations (4.14) and (4.15) is shown in Figure 4.23 assuming a mean gas pressure of 5 bar (as used during this test programme). It will be seen that the equation tends to over estimate the value of k_l when derived from k_g . Clearly, the relationship between k_l and the constant b, derived for oil sands does not apply to concrete. An alternative relationship between k_l and b has therefore been derived from the results of the current programme.

GAS PERMEABILITY COEFFICIENT (m²)

Data from Ref. 74

API Relationship (Ref. 75)

LINE OF EQUALITY

WATER PERMEABILITY COEFFICIENT (m²)
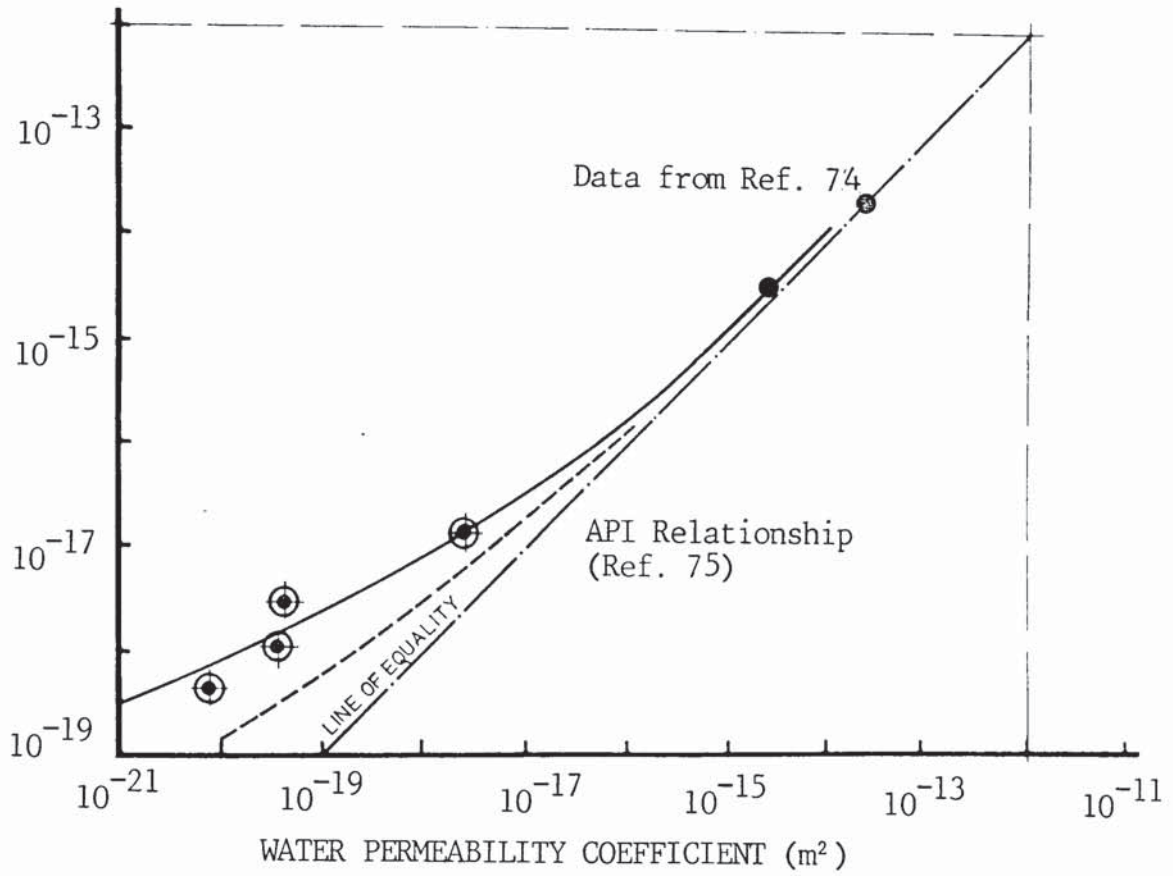
FIGURE 4.23. Theoretical relationship between water permeability and gas permeability coefficients based on Klinkenberg's equation and API Data for oil sands.

Values of b , calculated from the average values of water permeability k_l and gas permeability, k_g , for each of the four concretes tested, are illustrated in Figure 4.24. Also included is the relationship for oil sands proposed by the API and some original data published by Kinkenberg for Jena Glass and core samples. It would appear that a single relationship can be derived which is applicable to both Klinkenbergs data and the results for concrete. This is of the form

$$b = \frac{1 \cdot 635 \ k_l^{-0 \cdot 5227}}{10^8} \qquad (4.16)$$

where k_l is measured in units of m^2. Using this equation to calculate values for b, and by substitution in equation 4.14, the relationship between k_l and k_g has been derived. This is also shown in Figure 4.23 and provides a reasonable representation of the results obtained.

The slippage theory proposed by Klinkenberg to explain differences between permeabilities measured using liquid and gas, can therefore be applied to concrete. It should be noted however that other factors, such as moisture content, will influence the relationship between k_l and k_g . However, this is beyond the scope of the current work.

Having established that the slippage theory proposed by Klinkenberg can be used to explain differences between permeability coefficients for concrete measured using liquid and gas, it is possible to predict specific permeability from values of gas permeability and the applied test pressure. Figure 4.25 has been developed using equations 4.14 and 4.16 and illustrates the relationship between k_l and k_g for a range of mean pressures from 0.1 to 100 atmospheres. For typical structural concrete, which is likely to have an intrinsic permeability in the range 10^{-19} to 10^{-17} m^2[60], gas permeability values may be one to two orders of magnitude higher. For example, at a mean pressure of 5 atmospheres, concrete with a water permeability of
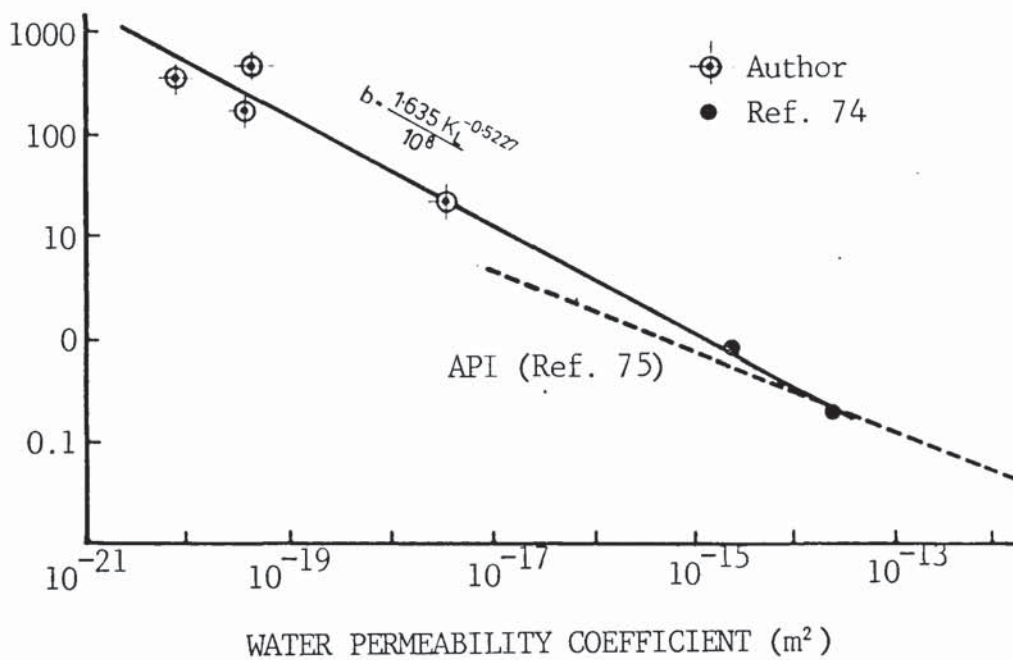
FIGURE 4.24. Relationship between water permeability and the constant b.

GAS PERMEABILITY
COEFFICIENT (m²)
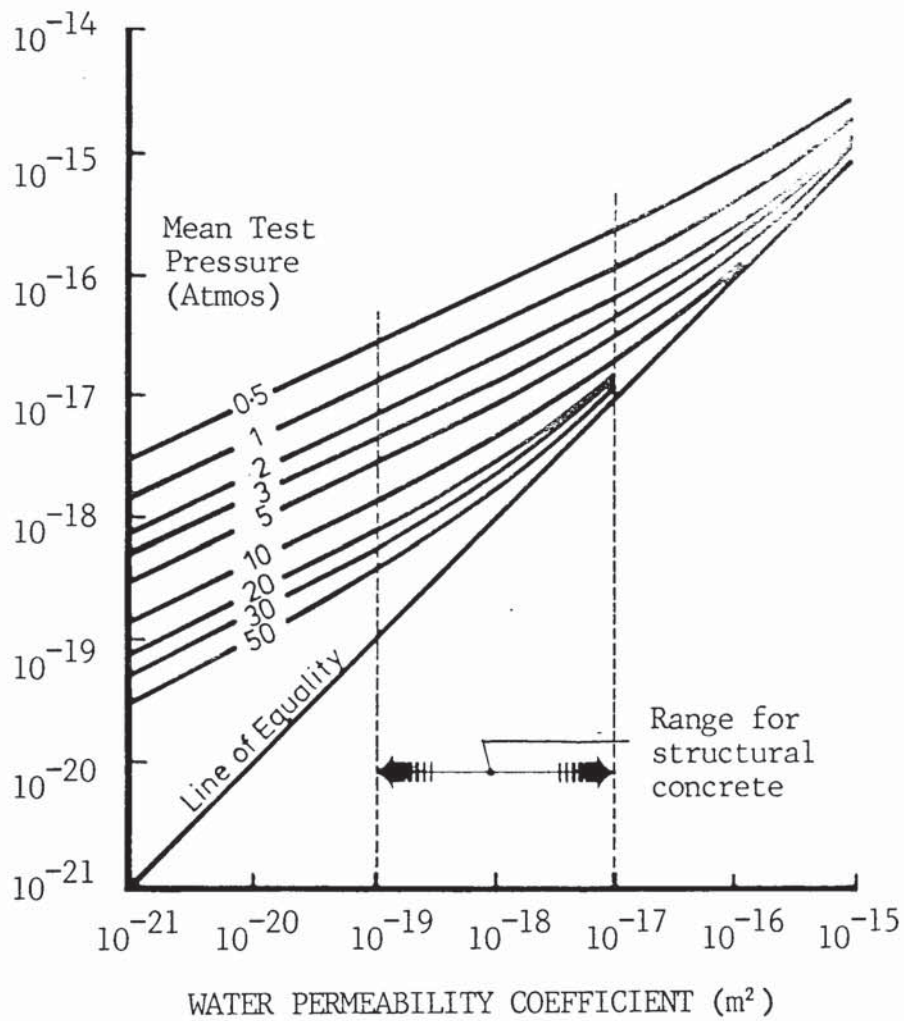
FIGURE 4.25. Proposed relationship between water permeability
and gas permeability and the influence of test
pressure.

10^{-18} m^2 may yield a gas permeability coefficient of about 10^{-17} m^2. The largest difference would occur when testing using a partial vacuum. For the typical structural concrete considered above, the difference between gas and water permeability could be as large as 100 times under such conditions. It is, therefore essential that when interpreting results obtained from measurements of gas permeability, the effect of slippage is taken into account.

This is of particular importance as there appears to be a move towards gas permeability measurements as a means of assessing quality. Test pressures vary from sub-atmospheric using the Figg test[76] to 1 MPa, used by the BRE in their recently proposed test using 100mm concrete cubes[77]. Without an understanding of the nature of gas flow through concrete, and the significance of test pressure, a comparison between the results from the different tests cannot be made.

5.   TENSILE CHARACTERISTICS

5.1 INTRODUCTION

The ability of concrete to resist cracking is determined primarily by
its tensile properties. Either the tensile strength must exceed the
imposed tensile stress, or the tensile strain capacity must exceed the
tensile strain. When the strains are thermally induced the thermal
expansion coefficient of the concrete is also an important factor. If
the thermal expansion coefficient is low, the strain associated with a
given temperature change will also be low. Hence, to minimise cracking
in a structure which will be subject to thermal load, the concrete
should have a low thermal expansion coefficient combined with a high
strain capacity.

Tests have been carried out to measure these characteristics for the
four selected concretes described in Table 4.1. The tensile behaviour
has been measured both in direct tension and under flexural load. The
measurement of thermal expansion coefficient is described in
Chapter 6.

5.2 EXPERIMENTAL DETAILS

5.2.1 Strain Measurement

The measurement of strain capacity, whether in direct tension or
in flexure, over the temperature range imposed upon a LNG tank in
service, required a method of strain measurement which would
operate down to -165°C. Vibrating Wire Strain Gauges (VWG's) had
been extensively used by Taylor Woodrow at elevated
temperatures[78] and it was, therefore, decided to evaluate
their performance at cryogenic temperature. As the name
indicates, VWG's operate on the principal of changing frequency
of vibration with changing stress in a tensioned wire. (Figure
5.1). When a gauge is embedded into, or fixed to the surface of,
a concrete specimen, changes in strain in the concrete are
measured as changes in the period of vibration for 100 cycles.
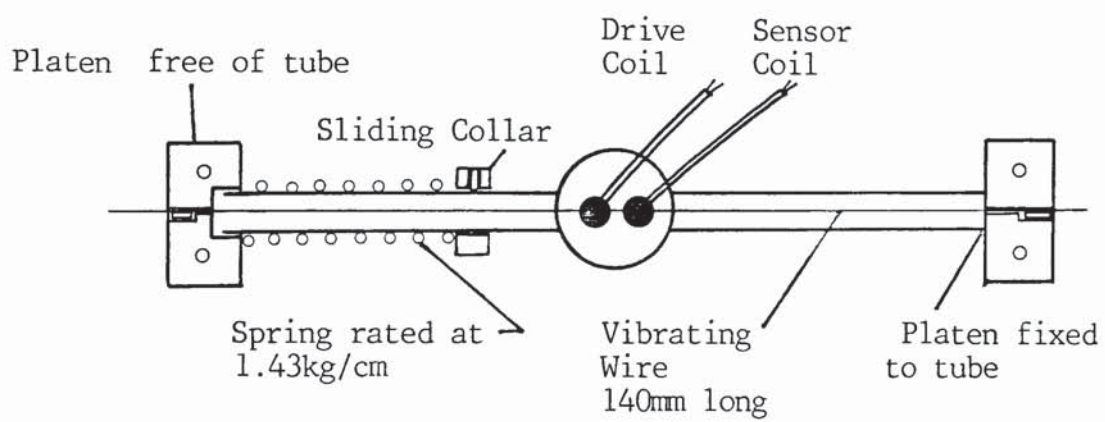
FIGURE 5.1. Vibrating wire strain gauges (VWG)

The frequency of vibration (f), is given by equation:-

$$f = \frac{1}{2L}\sqrt{\frac{P}{m}}$$ (5.1)

where L = length of the wire (in m)

P = load in the wire (in N)

m = mass per unit length of wire (in kg/m).

The load in the wire $P = f_t . A$

Where f_t = stress (in N/m^2)

A = cross section area (in m^2).

But, $f_t = E.\varepsilon$

where E = elastic modulus of the wire (in N/m^2)

ε = strain in the wire (in m/m)

Hence $P = E.\varepsilon.A$

Substituting in equation 5.1.

$$f = \frac{1}{2L}\sqrt{\frac{E.\varepsilon.A}{m}}$$

Rearranging,

$$\varepsilon = \frac{4L^2.f^2.m}{A.E}$$

The change in strain is calculated from the change in period reading, where $p = \frac{1}{f}$

Hence, $\Delta\varepsilon = \varepsilon_2 - \varepsilon_1 = \frac{4L^2 m}{E.A}\left(\frac{1}{p_2^2} - \frac{1}{p_1^2}\right)$ (5.2)

The term $\frac{4L^2 m}{E.A}$ is the gauge factor, as the values L, A, m, E are generally fixed for a particular gauge. The influence of temperature on each of these factors has been considered in relation to the change in gauge factor likely to occur at $-165°C$. In a gauge which is unrestrained, the length will change in proportion to the thermal expansion coefficient of the stainless steel tube which separates the plattens to which the wire is clamped. From a review of the literature on the cryogenic properties of steel, summarised in reference 79, the average thermal expansion coefficient will be about 9 microstrain per °C, resulting in a total shortening of 1665 microstrain between 20°C and $-165°C$.

This is about 0.17%. As the wire shortens, the weight per unit length will increase by a similar amount. In addition, the cross sectional area will reduce by about 0.35%. The major change will occur in the elastic modulus. For reinforcing steel and prestressing strand, the modulus increases as the temperature is reduced[79]. At $-165°C$ the modulus is 5-10% higher than at 20°C. The changes resulting from thermal contraction and its effect on weight per unit length and c.s.a. amount to about 0.5% and are not, therefore, considered to be significant. The change in modulus of the wire, however, would be expected to reduce the gauge factor by between 5 and 10%.

Calibration tests were carried out to check the gauge factor at ambient temperature, and to determine the change in gauge factor as the temperature reduced to $-165°C$. A rig was manufactured specifically for this purpose. This is illustrated in Figure 5.2 and full details of the gauge calibration tests are given in Appendix 3. To check the gauge factor at ambient temperature, four dial gauges were incorporated into the system. Strain was imposed on the gauges using a differential screw system which gave 478.5 microstrain ($\pm$ 2%) per revolution over the 140mm gauge length. Calibration tests were carried out as follows:-

i)   Three test runs with all eight gauges at ambient temperature to determine the gauge factor at 20°C.

Differential Screw

Vibrating Wire Gauges (4 No.)
(NB. For ambient calibration tests
2 No. VWG's were replaced by dial
gauges)

Insulated Cabinet

Temperature Controlled Environ-
ment (ambient to $-196°C$)

Gauges for Calibration
at Low Temperature
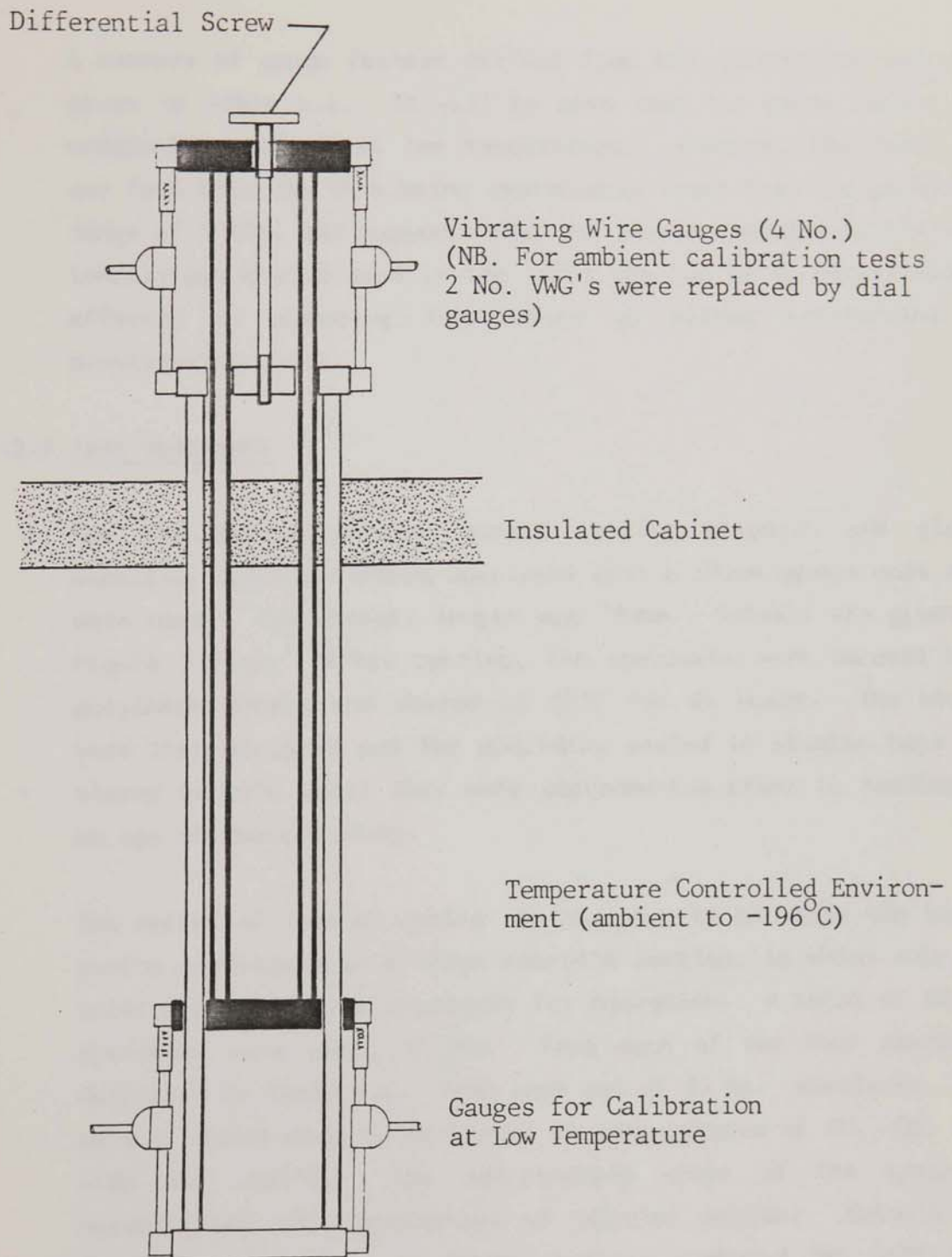
FIGURE 5.2. Test rig for VWG calibration at ambient and cryogenic
temperature.

ii) Four test runs with four gauges at 20°C and four gauges at
    -162°C.

A summary of gauge factors derived from the calibration tests is
given in Table 5.1. It will be seen that the gauge factor was
marginally reduced at low temperature. However, the reduction
was less than 2%, this being appreciably lower than the predicted
range of 5-10%, and suggests that the elastic modulus of the high
tensile piano wire used in the VWG's may not be as significantly
affected by reducing temperature as either reinforcing or
prestressing steel.

5.2.2 Test Specimens

For the measurement of direct tensile strength and strain
capacity, dog-bone shaped specimens with a 100mm square neck area
were used. The overall length was 750mm. Details are given in
Figure 5.3(a). After casting, the specimens were covered with
polythene sheets and stored at 20°C for 24 hours. The moulds
were then stripped and the specimens sealed in plastic bags and
stored at 20°C until they were instrumented prior to testing at
an age of about 8 weeks.

The method of 'sealed curing' is designed to simulate the insitu
curing conditions in a thick concrete section, in which only the
initial mix water is available for hydration. A total of 60 No.
specimens were cast, 15 No. from each of the four concretes
described in Table 4.1. From each set of 15 No. specimens, five
sets of three were to be tested at temperatures of 20, -20, -70,
-120 and -165°C. The non-standard shape of the specimens
necessitated the manufacture of special moulds. Details are
given in Appendix 1 on three drawings numbered TWC D6351/014,
Sheets 1-3.

For the measurement of strength and strain capacity in flexure,
standard beams measuring 100 x 100 x 500mm long were used in
compliance with BS 1881[50]. Details are given in Figure

(a) TENSILE TEST SPECIMEN
100 x 100mm square neck

200

100

240

750

VWG's located on two
faces at mid point
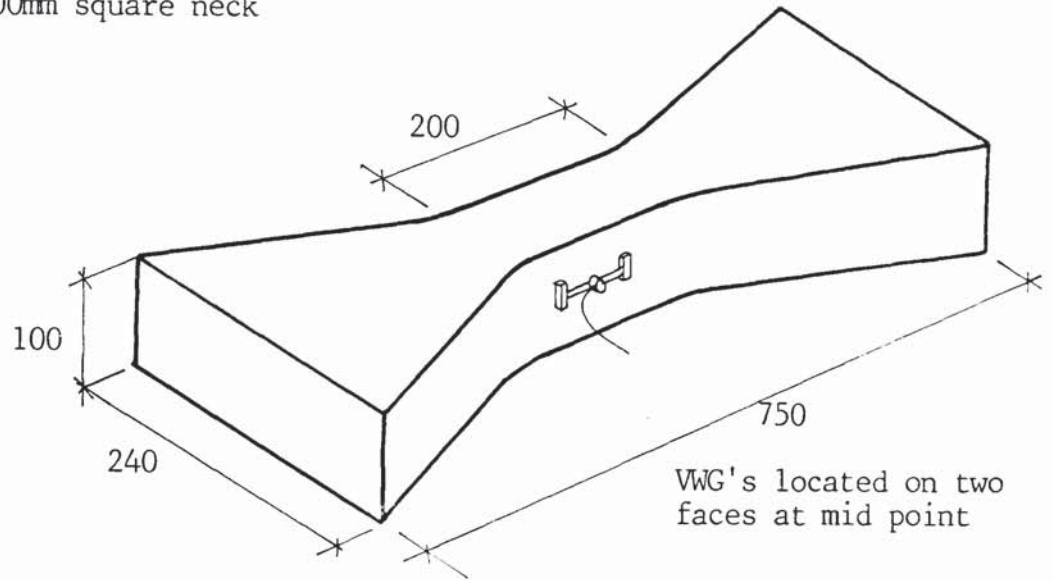
VWG's located 15mm
from top and bottom
edges.

100

100

500
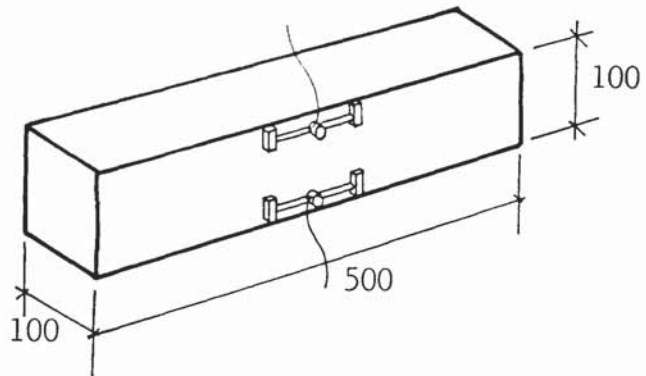
(b) FLEXURAL TEST SPECIMEN

FIGURE 5.3. Test specimens for the measurement of direct tensile
strength and flexural strength.

5.3b. Curing and storage conditions were identical to those used for the tensile test specimens. Fifteen specimens were again cast from each of the four mixes, three to be tested at 20, -20, -70, -120 and -165°C.

5.2.3 Specimen Casting and Allocation

For each mix, five 200kg batches of concrete were cast over a period of 10 days. From each batch, three dog-bone specimens and three 100 x 100 x 500mm prisms were cast. The specimens were then allocated to a particular test temperature as shown in Table 5.2. Tensile and flexural test specimens were allocated in pairs, with both a tensile test and a flexural test being carried out at a particular temperature on specimens from the same batch.

5.2.4 Fixing of VWG's

To measure the stress-strain behaviour of the concrete in direct tension up to failure, two continuously vibrating wire strain gauges were fixed to the neck of the dogbone specimens along the axis of loading and on opposite faces as shown in Figure 5.3(a).

The gauges were attached using a two part epoxy resin after having carefully prepared the concrete surface. This involved allowing the surface to dry and removing the paste layer from the surface to expose the aggregate. Prior to fixing the gauges the specimens were wrapped in plastic film. Only those areas required for gauge attachment were exposed to prevent a significant change in the moisture content of the specimen.

To ensure that the initial gauge length was the same for all gauges, they were set up on a template before being tensioned and adhered to the concrete. This ensured that no variations in gauge factor would occur as a result of individual gauges being of marginally different lengths. Also, by maintaining the end platens at a fixed distance apart, the load generated on the platens when the wire was tensioned (about 10 Newtons) was not transferred to the adhesive. This minimised the risk of the gauges becoming debonded during the 24 hour period whilst the

TEST NO.	TEMPERATURE ($^{\circ}$C)	GAUGE FACTORS	AVERAGE G.F.
1	20	2.922	
2	20	2.933	
3	20	2.927	2.927
4	−162	2.890	
5	−162	2.832	
6	−162	2.889	
7	−162	2.952	2.888

TABLE 5.1. Gauge factors derived from calibration tests at 20°C and −162°C

BATCH NO.	TEST TEMPERATURE ($^{\circ}$C)				
	20	−20	−70	−120	−165
1	●			●	●
2	●	●			●
3	●	●	●		
4		●	●	●	
5			●	●	●

TABLE 5.2. Specimen allocation for tensile and flexural tests.

resin adhesive was curing. The templates were then removed. A further precaution to minimise debonding after removal of the template, was to modify the gauges by the incorporation of a collar and spring as shown in Figure 5.1. The collar was adjusted to induce a load in the spring which was approximately equal to the load in the tensioned wire. Hence the load in the wire was transferred through the stainless steel wire-housing tube and not through the concrete via the adhesive.

To measure the stress-strain behaviour of the prisms in flexure, four VWG's were located at mid span, two on each of the opposite vertical faces. The gauges were orientated along the horizontal axis of the prisms, one gauge being mounted close to the top surface and one close to the bottom. The method of fixing was identical to that described above.

5.2.5 Loading Rigs

The design of the direct tensile test rig was based on a method previously used by Komlos[80]. A general arrangement is shown in Figure 5.4 and working drawings (TWC/D 6351/011A, Sheets 1-5) are included in Appendix 1. The rig comprised a reaction frame which separates two jaws which have universal joints. One jaw is fixed, the other being connected to a 200kN jack and free to slide. The specimen is located horizontally, with the jaws and the specimen being supported on rods fixed to the reaction frame. To avoid problems of embrittlement at low temperature, the rig was fabricated using stainless steel EN 58B.

The flexural test rig was designed to meet the requirements of BS 1881[50]. A general arrangement is shown in Figure 5.5 and working drawings (TWC/D 6351/012 A - Sheets 1-4) are also included in Appendix 1. Load was applied using either a 45 kN jack at temperatures down to -20°C, or a 120 kN jack at lower temperatures. Again stainless steel was used to avoid embrittlement at low temperature.

ELEVATION

PLAN
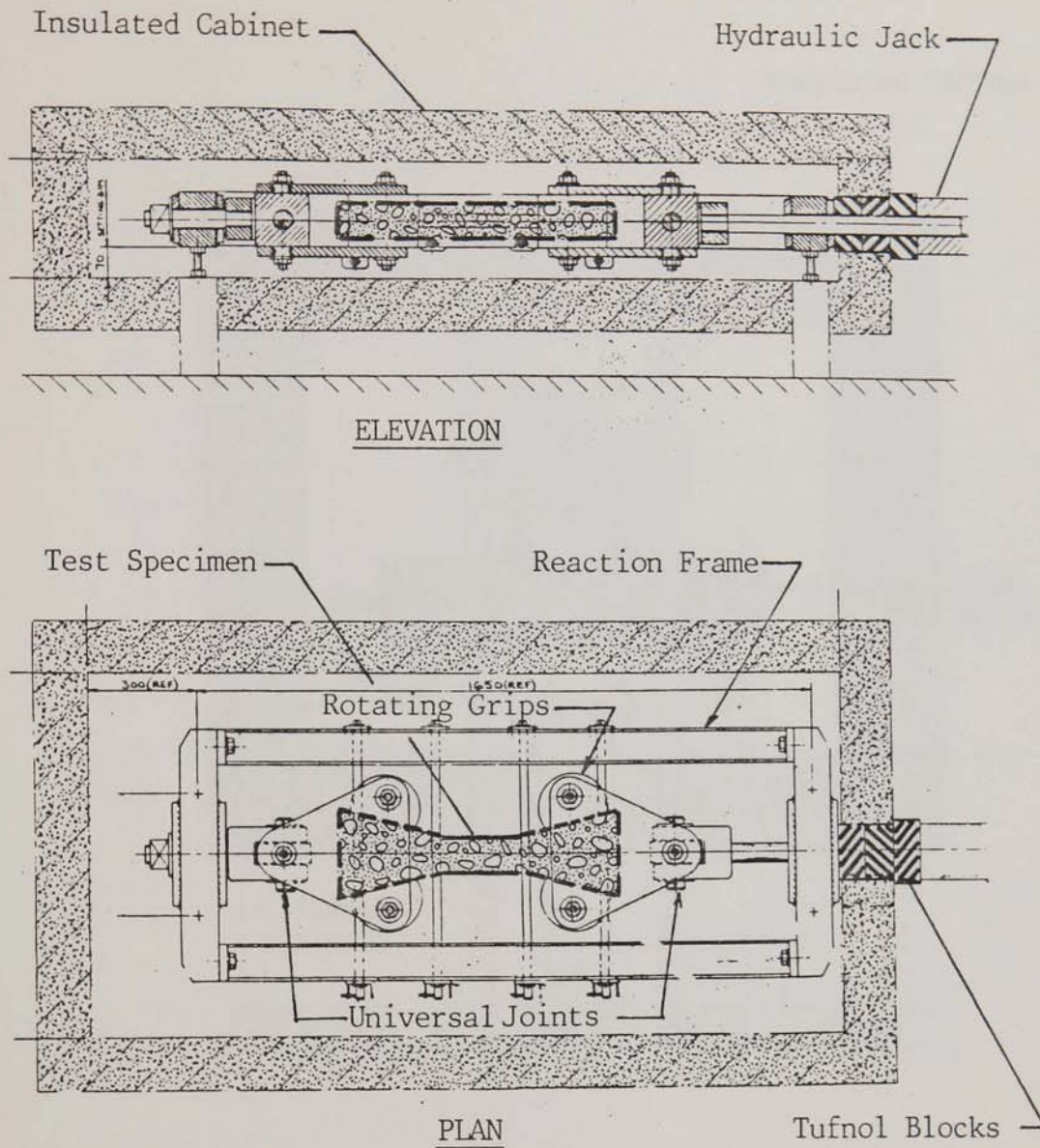
FIGURE 5.4. General arrangement of the loading rig for the measurement of direct tensile strength.
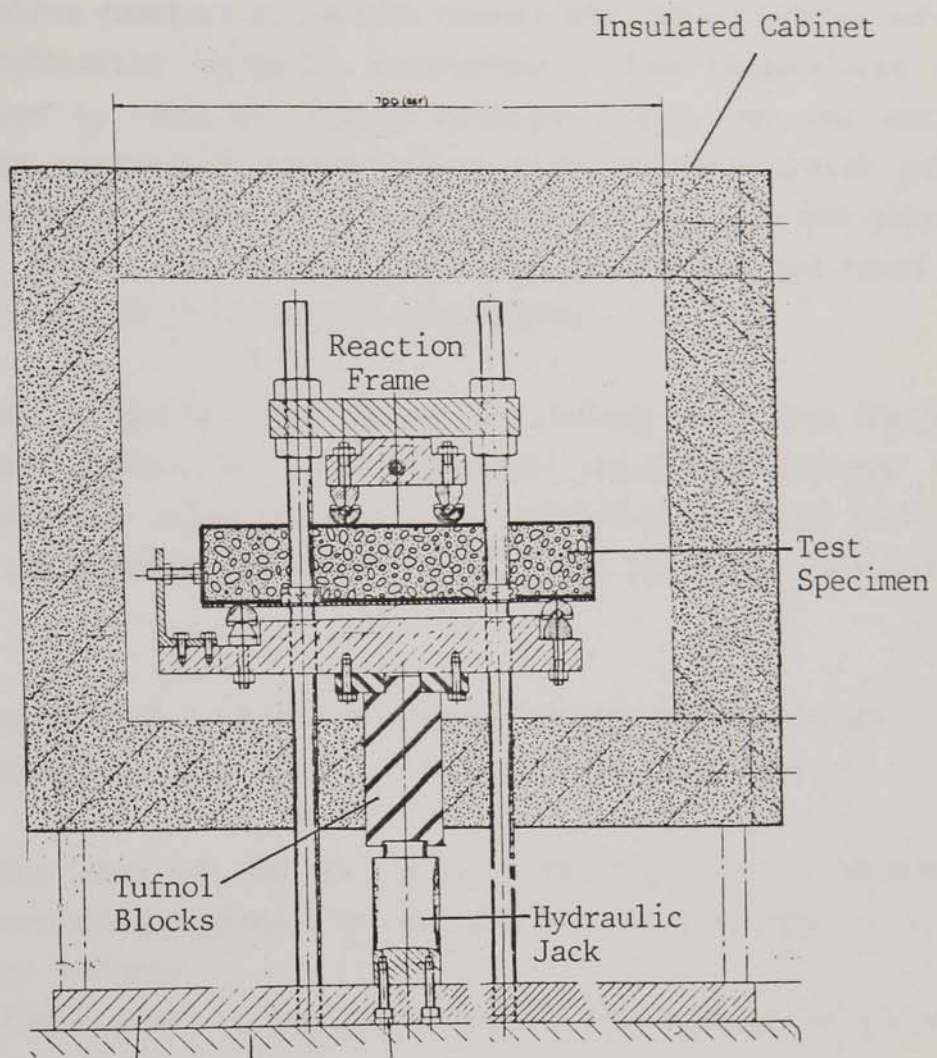
FIGURE 5.5.   General arrangement of the loading rig for the
measurement of flexural strength.

5.2.6 Cryogenic Containments

To achieve the low temperatures required for testing, the test rigs were housed in stainless steel insulated cabinets, as shown in Figures 5.4 and 5.5. The systems were designed such that the hydraulics remained at ambient temperature, being located outside the controlled cryogenic environment. Low temperatures were achieved by spraying liquid nitrogen (LN_2) into the cabinet through perforated copper pipes fixed to the inside walls. Thermocouples linked to a temperature control unit and solenoid valve limited the flow of LN_2 into the cabinet and hence the temperature of the cryogenic environment.

To achieve load transfer through the cabinet walls from the jacks located externally, high strength insulating spacers were incorporated, using Tufnol. This prevented excessive heat flow into the cabinets where the loading bar penetrated the cabinet wall.

It was decided to house the whole of the loading frames inside the cryogenic environment for the following reasons:-

i)   The mass of the loading rig would provide a degree of temperature stability, particularly in the event of a loss of coolant.

ii) Temperature gradients within the specimen would be minimised.

5.2.7 Test Procedures

Rates of cooldown likely to occur in a LNG containment are of the order of 1°C per hour. At this rate, cooling the specimens from +20°C to -165°C would take nearly 8 days. To cool 60 specimens individually in the loading rig at this slow rate would require a period of about 16 months. To overcome this problem two decisions were made. Firstly the rate of cooling

would be doubled to 2°C per hour. Secondly the specimens would be cooled in a separate chamber so that several specimens could be cooled simultaneously. These two changes enabled the 60 tests to be completed in each rig within an 8 weeks period, two weeks for each of the 4 concretes. The programme of cooling and testing over a typical 2 week period is shown in Table 5.3.

The main problem in cooling and testing the specimens in different cabinets was in ensuring a minimal change of temperature during transfer. Tests were carried out to determine the rate of warm up when specimens at -165°C were removed from the cooling cabinet. For the first five minutes the rate of heating was approximately constant being 5°C per minute at the surface. The time for transfer was generally less than 1 minute and not therefore considered to be a problem.

Having located the specimen within the loading rig the gauge leads were connected and a period of at least 30 minutes allowed for stabilization of the gauges and the environment. Stability was detected by observing the strain gauge output. Having achieved temperature stability, datum readings were taken on the gauges and loading commenced. An electric pump was used to apply the hydraulic load such that the stress on the specimen increased at a rate of approximately 1.5 N/mm^2 per minute. Both stress and strains were displayed on a U-V recorder which provided a permanent record of the data up to failure.

Tensile and flexural test specimens, with VWG's attached, and located in the loading rigs are shown in Plates 5.1 and 5.2.

5.3 TEST RESULTS

5.3.1 Direct Tensile Strength

Values of direct tensile strength recorded for each of the 60 specimens tested are given in Table 5.4 together with mean values at each of the five temperature levels. The results are presented graphically in Figure 5.6 which shows the influence of temperature on the tensile strength of the four concretes tested.

T = Tensile Test   F = Flexural test

WEEK 1		TESTING
Monday:	6T and 6F located in cooling cabinet, cooling rate set at 2°C/hour to -20°C.	3T) at 20°C 3F)
	After 20°C tests, rigs cooled to -20°C overnight.	
Tuesday:	Cabinet maintained at -20°C until 3T and 3F tested. Cooling rate set at 2°C/hour to -70°C.	3T) at -20°C 3F)
	Test rigs maintained at -20°C.	
Wednesday:	Test rigs cooled down to -70°C overnight.	
Thursday:	Cabinet maintained at -70°C until 3T and 3F tested, then allowed to warm up to ambient.	3T) at -70°C 3F)
Friday:	6T and 6F located in cabinet; cooling rate set at 2°C/hour to -120°C.	
	Test rigs maintained at -70°C.	
Saturday/ Sunday:	Specimens cooling to -120°C, rigs maintained at -70°C.	
WEEK 2		
Monday:	Test rigs crash cooled to -120°C. Cooling cabinets maintained at -120°C until 3T and 3F tested, then set at 2°C/hour to -165°C.	3T) at -120°C 3F
	Test rigs maintained at -120°C.	
Tuesday:	Specimens cooling to -165°C. Test rigs cooled to -165°C overnight.	
Wednesday:	Cooling cabinet maintained at -165°C until 3T and 3F tested, then allowed to warm up to ambient.	3T) at -165°C 3F)
Thursday:	Test rigs allowed to warm up to ambient.	
Friday:		
Saturday/ Sunday:		

NB. Days with no testing were used to retrieve and clean gauges and instrument new specimens prior to cooling.

TABLE 5.3.   Cooling and testing programme for direct tensile and flexural strength.
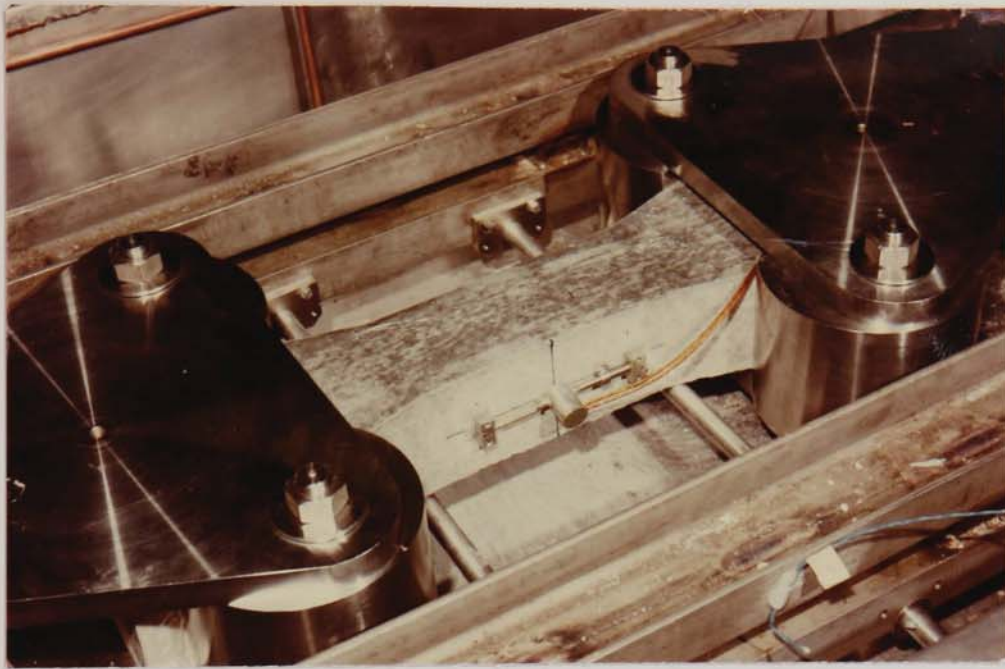
PLATE 5.1. Direct tensile test specimen located in the loading rig.
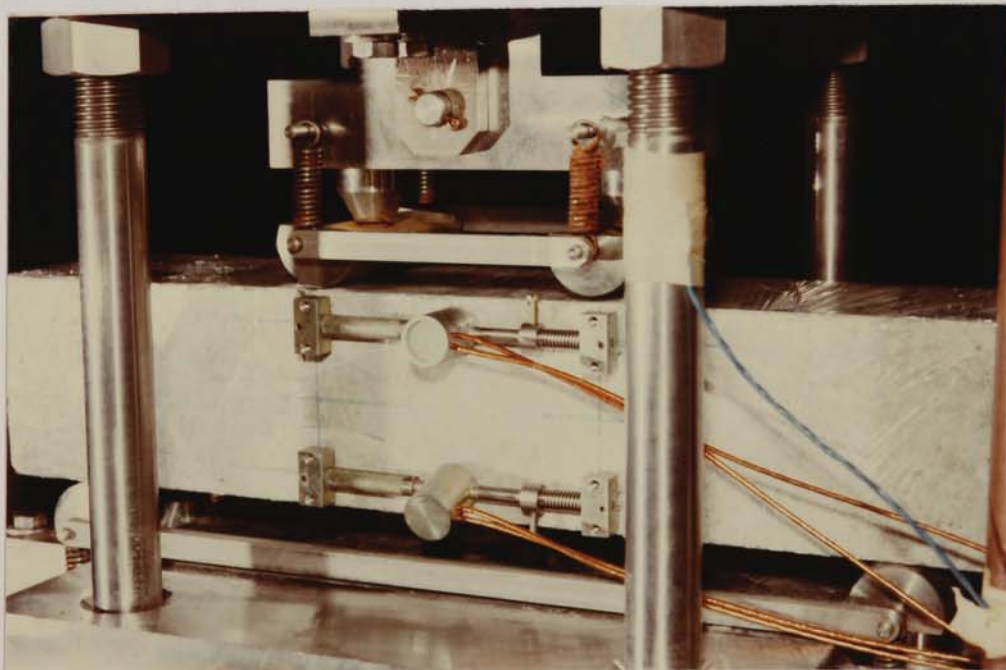
PLATE 5.2. Flexural test specimen located in the loading rig.

| MIX NO. | DIRECT TENSILE STRENGTH (N/mm²) AT TEMPERATURES INDICATED | | | | |
	20°C	-20°C	-70°C	-120°C	-165°C
AEC	1.18[+]	1.61(2.43)	0.58*	5.13(5.78)	3.97(4.79)
	1.39(1.76)	2.02(2.71)	5.80(6.09)	5.22(6.41)	5.34(5.34)
	1.60(1.79)	2.74(3.11)	4.14(6.04)	4.97(5.36)	4.31(5.15)
Mean	1.39	2.21	4.97	5.11	4.59
HS	1.71(2.48)	2.09	4.14(5.15)	5.53(6.64)	5.49[+]
	2.21(4.42)	2.52	6.11[+]	6.21(6.85)	4.93(6.28)
	2.61(3.86)	2.38	5.59[+]	4.62(5.27)	5.18(5.42)
Mean	2.18	2.33	5.28	5.45	5.20
LW	2.14(2.91)	3.00(3.69)	2.41(2.85)	5.49(5.82)	3.16(3.98)
	1.55[+]	2.85(3.66)	3.40(4.14)	5.35(6.46)	4.55(7.69)
	1.76[+]	3.54(4.74)	-	3.07(3.49)	4.90(7.36)
Mean	1.82	3.13	2.91	4.64	4.20
PFA	2.19(2.73)	3.63(4.01)	5.69(6.56)	5.30(7.33)	7.66(8.46)
	2.43(2.65)	2.38(2.83)	4.50(4.61)	5.85(6.44)	4.55(6.17)
	2.21(2.55)	2.90(3.14)	6.04(6.63)	-	5.86(6.73)
Mean	2.28	3.00	5.41	5.63	6.02

* Premature failure, data not included in the mean.

+ Only one gauge working.

() Indicates calculated stress at location of gauge indicating the highest strain at failure.

TABLE 5.4. Direct tensile strength recorded at temperatures down to -165°C.

For the three normal weight mixes the rate of strength gain was most noticeable in the range -20 to -70°C. Between 20 and -20°C there was a small increase, of the order of 30%, and below -70°C there was no significant change in strength. Between -20°C and -70°C the strength more than doubled. These results are consistent with published data, reported in Section 2.5.1, for the influence of temperature on the tensile splitting strength, and support the hypothesis that all the free water in concrete has frozen at -70°C.

The rate of strength increase of the lightweight concrete differed from the normal weight mixes. The most significant increase in strength occurred within the temperature range +20 to -20°C. Between -20 and -70°C there was a marginal reduction in the average strength. Below -70°C, the strength increased again down to -120°C followed by a further small reduction in the range -120 to -165°C.

The difference in the behaviour of the normal and lightweight concretes is believed to be, at least in part, due to the difference in pore structure. The increase in strength of the lightweight mix between +20 and -20°C is most likely due to the high proportion of larger pores, as shown in Figure 4.19, in which the water will have frozen once the temperature has reached about -5°C (see Section 2.2). The lack of strength gain between -20°C and -70°C, together with the continued increase in strength below -70°C would indicate that the capillary pores in the lightweight concrete are smaller than those present in the normal weight mixes. Results of porosimetry measurements, however, show a higher proportion of pores in the lightweight mix over the size range 50 to 75000 Å (Figure 4.19). This suggests that either the moisture in the lightweight mix is predominant in pores smaller than 50Å or that the moisture content is small in relation to the pore volume available and ice formation is therefore less effective in filling the voids and reducing the porosity.

5.3.2 Flexural Strength (Modulus of Rupture)

Values of flexural strength recorded for each of the 60 specimens

MIX NO.	FLEXURAL STRENGTH (N/mm^2) AT TEMPERATURES INDICATED				
	20°C	-20°C	-70°C	-120°C	-165°C
AEC	3.20	4.14	8.50	9.29	9.23
	3.12	4.87	9.23	8.86	9.57
	3.50	3.50	8.99	9.76	10.96
Mean	3.27	4.17	8.91	9.30	9.65
HS	4.52	5.49	8.62	11.90	10.33
	4.35	4.10	8.99	11.66	10.35
	4.26	4.97	9.62	11.66	-
Mean	4.38	4.85	9.08	11.74	10.34
LW	4.12	6.87	6.13	7.37	9.08
	3.80	6.37	6.40	7.93	8.73
	3.74	6.20	5.92	7.43	10.01
Mean	3.89	6.48	6.15	7.58	9.27
PFA	3.42	6.67	11.79	10.43	10.82
	1.53[+]	5.22	9.49	7.93	9.70
	3.77	6.20	9.85	10.97	12.39
Mean	3.60	6.03	10.38	9.68	10.97

+ Only one gauge working

TABLE 5.5. Flexural strength and strain capacity recorded at temperatures down to -165°C.
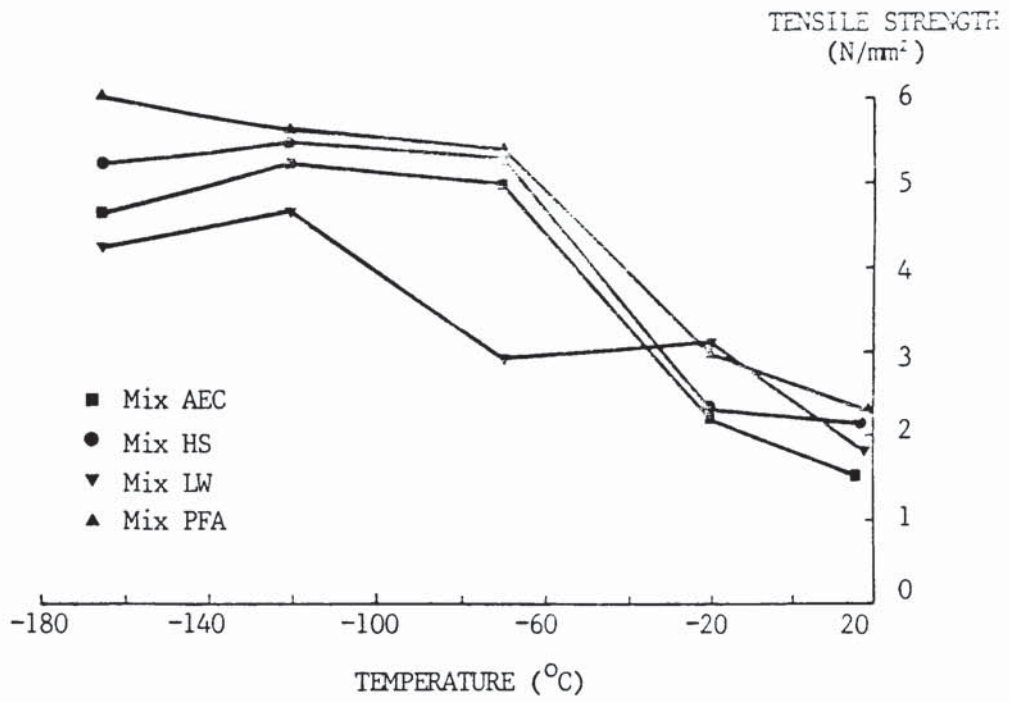
FIGURE 5.6.   The influence of temperature on direct tensile
strength
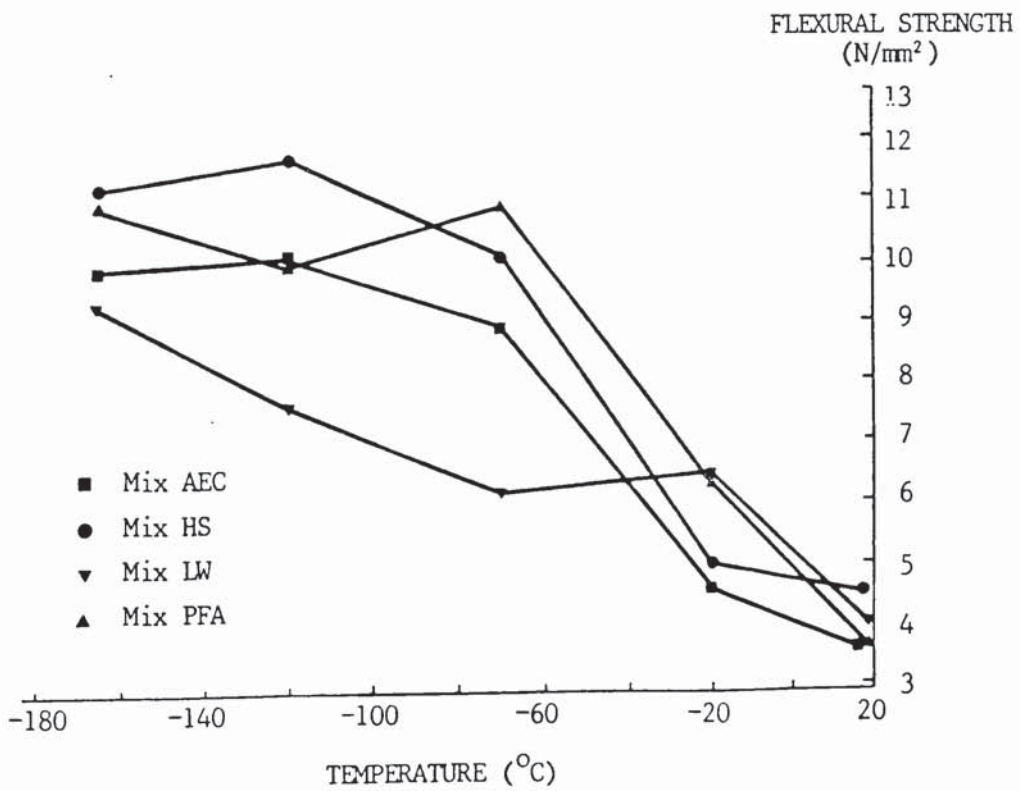
FIGURE 5.7.   The influence of temperature on flexural strength.
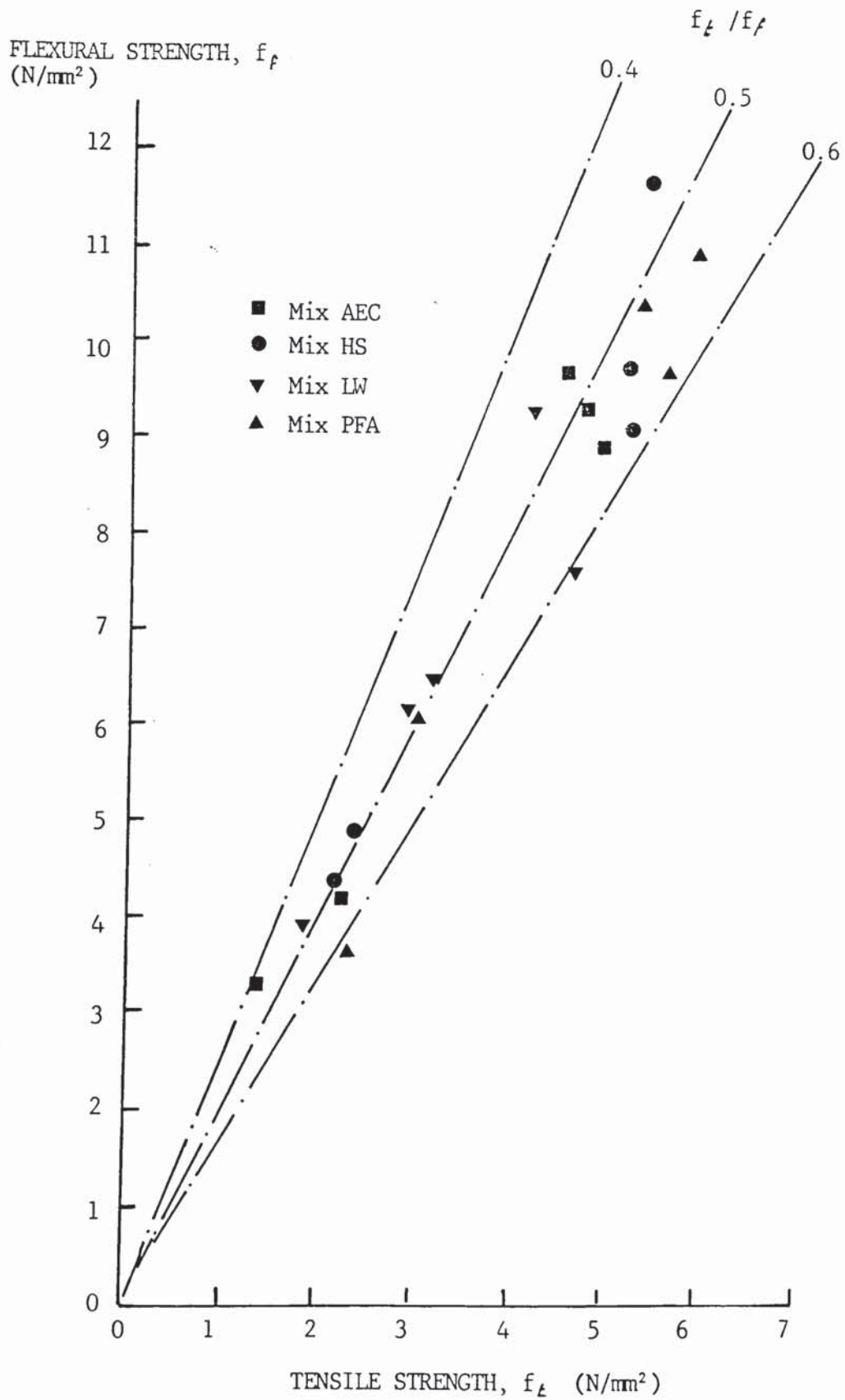
FIGURE 5.8. The relationship between direct tensile and flexural
strength over the temperature range 20°C to −165°C.

tested are given in Table 5.5. The results are summarized in
Figure 5.7 which shows the influence of temperature on the four
concretes tested. It will be seen that the flexural strength
increased with reducing temperature in much the same way as the
direct tensile strength. However, the magnitude of flexural
strength was approximately double the tensile strength over the
range of temperatures investigated. This is shown in Figure 5.8
which illustrates the relationship between tensile and flexural
strength for all four concretes over the range of test
temperatures.

5.3.3 Strain Capacity in Direct Tension

Stress-strain curves for each concrete are illustrated in Figure
5.9 (a-d) for mixes AEC, HS, LW and PFA respectively. Each
figure includes the five stress-strain curves recorded at 20,
-20, -70, -120 and -165°C, and each curve represents the average
from three specimens tested for each mix, at each temperature.

The magnitude of tensile strain capacity of the concrete, i.e.
the strain at failure, can be derived in a number of ways. The
most straightforward interpretation is to simply take the mean
strain recorded across the specimen at failure. These values are
given in Table 5.6. Being highly sensitive to the "weakest link
theory" values of tensile strain capacity (and tensile strength)
tended to be scattered. A closer examination of the results,
however, shows that some of this scatter can be explained by
non-axial loading of specimens. Failure occurs when the stress
(or strain) at any point in the specimen exceeds the strength (or
strain capacity). If the specimen is non-axially loaded, as
indicated by differential elongation during the test, the actual
stress at the point of failure will be in excess of the mean
value. Hence representing strain capacity in terms of the mean
value provides a conservative estimate. Values of maximum strain
at failure are also given in Table 5.6 for each specimen, it
being assumed that cracking was initiated at the location of the

STRESS
(N/mm²)

(a) Mix AEC

(b) Mix HS

(c) Mix LW

(d) Mix PFA

STRAIN (Microstrain)
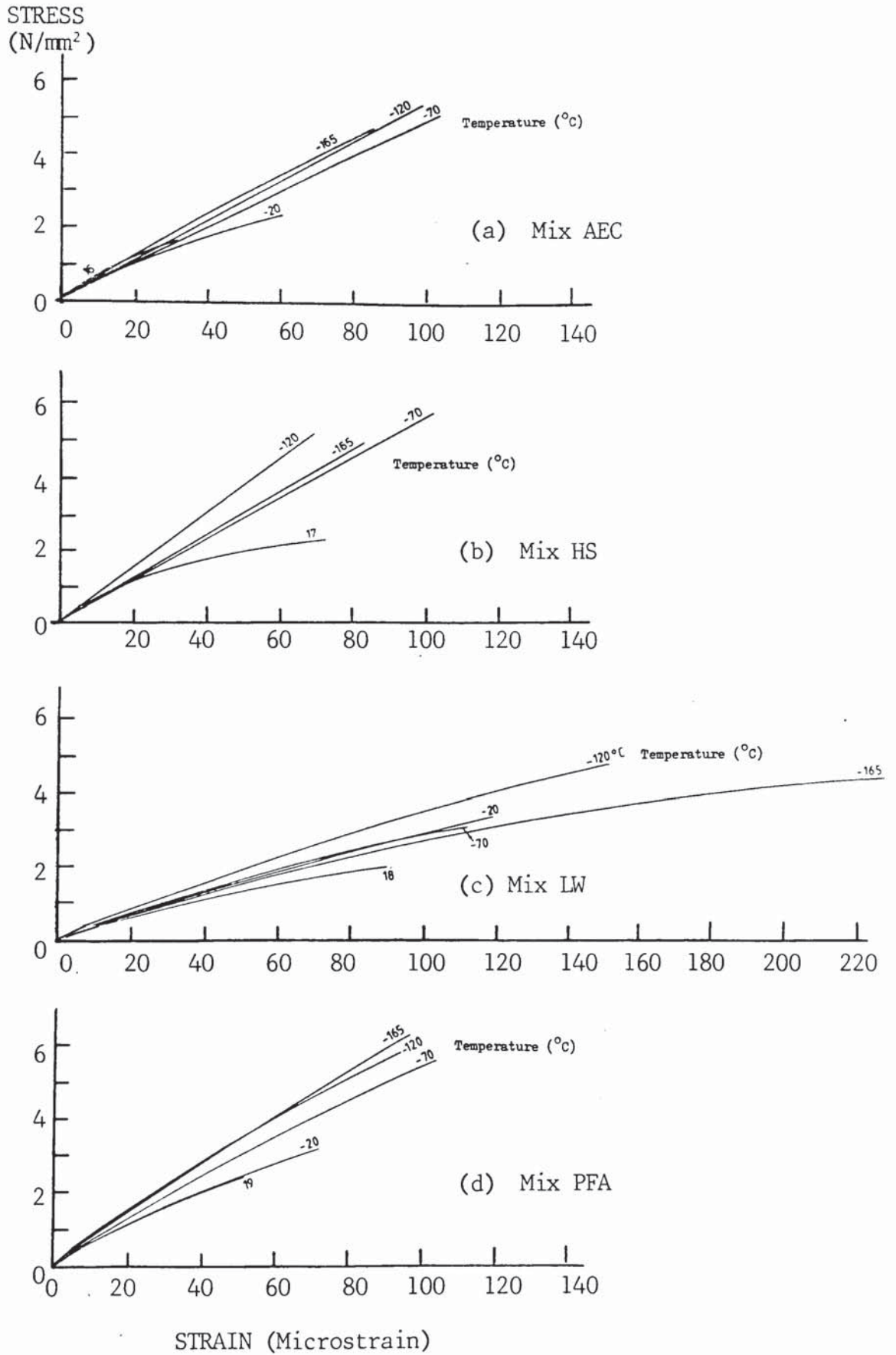
FIGURE 5.9. Stress-strain curves measured in direct tension.
Each curve represents the average from three test
specimens.

| MIX NO. | DIRECT TENSILE STRAIN CAPACITY (1×10^{-6}) AT TEMPERATURE INDICATED | | | | |
	20°C	-20°C	-70°C	-120°C	-165°C
AEC	42$^+$	58 (75)	7*	101(110)	74 (86)
	34 (43)	40 (53)	118 (124)	105 (129)	108 (108)
	33 (37)	81 (92)	87 (127)	88 (93)	72 (86)
Mean	36	61	103	98	85
HS	69 (100)	–	70 (87)	55 (66)	92$^+$
	73 (146)	–	100$^+$	78 (86)	73 (93)
	75 (110)	–	103$^+$	71 (81)	–
Mean	72	–	91	68	83
LW	80 (102)	112 (135)	94 (109)	190 (199)	162 (193)
	87$^+$	111 (140)	126 (149)	195 (231)	267 (436)
	90$^+$	132 (176)	–	92 (100)	130 (196)
Mean	86	118	110	189	186
PFA	39 (48)	86 (95)	109 (125)	81 (112)	125 (138)
	55 (60)	54 (61)	84 (86)	106 (114)	58 (78)
	59 (68)	74 (80)	122 (134)	–	99 (107)
Mean	51	71	105	94	94

* Premature failure, data not included in the mean.

+ Only one gauge working.

() Indicates strain recorded at gauge with greatest elongation.

TABLE 5.6. Strain capacity measured in direct tension at temperatures down to -165°C

gauge exhibiting the higher strain. The difference between the mean and the maximum strain values indicate the degree of non-axiality of loading.

The relationship between the mean tensile strain capacity and temperature is shown in Figure 5.10 for the four concretes tested. In every case the strain capacity increased as temperature was reduced in much the same way as strength. The strain capacity of the lightweight concrete was however, noticeably different from the normal weight concretes being of consistently greater magnitude; this despite the fact that the tensile strength was not appreciably different from the other three concretes. This is largely due to the lower elastic modulus of the lightweight concrete and the different mode of failure. Failure of the normal weight concrete occurred due to breakdown of the aggregate/cement paste bond. The lightweight aggregate did not debond, however, with failure occurring through the aggregate particles and hence utilizing the inherent strength and strain capacity of the aggregate.

Considering the normal weight concretes as a single population, the strain capacity increased from about 50 to 100 microstrain over the range 20 to -70°C with a small reduction to about 90 microstrain at -165°C. The strain capacity of lightweight concrete increased from 86 to 160 microstrain. Both normal and lightweight aggregate concrete therefore became appreciably more crack resistant as the temperature reduced down to cryogenic levels, the lightweight concrete gaining most benefit from the low temperatures.

5.3.4 Strain Capacity in Flexure

Stress-strain curves for each concrete are illustrated in Figure 5.11(a-d). Each curve represents the average from three specimens tested for each mix at each temperature. These stress-strain curves do not however, represent the behaviour of the extreme fibre as the gauges were located only 35mm below the neutral axis. (This was necessary in order to avoid damaging the
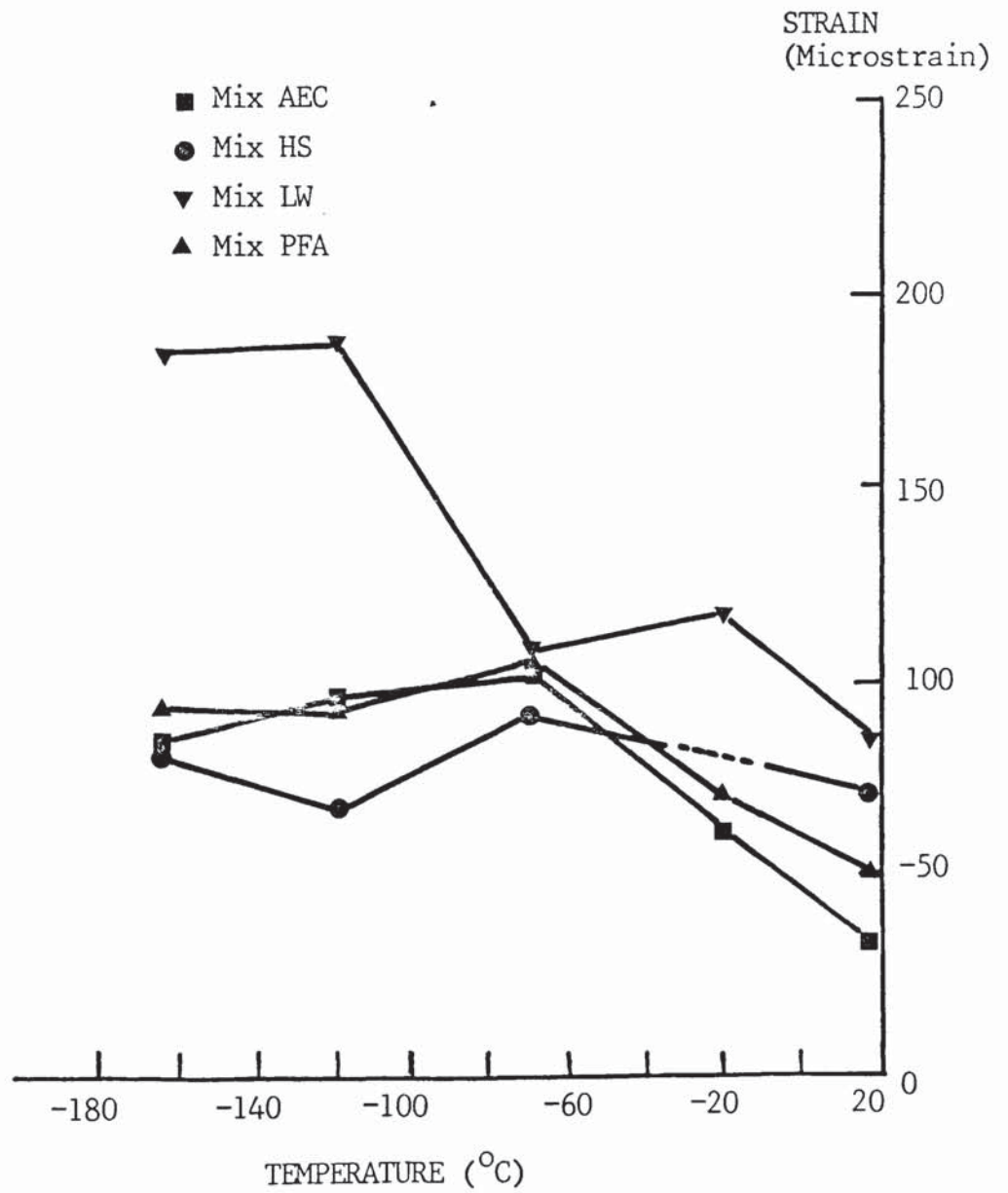
FIGURE 5.10. The influence of temperature on the strain capacity measured in direct tension.
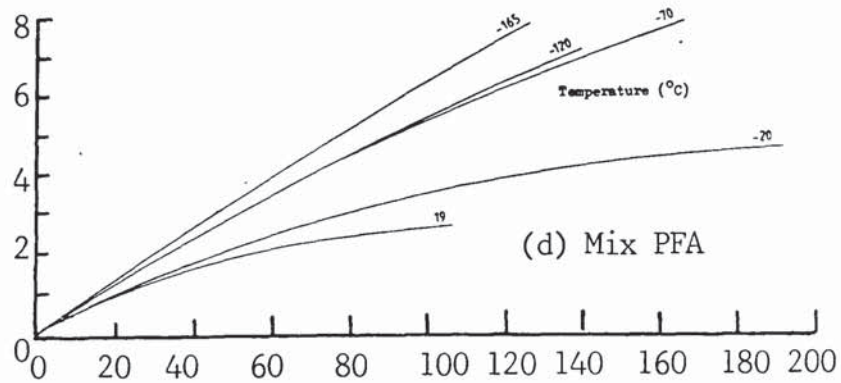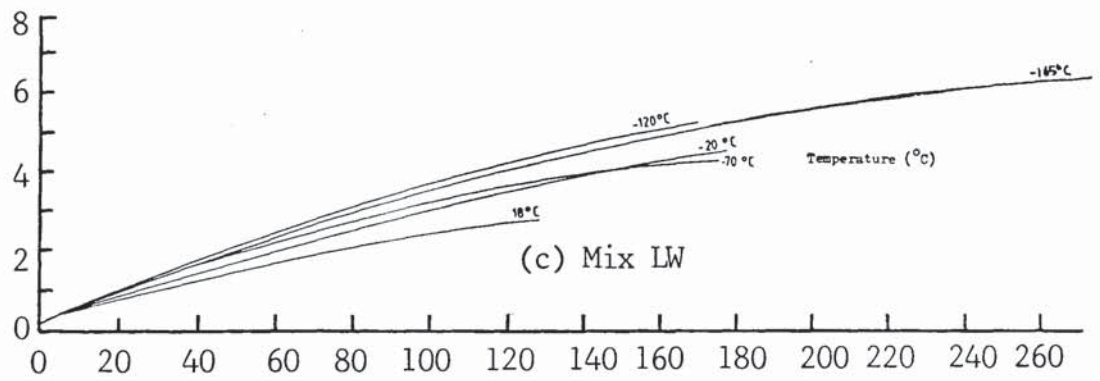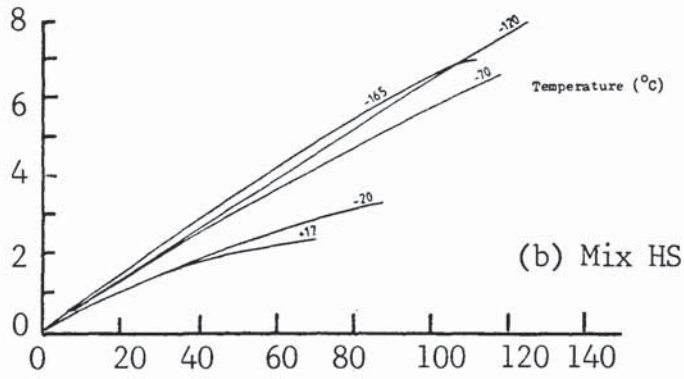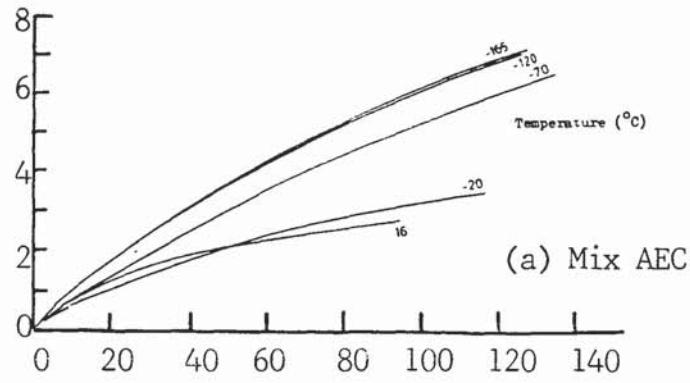
FIGURE 5.11. Stress-strain curves measured in flexure. Each curve represents the average from three test specimens.

MIX NO.	FLEXURAL STRAIN CAPACITY (1×10^{-6}) AT TEMPERATURE INDICATED				
	20°C	-20°C	-70°C	-120°C	-165°C
AEC	113	91	108	138	115
	72	133	144	135	108
	96	123	148[+]	103	157
Mean	94 (134)	116 (166)	133 (190)	125 (179)	127 (181)
HS	147	66[+]	98[+]	132	118[+]
	115	65	115	127	144
	63[+]	110[+]	120	108	-
Mean	108 (154)	80 (114)	111 (159)	122 (174)	131 (187)
LW	141	211	194	154	293
	128	199	170	168	265
	136	161	166	202	256
Mean	135 (193)	190 (272)	177 (253)	175 (250)	271 (387
PFA	95[+]	161	187	137	140
	106	207	128	130	139
	119	216	158	152	189
Mean	107 (153)	195 (279)	158 (226)	139 (199)	156 (223)

+ Only one gauge working.

() Indicates calculated extreme fibre strain at failure.

TABLE 5.7. Strain capacity measured in flexure at temperatures down to -165°C.

gauges when the specimen failed). Assuming a linear strain distribution throughout the specimen the strain at the extreme fibre would be greater than the measured strain by a factor of 50 ÷ 35 = 1.429.

Values of flexural strain capacity are given in Table 5.7. Included are the individual mean strains recorded for each specimen together with the mean strain for each concrete at each temperature and the corresponding extreme fibre strain calculated using the factor of 1.429.

The relationship between the mean flexural strain capacity, calculated for the extreme fibre, and temperature is shown in Figure 5.12 for the four concretes tested. In every case the strain capacity increased as the temperature reduced. At -165°C the strain at failure was typically 30-50% greater than recorded at ambient temperature. Again the lightweight aggregate concrete was noticeably different from the normal weight concretes, having a significantly higher strain at failure. The most pronounced difference was at -165°C when the lightweight concrete exhibited about double the strain recorded for the other three mixes. At higher temperatures the difference was typically 30-50%.

The relationship between the flexural strain capacity and the tensile strain capacity is shown in Figure 5.13. The former was of the order of 60% greater in magnitude based on measured strains, but some 100% greater based on estimated extreme fibre strains at failure.

5.3.5 Relationship Between Strength and Strain Capacity

Relationships between strength and strain capacity are given in Figure 5.14. Data are included from both the direct tensile tests and flexural tests. For the lightweight concrete there appears to be a single linear relationship between strength and strain capacity which applies both in direct tension and to the extreme fibre stress in bending. For the three normal weight mixes, however, the strain capacity does not increase in direct proportion to strength. At the higher strength levels there
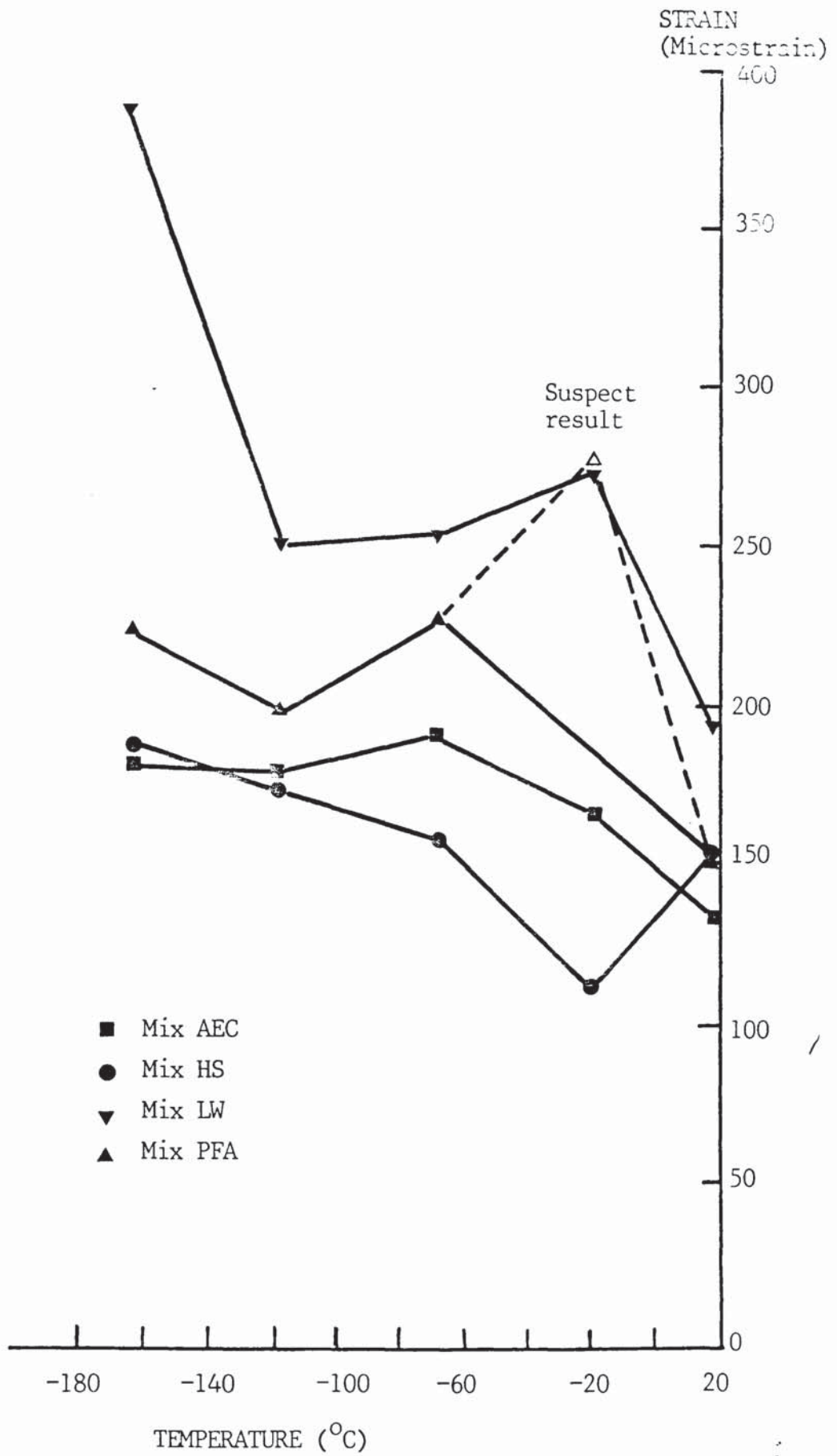
FIGURE 5.12. The influence of temperature on the strain capacity measured in flexure.
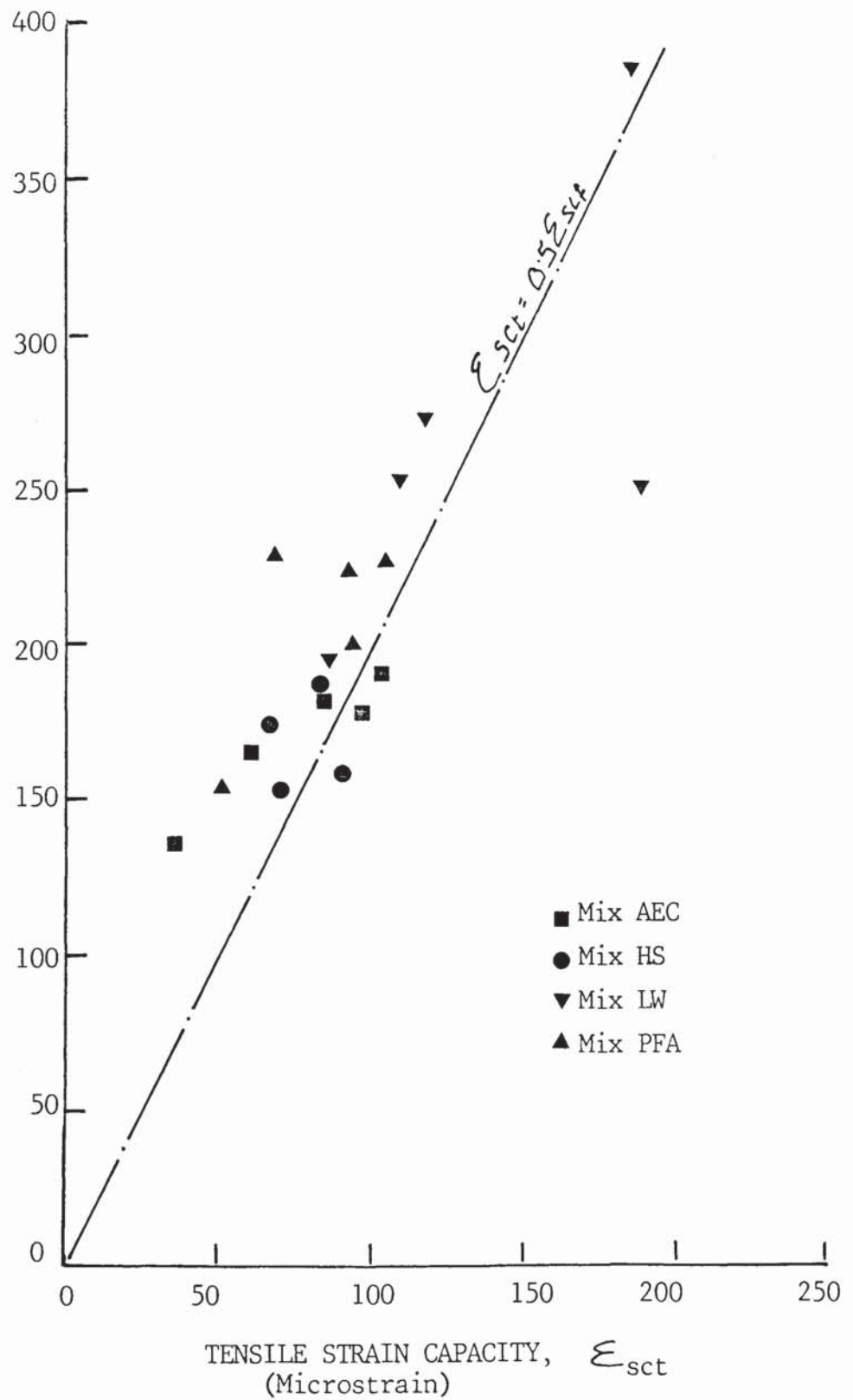
FIGURE 5.13. The relationship between strain capacity measured in direct tension and in flexure.
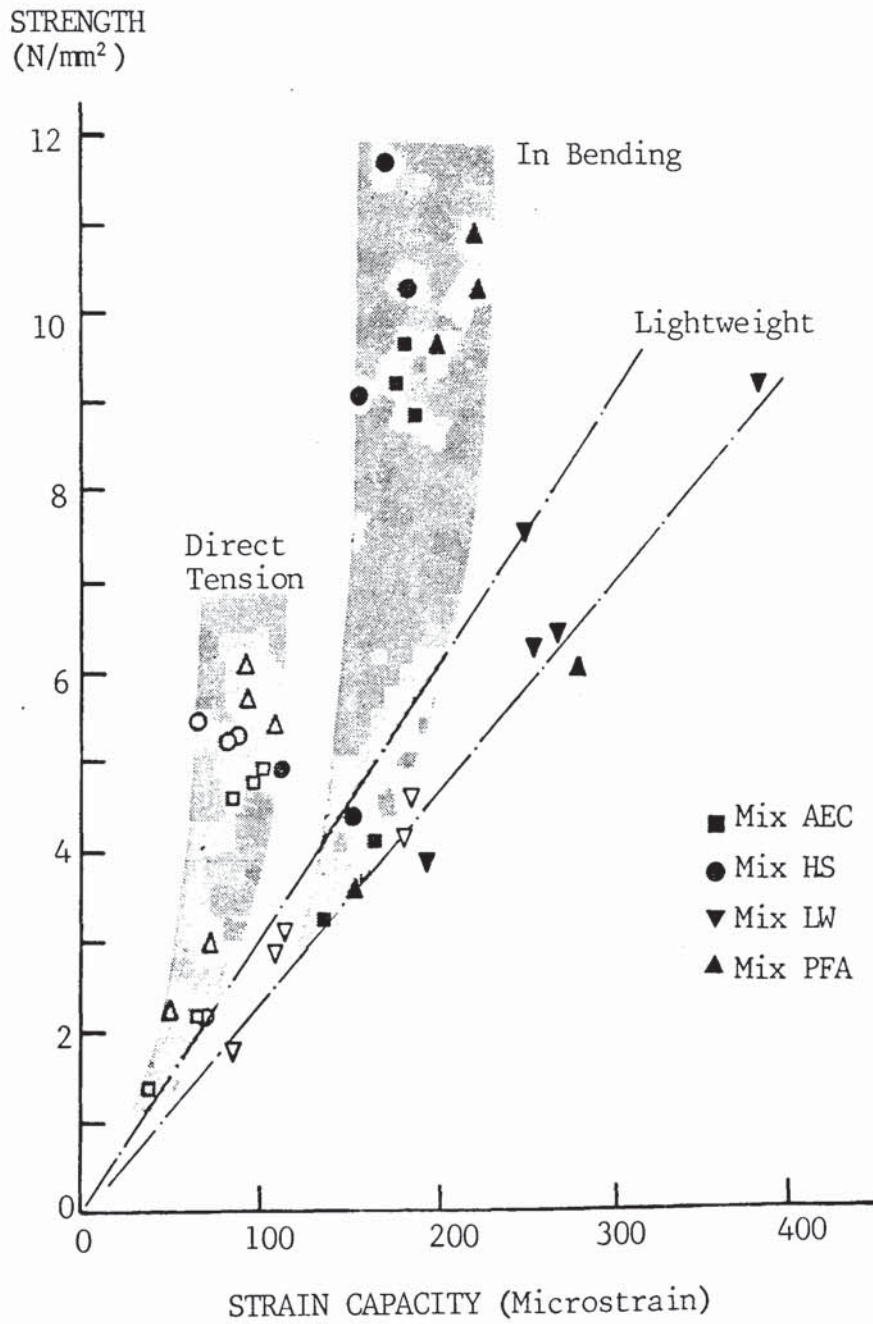
FIGURE 5.14. The relationships between strength and strain
capacity measured in both direct tension and in
flexure.

appears to be a limiting strain value which it is difficult to exceed. In direct tension this value is about 110 microstrain: in flexure the equivalent value is of the order of 220 microstrain, about double the value in tension.

Whilst the tensile strain behaviour at cryogenic temperature has not been investigated previously, considerable research has been carried out on concrete at ambient temperature. A summary of tensile strain capacities reported in the literature (81-85) is given in Table 5.8. Whilst reported values of tensile strength varied from less than 1 N/mm^2 up to 4.5 N/mm^2 the tensile strain capacity remained largely within the range 50-100 microstrain, these values being compatible with the authors results.

REF. NO.	SOURCE		STRENGTH (N/mm^2)	STRAIN CAPACITY (Microstrain)
81	Cornelissen & Reinhardt		2.5	100
82	Zielinski & Reinhardt			
	- Mortar		1.9	110
	- Microconcrete		2.5	110
	- Concrete		2.5	140
83	Hughes & Chapman*		1.52	90
			1.24	80
			1.14	80
			1.17	60
			0.76	65
84	Domone	Immersed	2.60	83
			2.35	88
			2.20	85
			2.15	78
			2.15	65
			2.05	80
		Sealed	2.20	77
			1.85	70
			1.90	69
			1.80	64
			1.65	61
			1.65	65
85	Lydon & Balendran	Limestone	3.45	75
			3.45	85
			3.85	83
			3.90	80
			3.90	90
			3.95	90
			4.05	97
			4.35	95
			4.35	87
			4.50	100

TABLE 5.8. A summary of published results on tensile strength and strain capacity.

6. THERMAL EXPANSION COEFFICIENT AND ELASTIC MODULUS

6.1 INTRODUCTION

The most significant loads to be imposed upon the wall of a cryogenic storage tank may be thermally induced. It is, therefore, essential that the thermal expansion coefficient of the concrete is known over the range of operating temperatures. Furthermore, the magnitude of thermally induced stresses will be determined by the elastic modulus of the concrete. Tests have, therefore, been carried out to measure both the thermal expansion coefficient and elastic modulus over the temperature range +20 to -165°C.

6.2 EXPERIMENTAL DETAILS

6.2.1 Strain Measurement

To record both load induced and thermally induced strains, embedded Vibrating Wire Strain Gauges were used. The method of operation of VWG's is described in Section 5.2.1, together with details of calibration tests at ambient and cryogenic temperature which were undertaken to establish the variation in gauge factor for surface mounted gauges. The results showed that the influence of temperature was unlikely to change the gauge factor by more than 2% and for the strain capacity measurements no adjustments were made. In all previous tests, the temperature was maintained at a constant level for the duration of loading. Measurement of the thermal expansion coefficient, however, necessarily involved the measurement of strain under conditions of changing temperature. Further calibration tests were carried out, therefore, to determine the temperature correction factor for the VWG's under transient thermal conditions and to check the gauge factor for the embedded gauges.

The temperature correction factor is necessary to take account of the thermal expansion coefficient of the steel wire within the gauge. Consider the strain change in the concrete $\Delta \varepsilon$ for a temperature change $\Delta \theta$. For the same temperature change the

length of the vibrating wire will change by $\Delta\theta.\alpha_\omega$ where α_ω is the thermal expansion coefficient of the wire. The recorded strain change $\Delta\varepsilon_r$ will therefore be:-

$$\Delta\varepsilon_r = \Delta\varepsilon - \alpha_\omega \Delta\theta \qquad (6.1)$$

Where expansion is positive.

Hence, the actual strain change in the concrete, is given by the equation,

$$\Delta\varepsilon = \Delta\varepsilon_r + \alpha_\omega \Delta\theta \qquad (6.2)$$

Consider a concrete specimen which is cooled from 30°C to 10°C, and which under ambient conditions has a thermal expansion coefficient of 11 microstrain per °C. The real contraction of the concrete is 20 x 11 = 220 microstrain. However, over the same 20°C temperature change the wire in the VWG will have also contracted. The thermal expansion coefficient of the steel wire under ambient conditions is 12 microstrain per °C, hence the wire will have contracted by 20 x 12 = 240 microstrain. As the concrete has contracted by only 220 microstrain, the wire will therefore be in greater tension. The recorded gauge reading would therefore indicate expansion of the concrete by 20 microstrain. Applying the above equation, however:-

$\Delta\varepsilon = 20 + (12).(-20)$
$\quad = 20 - 240 = -220$ microstrain

Calibration tests were carried out as follows:-

(1) Two gauges, tensioned at different frequencies, were cooled down to -178°C in increments, and the apparent strain resulting from differential contraction of the wire and the body of the gauge was recorded. This test was carried out three times.

(2) Gauges were fixed to both copper and nickel bars, with pre-defined thermal contraction characteristics, and these

were cooled from 20°C to -178°C. In each case four gauges were used, in two pairs, each pair being tensioned to a different frequency.

(3) Three concrete cylinders were cast, 150mm diameter by 450mm long, each with an embedded gauge at the centre and three surface mounted gauges fixed at equal intervals around the surface. Gauge readings were taken at 18°C and after cooling to -173°C.

(4) The three concrete cylinders were subjected to loading at temperatures of 20, -20, -70, -115 and -165°C, and the strain monitored at a stress level of 13.8N/mm².

Specific details of the thermal and load calibration tests are given in Appendix 3. The temperature corrections, derived from the calibration tests using nickel and copper bars, are shown in Figure 6.1. There are a series of curves, the temperature correction being influenced by the initial frequency of the wire as shown in Figure 6.2. This is described in Appendix 3 in more detail, in which it is shown that the change in the temperature correction factor, $\Delta \mathcal{E}_{\angle c}$, is linearly related to (frequency)². and hence the initial strain in the wire. The reason for this has not been identified, but the effect has been taken into account by ensuring that for the thermal expansion coefficient and elastic modulus tests, all the gauges were tensioned within a narrow frequency band.

The results of tests on the three concrete cylinders with both embedded and surface mounted gauges are included in Tables 6.1, 6.2 and 6.3. The results obtained when the specimens were cooled directly from 18°C to -173°C are given in Table 6.1. The variation in thermal contraction for the three specimens, after correcting for contraction of the gauge wire, was insignificant. However, the same difference was observed between internal and external strain for each specimen, the former being about 6% higher. For this difference to be attributed to a change in gauge factor for the embedded gauges, an increase of about 15% would be needed ie. the average difference between values of measured strain change before temperature correction. Hence to
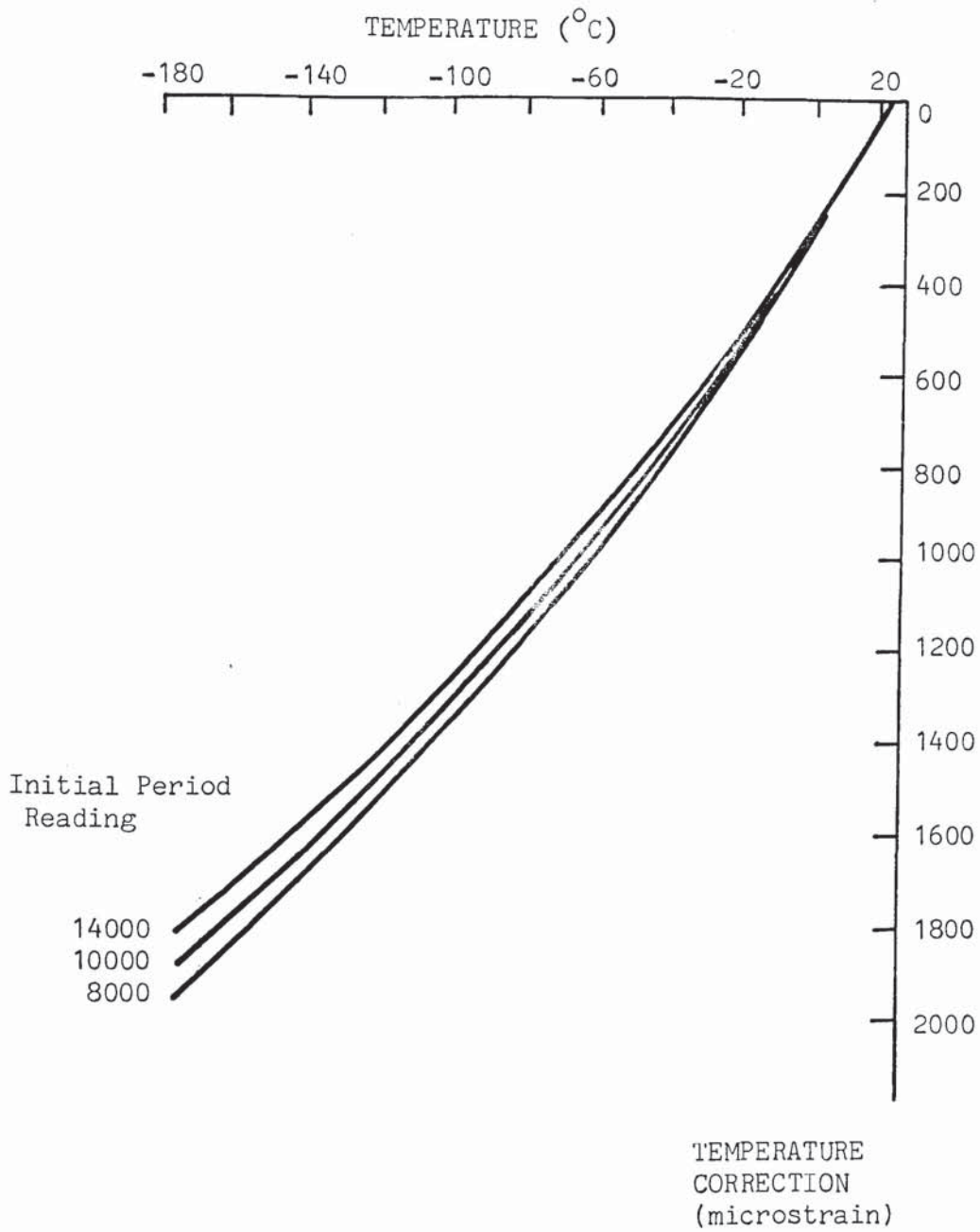
FIGURE 6.1.   Temperature correction curves for vibrating wire
strain gauges derived using copper and nickel test
pieces with defined thermal expansion coefficients.

CHANGE IN TEMPERATURE
CORRECTION FACTOR
(microstrain)
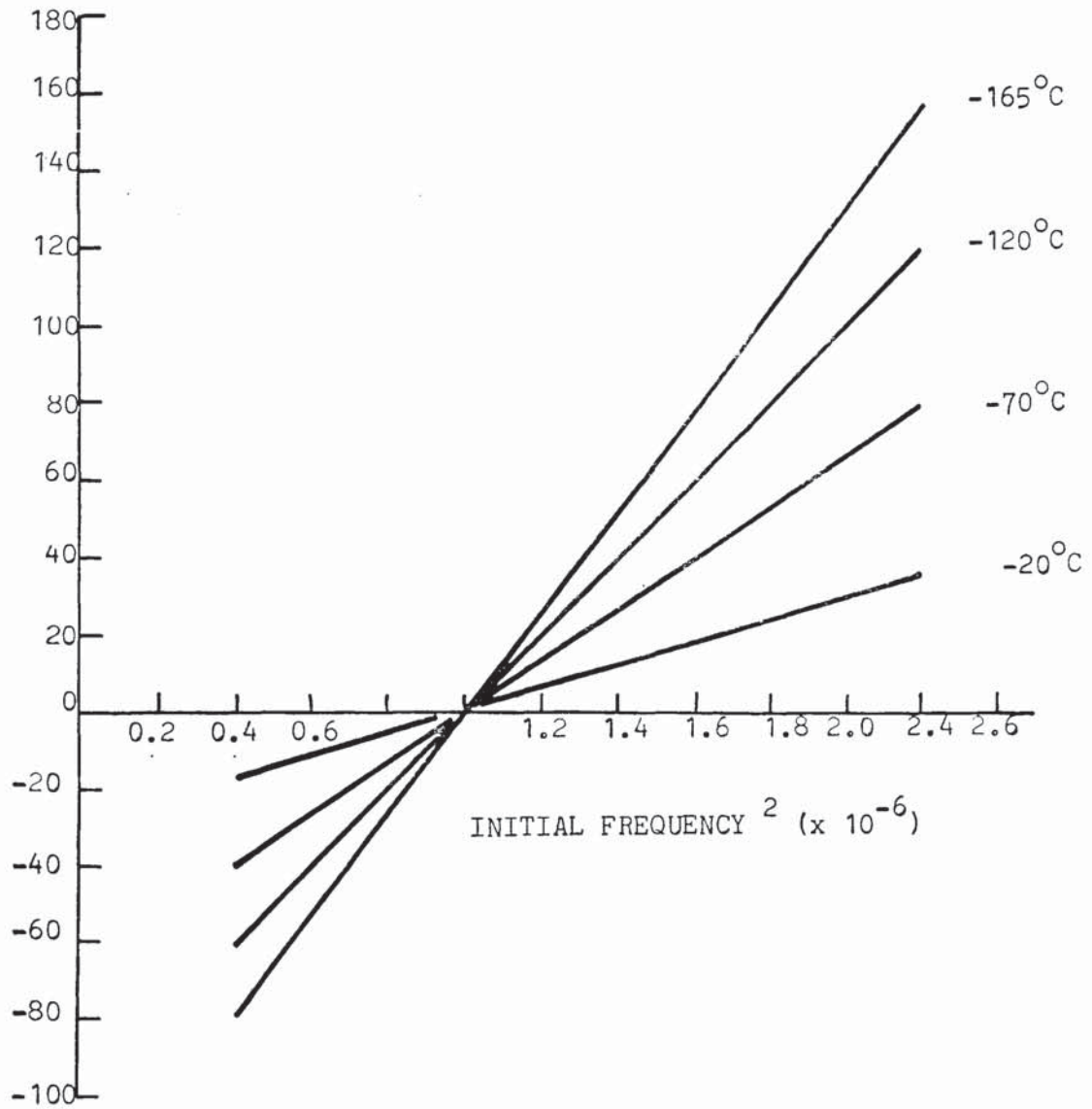
FIGURE 6.2.   Change in temperature correction factor with
              initial gauge frequency.

SPEC NO			INITIAL FREQUENCY Hz	MEASURED STRAIN $\mathcal{E}_r$	TEMPERATURE CORRECTION $\mathcal{E}_{tc}$	THERMAL CONTRACTION $\mathcal{E}_c$
1	EXTERNAL	Gauge 1	1420	675	−1950	−1275
		Gauge 2	1395	679	−1945	−1266
		Gauge 3	1406	643	−1950	−1307
		Average				−1283
	INTERNAL		1419	585	−1950	−1365
2	EXTERNAL	Gauge 1	1071	527	−1840	−1313
		Gauge 2	1116	631	−1850	−1219
		Gauge 3	1114	541	−1850	−1309
		Average				−1288
	INTERNAL		1126	498	−1855	−1357
3	EXTERNAL	Gauge 1	868	489	−1785	−1298
		Gauge 2	868	520	−1785	−1265
		Gauge 3	866	505	−1795	−1281
		Average				−1281
	INTERNAL		861	423	−1785	−1362

TABLE 6.1. Summary of results obtained from tests to establish the correction factor for VWG's under transient temperature conditions.

obtain similar values of internal and external strains, the gauge factor for embedded gauge would need to be increased from 2.927 to about 3.4.

To check the gauge factor of the embedded gauges, a second series of tests were carried out in which the specimens were cooled in four increments, and load tested at each temperature. Values of temperature corrected thermal strains are given in Table 6.2. Again the external strains were higher, in this case by about 10% However, the results of the load tests, summarised in Table 6.3, indicated no significant change in gauge factor. On average the gauge factor was about 2.5% lower for the internal gauges. The difference in thermal strain could not, therefore, be attributed to a change in gauge factor. The influence may, therefore, be a true measure of the relative thermal contraction through the specimen. For the test programme proper, the gauge factor has not been changed.

6.2.2 Test Specimens

The thermal contraction and elastic modulus were measured using the same set of specimens. For each concrete, three 150mm diameter by 450mm cylinders were cast, each with a 150mm long embedded Vibrating Wire Strain Gauge located along the axis of the cylinder in the middle third as shown in Figure 6.3. After casting at a mix temperature of 20°C, the moulds were covered and stored in a constant temperature room for 24 hours. The specimens were then de-moulded, sealed in heavy duty polythene bags and maintained at 20°C until the time of testing. Prior to . testing the trowelled end of each cylinder was capped to provide a flat bearing surface.

6.2.3 Loading Rigs

Three hydraulic loading rigs were used to enable one set of three specimens to be tested simultaneously. A section through a rig is shown in Figure 6.3. and working drawings are given in Appendix 1. Stainless steel, EN58B, was used to avoid embrittlement problems during low temperature testing. The rig design is

TEMPERATURE °C	SPECIMEN 1		SPECIMEN 2		SPECIMEN 3		AVERAGE	
	Int	Ext	Int	Ext	Int	Ext	Int	Ext
17 to -20	-386 (1.052)	-367	-398 (1.147)	-347	-395 (0.995)	-397	-393 (1.062)	-370
-20 to -70	-289 (1.125)	-257	-302 (1.127)	-268	-296 (1.161)	-255	-296 (1.139)	-260
-70 to -115	-277 (1.070)	-259	-291 (1.124)	-259	-277 (1.117)	-248	-282 (1.106)	-255
-115 to -165	-255 (1.081)	-236	-265 (1.123)	-236	-250 (1.147)	-218	-257 (1.117)	-230
17 to -165	-1207 (1.079)	-1119	-1256 (1.132)	-1110	-1218 (1.089)	-1118	-1228 (1.103)	-1115

( ) Indicates ratio of internal to external strain.

TABLE 6.2. Results of tests to establish the gauge factor for embedded gauges under conditions of changing temperature.

TEMPERATURE (°C)		STRAIN AT 13.8N/mm² ASSUMING GF = 2.927			MEAN
		Spec. 1	Spec. 2	Spec. 3	
20	Int	439	489	445	464
	Ext	416	457	345*	437
	Ratio	0.948	0.935	0.775*	0.942
		GF for Embedded Gauge			2.757
-20	Int	478	513	452	481
	Ext	430	487	440	452
	Ratio	0.900	0.949	0.974	0.940
		GF for Embedded Gauge			2.751
-70	Int	448	475	427	450
	Ext	422	477	423	441
	Ratio	0.942	1.004	0.991	0.979
		GF for Embedded Gauge			2.866
-125	Int	413	455	423	430
	Ext	406	452	408	422
	Ratio	0.983	0.993	0.965	0.981
		GF for Embedded Gauge			2.871
-165	Int	395	421	395	404
	Ext	408	440	403	417
	Ratio	1.033	1.045	1.020	1.032
		GF for Embedded Gauge			3.021

$$\text{GF for Embedded Gauge} = \frac{\text{External Strain}}{\text{Internal Strain}} \times 2.927$$

TABLE 6.3. Results of tests to establish the gauge factor for embedded gauges under load, at temperatures from 20°C to -165°C.
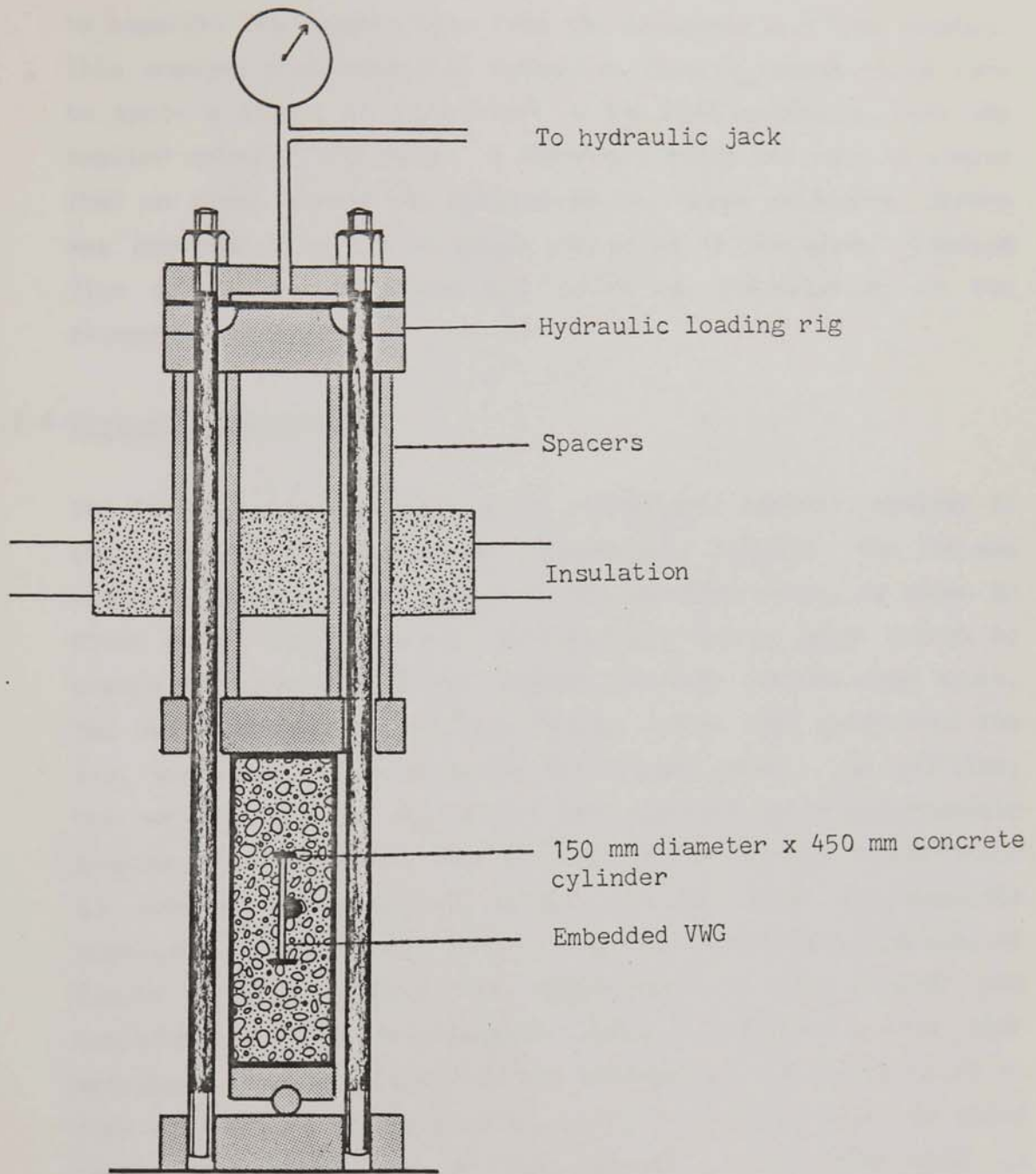
FIGURE 6.3.   Section through the loading rig and test specimen.

similar to that used by Taywood Engineering (78) for creep testing at ambient and elevated temperatures, the most significant difference being the extended reaction frame required to separate the loading head from the cryogenic specimen housing. This enabled a conventional hydraulic loading system to be used to apply a stress of 13.8 N/mm^2 to the test cylinders. Load was applied using a hand pump. A three-way valve was used to ensure that an equal stress was applied to all three cylinders. Stress was recorded from a dial gauge connected to the pump. Loading rigs are shown in Plate 6.1 prior to installation in the cryogenic cabinet.

6.2.4 Cryogenic Containment

The loading rigs were located in a cryogenic cabinet, similar to that used for low temperature permeability testing. The lid was modified to allow penetration of the reaction frame, as shown in Plate 6.2. This involved cutting three holes, large enough to enable the specimens to be lowered into the cabinet from above. The seals around the reaction frames, where they penetrated the lid, were made using expanded polystyrene plugs. In addition, the set temperature controller was replaced by a programmable temperature controller, and the base of the cabinet strengthened to support the combined weight of the rigs and concrete specimens. Cooling was achieved by the controlled injection of liquid nitrogen (LN$_2$). The temperature in the cabinet was monitored using a thermocouple located adjacent to the test specimens. This was linked to the temperature controller which in turn activated a solenoid valve in the LN$_2$ supply line. To avoid temperature variations in the cabinet, a fan was used to circulate the cold gas and baffles at the LN$_2$ inlet point both dispersed the gas around the chamber and prevented LN$_2$ from being sprayed directly onto the test specimens.

6.2.5 Test Procedure

After sealed curing for 8 weeks, one set of specimens was removed from the plastic bags and located in the loading rigs. They were then wrapped in plastic film to prevent moisture movement during

PLATE 6.1. Cylindrical specimens located in the hydraulic loading rigs prior to installation into the cryogenic cabinet.

PLATE 6.2. Three loading rigs installed in the cryogenic test rig prior to testing.

the test. The loading rigs were installed into the cryogenic cabinet and strain readings taken to provide a datum at the start of the test. The specimens were loaded in increments of $3.45N/mm^2$ up to a maximum stress of $13.8N/mm^2$ and strain readings taken after each increment of load to determine the elastic modulus, E, of the three specimens at ambient temperature. The load was then released and the strain again recorded.

To cool the specimens, the programmable temperature controller was set at a rate of $-2°C$ per hour. After 20 hours when the temperature had dropped from $+20$ to $-20°C$, the temperature was held for one hour. During the one hour dwell period the VWG was monitored to ensure that no strain changes were occurring, hence indicating that the concrete specimen was in thermal equilibrium with the environment in the cryogenic cabinet. The strain was then recorded and the specimens load cycled, the procedure being the same as at $20°C$. Cooling was then continued at a rate of $2°C$ per hour and load cycling repeated at temperatures of -70, -120 and $-165°C$. The data obtained, therefore, provided information on both the elastic modulus, E, for each load cycle, and thermal contraction over the range $+20$ to $-165°C$.

6.3 TEST RESULTS

Gauge readings for individual test specimens obtained throughout the test regime described above are given in Table 6.4, together with calculated strain values. A gauge factor of 2.927×10^{-3} microstrain per frequency^2 has been used throughout. Furthermore, the temperature correction curve for gauges tensioned to an initial frequency of $1,000Hz$ has also been used throughout. Initial frequencies, given in Table 6.4, were all in the range 928 to $1,009Hz$. From Figure 6.2, which illustrates the relationship between temperature correction factor $\mathcal{E}_{tc}$ and frequency^2, it will be seen that the variation in $\mathcal{E}_{tc}$ due to the variation in initial frequency will have been less than 25 microstrain when cooling from $20°C$ to $-165°C$. As the recorded thermal contraction was of the order of $1,700$ microstrain, the change in $\mathcal{E}_{tc}$ has been ignored, being equivalent to less than 1.5% of the total thermal contraction.

Mix AEC

SPECIMEN NO.	TEMP (°C)	0	3.45	6.90	10.35	13.80	0
1	16	10180 -	10342 (-68)	10517 (-178)	10699 (-267)	10909 (-365)	10276 (-52)
2	16	10271 -	10433 (-85)	10622 (-180)	10823 (-276)	11052 (-378)	10292 (-11)
3	16	10212 -	10397 (-99)	10573 (-188)	10762 (-279)	10979 (-377)	10266 (-29)
Ave.	16		(-91)	(-182)	(-274)	(-373)	(-30)
1	-20	10228 -	10306 (-42)	10454 (-120)	10642 (-213)	10855 (-314)	10243 (-6)
2	-20	GAUGE FAILURE					
3	-20	10264 -	10402 (-73)	10570 (-158)	10768 (-254)	10984 (-352)	10283 (-10)
Ave.	-20		(-58)	(-139)	(-234)	(-333)	(-9)
1	-70	10206 -	10271 (-35)	10394 (-101)	10549 (-179)	10710 (-258)	10213 (-4)
2	-70	GAUGE FAILURE					
3	-70	10245 -	10365 (-64)	10514 (-141)	10686 (-225)	10856 (-305)	10262 (-9)
Ave.	-70		(-50)	(-121)	(-202)	(-282)	(-7)
1	-120	10283 -	10298 (-8)	10410 (-67)	10549 (-138)	10691 (-207)	10303 (-11)
2	-120	GAUGE FAILURE					
3	-120	10310 -	10405 (-50)	10540 (-119)	10692 (-193)	10844 (-264)	10317 (-4)
Ave.	-120		(-29)	(-93)	(-166)	(-236)	(-8)
1	-165	10392	10393 (0)	10482 (-46)	10608 (-109)	10755 (-180)	10412 (-10)
2	-165	GAUGE FAILURE					
3	-165	10392	10487 (-49)	10614 (-112)	10757 (-181)	10912 (-252)	10397 (-3)
Ave.			(-25)	(-79)	(-145)	(-216)	(-7)

Mix HS

SPECIMEN NO.	TEMP (°C)	0	3.45	6.90	10.35	13.80	0
1	15	10415 -	10527 (-57)	10690 (-137)	10861 (-217)	11037 (-295)	10415 (0)
2	15	10776 -	10917 (-65)	11090 (-141)	11285 (-222)	11510 (-311)	10776 (0)
3	15	10093 -	10357 (-70)	10522 (-143)	10684 (-213)	(-?)	10093 (-?)
Ave.	15		(-64)	(-141)	(-219)	(-307)	(0)
1	-20	10433 -	10568 (-68)	10698 (-132)	10851 (-203)	11031 (-283)	10433 (0)
2	-20	10798	10941 (-65)	11117 (-142)	11295 (-216)	11503 (-298)	10800 (-1)
3	-20	10138	10237 (-55)	10379 (-131)	10520 (-203)	10682 (-282)	10136 (1)
Ave.	-20		(-63)	(-135)	(-207)	(-288)	(2)
1	-70	10123	10209 (-48)	10344 (-121)	10475 (-189)	10630 (-266)	10124 (-6)
2	-70	10757	10881 (-57)	11047 (-131)	11214 (-202)	11394 (-275)	10761 (-2)
3	-70	10186	10314 (-49)	10447 (-119)	10593 (-188)	(-262)	10110 (-7)
Ave.	-70		(-51)	(-124)	(-193)	(-268)	(-5)
1	-120	10128	10223 (-53)	10337 (-114)	10440 (-168)	10663 (-279)	10115 (7)
2	-120	10804	10922 (-54)	11066 (-117)	11220 (-182)	11389 (-251)	10603 (0)
3	-120	10132	10217 (-47)	10328 (-107)	10448 (-170)	10584 (-238)	10136 (-2)
Ave.	-120		(-51)	(-113)	(-173)	(-256)	(-3)
1	-165	10188	10307 (-65)	10396 (-117)	10517 (-174)	10636 (-232)	10188 (0)
2	-165	10911	11033 (-54)	11169 (-112)	11314 (-172)	11469 (-233)	10907 (2)
3	-165	10276	10344 (-36)	10453 (-93)	10564 (-149)	10684 (-208)	10274 (-1)
Ave.	-165		(-41)	(-107)	(-165)	(-224)	(1)

Mix LW

SPECIMEN NO.	TEMP (°C)	0	3.45	6.90	10.35	13.80	0
1	18	10057 -	10287 (-128)	10566 (-272)	10916 (-437)	11325 (-611)	10083 (-15)
2	18	09915 -	10135 (-128)	10394 (-268)	10712 (-426)	11063 (-585)	09955 (-24)
3	18	10097 -	10336 (-131)	10625 (-278)	10986 (-446)	11379 (-610)	10710 (-319*)
Ave.	18		(-129)	(-273)	(-436)	(-602)	(-20)
1	-20	09925 -	10144 (-127)	10439 (-285)	10753 (-439)	11096 (-594)	09945 (-12)
2	-20	09800 -	10006 (-124)	10276 (-276)	10555 (-420)	10857 (-564)	09826 (-16)
3	-20	10581 -	10574 (3)	10578 (1)	10881 (-142)	11230 (-293)	10677 (-48)
Ave.	-20		(-126)	(-281)	(-430)	(-579)	(-14)
1	-70	09940 -	10172 (-133)	10454 (-284)	10771 (-439)	11121 (-595)	09953 (-8)
2	-70	09835 -	10055 (-131)	10313 (-274)	10593 (-417)	10897 (-561)	09853 (-11)
3*	-70	10468 -	10385 (+43)	10578 (-55)	10885 (-201)	11234 (-352)	10926 (-219)
Ave.	-70		(-132)	(-279)	(-428)	(-578)	(-10)
1	-120	09586 -	09720 (-87)	09921 (-211)	10140 (-338)	10360 (-458)	09598 (-8)
2	-120	09471 -	09597 (-85)	09781 (-203)	09982 (-325)	10178 (-437)	09481 (-7)
3*	-120	10370 ; -	10361 (+5)	10329 (+22)	10545 (-90)	10771 (-199)	10377 (-4)
Ave.	-120		(-86)	(-207)	(-332)	(-448)	(-8)
1	-165	09529 -	09649 (-80)	09806 (-179)	09986 (-288)	10164 (-390)	09518 (7)
2	-165	09413 -	09528 (-79)	09678 (-178)	09846 (-284)	10010 (-382)	09405 (6)
3	-165	09867 -	09991 (-74)	10159 (-170)	10353 (-275)	10550 (-376)	10298 (-246)
Ave.	-165		(-78)	(-176)	(-282)	(-382)	(7)

Mix PFA

SPECIMEN NO.	TEMP (°C)	0	3.45	6.90	10.35	13.80	0
1	16	10268 -	10402 (-71)	10585 (-164)	10782 (-258)	11018 (-365)	10290 (-12)
2	16	10148 -	10253 (-58)	10398 (-135)	10556 (-215)	10740 (-305)	10166 (-10)
3	16	10248 -	10368 (-64)	10544 (-154)	10734 (-246)	10961 (-351)	10280 (-17)
Ave.	16		(-64)	(-151)	(-240)	(-340)	(-13)
1	-20	10309 -	10442 (-70)	10638 (-168)	10841 (-264)	11033 (-351)	10337 (-15)
2	-20	10193 -	10294 (-55)	10443 (-134)	10610 (-218)	10764 (-292)	10211 (-10)
3	-20	10299 -	10415 (-61)	10598 (-154)	10799 (-250)	10981 (-330)	10318 (-10)
Ave.	-20		(-62)	(-152)	(-244)	(-324)	(-12)
1	-70	10268 -	10370 (-54)	10522 (-132)	10691 (-215)	10858 (-293)	10296 (-15)
2	-70	GAUGE FAILURE					
3	-70	10254 -	10349 (-51)	10492 (-125)	10654 (-205)	10817 (-282)	10270 (-9)
Ave.	-70		(-53)	(-129)	(-210)	(-288)	(-12)
1	-120	10319 -	10418 (-52)	10553 (-120)	10692 (-188)	10834 (-255)	10329 (-5)
2	-120	GAUGE FAILURE					
3	-120	10296 -	10386 (-48)	10516 (-114)	10648 (-179)	10790 (-247)	10296 (0)
Ave.	-120		(-50)	(-117)	(-184)	(-251)	(-3)
1	-165	10398 -	10500 (-52)	10620 (-112)	10750 (-174)	10884 (-236)	10397 (0)
2	-165	GAUGE FAILURE					
3	-165	10358 -	10456 (-51)	10572 (-109)	10698 (-171)	10827 (-231)	10349 (5)
Ave.	-165		(-52)	(-111)	(-173)	(-234)	(3)

TABLE 6.4. Individual gauge results obtained during the tests to measure both elastic modulus and thermal contraction.

6.3.1 Thermal Contraction

The thermal contraction recorded over the temperature range -15°C to -165°C is illustrated in Figure 6.4. Each point represents the average value obtained from the three specimens tested for each of the four concrete mixes.

The results are also given in Table 6.5 presented in terms of thermal expansion coefficients within each of the four temperature increments and the average value over the full range. On examination of the results presented in Figure 6.4 and Table 6.5, it can be seen that there was little difference between the three normal weight concretes, whilst the lightweight concrete exhibited lower thermal expansion coefficients. Values of total thermal contraction for mixes AEC, HS and PFA were 1,710 1,789 and 1,784 microstrain respectively, i.e. all values were within 3% of the mean of 1,761 microstrain. The contraction was not uniform throughout the range of test temperatures; the coefficient of thermal expansion reduced from an average value of 13.16 microstrain per °C over the range +15 to -20°C, to 9.75 microstrain per °C over the range -120 to -165°C.

The thermal contraction of the lightweight aggregate concrete was less than exhibited by the normal weight mixes with an average value of 1,386 microstrain over the range +18 to -165°C. The thermal expansion coefficient reduced from 10.24 microstrain per °C in the range +18 to -20°C to 7.57 microstrain per °C in the range -120 to -165°C. There are two reasons for the reduced thermal contraction of the lightweight concrete:-

(1) The thermal expansion coefficient of the concrete is determined largely by the thermal expansion coefficient of the aggregate, which constitutes about 70% of the volume. The lighweight aggregate has a lower coefficient than the gravel aggregate used in the three normal weight mixes.

(2) The moisture content of lightweight concrete is higher than that of the normal weight concrete by virtue of the porous nature of the lightweight aggregate. During cooldown,

TEMPERATURE °C

Range of published results

Mix AEC
Mix HS
Mix LW
Mix PFA

THERMAL STRAIN
(microstrain)
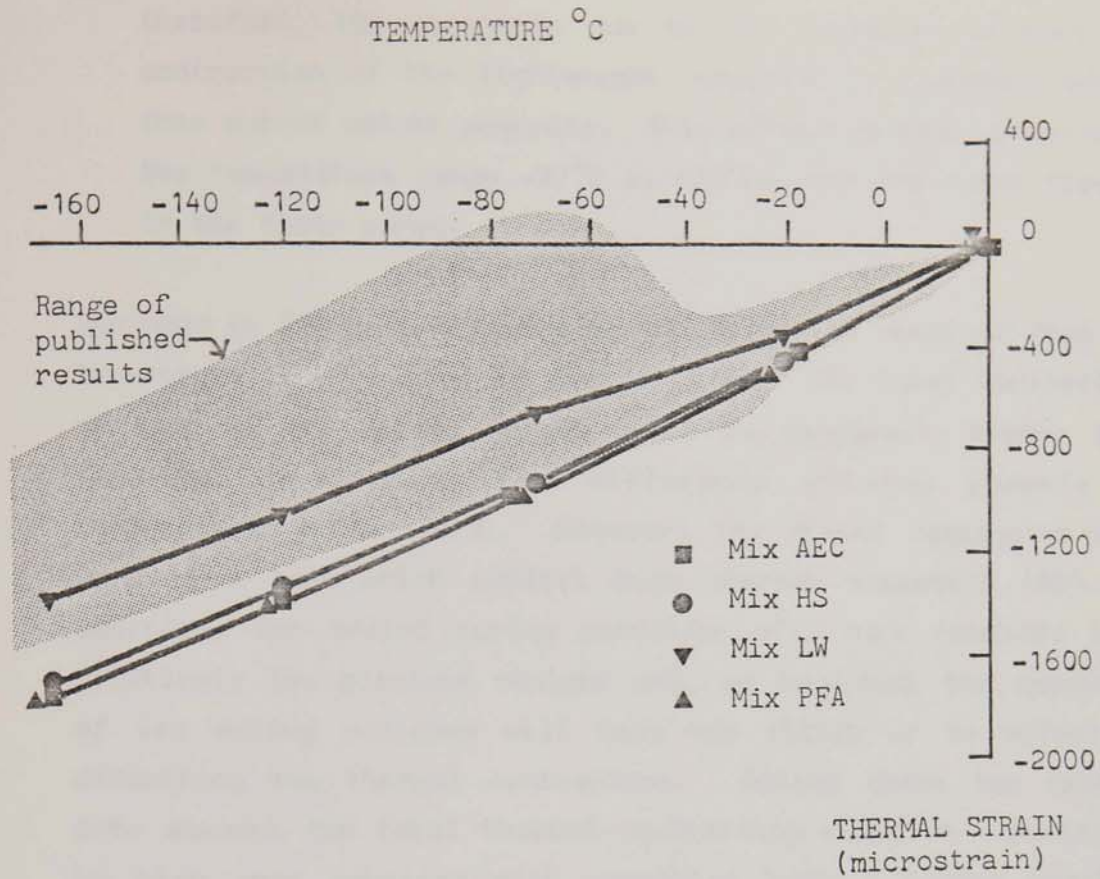
FIGURE 6.4.   Thermal contraction recorded over the temperature
range 20°C to -165°C.

TEMPERATURE RANGE °C	THERMAL EXPANSION COEFF. (Microstrain per °C)			
	AEC	HS	LW	PFA
15 to -20	12.53	13.57	10.24	13.39
-20 to -70	9.64	8.84	5.42	9.48
-70 to -120	9.24	8.80	7.66	8.86
-120 to -165	8.76	7.84	7.62	8.55
Ave 15 to -165	9.88	9.50	7.57	9.86

TABLE 6.5.   Thermal expansion coefficients.

therefore, the expansion due to ice formation offsets the contraction of the lightweight concrete to a greater extent than normal weight concrete. This effect is most apparent in the temperature range -20°C to -70°C, when the water freezes in the finer pores.

Included in Figure 6.4 is the range of results obtained from the literature as discussed in Section 2.6.1. The total contraction of each of the normal weight mixes is marginally higher than recorded previously, the difference arising largely at temperatures below -70°C. However, the gravel aggregates used were of a type which exhibit high thermal expansion (86). In addition, the sealed curing condition will have resulted in a relatively low moisture content and, as recorded, the expansion of ice during cooldown will have had little or no effect in offsetting the thermal contraction. Taking these two factors into account the total thermal contraction would be expected to be high when compared with concretes with a higher moisture content and containing aggregates with lower thermal expansion coefficients.

6.3.2 Elastic Modulus

Stress-strain curves obtained for each of the four concretes at five test temperatures are given in Figure 6.5 (a-d). Each curve represents the average of three test specimens. The elastic modulus has been obtained graphically by plotting the best straight line (determined visually) through the four strain values recorded at stress levels of 3.45, 6.90, 10.35 and 13.8 N/mm^2. The gradient has then been determined by extrapolating the line back to the vertical stress axis, and dividing the apparent strain change by the nett stress.

Calculated values of elastic modulus, E_c, are given in Table 6.6 together with stress and strain values used in the derivation. Again there was close agreement between the three normal weight mixes, particularly at temperatures below -70°C. The high strength mix yielded the higher values down to -20°C, this being consistent with the higher strength. The elastic
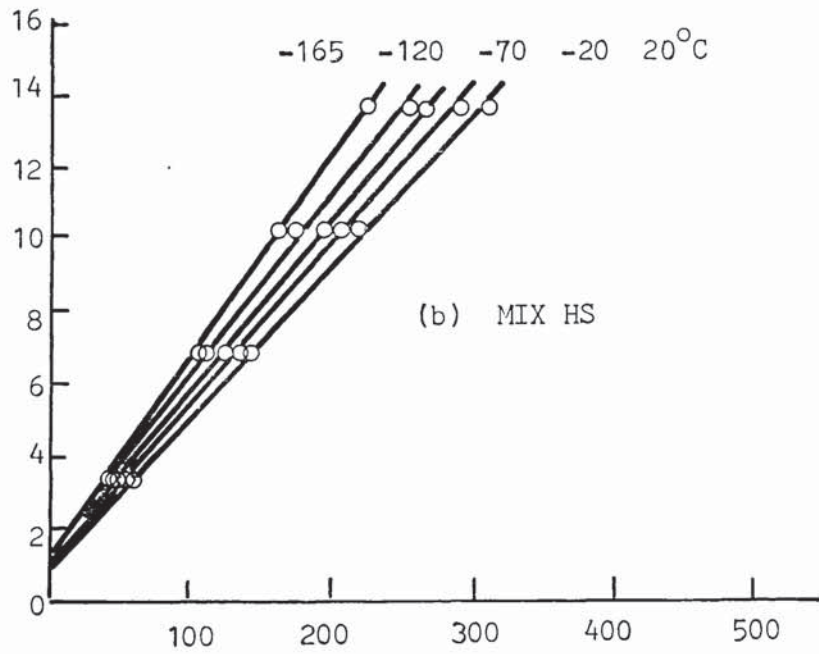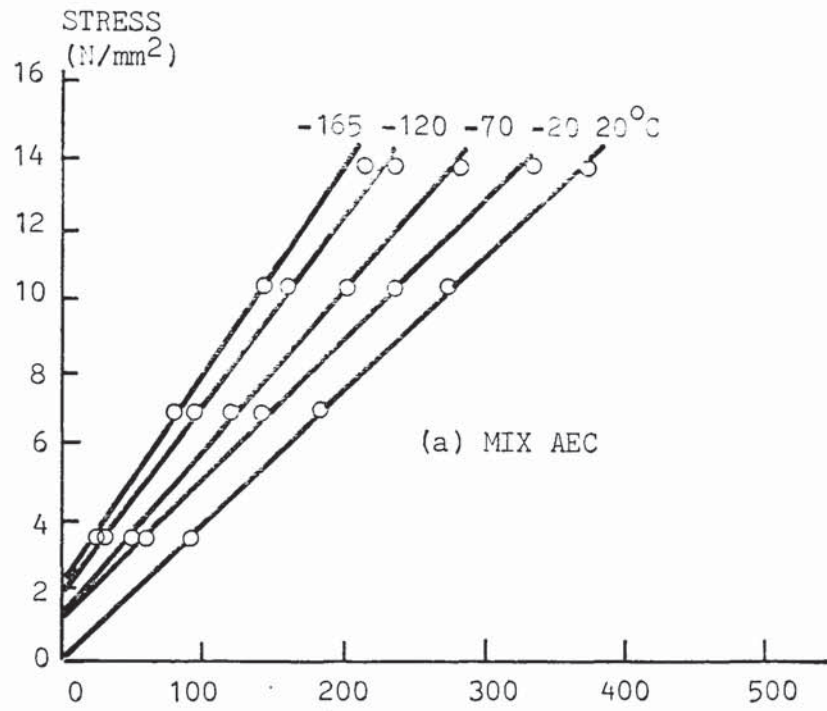
FIGURE 6.5. Stress-strain curves for specimens loaded to a stress of 13.8N/mm² at temperatures from 20°C to −165°C.

FIGURE 6.5. Stress-strain curves for specimens loaded to a stress of 13.8N/mm² at temperatures from 20°C to -165°C.

- 231 -
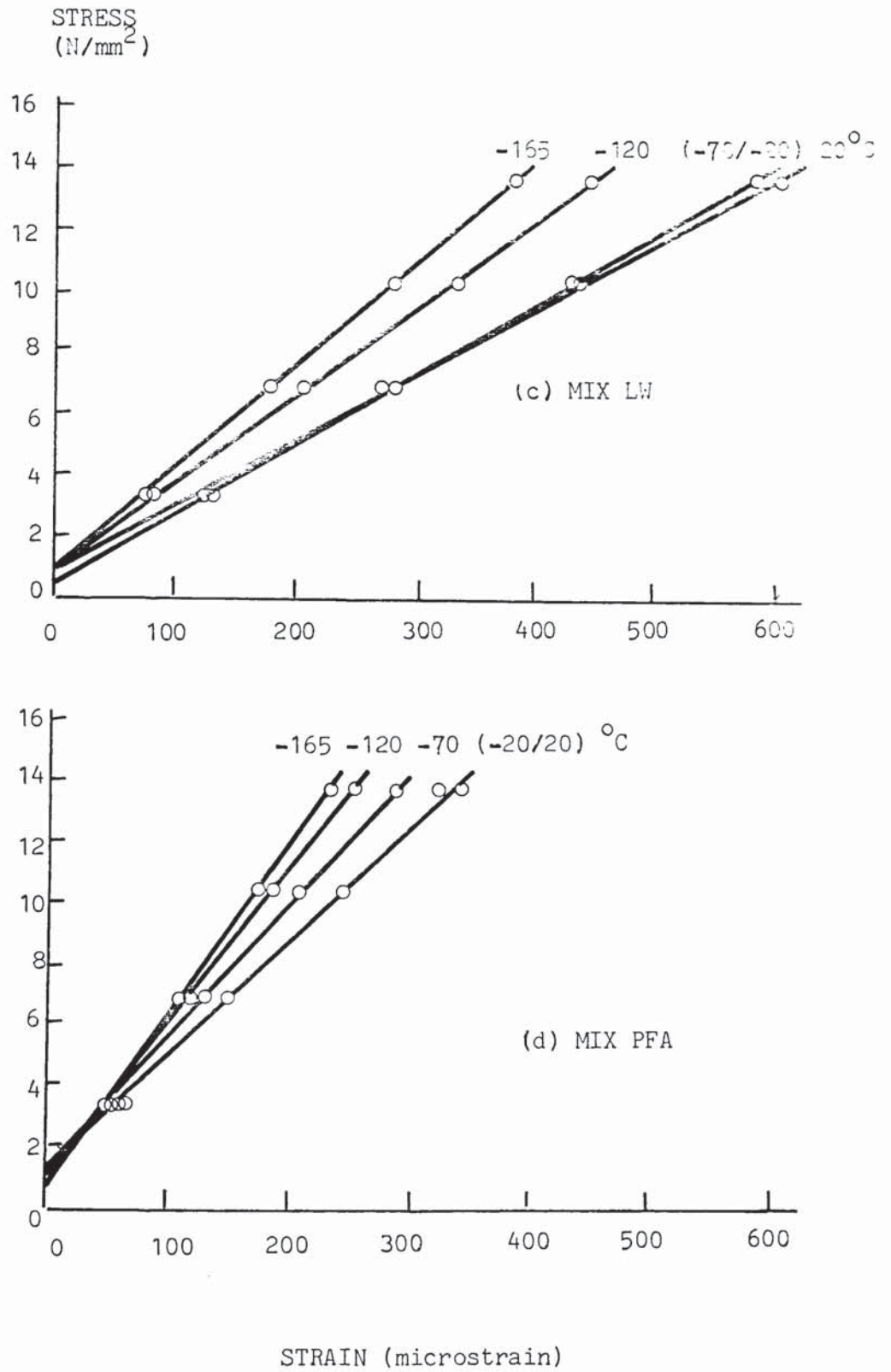
CONCRETE MIX	TEST TEMP ($^{\circ}$C)	STRESS RANGE (MPa)	STRAIN (Microstrain)	ELASTIC MODULUS (kN/mm^2)
HS	15	13.8 − 0.9 = 12.9	302	42.7
	−20	13.8 − 0.9 = 12.9	283	45.6
	−70	13.8 − 1.1 = 12.7	268	47.4
	−120	13.8 − 1.1 = 12.7	247	51.4
	−165	13.8 − 1.1 = 12.7	224	56.7
AE	16	13.8 − 0 = 13.8	372	37.1
	−20	13.8 − 1.1 = 12.7	320	39.7
	−70	13.8 − 1.2 = 12.6	275	45.8
	−120	13.8 − 1.8 = 12.0	227	52.9
	−165	13.8 − 2.1 = 11.7	202	58.5
LW	16	13.8 − 0.8 = 13.0	600	21.7
	−20	13.8 − 0.5 = 13.3	580	22.9
	−70	13.8 − 0.5 = 13.3	580	22.9
	−120	13.8 − 0.8 = 13.0	450	28.9
	−165	13.8 − 0.8 = 13.0	382	34.0
PFA	16	13.8 − 1.3 = 12.5	335	37.3
	−20	13.8 − 1.3 = 12.5	335	37.3
	−70	13.8 − 1.3 = 12.5	288	43.7
	−120	13.8 − 1.0 = 12.8	251	51.0
	−165	13.8 − 0.7 = 13.1	234	56.0

TABLE 6.6. Results used in the calculation of elastic modulus.

modulus of the lightweight concrete was appreciably lower than that of the normal weight mixes at all test temperatures, due to the lower stiffness of the lightweight aggregate. Values were generally 50-60% of those recorded for the normal weight mixes.

The influence of temperature on elastic modulus is illustrated in Figure 6.6 together with the range of results obtained from the literature. The results are generally consistent with data reported by other workers (see Section 2.7). With respect to the ambient value, at -165°C the modulus increased by about 55% for mixes AEC, LW and PFA. An increase of 33% was recorded for the high strength mix, which had the highest ambient value.
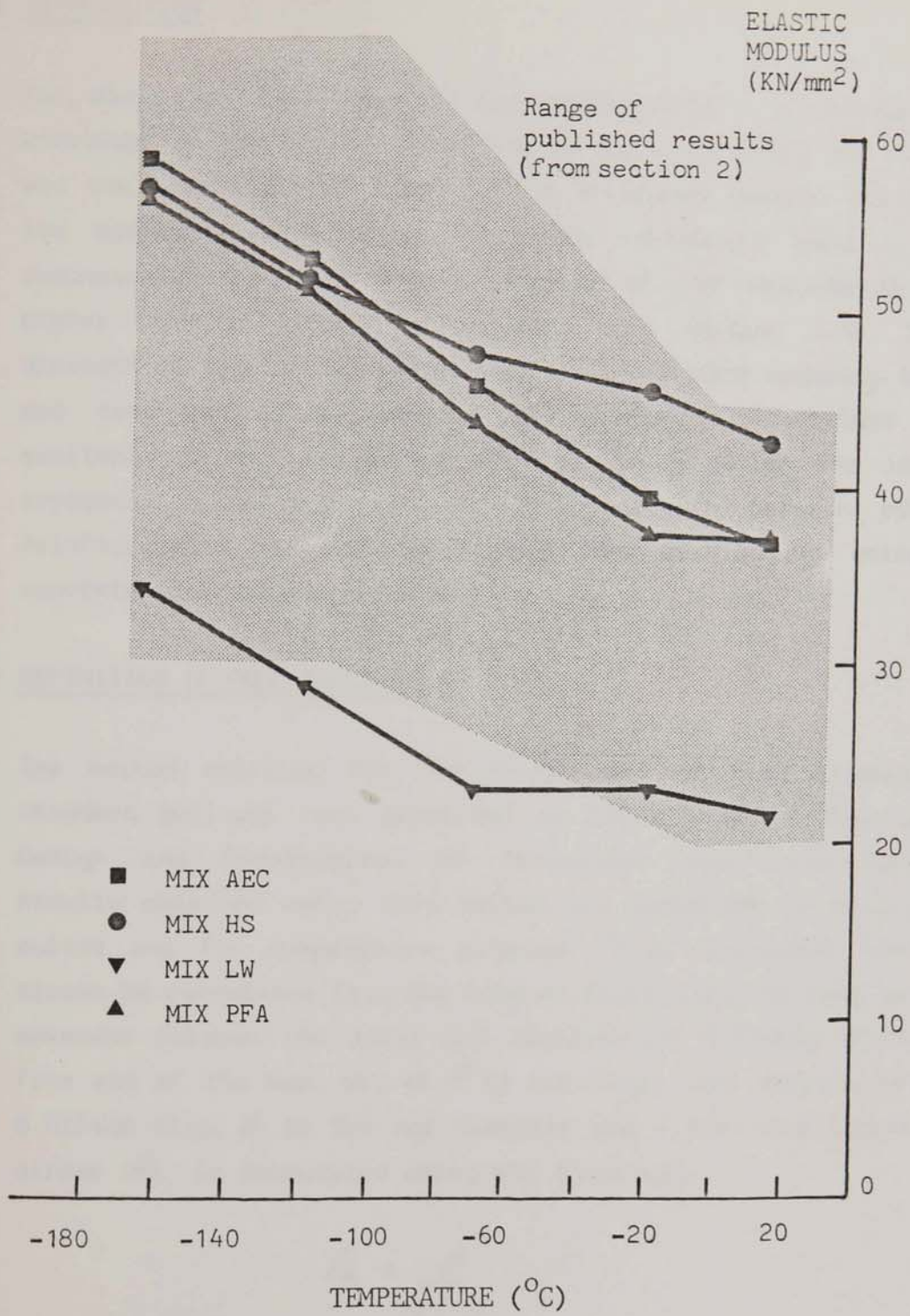
FIGURE 6.6. The influence of temperature on elastic modulus.

7. BOND TO REINFORCEMENT

7.1 INTRODUCTION

The design of reinforcement for crack control is dependant upon a knowledge of the tensile behaviour of both the steel and the concrete, and the bond strength which can be developed between the two. At the low operating temperature in tanks containing LNG, it has been demonstrated that the tensile strength of the concrete is about 150% higher than at ambient temperature (see section 5.3). The tensile strength of reinforcing steel also increases with reducing temperature, and data on its performance at cryogenic temperature is widely available in the literature [79]. To establish the influence of cryogenic temperature on the bond strength between concrete and reinforcement, pull-out tests have been carried out using the four concrete mixes given in Table 4.1.

7.2 DEFINITION OF BOND STRENGTH

The method selected for the measurement of bond strength was the standard pull-out test described in CP114 "Code of Practice for the Design and Construction of Structural Reinforced Concrete"[87]. Results obtained using this method are presented as bond stress/slip curves and for comparative purposes CP114 recommends that the bond stress be calculated from the load at first slip, defined as a relative movement between the steel and concrete of 0.0254mm (0.001") at the free end of the bar. So, if P is the total load applied to the bar at 0.0254mm slip, d is the bar diameter and L the bond length, the bond stress f_b is calculated using the equation:-

$$f_b = \frac{P}{\pi . L . d}$$

(7.1)

7.3 EXPERIMENTAL DETAILS

7.3.1 Test Specimens

Specimens comprised 150mm cubes each with a cast in 20mm diameter

reinforcing bar. The specimens were manufactured using BS cube moulds modified to enable the 960mm long bar to penetrate vertically through the centre as illustrated in Figure 7.1. To conform as closely as possible to the method desribed in CP114, helical reinforcement, also detailed in Figure 7.1, was provided in each cube to prevent bursting of the concrete during testing. The rebar was turned down at each end prior to installation in the mould. This was required to enable a deformation transducer to be located at one end and the jacking system at the other.

A total of 15No. specimens were cast from each concrete, 3 No. to be tested at 20, -20, -70, -120 and -165°C. The concrete was cured by sealing the cubes in polythene bags immediately after stripping the moulds. This method of "sealed curing" is designed to simulate the insitu condition in a structural member, in which only the initial mix water is available for hydration. Curing in water at 20°C, as required by BS1881[50], does not accurately represent insitu curing conditions. The limited number of moulds available meant that the specimens for each mix had to be cast from three seperate batches. To check batch variation, 6 No. 100mm cubes were also cast from each batch for testing at 7 and 28 days. The results are given in Table 7.1, which shows the high degree of batch to batch consistency achieved for each mix.

Two types of deformed reinforcement were used, both with a nominal diameter of 20mm. For mix AEC and mix HS, 9% nickel steel bar was used, supplied by George Clarke (Sheffield) Ltd. This special cryogenic steel was selected to avoid the problem of brittle fracture associated with conventional reinforcing steel. The two remaining mixes, LW and PFA, were tested using Krybar, manufactured by Trade Arbed in Luxembourg. This steel was developed specifically for low temperature applications and is supplied at a significantly lower cost than the 9% nickel steel. The decision to use Krybar for mixes LW and PFA, largely for commercial reasons, delayed casting of the test specimens. As a result, when the bond strength programme was carried out, the test specimens containing 9% nickel steel bar were about 4 months old, compared with 6 weeks for the Krybar specimens. In view of
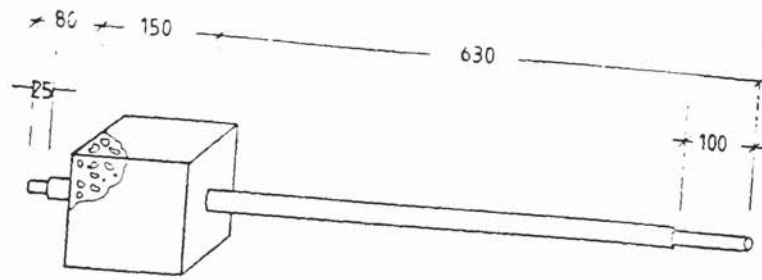
20mm bar cast into a 150mm cube
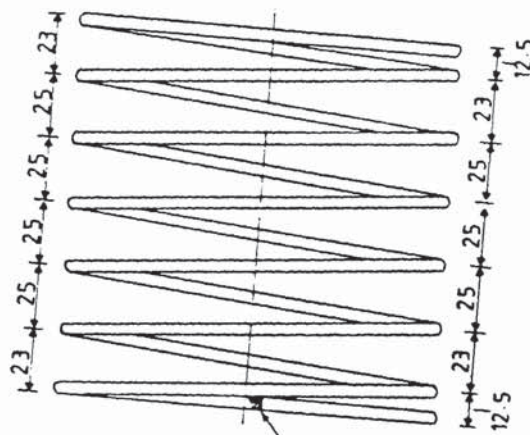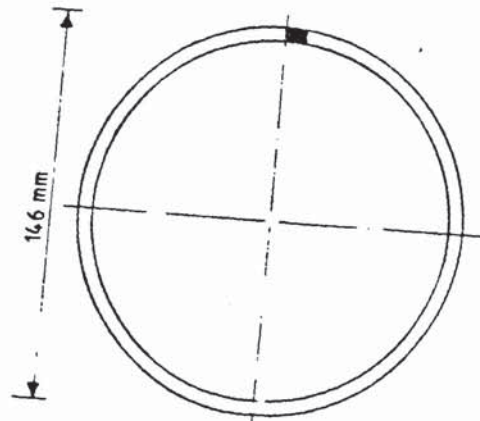
ELEVATION

Helix bent from
6mm mild steel
round bar complying
with BS785.

PLAN

FIGURE 7.1. Bond test specimen details.

MIX	BATCH	COMPRESSIVE STRENGTH (N/mm^2)					
		7 Days			28 Days		
AEC	1	44.2	42.2	43.6	54.4	54.5	53.0
	2	42.0	42.0	41.2	50.0	52.0	52.0
	3	42.6	42.8	41.8	50.8	50.2	49.0
HS	1	71.5	78.0	72.8	91.0	86.0	86.0
	2	67.6	68.6	69.4	85.0	87.0	82.0
	3	71.5	73.5	74.1	85.0	86.0	86.0
LW	1	38.2	37.2	39.8	49.8	47.2	48.4
	2	39.2	40.8	41.2	52.4	51.4	52.2
	3	38.8	38.3	40.6	49.4	48.0	49.3
PFA	1	41.5	43.5	49.0	58.0	62.0	60.0
	2	46.0	45.0	46.0	55.0	59.5	61.0
	3	42.5	45.6	44.8	52.4	51.4	52.2

TABLE 7.1.   Test cube results.

the method of curing, however, this age difference is not believed to have significantly affected the concrete properties.

7.3.2 Loading Rig

A schematic representation of the test arrangement is shown in Figure 7.2. Testing conformed to the requirements of CP114, with the exception of the need for the low temperature. Load was applied to the rebar using a 50 tonne Enerpac hydraulic cylinder. The system was arranged such that the hydraulics were remote from the cold environment to prevent freezing of the hydraulic oil. Load was transferred from the rebar to the cube through load bearing Tufnol insulation. Details of the loading system are given in the working drawings in Appendix 1.

7.3.3 Cryogenic Containment

The specimens were located within an insulated stainless steel tank designed to operate in the range +20 to -196°C. Only the long end of the rebar protruded through the cabinet base, to be connected to the loading system described above. Low temperatures were achieved by spraying liquid nitrogen (LN_2) into the cabinet through perforated copper pipes. Thermocouples linked to a temperature control unit and solenoid valve limited the flow of LN_2 into the cabinet and hence the temperature of the cryogenic environment.

7.3.4 Instrumentation

A deformation transducer, based on the continuously vibrating wire principle was developed to measure movement between the top of the concrete and the protruding end of the reinforcing bar. A schematic diagram of the transducer, illustrating the method of measurement is shown in Figure 7.3. Working drawings are included in Appendix 1. The transducer was calibrated at ambient temperature using slip gauges, these in turn being checked using a micrometer. The calibration was carried out up to a slip of 0.25mm. The results are given in Figure 7.4, which shows the relationship between the change in frequency[2] and slip to be

Cryogenic Chamber

Slip Transducer

Concrete Specimen

Tufnol Blocks

Hydraulic Jack

Grip

LN_2 Inlet

LN_2 EXHAUST
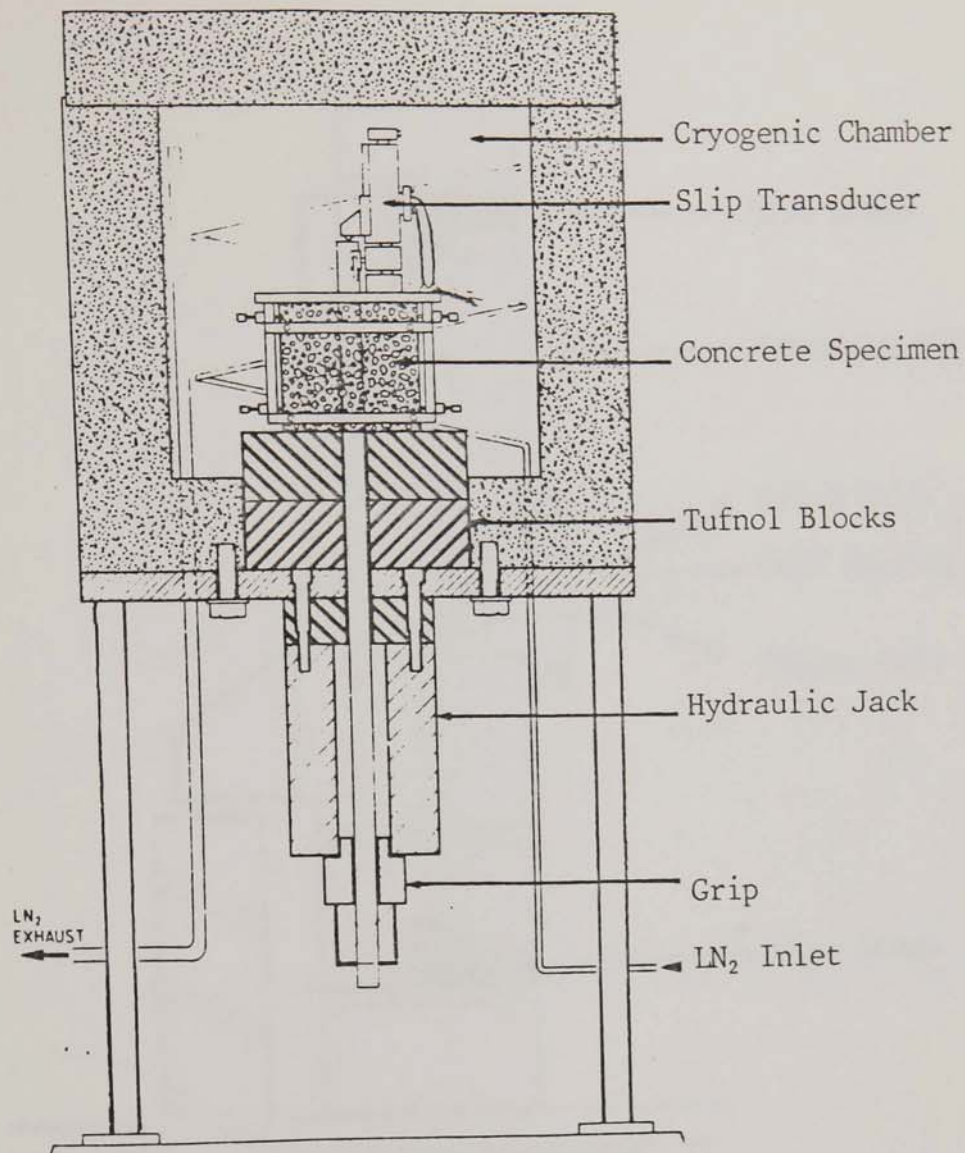
FIGURE 7.2.   Bond test arrangement.
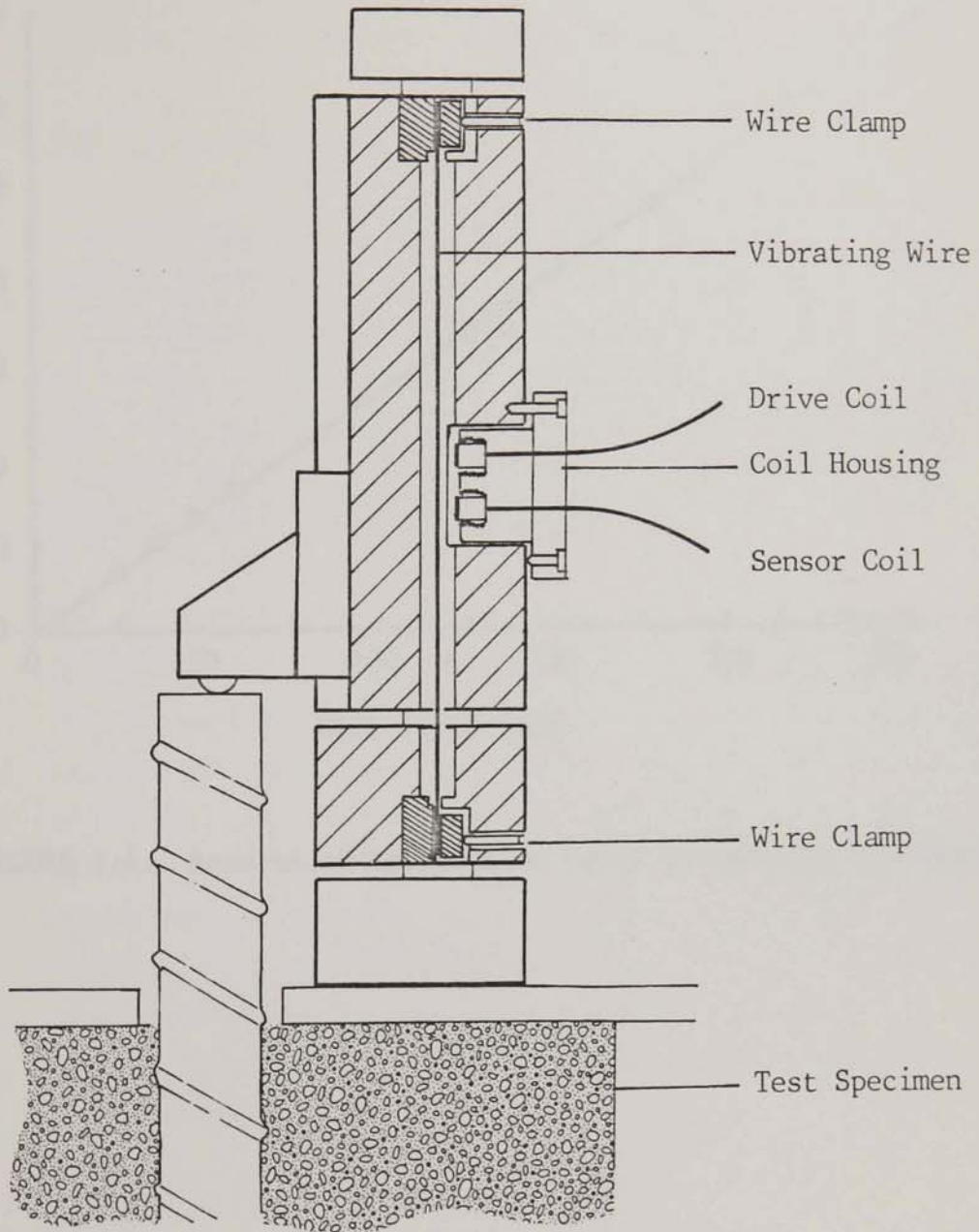
FIGURE 7.3. Section through the transducer for measurement of slip.

CHANGE IN FREQUENCY^2
$(1 \times 10^4 Hz)$

SLIP $(x \ 10^{-3} mm)$
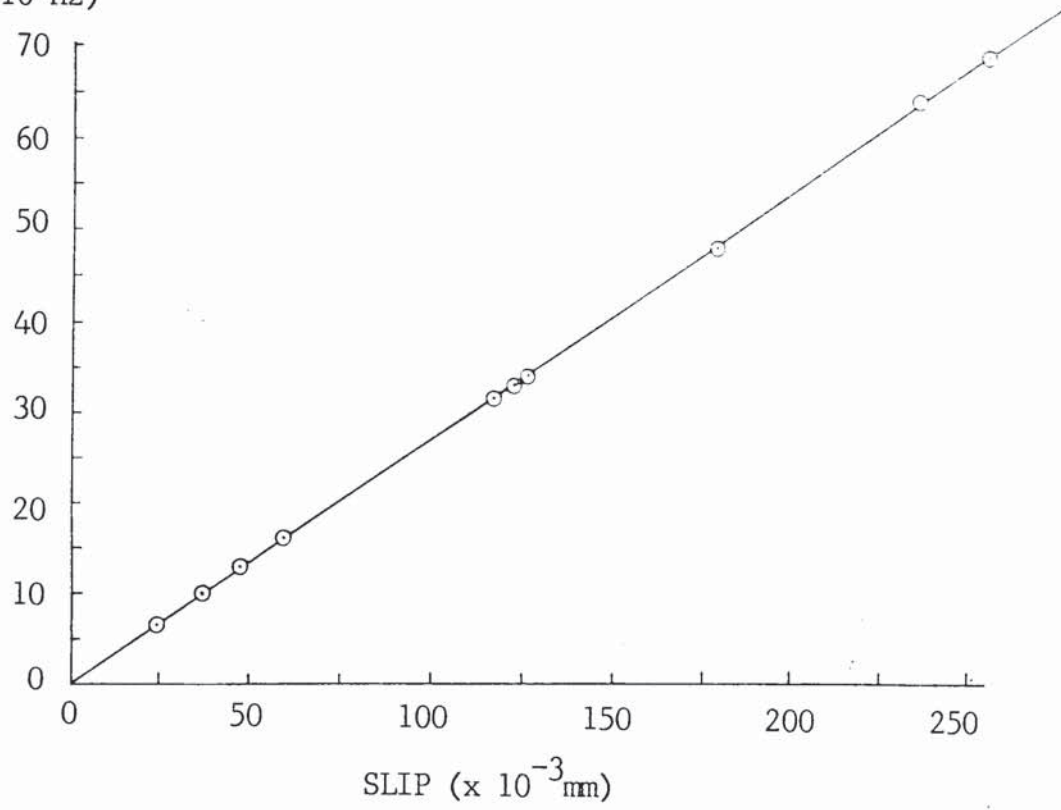
FIGURE 7.4. Results of calibration tests on the slip transducer.

linear. As previous tests on vibrating wire gauges at low temperature had shown no significant change in gauge factor. no further calibration tests were considered to be necessary. Furthermore, as all sixty specimens were tested using the same transducer, and tests were carried out at constant temperature, no corrections were required for either differences in initial frequency or changes in temperature.

7.3.5 Test Procedure

The test specimens were initially cooled down in a cryogenic cabinet adjacent to the bond test chamber. This enabled the 12 low temperature test specimens for each mix to be cooled slowly, at a rate of 2°C per hour, without prolonging the test period. Each mix was tested over a period of 5 days with the three ambient tests on Day 1 and three tests at -20, -70, -120 and -165°C on Days 2,3,4 and 5 respectively.

For the low temperature tests the loading rig and cabinet were precooled to the required test temperature. The test specimen was then transferred from the cooling cabinet to the test chamber and allowed to stabilise before the test commenced. Temperature stability was established by monitoring both a thermocouple located in the test chamber and the slip transducer. When temperature stability was achieved, usually within about 30 minutes, loading was applied to the reinforcing bar at a maximum rate of 30kN/minute until the slip exceeded 0.04mm. Output from the hydraulic pump and the transducer were permanently plotted on a U-V recorder.

7.4 TEST RESULTS

Summary graphs for each of the four concretes tested are given in Figures 7.5 (a-d) in which average curves derived from the three specimens tested at each temperature are presented. Values of bond stress for individual test specimens recorded at a slip of 0.0254mm are given in Table 7.2, together with average values for each concrete at each test temperature. These average values are included in Figure 7.6(a) which illustrates the change in bond stress with temperature for
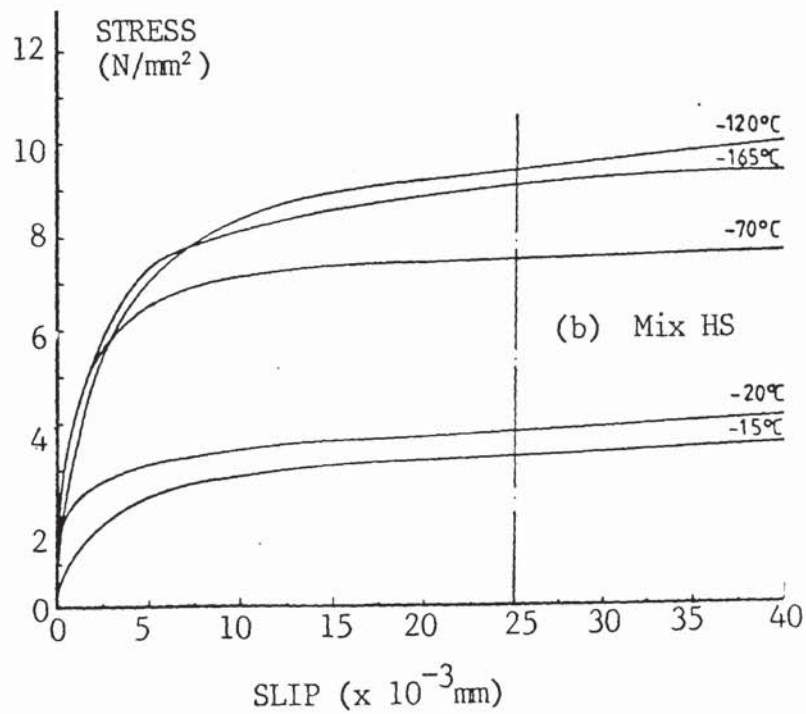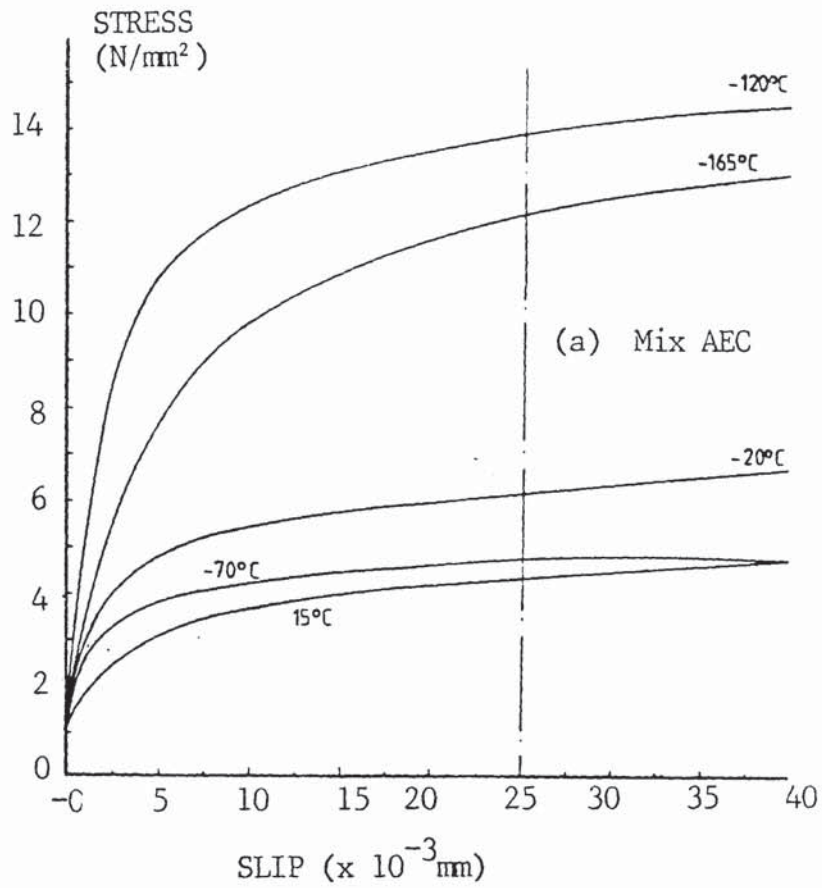
FIGURE 7.5. Bond stress vs slip curves recorded at temperatures down to -165°C.
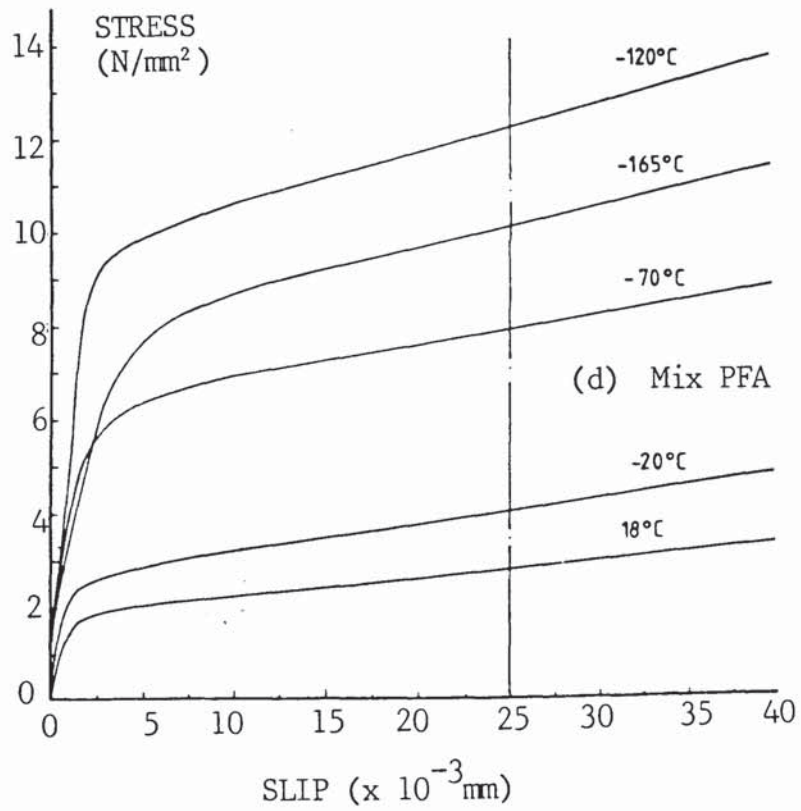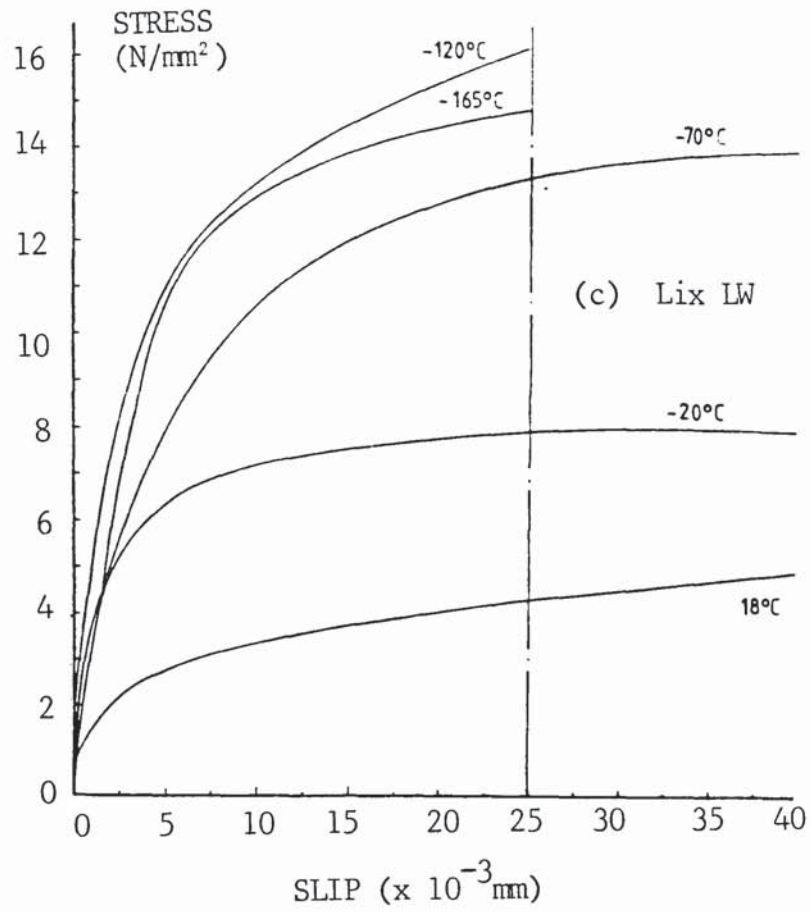
FIGURE 7.5. Bond stress vs slip curves recorded at temperatures down to −165°C.

TABLE 7.2. Bond test results obtained for individual specimens.

TEST TEMP (°C)	MIX AEC			MIX HS			MIX LW			MIX PFA		
	Batch	Age (Days)	Bond Stress (N/mm²)	Batch	Age (Days)	Bond Stress (N/mm²)	Batch	Age (Days)	Bond Stress (N/mm²)	Batch	Age (Days)	Bond Stress (N/mm²)
15	1	94	2.13	1	119	5.47	1	46	-	1	42	2.55
	1	94	3.88	1	119	3.06	1	46	4.32	1	42	2.90
	1	94	3.78	1	119	4.50	1	46	4.18	2	40	2.63
	Ave		3.26	Ave		4.34	Ave		4.25	Ave		2.69
-20	1	95	3.82	1	120	6.04	1	47	6.60	1	43	3.45
	1	95	2.60	1	120	6.35	1	47	9.76	1	43	4.45
	1	95	5.10	1	120	6.04	2	41	7.32	1	43	3.88
	Ave		3.84	Ave		6.14	Ave		7.89	Ave		3.93
-70	2	95	8.07	2	119	4.57	2	42	11.13	2	42	8.41
	2	95	7.07	2	119	5.44	2	42	14.75	2	42	6.57
	2	95	2.10*	3	119	3.95	2	42	14.29	2	42	8.69
	Ave		7.57	Ave		4.65	Ave		13.42	Ave		7.89
-120	2	97	8.79	2	121	15.58	2	43	16.88+	3	38	13.01
	2	97	4.57	2	121	12.17	3	41	16.50+	2	43	10.26
	3	92	15.07	3	-	-	3	41	15.31+	3	38	13.57
	Ave		9.48	Ave		13.88	Ave		16.23	Ave		12.28
-165	3	119	9.25	3	139	9.01	3	42	15.13	3	43	8.13
	3	119	8.88	3	139	15.26	3	42	17.25	3	43	16.00
	3	119	8.88	3	139	11.95	3	42	12.31	3	43	7.07
	Ave		9.00	Ave		12.07	Ave		14.90	Ave		10.04

* Not included in average   + Maximum stress when bar failed

each of the four concretes tested. With the exception of mix HS all the concretes exhibited similar bond-stress/temperature relationships. The bond strength increased steadily over the range 20 to -120°C with little change at the lower temperatures. The low value for mix HS at -70°C cannot be readily explained. The concrete batch from which the specimens were cast yielded a 28 days compressive cube strength similar to the other two batches so a dramatic change in materials proportions was unlikely. It is possible that the specimens were not adequately sealed, resulting in drying during the curing period. As demonstrated previously, a change in concrete properties at low temperature is primarily related to moisture content (see Section 2). A loss of moisture would be expected to reduce the amount by which the property changes with temperature. The increase in bond stress with reducing temperature is illustrated in Figure 7.6(b). Whilst the results are varied, it will be seen that the normal weight concretes tend to respond to temperature in approximately the same way. Little change occurred down to -20°C; between -20 and -120°C there was a progressive increase of up to $10N/mm^2$; and between -120 and -165°C there was a small reduction. For the lighweight mix, however, there was a considerable increase in bond at -20°C, and a continuing increase at about the same rate down to -70°C. Below -70°C the bond increased, but at a slower rate, down to -120°C and between -120°C and -165°C there was again a small reduction.

The difference in rate of increase in bond strength with reducing temperature for the normal weight and lightweight concrete is believed to be due largely to the differing moisture contents. It has been shown that water in concrete freezes progressively with reducing temperature starting in the larger pores. In lightweight concrete, the aggregate is porous and the moisture content can be double that in normal weight concrete (8% by weight compared with 4%). Furthermore, much of this water is contained in large pores in the aggregate which freezes at the higher temperatures resulting in a rapid response to temperature change. The majority of water in normal weight concrete is contained in much smaller pores and hence requires a much lower temperature to initiate freezing. Hence, whilst other properties, such as compressive and tensile strength appear to be affected most significantly by ice formation in the finer pores, the bond strength also appears to be affected by freezing in the larger capillaries.
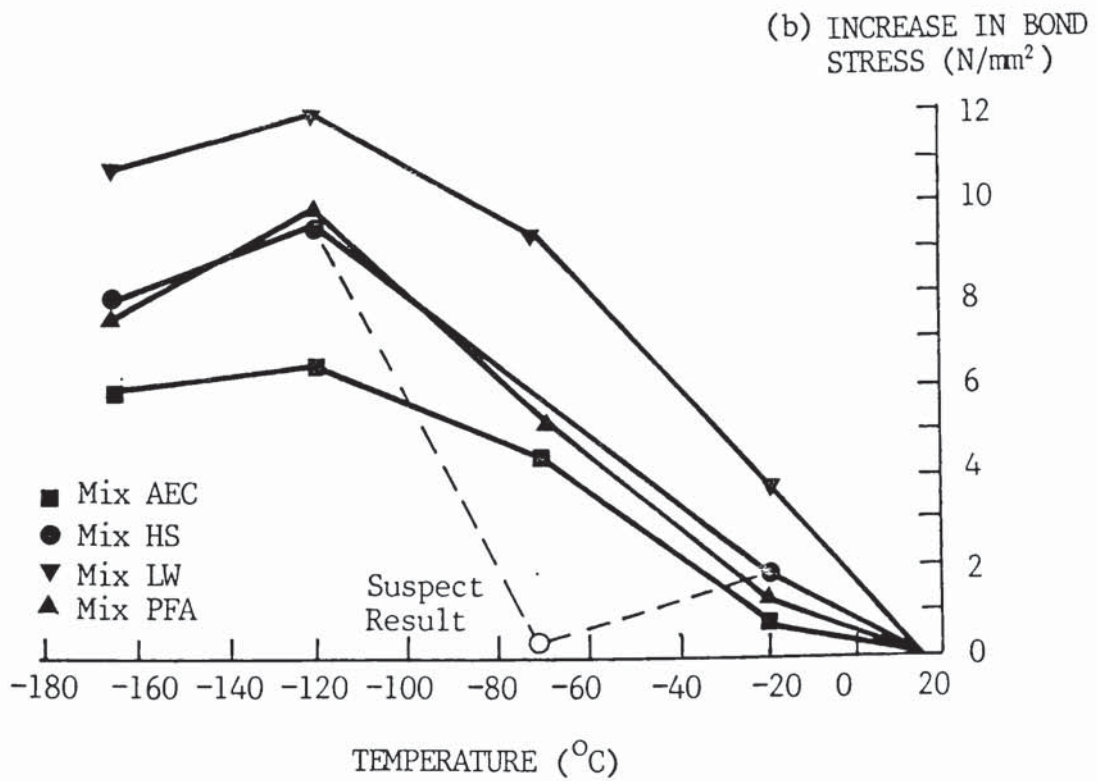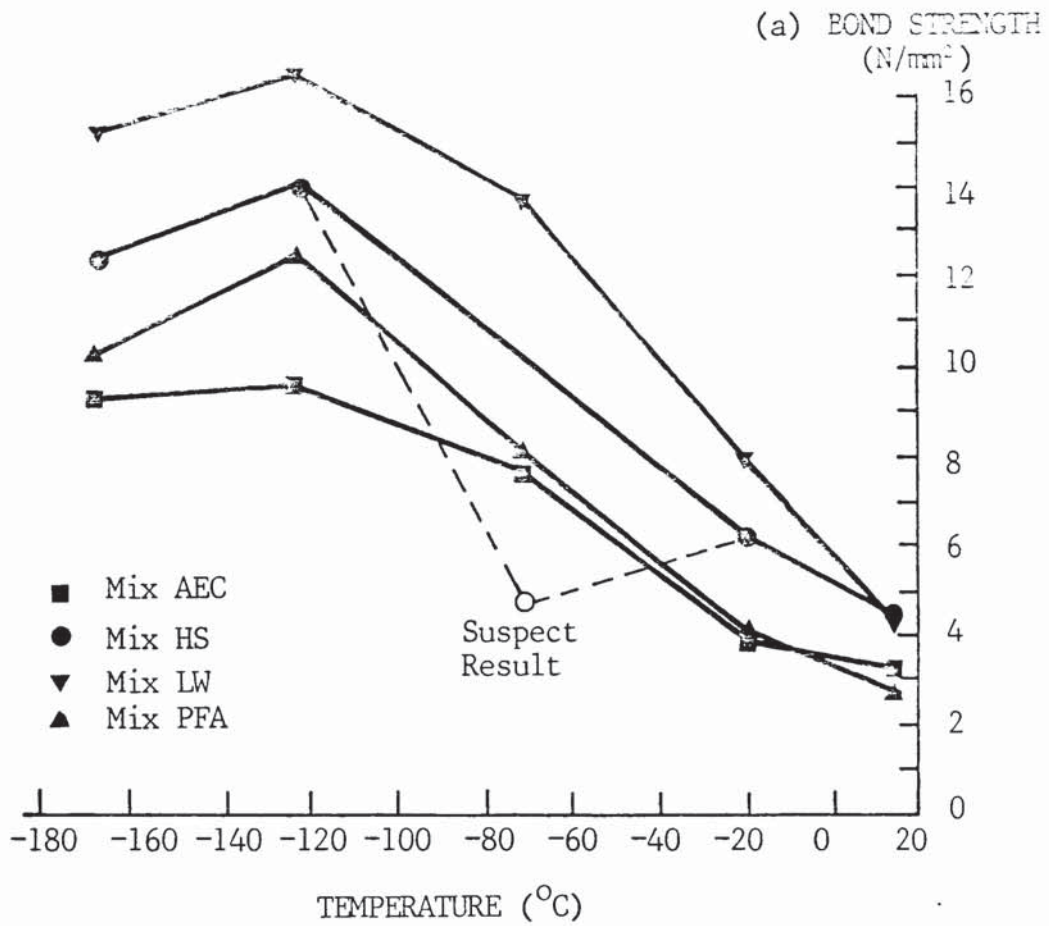
FIGURE 7.6. The influence of temperature on bond strength.

8. DISCUSSION OF RESULTS

8.1 INTRODUCTION

A range of tests have been carried out on four selected concretes to establish their suitability for use in cryogenic storage facilities. Properties measured include:-

(i)   Gas permeability
(ii)   Strength in direct tension and in bending.
(iii) Strain capacity in direct tension and in bending.
(iv)   Thermal expansion coefficient.
(v)   Elastic modulus
(vi)   Bond to reinforcement.

Tests were undertaken to establish the effect of temperature, within the range +20 to -165°C on the above properties. In addition, gas permeability tests were carried out to determine the residual gas permeability after both slow and rapid thermal cycles between ambient and cryogenic temperature. This section includes a discussion of the results obtained with regard to the following:-

-    The effect of temperature on the various properties.
-    The relationship between different properties.
-    The relative performance of the concretes tested.

8.2 EFFECT OF TEMPERATURE

Property changes with temperature are shown in Figures 8.1 to 8.4 for each of the four concrete mixes AEC, HS, LW and PFA respectively. The low temperature results are expressed as a percentage of the ambient values. In every case the most substantial changes occurred in tensile strength, flexural strength and bond to reinforcement. At -165°C, the increase in tensile and flexural strength was typically of the order of 150%. The bond strength was most significantly affected, with typical increases of the order of 200%, and up to 300% for mix PFA.

The effect of temperature on strain capacity was far less consistent. The increase at -165°C varied from only 20% for mix HS, to more than
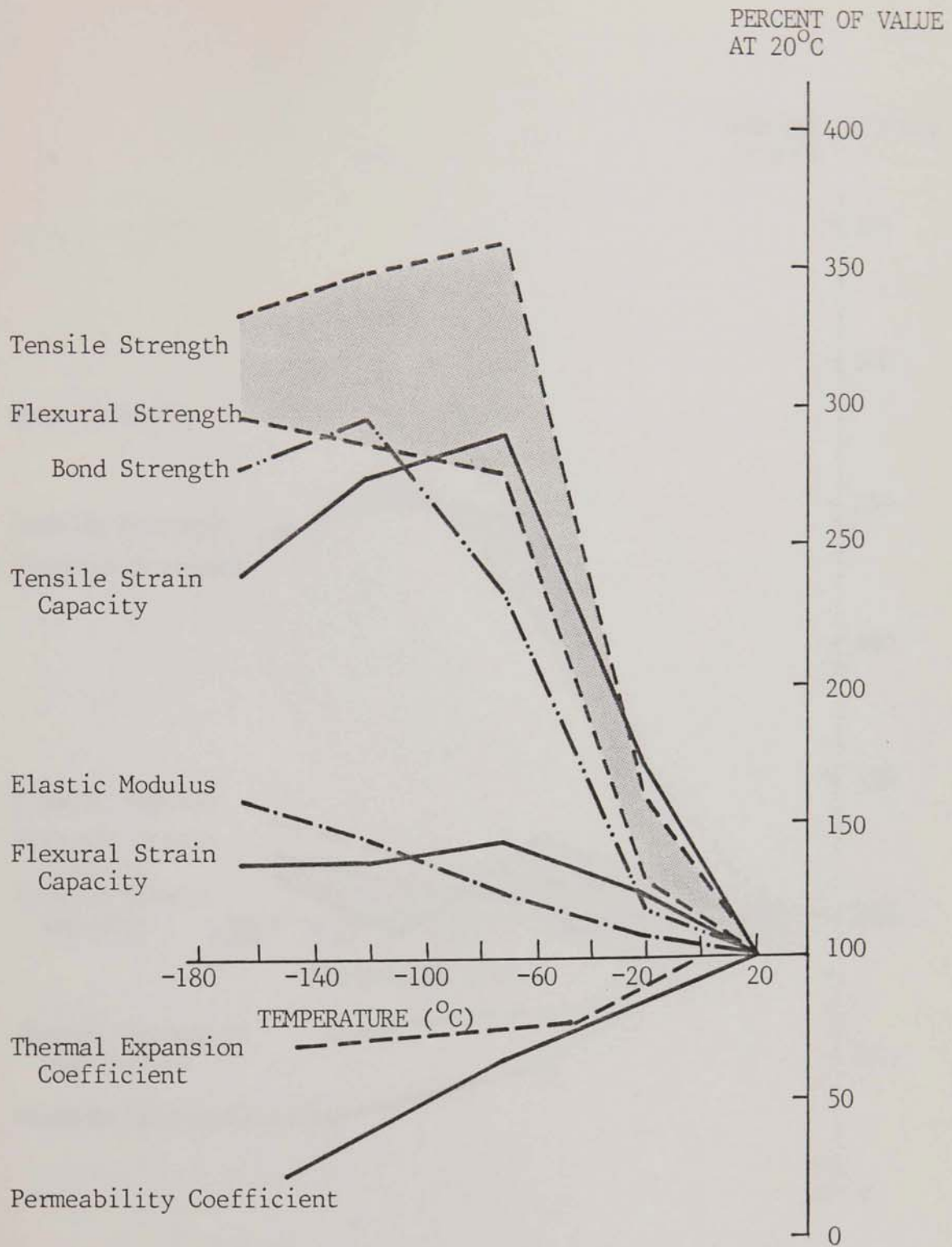
FIGURE 8.1. Percentage change in the properties of Mix AEC
with reducing temperature.
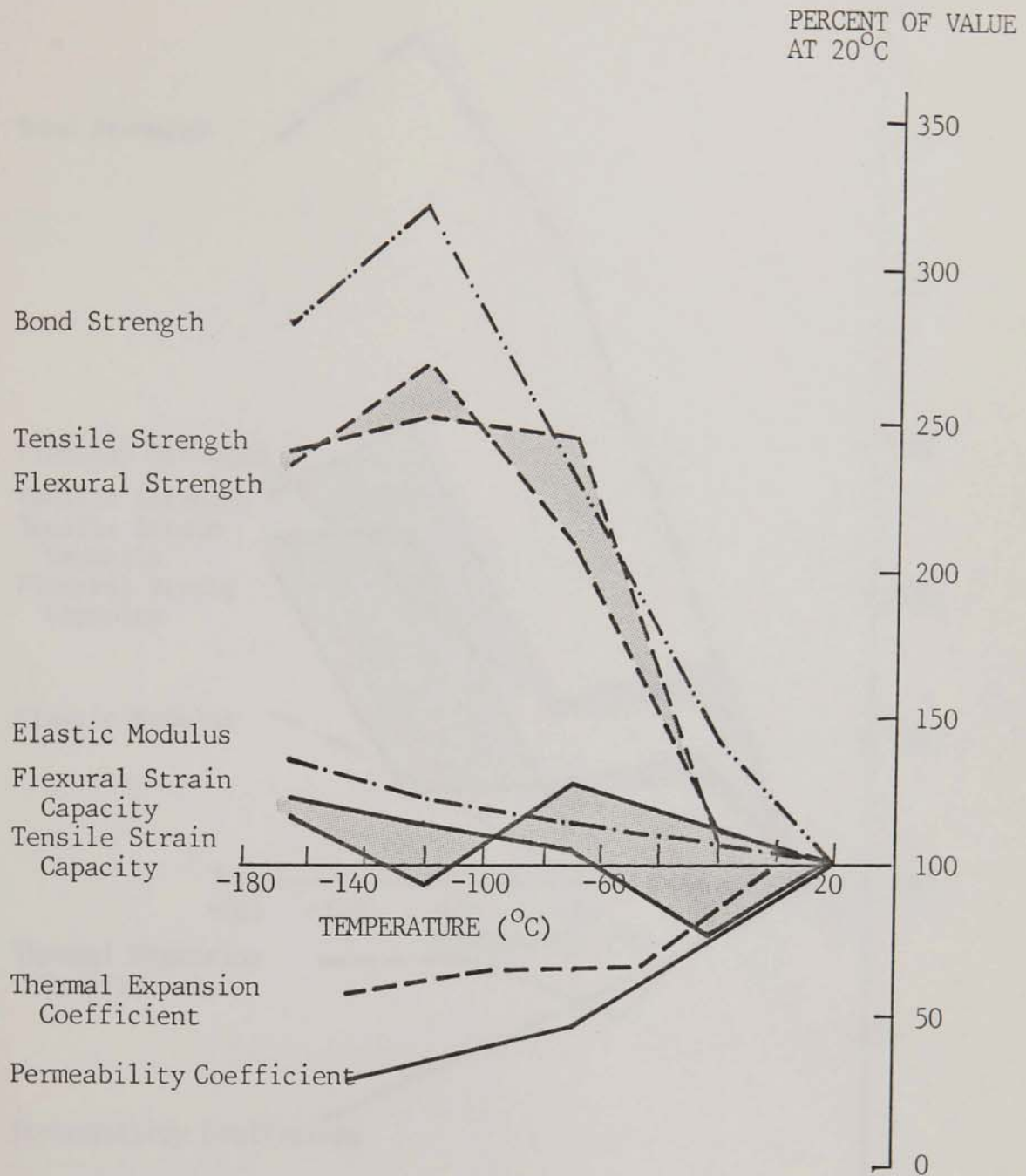
FIGURE 8.2.   Percentage change in the properties of Mix HS
with reducing temperature.
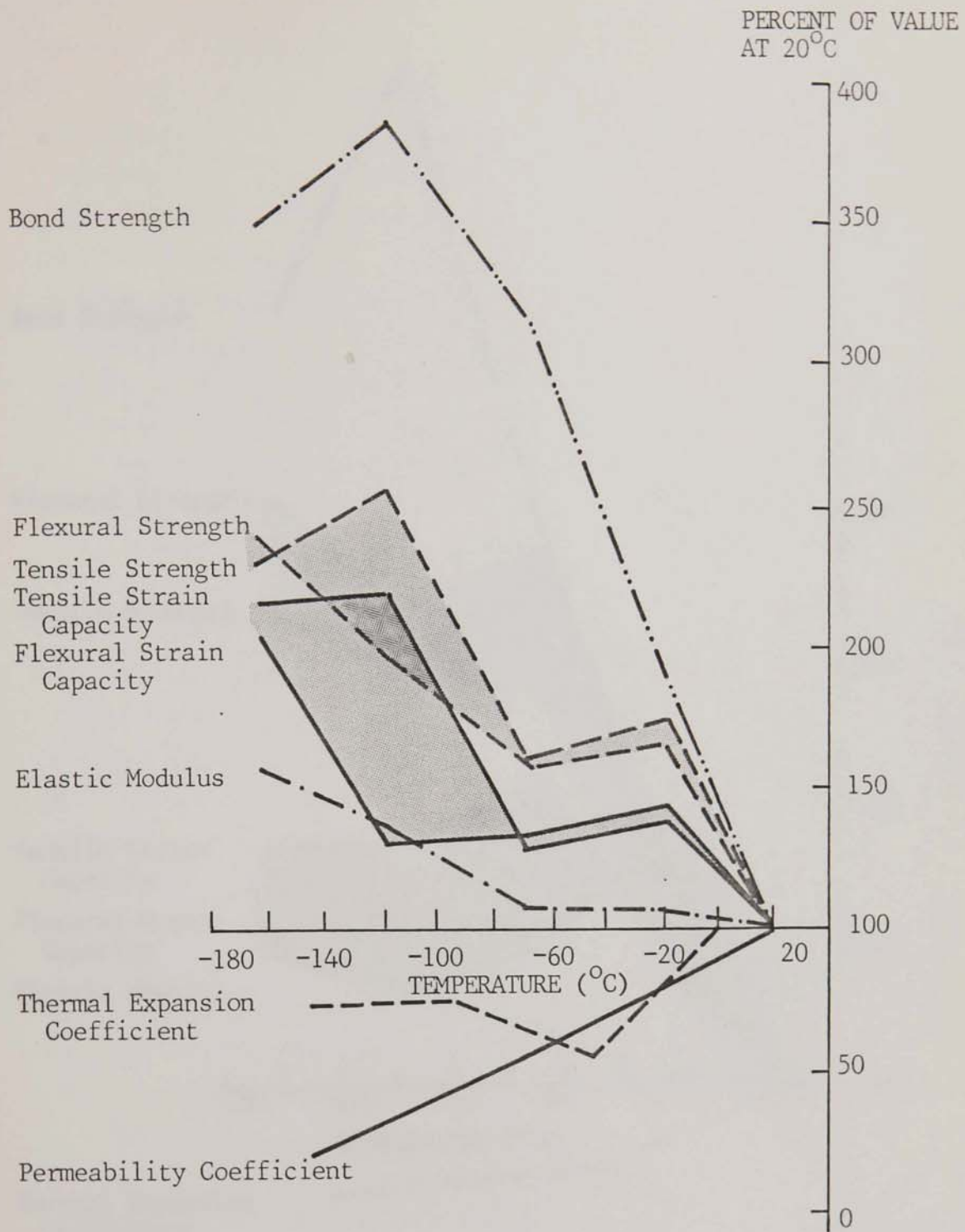
FIGURE 8.3. Percentage change in the properties of Mix LW with reducing temperature.

Bond Strength

Flexural Strength

Tensile Strength

Tensile Strain
Capacity

Flexural Strain
Capacity

Elastic Modulus

Thermal Expansion
Coefficient
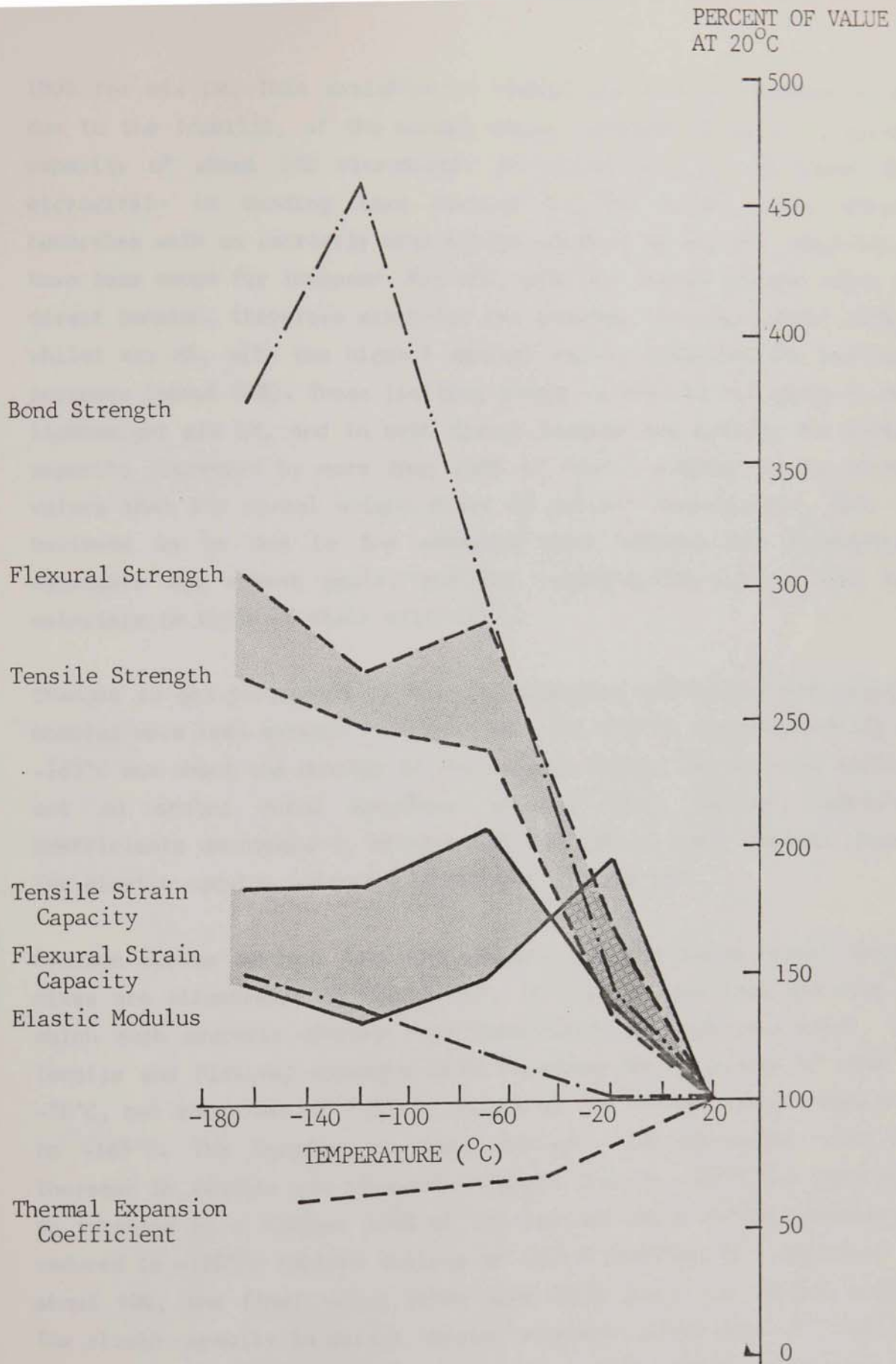
FIGURE 8.4.   Percentage change in the properties of Mix PFA
with reducing temperature.

100% for mix LW. This variation in percentage increase appears to be due to the inability of the normal weight concrete to exceed a strain capacity of about 110 microstrain in direct tension and about 220 microstrain in bending (see section 5.3.5). Hence normal weight concretes with an initially high strain capacity at ambient temperature have less scope for increase. Mix AEC, with the lowest ambient value in direct tension, therefore exhibited the greatest increase (about 150%), whilst mix HS, with the highest ambient value, exhibited the smallest increase (about 20%). These limiting strain values did not apply to the lightweight mix LW, and in both direct tension and bending the strain capacity increased by more than 100% at -165°C despite having higher values than the normal weight mixes at ambient temperature. This is believed to be due to the enhanced bond between the lightweight aggregate and cement paste, and the compatibility between the two materials in terms of their stiffness.

Changes in gas permeability, thermal expansion coefficient and elastic modulus were less marked. For mixes AEC, HS, and LW the permeability at -165°C was about one quarter of the ambient value. (No test was carried out on sealed cured specimens of mix PFA). Thermal expansion coefficients decreased to between 55% and 75% of their ambient value. The elastic modulus increased by between 33% and 55%.

Average curves derived from the results for the three normal weight mixes are illustrated in Figure 8.5. It will be seen that the rate at which each property changed with temperature was not consistent. The tensile and flexural strength both increased by in excess of 150% at -70°C, but there was no further change as the concrete was cooled down to -165°C. The increase in bond strength was consistent with the increase in tensile and flexural strength down to -70°C, but continued to increase by a further 100% of the ambient value as the temperature reduced to -120°C; further cooling to -165°C resulted in a reduction of about 50%, the final value being some 200% above the ambient value. The strain capacity in direct tension reached a peak value at -70°C and dropped marginally on further cooling to -165°C, whilst in bending the peak occurred at -20°C with little change thereafter. The permeability reduced almost linearly over the range +20 to -165°C, whilst the elastic modulus increased in a similar manner by about 50%. The thermal expansion coefficient reduced rapidly at temperatures down to -70°C and

PERCENT OF VALUE
AT 20°C

Bond Strength

Flexural Strength

Tensile Strength

Tensile Strain
  Capacity

Elastic Modulus

Flexural Strain
  Capacity

TEMPERATURE (°C)

Thermal Expansion
  Coefficient

Permeability Coefficient
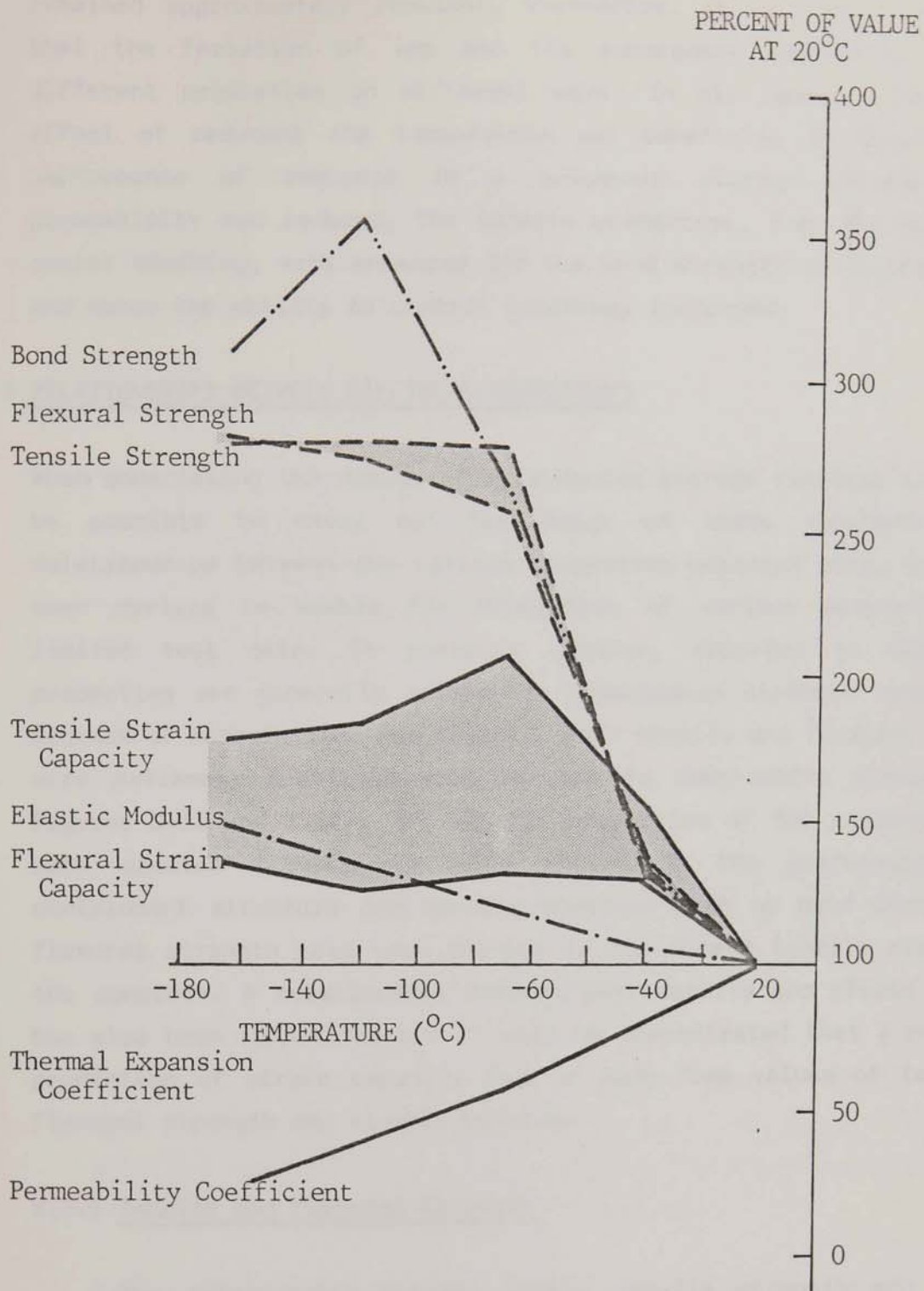
FIGURE 8.5. Average percentage change in the properties of the
            three normal weight mixes with reducing
            temperatures.

remained approximately constant, thereafter. It is clear, therefore, that the formation of ice and its subsequent contraction affects different properties in different ways. In all cases, however, the effect of reducing the temperature was beneficial in terms of the performance of concrete in a cryogenic storage structure. The permeability was reduced, the tensile properties, i.e. the ability to resist cracking, were enhanced and the bond strength to reinforcement, and hence the ability to control cracking, increased.

8.3 RELATIONSHIPS BETWEEN DIFFERENT PROPERTIES

When undertaking the design of a cryogenic storage facility it may not be possible to carry out the range of tests reported herein. Relationships between the various properties measured have, therefore, been derived to enable the prediction of various properties from limited test data. In previous studies, reported in Section 2, properties are generally related to compressive strength with varying degrees of correlation. For example, both tensile and flexural strength were extremely scattered when related to compressive strength (see Figures 2.11 and 2.12). The tensile properties of the concrete are of much greater significance with regard to the performance of a containment structure and hence properties such as bond strength and flexural strength have been related to the direct tensile strength of the concrete. A relationship between permeability and strain capacity has also been identified and it will be demonstrated that a reasonable prediction of strain capacity can be made from values of tensile or flexural strength and elastic modulus.

8.3.1 Tensile and Flexural Strength

The relationship between direct tensile strength and flexural strength is discussed briefly in section 5.3.4. The results are plotted in Figure 5.8 and show direct proportionality between these two properties, over the temperature range +20 to -165°C. The relationship can be approximated by a straight line where $f_t = 0.5 f_f$. There was some scatter of results but all the points lie within two lines represented by the equations,

$$f_t = 0.45 f_f$$

and $f_t = 0.68 f_f$

These limits are consistent with ACI 224.212-86[88] which quotes values of f_t within the range 0.48 to 0.65 f_f for concrete at ambient temperature. As a first approximation, however, the equation $f_t = 0.5 f_f$ should be used.

8.3.2 Bond Strength and Tensile Strength

The relationship between bond strength, f_b, defined as the stress at a slip of 0.0254mm, and direct tensile strength f_t is illustrated in Figure 8.6. Equations for the prediction of bond strength and tensile strength are given in Section 2 as follows:-

Equation 2.7 $f_t = 0.181 f_c^{3/4}$
Equation 2.14 $f_b = 0.142 f_c$

Combining these two equations and eliminating compressive strength, f_c, gives the following relationship.

$$f_b = 0.7845 f_t^{4/3} \tag{8.1}$$

The curve represented by equation 8.1 has been included in Figure 8.6 and represents a lower bound bond strength. Using this equation for predictive purposes will therefore ensure that there is always a safety factor on bond strength.

Equation 8.1 only applies to the normal weight concretes tested and will grossly underestimate the bond strength of lightweight concrete, which for a given tensile strength, has about double the bond strength. A more appropriate equation for lightweight concrete is therefore:-

$$f_b = 2 f_t^{4/3}$$

This is also presented graphically in Figure 8.6.
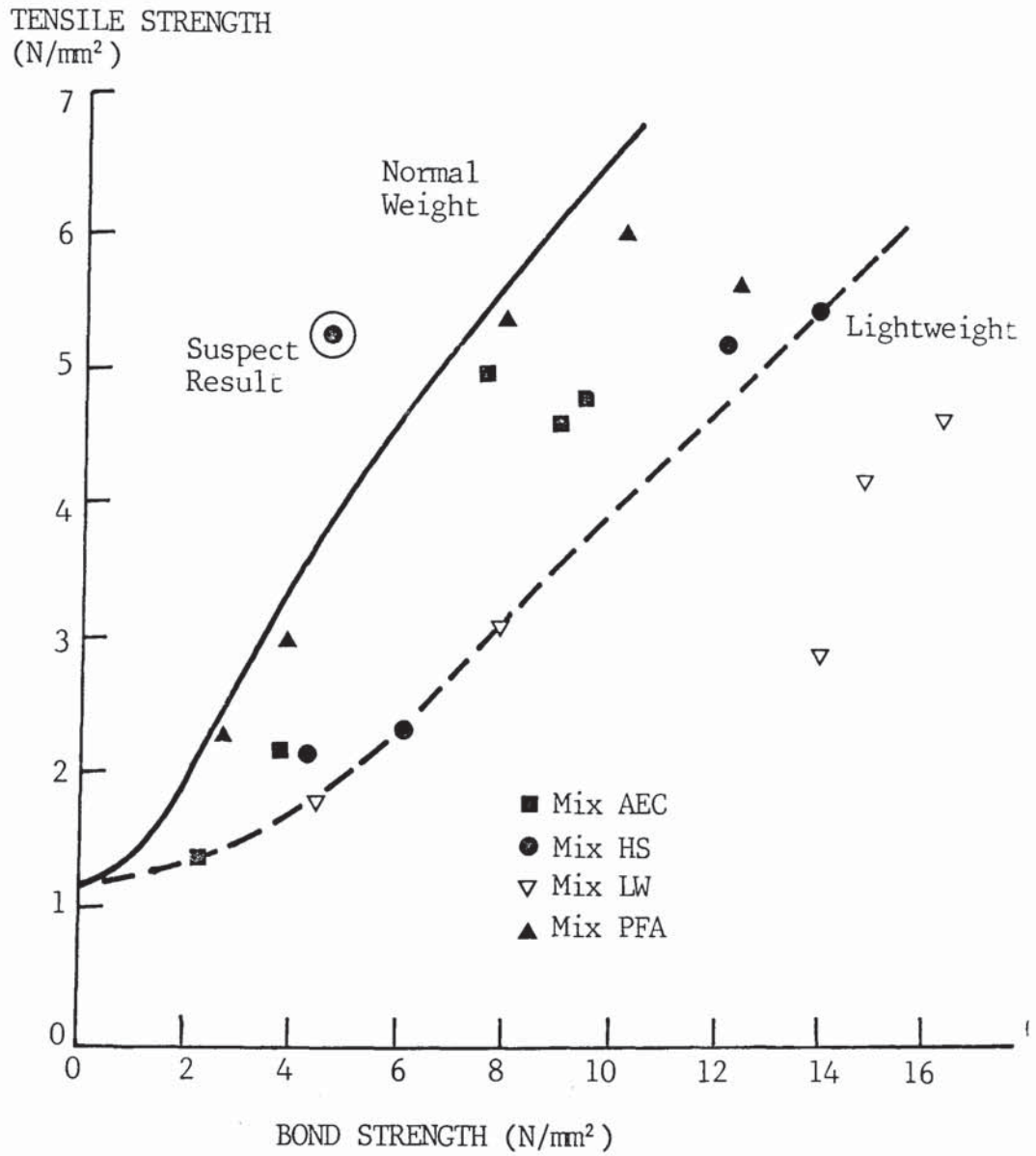
FIGURE 8.6. The relationship between bond strength and tensile strength.

8.3.3 Prediction of Strain Capacity

As the stress-strain relationship in tension and flexure is approximately linear up to failure, particularly at low temperature, the strain capacity, ε_{sct}, of the concrete can be calculated from the tensile strength f_t and elastic modulus. E. In direct tension the strain capacity $\varepsilon_{sct} = \frac{f_t}{E}$ where f_t is the direct tensile strength. Similarly, in bending $\varepsilon_{scf} = \frac{f_f}{E}$ where f_f is the modulus of rupture. Values of elastic modulus have been measured for each of the four concretes over the complete range of test temperatures and a comparison between measured and predicted strains can therefore be made. Values of elastic modulus, tensile and flexural strength, and the calculated strain capacity are given in Table 8.1, together with the measured strain capacity. The predicted and measured values are plotted in Figure 8.7 which illustrates that, with few exceptions, the two values are in close agreement. Where there are large discrepancies, this is generally due to the predicted value underestimating the measured value hence being conservative in terms of structural performance. For design purposes, it is recommended that the following equation be used:-

$$\varepsilon_{sct} = \frac{0.8\, f_t}{E} \qquad (8.2)$$

The curve represented by this equation is included in Figure 8.7 and provides a lower bound value taking into account the scatter of results.

8.3.4 Strain Capacity and Permeability

Two noticeable features of mix LW were its low permeability and high strain capacity, compared with the normal weight mixes. These differences in the two most important properties with regard to containment, prompted an examination of the relationship between permeability and strain capacity for all four concretes. The results obtained at ambient temperature are illustrated in Figure 8.8(a) and indicate an approximately linear relationship between log permeability and strain capacity in both

MIX	DIRECT TENSION				FLEXURE		
	Elastic Modulus kN/mm^2	f_t N/mm^2	Strain Capacity		f_f N/mm^2	Strain Capacity	
			Pred	Measured		Pred	Measured
AEC	37.1	1.39	38	36	3.27	88	134
	39.7	2.21	56	61	4.17	105	166
	45.8	4.97	109	103	8.91	195	196
	52.9	4.79	91	98	9.30	176	179
	58.5	4.59	79	85	9.65	165	181
HS	42.7	2.18	51	72	4.38	103	154
	45.6	2.33	51	–	4.85	106	114
	47.4	5.28	111	91	9.08	192	159
	51.4	5.45	106	68	11.74	228	174
	56.7	5.20	92	83	10.34	182	187
LW	21.7	1.82	84	86	3.89	179	193
	22.9	3.13	137	118	6.48	283	272
	22.9	2.91	127	110	6.15	269	253
	28.9	4.64	161	189	7.58	262	250
	34.0	4.20	124	186	9.27	273	387*
PFA	37.3	2.28	61	51	3.60	97	153
	37.3	3.00	80	71	6.03	162	279*
	43.4	5.41	125	105	10.38	239	226
	51.0	5.63	110	94	9.68	196	199
	56.0	6.02	108	94	10.97	196	223

TABLE 8.1. Measured strain capacities, and vaues predicted using the measured tensile or flexural strength and elastic modulus.
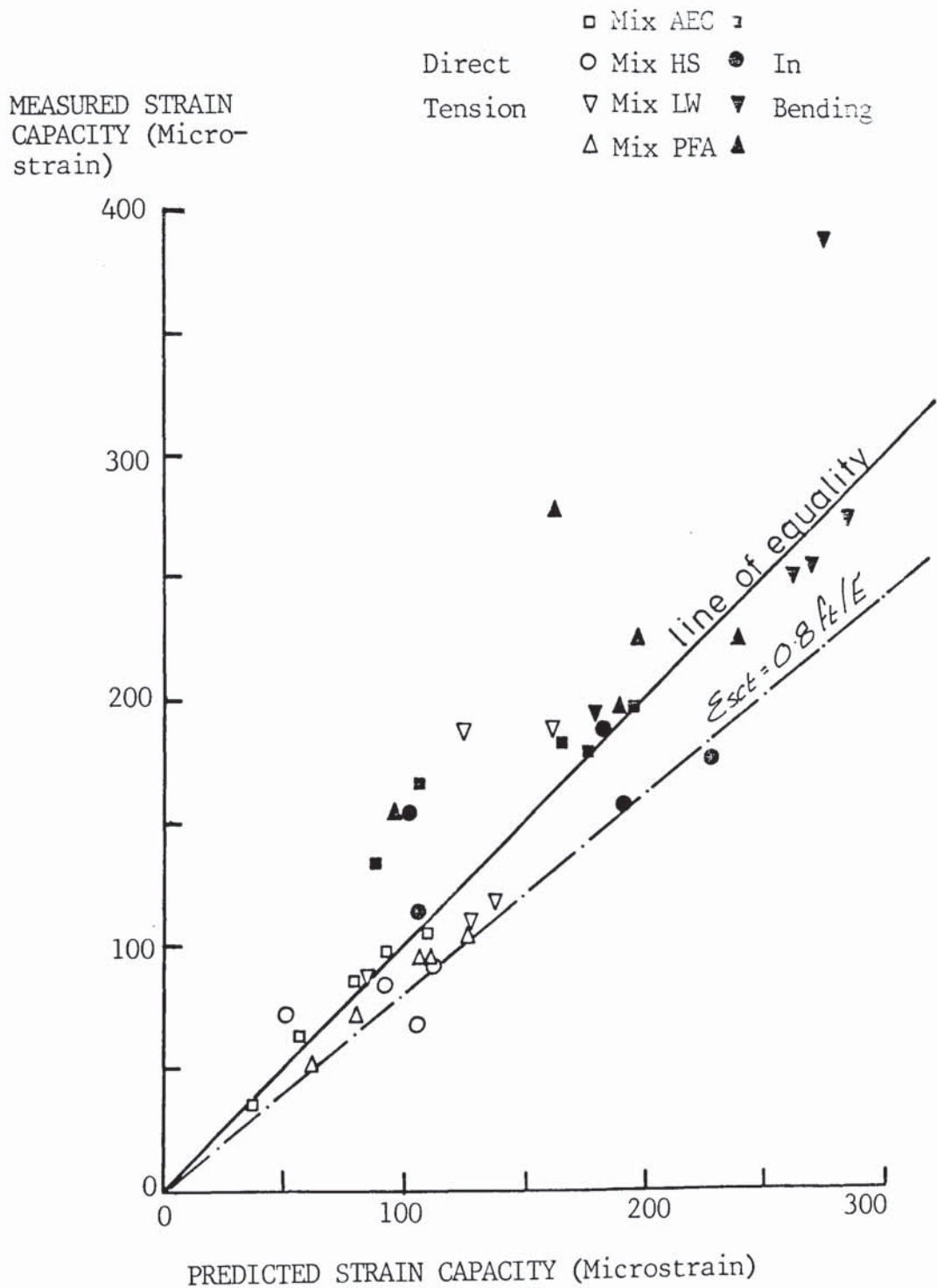
FIGURE 8.7. Measured strain capacity vs calculated strain capacity using tensile or flexural strength and elastic modulus.
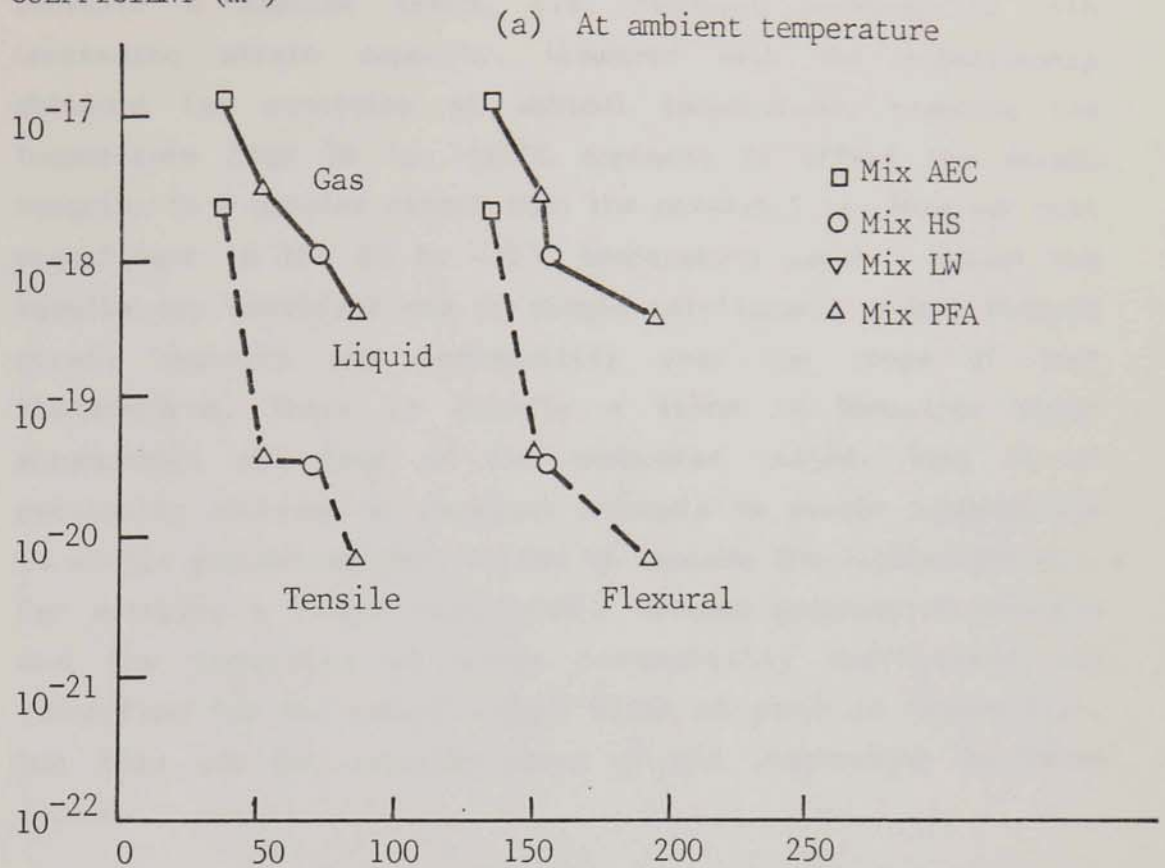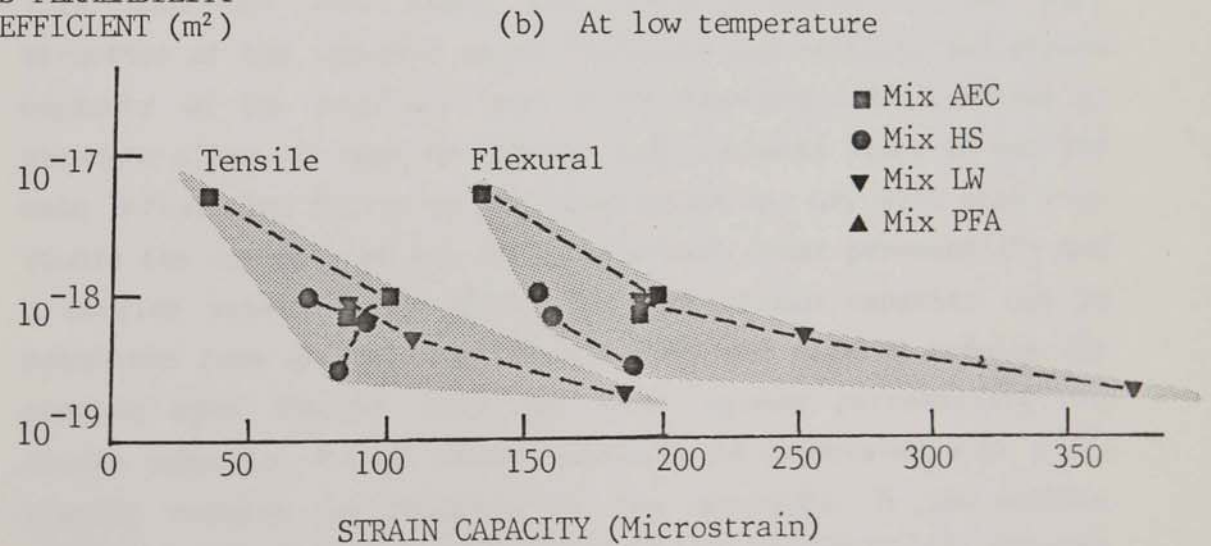
FIGURE 8.8. The relationship between permeability and measured strain capacity.

direct tension and bending. Figure 8.8(b) illustrates the low temperature test results given in Tables 4.6, 5.4 and 5.6, which indicate a similar trend, i.e. reducing permeability with increasing strain capacity. Compared with the relationship obtained for concretes at ambient temperature, reducing the temperature from 20 to -165°C appeared to affect the strain capacity to a greater extent than the permeability. This was most significant in the 20 to -70°C temperature range. Whilst the results are scattered and no single relationship exists between strain capacity and permeability over the range of test temperatures, there is clearly a trend in behaviour which encompasses all four of the concretes tested. This is of particular interest as previous attempts to relate permeability to single properties have failed to include the lightweight mix. For example, a linear relationship between compressive strength and the logarithm of water permeability coefficient was identified for the normal weight mixes as shown in Figure 3.11, but this was not representative of the lightweight concretes tested.

This indicates that there are characteristics of the pore structure of the concrete which influence permeability and strain capacity in the same way, but which may have little effect on strength alone. It must be assumed that porosity alone is not the main influencing factor as the lightweight mix LW, with more than double the porosity of mix AEC, had a much lower permeability and a similar strength. The fact that the strain capacity can be predicted from measurements of strength and elastic modulus may provide some insight into the link between permeability and strain capacity. A high strain capacity is associated with a low elastic modulus in relation to the strength. A low modulus indicates the ability to accommodate and redistribute internal stress and hence minimise microcracking arising from differential strains between the aggregate and cement paste. A concrete with less microcracking will be more impermeable.

The relationship between predicted strain capacity, (strength divided by elastic modulus) and permeability is shown in Figure 8.9. It would appear that an estimate of both strain capacity and permeability can be made from measurement of strength and elastic
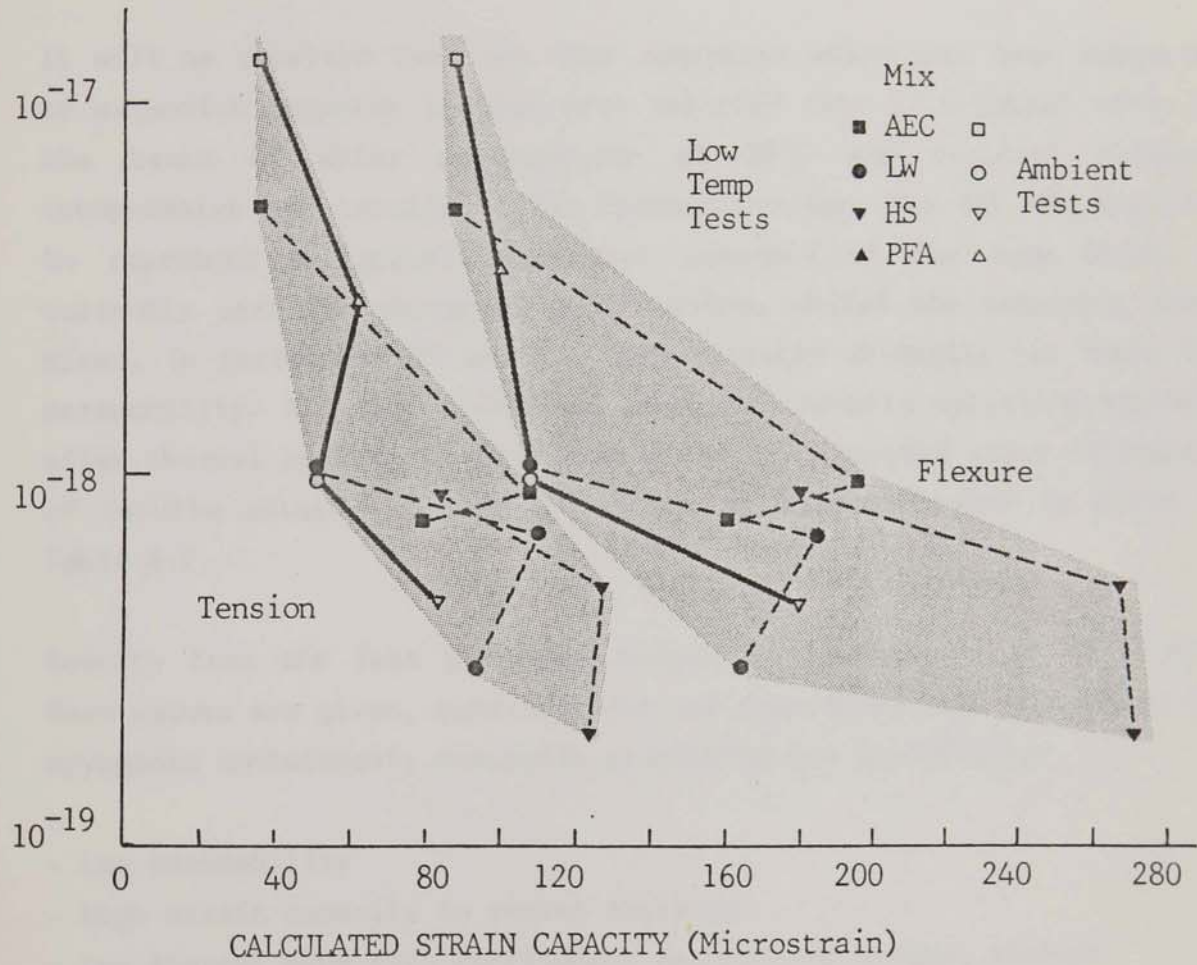
FIGURE 8.9. The relationship between permeability and calculated
strain capacity.

modulus. Standard techniques exist for measuring both flexural strength (BS1881: Part 118 :1983)[50] and elastic modulus (BS1881:Part 121;1983)[50], and with supporting data it may be possible to evaluate concretes for containment structures in terms of both inherent permeability and resistance to cracking using only these two properties, which are relatively simple to measure.

8.4 RELATIVE PERFORMANCE OF CONCRETES TESTED

It will be recalled that the four concretes which have been subjected to extensive property testing were selected from 17 original mixes on the basis of water permeability at 20°C and residual strength (compressive and tensile) after thermal cycling. Mix AEC was included to represent a typical structural concrete of the type which is currently used for cryogenic applications, whilst the remaining three mixes, in particular HS and LW, were selected primarily for their low permeability. All four mixes had a residual tensile splitting strength after thermal cycling in excess of 90% of the uncycled value. A summary of results obtained during the screening test programme is given in Table 8.2.

Results from the test programme proper are summarised in Table 8.3. Mean values are given, generally derived from three test specimens. For cryogenic containment, desirable properties are as follows:-

- Low permeability
- High strain capacity to resist cracking
- Low thermal expansion coefficient to minimise thermal strains
- Low elastic modulus to minimise thermal stress
- High bond to reinforcement for minimum crack widths
- Resistance to thermal cycling

With the exception of resistance to thermal cycling, the performance of the lightweight concrete was best on all counts at both ambient and cryogenic temperature. Compared with the control mix AEC, a standard air-entrained structural concrete, the lightweight mix of approximately the same compressive strength, had appreciably lower permeability; the strain capacity was higher; the thermal expansion was lower; elastic

	AE2	S6	A4	Cl
Compressive Strength (N/mm²)				
– at 20°C	50.0	100.3	40.9	42.8
– at –165°C	105.0	171.0	117.5	102.5
– after cycling	56.1	97.0	46.8	45.3
– % residual strength	112.2	96.7	114.4	105.8
Tensile Splitting Strength (N/mm²)				
– at 20°C	1.82	3.88	2.10	1.72
– at –165°C	2.34	7.89	4.95	6.09
– after cycling	1.85	3.54	1.98	1.82
– % residual strength	101.7	91.2	94.3	105.8
Water Permeability x 10^{-18} m²	3.87	0.024	0.012	3.20

TABLE 8.2. Summary of results obtained during the screening test programme for the four concretes selected for further testing.

Table 8.3 — Summary of results obtained from the main test programme.

PROPERTY AND UNITS	°C	MIX AEC 20	−20	−70	−120	−165	MIX HS 20	−20	−70	−120	−165	MIX LW 20	−20	−70	−120	−165	MIX PFA 20	−20	−70	−120	−165
PERMEABILITY COEFFICIENTS																					
– to water at 20°C (x $10^{-20}\,m^2$)		239.0					3.6					0.7					3.8				
– to nitrogen (x $10^{-18}\,m^2$) at 20°C		13.4					1.0					0.4					3.0				
after slow cycling		15.3					1.0					32.9					2.7				
after rapid cycling		88.8					27.7					42.2					13.6				
– to methane (x $10^{-18}\,m^2$)		5.3	–	0.9	–	0.8	1.1	–	0.7	–	0.3	0.9	–	0.5	–	0.2	NO RESULTS				
TENSILE STRENGTH (N/mm²)		1.4	2.2	5.0	4.8	4.6	2.2	2.3	5.3	5.5	5.2	1.8	8.1	2.9	4.6	4.8	2.3	3.0	5.4	5.6	6.0
FLEXURAL STRENGTH (N/mm²)		3.3	4.2	8.9	9.3	9.7	4.4	4.9	9.1	11.7	10.3	3.9	6.5	6.2	7.6	9.3	3.6	6.0	10.4	9.7	11.0
TENSILE STRAIN CAPACITY (x 10^{-6})		36	61	103	98	85	72	–	91	68	83	86	118	110	189	186	51	71	105	94	94
FLEXURAL STRAIN CAPACITY (x 10^{-6})		134	166	190	179	181	154	114	159	174	187	193	272	253	250	387	153	279	226	199	223
THERMAL EXPANSION COEFFICIENT (Microstrain/°C)		12.5	9.6		9.2	8.8	13.6	8.8		8.8	7.8	10.2	5.4		7.7	7.6	13.4	9.5		8.9	8.6
ELASTIC MODULUS (kN/mm²)		37.1	39.7	45.8	52.9	58.5	42.7	45.6	47.4	51.4	56.7	21.7	22.9	22.9	28.9	34.0	37.3	37.3	42.7	51.0	56.0
BOND TO REINFORCEMENT (N/mm²)		3.3	3.8	7.6	9.5	9.0	4.3	6.1	4.7	13.9	12.1	4.3	7.9	13.4	16.2	14.9	2.7	3.9	7.9	12.3	10.0

TABLE 8.3. Summary of results obtained from the main test programme.

modulus was lower; and bond to reinforcement was increased. Except for their permeability coefficients, the three normal weight mixes did not differ significantly, compared with the difference resulting from the use of the lightweight aggregate. A marginal improvement over the control mix AEC, was recorded for the high strength mix HS with higher strain capacity at ambient temperature and increased bond strength at both ambient and cryogenic temperature. The use of PFA marginally increased strain capacity at both ambient and cryogenic temperature but had little effect on thermal expansion coefficient, elastic modulus or bond.

With regard to permeability there were significant differences between the normal weight mixes, confirming the results obtained during the screening test programme. Compared with the control mix AEC, a reduction in water permeability of about two orders of magnitude was achieved by mix HS, the gas permeability reducing by a factor of more than 10. The use of PFA caused a similar reduction in water permeability and reduced the gas permeability by a factor of 4.

The relative performance of the four mixes changed significantly when assessed on the basis of residual gas permeability after thermal cycling. Slow cooldown, at 4°C per hour, had little effect on the three normal weight mixes, but increased the permeability of the lightweight mix by about 80 times. Hence, whilst the rank order of performance of mixes AEC, HS and PFA remained the same, mix LW moved from best to worst, with a residual gas permeability about double that of the control mix AEC. Rapid cycling by immersion in LN_2 had a significant effect on all four concretes, with increases of x7, x30, x100 and x5 for mixes AEC, HS, LW and PFA respectively. The highest residual value was recorded for the control mix, whilst the lowest residual value was recorded for mix PFA. The difference between these two extreme values was relatively small, however (about x7) compared with initial values prior to thermal cycling which varied by a factor of 30. Reasons for the considerable increase in permeability of the lightweight concrete compared with the normal weight mixes are discussed in section 4.4.2, but it should be noted here that the one sample which was cycled under restraint in the low temperature permeability cell appeared unaffected. Hence, in a prestressed concrete structure, the effect of thermal cycling may be less severe then recorded for the unrestrained samples for which the majority of results were obtained.

9. STRUCTURAL IMPLICATIONS

9.1 INTRODUCTION

The changes in the properties of concrete as affected by constituent materials, mix proportions and reducing temperature all have an impact on the design of cryogenic storage facilities and subsequent structural performance. The principal objective of a cryogenic storage facility is containment of the product. Unacceptable losses can occur as a result of either high permeability concrete or cracking of the containment. The implications of the test results have therefore been considered in these two respects.

9.2 PERMEABILITY

9.2.1 Assumptions

Containment systems for LNG most commonly comprise a double walled cylindrical tank with the annular space filled with insulation. The inner tank (or primary containment) has to contain the LNG under hydrostatic pressure plus a small overpressure of about 0.158bar, whilst at a uniform temperature of -165°C.

The outer tank (or secondary containment) has to prevent the escape of gas at a pressure of 0.158 bar, and the ingress of moisture whilst at ambient temperature. Calculations have been carried out to establish the escape of LNG or gaseous methane through the primary and secondary containments, and to determine the acceptability of values of permeability coefficient derived from tests.

Only flow through the concrete has been considered; no account is taken of flow through joints or cracks. The following assumptions have been made to enable acceptable permeability coefficients to be calculated:-

(a) Primary tank internal diameter = 50m

(b) Primary tank height = 28m

(c) Head of LNG = 25m

(d) Primary tank wall thickness = 0.5m

(e) Secondary tank internal diameter = 53m

(f) Secondary tank height = 30m

(g) Secondary tank wall thickness = 0.5m

(h) Viscosity of LNG at $-165°C = 142 \times 10^{-6} Nsec/m^2$

(i) Viscosity of methane at $20°C = 10.3 \times 10^{-6} Nsec/m^2$

(j) Density of LNG = $450kg/m^3$

(k) Internal gas pressure = $1.158 \times 10^5 N/m^2$ (absolute)

(l) External pressure = $1.0 \times 10^5 N/m^2$ (absolute)

9.2.2 Primary Containment

To be acceptable as a primary containment it is desirable, but not essential, that no LNG escapes through the wall or base of the primary tank during the life of the structure. To calculate an acceptable permeability coefficient, it has therefore been assumed that, in a 30 year design life, LNG does not penetrate to more than half the thickness of the wall, i.e. 0.25m.

Combining equations (3.3) and (4.3) and re-arranging:-

$$k_l = \frac{x^2 . \eta . \nu}{2t(P_1 - P_2)}$$

The most severe case will be at the base of the tank where the hydrostatic pressure is greatest, and

$$P = h\rho g = 25m \times 450kg/m^3 \times 9.81m/sec^2$$
$$= 1.104 \times 10^5 N/m^2$$

In absolute terms, adding the internal gas pressure of $0.158 \times 10^5 N/m^2$ and atmospheric pressure:-

$$P_1 = (1.104 + 1.000 + 0.158) \times 10^5 N/m^2$$
$$= 2.262 \times 10^5 N/m^2$$

Hence, $k_l = \dfrac{0.25^2 \times 142 \times 10^{-6} \times 0.05}{2 \times (30 \times 365 \times 25 \times 3600) \times (2.262 - 1.000) \times 10^5}$

- 270 -

$$= \underline{\underline{1.858 \times 10^{-21}m^2}}$$

As the maximum acceptable value of k is a function of the square of the allowable depth of penetration, permitting full depth penetration through a 0.5m wall would allow k to be increased by 4 times, to 7.432 x $10^{-21}m^2$. Increasing the wall thickness at the base of the tank will also permit higher values of k as shown by Figure 9.1, which illustrates the relationship between permeability coefficient, wall thickness and penetration depth. Also included in Figure 9.1 are measured values of liquid permeability for the four concretes tested. These values are the coefficients measured using water at 20°C, divided by a factor of 4, i.e. the recorded reduction in gas permeability. This is a conservative reduction as the change in liquid permeability is likely to be greater than the change in gas permeability as discussed in section 4.4.4 and illustrated in Figure 4.23. Based on the above assumptions, the permeability would be required to be less than 1.86 x $10^{-21}m^2$. Only mix LW was sufficiently impermeable to satisfy this requirement. Mixes HS and PFA would be acceptable if either the wall thickness was incresed to about 1.1m, or the permissible penetration depth was increased to 600mm regardless of wall thickness. Using mix AEC it would be impossible to meet the assumed requirements with a practical wall thickness.

Once complete penetration of the tank is achieved, steady state conditions will exist. In this case the flow rate will be governed by equation (4.3):-

$$Q = \frac{k_{l} A (P_{1} - P_{2})}{\eta x}$$

Considering a $1m^2$ area at the base of the tank wall where P_1 = 2.262N/m²:

$$Q = k_{l} \frac{(2.262 - 1.000)10^5}{142 \times 10^{-6} \times x}$$
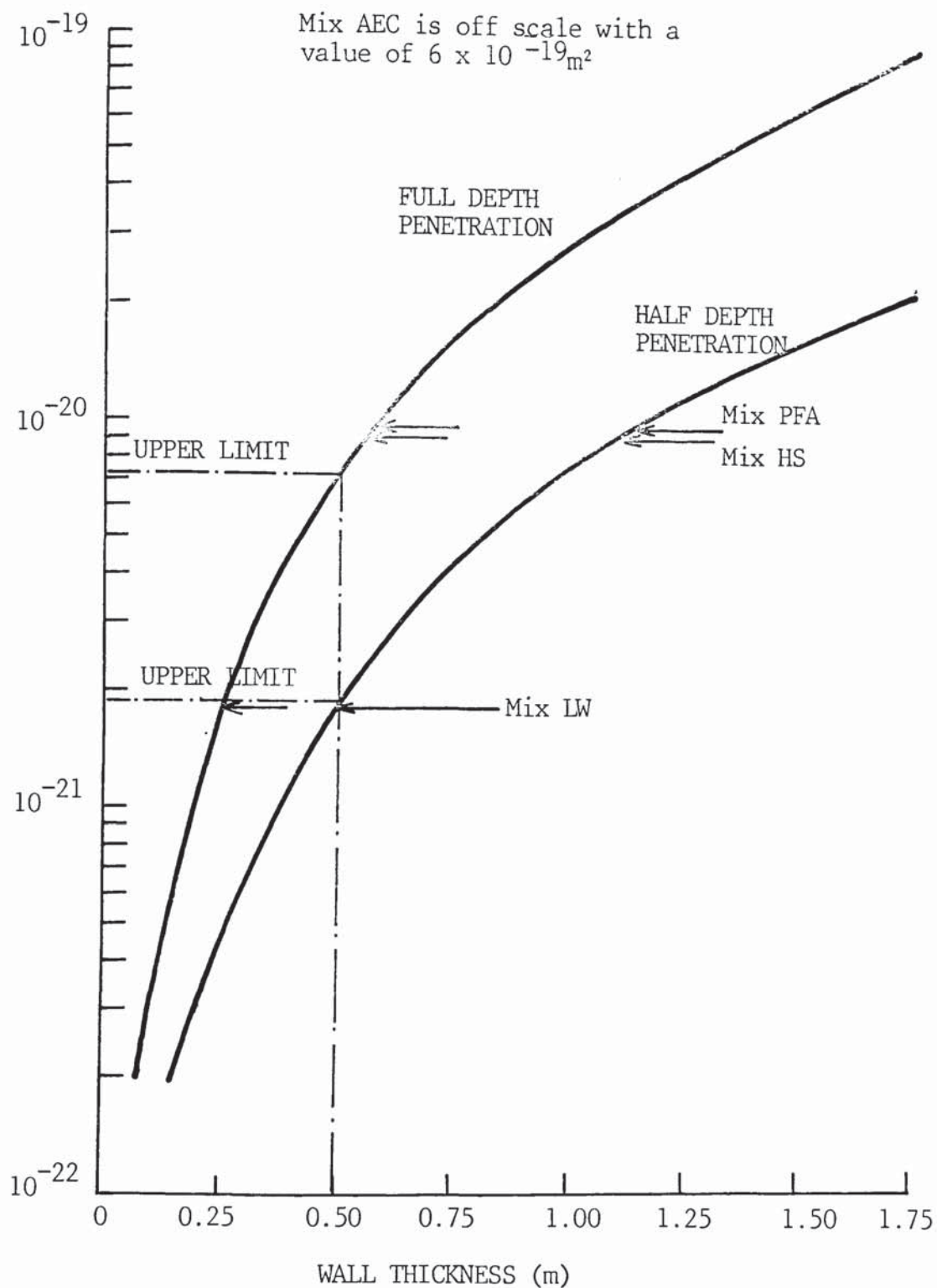
FIGURE 9.1. The relationship between liquid permeability coefficient and the penetration of LNG into a typical storage tank wall during a 30 year design life.

$$= \frac{k_l}{x} \quad 8.887 \times 10^8 m^3/sec/m^2$$

The wall area is equal to $\pi \times 50 \times 25 = 3,927 m^2$. The average pressure differential over the height of the wall is, however, half the pressure differential at the base, hence the total flow rate through the wall:-

$$Q = \frac{k_l}{x} \quad 8.887 \times 10^8 \times \frac{3,927}{2} \quad m^3/sec$$

$$= \frac{k_l}{x} \quad 1.745 \times 10^{12} m^3/sec$$

The relationship between flow rate, permeability coefficient and wall thickness is represented graphically in Figure 9.2. The flow rate is defined in terms of both the volume per day and the percentage of boil-off. Estimated low temperature liquid permeability coefficients are again included. It will be seen that even if mix AEC is used, the flow through the tank will be only $0.2 m^3/day$. The boil-off from an in-service LNG tank is of the order of 0.04% of the total volume; for the assumed $50,000 m^3$ tank this is $20 m^3/day$. Hence, the loss through the wall represents only 1% of the boil-off. If this seepage can be accomodated in the design of the tank it may therefore be acceptable to use a conventional structural concrete. The use of one of the lower permeability mixes would, however, reduce the seepage substantially.

9.2.3 Secondary Containment

Whilst leakage of liquefied gas is the main concern in the primary tank, the secondary containment is required to prevent the escape of methane gas into the environment. Under steady state conditions, gas leakage will be determined by equation 4.2:-

$$Q = \frac{k_g \, A \, . \, (P_1^2 - P_2^2)}{x . \eta . 2P}$$

- 273 -

LIQUID PERMEABILITY
COEFFICIENT (m²)

FLOW RATE (m³ per day)

PERCENT OF BOIL OFF
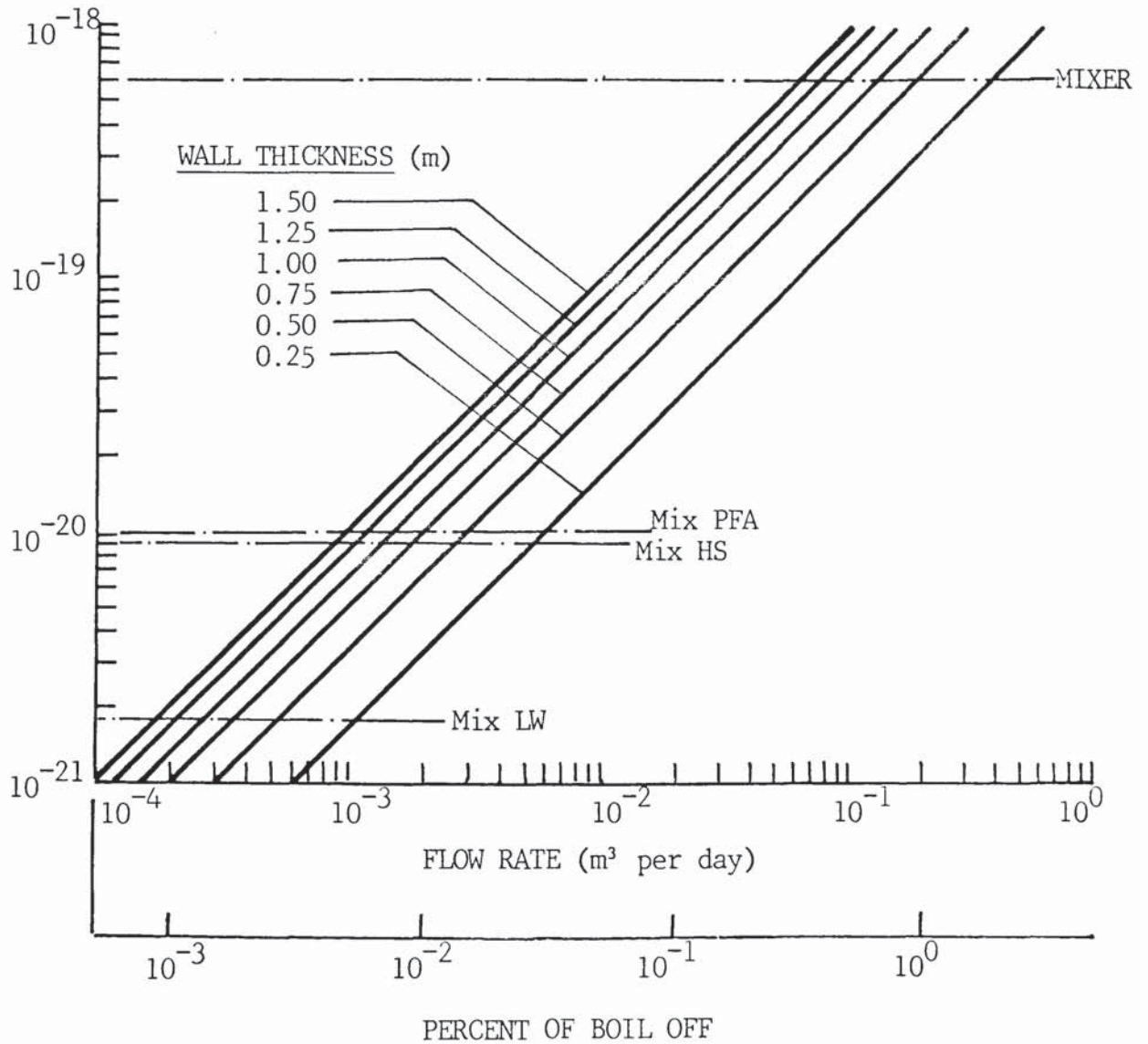
FIGURE 9.2. The relationship between LNG flow rate, wall thick-
ness and liquid permeability coefficient for a
100,000m³ storage tank.

Under normal operating conditions the internal pressure will be $1.158 \times 10^5 N/mm^2$. Hence the flow through a $1m^2$ area of tank wall will be:-

$$Q \quad \frac{k_g \left(1.158^2 - 1^2\right) 10^{10}}{x \left(10.3 \times 10^{-6}\right) 10^5}$$

(The viscosity of methane at 20°C has been used).

Hence, $Q = \frac{k_g}{x} . \ 1.655 \times 10^9 m^3/sec$ per m^2 area

The wall area $= \pi \times 30 \times 53 = 4,995 m^2$.

$\therefore Q = \frac{k_g}{x} \ 8.267 \times 10^{12} m^3/sec = \frac{k_g}{x} \ 7.143 \times 10^{17} m^3/day$

The relationship between flow rate, permeability coefficient and wall thickness is presented graphically in Figure 9.3. Even when using a conventional structural concrete, the gas loss through the wall is only $40m^3/day$, this being equivalent to less than 1% of the acceptable boil-off.

Using the lower permeability mixes this would reduce to less than 0.1% of boil-off. These very small losses are primarily due to the low internal pressure within the tank which operates at marginally above atmospheric pressure.

9.2.4 Effects of Thermal Cycling

Now consider the performance of a primary tank after thermal cycling. Whilst tanks are normally maintained at low temperature after initial cooldown, it may be necessary to carry out inspection or maintenance. This would require the tank to be allowed to return to ambient temperature. Having re-cooled and filled the tank the leakage rate through the wall will now be determined by the permeability of concrete which has been subjected to a "slow" thermal cycle. Test results have
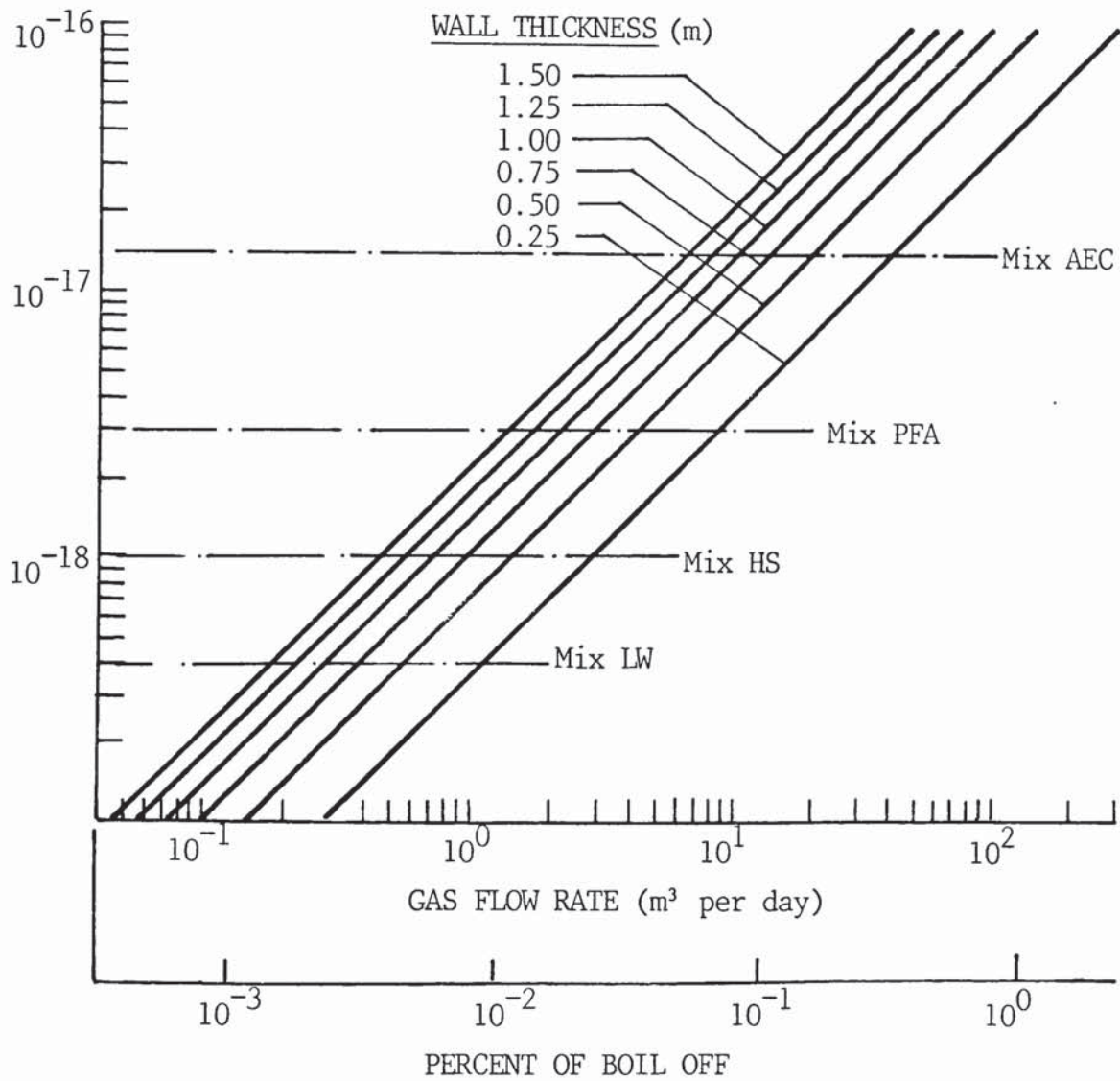
FIGURE 9.3. The relationship between methane gas flow rate, wall thickness and gas permeability coefficient.

demonstrated that for the normal weight mixes, the effect will be negligible. However, the gas permeability of the lighweight concrete increased from 0.43 to 32.9 x $10^{-18}m^2$ after slow thermal cycling. These values were measured at 20°C. Assuming a reduction to $\frac{1}{4}$ of this value at -165°C, as recorded, the residual gas permeability would reduce to about 8 x $10^{-18}m^2$. The liquid permeability associated with this value of gas permeability (derived from the relationship shown in Fig. 4.23) is 1.2 x $10^{-18}m^2$. At this level LNG would penetrate through the 500mm thick wall within 135 days and under steady state conditions the leakage rate would be equal to about $0.4m^3$ per day, or 2% of the boil-off. This is about double the leakage rate associated with the use of a conventional structural concrete.

9.3 CRACKING

Under commissioning and in-service conditions the most likely cause of cracking will be thermal stresses and strains arising from temperature differentials which occur locally through the wall or base of the tank, or globally when the tank is only part full. The magnitude of thermal strains will be determined by the thermal expansion coefficient of the concrete. The stresses which develop will be proportional to the elastic modulus of the concrete.

9.3.1 Resistance to Cracking

The likelihood of cracking can be considered in relation to either stress or strain. With regard to stress, for cracking to be avoided the tensile strength, f_t , must exceed the tensile stress which is in turn proportional to the temperature change $\Delta\theta$, the thermal expansion coefficient, α , and the elastic modulus, E . For no cracking:-

$$f_t \not< C.\Delta\theta.\alpha.E$$

(9.1)

where C is a function of the degree of restraint, taking into account creep.

In terms of strain, cracking is avoided when the strain capacity of the concrete exceeds the stress-induced strain which is proportional to the temperature change $\Delta\theta$ and the thermal expansion coefficient α , thus for no cracking:-

$$\mathcal{E}_{sct} \not> C.\Delta\theta.\alpha \qquad (9.2)$$

Referring to section 8.2.3, it will be seen that the strain capacity,$\mathcal{E}_{sct}$,can be predicted from values of tensile strength and elastic modulus by the equation:-

$$\mathcal{E}_{sct} = \frac{f_t}{E}$$

Substituting in equation (9.2):-

$$\frac{f_t}{E} \not> C.\Delta\theta.\alpha.$$

or

$$f_t \not> C\,\Delta\theta.\alpha.E$$

If it is assumed that the relationship holds between strain capacity, tensile strength and elastic modulus then both approaches will lead to the same conclusion with regard to crack proneness.

As the strains which lead to cracking are thermally induced, the relative performance of the concretes tested can be compared by estimating limiting values of temperature differential. Re-arranging equations 9.1 and 9.2:-

$$\Delta\theta \not> \frac{f_t}{C.\alpha.E} \qquad OR \qquad \frac{\mathcal{E}_{sct}}{C.\alpha}$$

In the most conservative case $C = 1$, i.e. the concrete is fully restrained and no creep relief occurs. On this basis, values of $\frac{f_t}{\alpha E}$ and $\frac{\mathcal{E}_{sct}}{\alpha}$ have been calculated and are given in Table 9.1. The results are also illustrated in Figure 9.4 which shows the effect of temperature on two parameters. Two features of the results are immediately apparent:-

| | PROPERTY VALUES | | | | CRACK RESISTANCE BY | |
| | | | | | Stress | Strain |
MIX	f_t	ε_{sct}	E	α	$\dfrac{f_t}{\alpha E}$	$\dfrac{\varepsilon_t}{\alpha}$
AEC	1.39	36	37.1	12.53	2.99	2.87
	2.21	61	39.7	9.64	5.78	6.33
	4.97	103	45.8	9.24	11.74	11.15
	4.79	98	52.9	8.76	10.10	11.42
	4.59	85	58.5	(8.76)	8.96	9.70
HS	2.18	72	42.7	13.57	3.76	5.31
	2.33	–	45.6	8.84	5.78	–
	5.28	91	47.4	8.80	12.70	10.34
	5.45	68	51.4	7.84	13.52	8.67
	5.20	83	56.7	(7.84)	11.70	10.59
LW	1.82	86	21.7	10.24	8.18	8.40
	3.13	113	22.9	5.42	28.20	21.77
	2.91	110	22.9	7.66	16.59	14.36
	4.64	189	28.9	7.62	21.07	24.88
	4.20	186	34.0	(7.52)	16.21	24.40
PFA	2.28	51	37.3	13.39	4.57	3.81
	3.00	71	37.3	9.48	8.48	7.49
	5.41	105	43.4	8.86	14.07	11.85
	5.63	94	51.0	8.55	12.91	16.99
	6.02	94	56.0	(8.55)	12.57	10.99

TABLE 9.1. Calculation of resistance to thermal cracking.

a) Based on stress

b) Based on strain
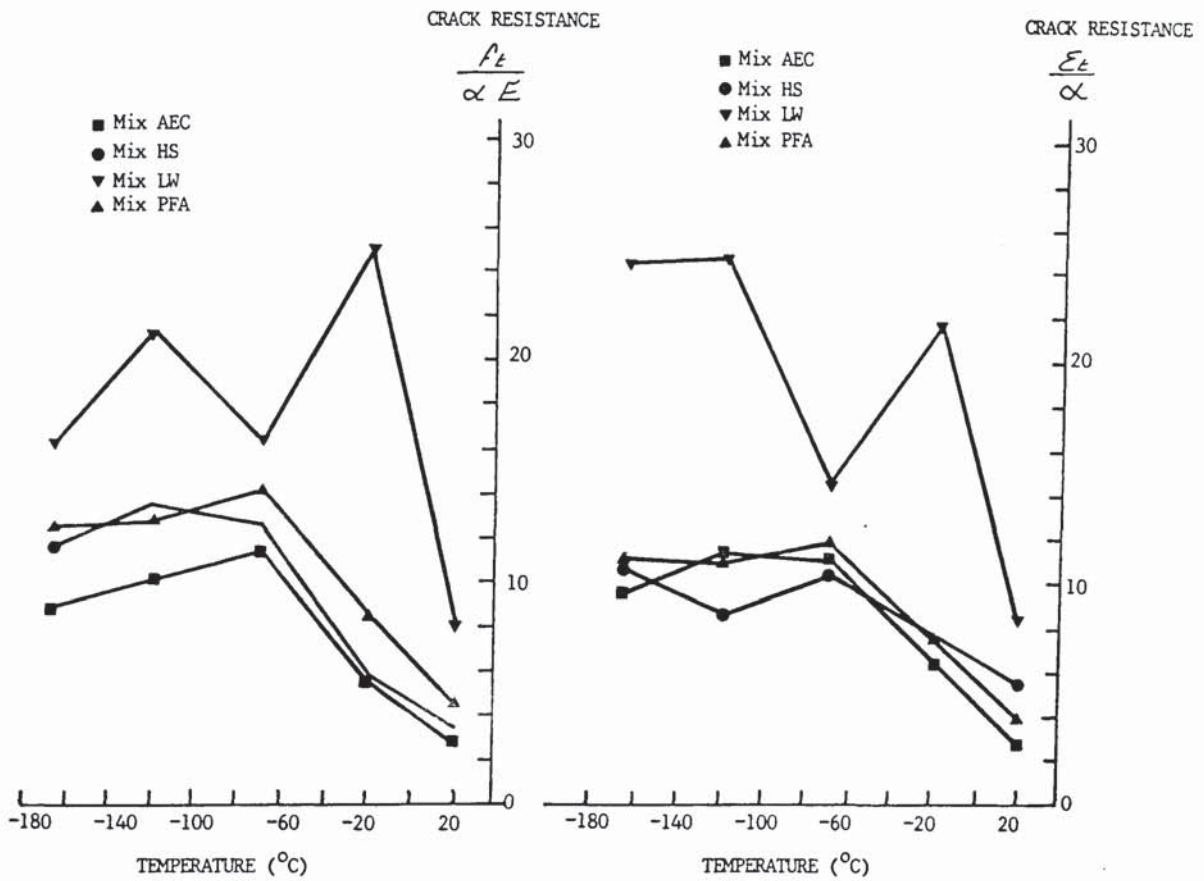
FIGURE 9.4.   The influence of temperature on crack resistance.

(1) The resistance to thermal cracking increased at low temperature.

(2) The lightweight concrete has appreciably higher crack resistance than the three normal weight mixes.

Hence for the avoidance of cracking, the use of lightweight concrete has clear advantages, more so at low temperatures. The combination of lower thermal expansion coefficient, resulting in less strain for a given temperature differential, and the ability to tolerate higher levels of strain, will enable the lightweight concrete to withstand approximately double the temperature differential which can be tolerated by a conventional structural concrete. In the case of a temperature crossfall through a wall, and assuming elastic behaviour, the thermal stress is equal to $\frac{1}{2}\Delta\theta.\alpha.E$ i.e. the effective restraint is 50%. In this situation, the temperature differential which can be sustained in an unstressed element will be double the figures quoted in Table 9.1. Calculated values at ambient and cryogenic temperature (-165°C) are given in Table 9.2. These are conservative values as creep relief has not been taken into account.

9.3.2 Control of Cracking

There are two criteria which must be met to ensure that cracking occurs in a controlled manner in a reinforced or prestressed concrete structure [89]:-

(1) The steel ratio must be such that when a crack occurs, the load transferred to the steel is insufficient to cause the steel to yield. This is achieved by calculating the critical steel ratio ρ_{crit}, using the equation:-

$$\rho_{crit} = \frac{f_t}{f_y} \tag{9.3}$$

where f_t is the direct tensile strength of the concrete.

f_y is the characteristic yield stress of the reinforcement.

(2) The reinforcement should be distributed in such a way as to provide adequate bond stress. When criterion (1) is met, the maximum spacing of cracks, is given by the formula:-

$$S_{max.} = \frac{f_t}{f_b} \cdot \frac{\phi}{2\rho} \qquad (9.4)$$

Where f_t/f_b is the ratio of the tensile strength of the concrete f_t to the bond strength between the concrete and steel, f_b.

ϕ is the bar diameter.

ρ is the steel ratio based on the gross concrete section.

To achieve minimum crack widths, the crack spacing must also be kept to a minimum. This can be achieved by reducing the bar size ϕ, increasing the steel ratio ρ or reducing the ratio f_t/f_b. Values of $\frac{f_t}{f_b}$ are given in Table 9.3 for the four mixes tested.

In the design of the steel two factors must therefore be taken into account. Firstly, the increase in the tensile strength of the concrete at low temperature will necessitate an increase in the amount of reinforcement used, to cover the possibility of cracking occurring at low temperature. The tensile strength of concrete typically increases by about 150%. However, the yield strength of the steel also increases by about 25%[79]. The steel required for controlled cracking will therefore be 250/125 = 2 x the ratio required at ambient temperature.

Secondly, for a given steel ratio, crack width and spacing will be lower when the ratio of f_t/f_b is small. The lightweight concrete has an advantage in this respect particularly at low temperatures. Values of f_t/f_b are about half those recorded for the control concrete. This gives the flexibility to either increase the bar size (and hence use less bars) or to reduce the steel ratio ensuring that the value always exceeds ρ_{crit}.

When designing the reinforcement, it must be assumed that cracking can potentially occur when the tensile strength of the concrete is at its maximum value. For all four concretes tested this occurred at about -120°C when values were as follows:-

MIX	LIMITING TEMPERATURE CROSSFALL ($^{\circ}$C)	
	Ambient	Cryogenic
AEC	6	18
HS	8	22
LW	16	40
PFA	8	22

TABLE 9.2. Limiting temperature crossfalls under ambient and cryogenic conditions.

TEMPERATURE ($^{\circ}$C)	MIX AEC	MIX HS	MIX LW	MIX PFA
20	0.426	0.502	0.428	0.848
-20	0.576	0.380	0.397	0.763
-70	0.657	(1.134)	0.191	0.686
-120	0.505	0.393	0.286	0.459
-165	0.510	0.430	0.282	0.60

TABLE 9.3. Calculated ratios of tensile strength to bond strength.

AEC - 4.79 N/mm^2
HS - 5.45 N/mm^2
LW - 4.64 N/mm^2
PFA - 6.63 N/mm^2

The lightweight concrete would, therefore, require the lowest level of ρ_{crit}. The lightweight mix also has the lowest ratio of f_t / f_b hence, in the event that cracking should occur, despite the lower proportion of steel, crack widths would be smaller also.

10.   CONCLUSIONS AND RECOMMENDATIONS

10.1 INTRODUCTION

The following conclusions are based on the results obtained from screening tests on 17 concrete mixes, and comprehensive property testing of 4 selected concretes. The latter were chosen on the basis of low water permeability at ambient temperature and resistance to cycling between ambient and cryogenic temperature assessed by measurement of compressive and tensile splitting strength. All the specimens were subjected to sealed curing conditions. The results of an extensive analysis of the literature have also been taken into account.

10.2 SCREENING TESTS

(i)   For all seventeen concretes tested, there was an increase in compressive strength when cooled from 20°C to -165°C. The average increase was about 50 N/mm^2, for typical structural concretes with average ambient cube strengths in the range 40 to 60 N/mm^2, although there was a tendency for concretes with a higher water content to exhibit a higher than average increase. Also the absolute change in compressive strength tended to be higher for very high strength mixes and less for lower strength mixes.

(ii)   Whilst all seventeen concretes exhibited a significant increase in tensile splitting strength, the results were considerably more variable than those recorded in compression. The average increase was about 3 N/mm^2.

(iii)   The effect on compressive strength of cooling to -165°C at a rate of 60°C per hour and reheating to ambient temperature, was insignificant. Residual strengths were never more than 10% less than the strength of the control cubes, and for 9 out of the 17 mixes the strength after the thermal cycle was higher than that of the control cubes.

(iv)   The residual tensile splitting strength after thermal cycling was reduced by an average of about 10%. The variability was

greater than that recorded for residual compressive strength, possibly indicating the greater sensitivity of tensile strength to any disruption which may have been caused by the thermal cycle.

(v)   The relationship between compressive and tensile strength was largely unchanged at cryogenic temperature. The tensile splitting strength was generally 4 to 6% of the compressive cube strength. It should be noted that the adopted method for the tensile splitting test was more severe than usual, the point loads being transferred to the concrete via stainless steel rods instead of timber which distributes the stress over a larger area.

(vi)   For the normal weight mixes, the water permeability coefficient was broadly related to compressive strength on a log-linear basis. Concrete with a mean cube strength of 16 N/mm^2 exhibited a coefficient of permeability more than 1000 times that of a concrete with a mean strength of 100 N/mm^2. For typical structural concretes with mean cube strengths in the range 40 to 60 N/mm^2, water permeability coefficients were generally in the range 10^{-18} to 10^{-17} m^2 (10^{-11} to 10^{-10} m/sec).

(vii)   For non-air entrained concretes, the permeability coefficient was also related to water/cement (w/c) ratio. The use of air entraining agents caused a reduction in permeability in relation to compressive strength, but when the assessment was made in terms of w/c ratio, this was found in all cases to cause an increase in permeability.

(viii) The permeability of the lightweight concretes did not conform to the relationships identified for the normal weight mixes. Permeability coefficients were more than two orders of magnitude lower than recorded for the normal weight mixes of similar strength and w/c ratio. Various reasons for this marked difference have been suggested related to mix

proportions, moisture content and aggregate/cement paste bond, but a more detailed investigation was beyond the scope of this programme.

(ix)   Four mixes were selected from the screening test programme for more comprehensive testing. Two of these, a high strength mix and a lightweight concrete were selected on the basis of low permeability. One mix was selected as being typical of the structural concrete currently used in cryogenic storage systems. The fourth mix, containing PFA, was selected for its relatively low permeability, within the typical range of values, and for other benefits associated with the use of PFA related to the construction process. All four mixes also exhibited acceptable resistance to thermal cycling defined by residual strengths (tensile and compressive) of not less than 90% of the control values.

10.3 CRYOGENIC PROPERTIES

10.3.1 Permeability

Considerable difficulties were encountered in the measurement of the gas permeability coefficient at cryogenic temperature and only seven concrete specimens were tested. Nevertheless, the results obtained are consistent within themselves and compatible with both the water permeability results obtained during the screening test programme and gas permeability measurements carried out to establish the effect of thermal cycling. The principal conclusions to be drawn from these tests are as follows:

(i)   At -165°C the gas permeability coefficient was reduced to about 10% to 20% of the value recorded at 20°C.

(ii)   The lightweight concrete consistently exhibited appreciably lower permeability coefficients when compared with normal weight mixes subjected to similar curing and storage conditions.

- 287 -

(iii)   Water cured concretes exhibited gas permeability
        coefficients which were about two orders of magnitude
        lower than the sealed cured concretes.

10.3.2 <u>Tensile Behaviour</u>

Tests were carried out in direct tension and in bending, to
determine both the strain capacity and strength of the concrete
with reducing temperature. Values obtained in bending were
generally double those obtained in direct tension for all four
concretes and at all test temperatures in the range 20 to
-165°C. This is consistent with published data on the tensile
strength at ambient temperature. The principal conclusions
from these tests were as follows:

(i)   The tensile capability, or crack resistance of all four
        concretes increased with reducing temperature. For the
        three normal weight mixes the increase occurred largely
        within the range -20°C to -70°C, with little change at
        lower temperatures. For the lightweight concrete the
        change was progressive over the complete range of test
        temperatures.

(ii)   At -165°C the tensile strength of the normal weight
        concretes was typically 150 to 200% higher than the
        value at 20°C. For the lightweight concrete the
        increase was about 130%.

(iii)   The increase in strain capacity was much less consistent
        from mix to mix with those mixes with the lower ambient
        values exhibiting the greatest percentage increase.
        However, this was the result of the normal weight mixes
        being unable to exceed a strain capacity ceiling of
        about 110 microstrain in direct tension and 220
        microstrain in bending. Hence for concretes with a high
        value at ambient temperature, the scope for increase was
        much less.

(iv)   The lightweight mix exhibited a higher strain capacity
       than the normal weight mixes throughout the range of
       test temperatures, the difference increasing as the
       temperature reduced.   Whilst at ambient temperature the
       strain capacity of the lightweight concrete was about
       50% higher than the average value for the three normal
       weight mixes, at -165°C it was about double.

10.3.3 Thermal Expansion Coefficient

(i)   The thermal expansion coefficient of all four concretes
       reduced with temperature.   Values recorded over the
       temperature range -120°C to -165°C were about 75% of the
       values recorded over the range +20°C to -20°C.

(ii)   Values of thermal contraction for the normal weight
       mixes over the temperature range +20 to -165°C were all
       within 3% of the average value of 1760 microstrain. The
       values were relatively high compared with previously
       published results, but this has been attributed to the
       high thermal expansion coefficient of the gravel
       aggregate used.

(iii) Lower thermal contraction was exhibited by the
       lightweight concrete. This was due to the lower thermal
       expansion coefficient of the lightweight aggregate and
       the higher moisture content of the lightweight concrete.
       The latter would result in a higher proportion of the
       thermal contraction being offset by the expansive
       formation of ice. The total contraction exhibited by
       the lightweight concrete was 1386 microstrain, 22% lower
       than the normal weight concrete.

10.3.4 Elastic Modulus

(i)   The elastic modulus of all four concretes increased with
       reducing temperature.

(ii)   For the normal weight mixes the increase from 20°C to
        -165°C varied from 33% to 58%, the biggest increase
        being associated with the lowest ambient value. At
        -165°C the moduli of all three normal weight mixes were
        almost identical with values of 58.5, 56.7 and 56.0
        kN/mm^2 for mixes AEC, HS and PFA respectively.

(iii)   The lightweight concrete exhibited values of elastic
        modulus which were 55 to 60% of the normal weight
        concrete, over the complete range of test temperatures.
        The values increased from 21.7 kN/mm^2 at 20°C to 34.0
        kN/mm^2 at -165°C, this being consistent with published
        data on the elastic modulus of lightweight aggregate
        concrete.

10.3.5 Bond to Reinforcement

Bond tests were carried out using two types of reinforcement,
and specimens were tested at ages ranging from 6 weeks to 4
months. Comparisons between the performance of the different
mixes can, therefore, only be approximate. As the specimens
were sealed cured the age effect is believed to be of only
secondary importance. However, the different bar types may
have had a significant effect. The following conclusions have,
therefore, been drawn with this in mind.

(i)   The bond strength increased substantially over the range
        +20°C to -165°C with values at -165°C being 200% to 300%
        higher than those recorded at ambient temperature.

(ii)   The rate of change of bond strength with respect to
        temperature was similar to that of tensile strength down
        to -70°C. However, as the temperature reduced further,
        continued increase in bond strength was exhibited, with
        peak values occurring at -120°C for all four concretes.

10.4 RESIDUAL PERMEABILITY AFTER THERMAL CYCLING

Tests to establish the residual gas permeability coefficient were

carried out using two rates of cooling. Slow cooling refers to a rate of 4°C per hour from 20°C down to -165°C, whilst rapid cooling refers to immersion of specimens into liquid nitrogen at -196°C. The results indicate the following:

(i)   For the normal weight mixes the permeability was increased by a factor of two when subjected to slow thermal cycling. Rapid cycling was more disruptive, increasing the gas permeability by up to 30 times for the high strength mix, but mixes AEC and PFA by only 7 times and 3 times respectively.

(ii)   The response of the lightweight mix to thermal cycling was considerably greater than that exhibited by the normal weight mixes. The gas permeability increased by about 100 times regardless of the rate of cooling, eliminating the considerable benefit associated with the low initial permeability of the lightweight mix. The increase was attributed to disruption due to ice formation, the lightweight mix having a higher moisture content than the normal weight mixes due to the porous nature of the aggregate. However, limited evidence from tests in the low temperature permeability cell indicated that if the concrete was confined, then disruption did not occur, the expansion of the concrete associated with the ice formation being prevented. For prestressed concrete, therefore, permeability may not be as severely affected as indicated by tests on unrestrained specimens.

10.5 RELATIONSHIP BETWEEN PERMEABILITY AND PORE STRUCTURE

The pore characteristics of two concretes were determined by mercury intrusion porosimetry before and after thermal cycling. The two concretes investigated were mix AEC, with the highest permeability of the four concretes tested, and mix LW, with the lowest permeability. Furthermore, the largest change in permeability was exhibited by mix LW whilst mix AEC was the least affected by thermal cycling. Despite the very wide range of permeability coefficients recorded no specific relationship could be derived between permeability and porosity. The low permeability lightweight concrete had the higher total porosity spread over the complete range of pore sizes from 50 to 75000Å. This

suggests that the permeability of concrete is determined largely by pores with a radius in excess of 75000Å which are outside the range of the mercury porosimeter. The only trend to be identified was that the largest increase in total porosity after thermal cycling was associated with the biggest increase in permeability.

10.6 RELATIONSHIP BETWEEN PERMEABILITY COEFFICIENTS MEASURED USING WATER AND GAS

(i)   Concrete permeability coefficients obtained using water and nitrogen differed significantly, the biggest difference being associated with concretes with the lowest permeability coefficients. This difference has been investigated and attributed to gas slippage, whereby the gas molecules close to the wall of a capillary have a finite velocity.

(ii)   Using the data obtained a relationship between water and gas permeability has been derived which enables the value of intrinsic permeability to be calculated from the gas permeability coefficient and the absolute pressure at which the test was carried out.

10.7 RELATIONSHIPS BETWEEN DIFFERENT PROPERTIES

Relationships have been derived to enable the prediction of a range of properties from limited test results.

(i)   The only property which could be related to permeability for all four mixes was the strain capacity. As strain capacity increased, so the permeability reduced. This reinforces the view that the permeability of concrete is determined by relatively large pores, beyond the range measured by mercury porosimetry, or microcracks, which would also directly affect the strain capacity.

(ii)   The strain capacity can be predicted from either the direct tensile strength or the modulus of rupture, together with the elastic modulus. Hence, if the relationship between

permeability and strain capacity holds for all concretes, it may be possible to estimate permeability from these measurements also.

(iii)   The modulus of rupture was about double the direct tensile strength for all concretes over the complete range of test temperatures.   Measurement of modulus of rupture was less variable and it is therefore recommended that predictions should be based on these values rather than direct tensile strength.

10.8 CONCRETE FOR LNG CONTAINMENT

The principal requirement of a cryogenic storage facility is containment of the product. Hence concrete which is selected for this application must have low inherent permeability and be able to withstand the stresses imposed upon it without cracking.

(i)   Of the four concretes tested, the lightweight mix, using a sintered PFA aggregate, was most suitable for cryogenic applications. Not only did it exhibit the lowest permeability coefficient, but also the combination of high strain capacity, low elastic modulus and low thermal expansion coefficient, which enable it to withstand significantly higher temperature differentials in service.

(ii)   Measured permeability coefficients for the lightweight concrete are compatible with the requirements for typical LNG storage tanks of $100000m^3$ capacity with regard to both containment of the liquid gas in a primary tank, and minimising gas leakage from a secondary containment.

(iii) The typical air-entrained structural concrete would be unlikely to be sufficiently impermeable to prevent the escape of LNG over the 30 year design life of a tank. The permeability could be reduced either by increasing the strength or by the use of PFA.

(iv)   The effect of thermal cycling was to increase the permeability
        of all four concretes tested. The increase was greatest when
        the temperature change was rapid. The most significant
        increase was recorded for the lightweight mix and has been
        attributed to the higher moisture content compared with the
        normal weight mixes. The consequence of this was that, after
        thermal cycling, all four concretes exhibited a similar
        permeability coefficient, despite the significant differences
        prior to the thermal cycle. There was limited evidence,
        however, to suggest that for prestressed concrete the
        permeability would be unaffected by thermal cycling.

10.9 RECOMMENDATIONS

(i)   There are clearly significant benefits which can be achieved by
        the use of lightweight concrete for cryogenic storage
        facilities with regard to leak tightness. Further work should
        be carried out to identify the primary influencing factors with
        respect to the low permeability and high strain capacity of
        concrete using sintered PFA aggregate. Furthermore, the
        reasons for the substantial increase in permeability after
        thermal cycling should be investigated.

(ii)   The relationship between permeability and strain capacity
        should be investigated for a wider range of concretes. The
        fact that a relationship was derived for the four concretes
        tested suggests that only those pores which are sufficiently
        large to initiate microcracking, will influence permeability.
        The prediction of strain capacity from more simple measurements
        of elastic modulus and either tensile strength or modulus of
        rupture should also be considered for further study. This may
        then lead to the direct prediction of permeability from
        currently standard tests.

(iii) Under constrained conditions, thermal cycling appeared to have
little affect on permeability. Hence for prestressed concrete
it may be possible to tolerate thermal cycling without loss of
performance. Limited results have been published on the
effects of prestress on the thermal contraction of concrete
which indicate that expansive ice formation is prevented.
Further work to investigate the effects of prestress on the
change in permeability after thermal cycling should therefore
be carried out, as cryogenic containments commonly use
prestressed concrete.

APPENDIX 1

WORKING DRAWINGS
OF EXPERIMENTAL APPARATUS

LIST OF WORKING DRAWINGS

Permeability test cylinder	TWC D6355/202A
Tensile test specimen mould	TWC/D6351/014 (3 Sheets)
Tensile test rig	TWC D6351/011A (5 Sheets)
Flexural test rig	TWC D6351/012A (4 Sheets)
Compression loading rig	014J/6354/01 (8 Sheets)
Bond test rig	TWC D6351/010B (2 Sheets)
Bond slip transducer	TWC 6355/87A (5 Sheets)

APPENDIX 2

DETAILS OF EPOXY RESIN USED FOR LOW
TEMPERATURE PERMEABILITY TESTING

APPENDIX 3

CALIBRATION OF VIBRATING WIRE STRAIN GAUGES
AT AMBIENT AND LOW TEMPERATURE

A3.1.   INTRODUCTION

One of the principal requirements of the research project was for a reliable means of measuring concrete deformation at cryogenic temperatures. Vibrating Wire Strain Gauges (VWG's) have a proven reliability for measurement both on, and within, concrete at ambient and elevated temperatures and were therefore considered for low temperature application. One of the main advantages of VWG's is that, unlike transducers which use electrical resistivity measuring elements, the VWG uses electrical means for generation and supply of strain measurement values without dependency on precise magnitude. Provided that the initiation and feed-back signals are sufficiently high at cryogenic temperature, then stable readings would be expected.

A3.2. MATERIALS AND COMPONENT CONSIDERATIONS

The first consideration in developing a suitable VWG for the project was to employ as many standard gauge components as possible. Apart from financial considerations, familiarity of use of components and materials would assist in achieving gauge factor uniformity.

A study of the materials used in standard gauges indicated two changes. These involved the use of cryogenic cable and sealant.

A3.2.1 CABLES

The cable insulation material was changed to Kapton Polymide which is recommended for service from -269°C to over 315°C. This has excellent resistance to abrasion and is treated for bondability.

A cable was chosen with a small overall diameter (0.92mm) supplied as a flat twin. The conductors were stranded silver plated copper wire.

A3.2.2 SEALANT

Standard gauges use an epoxy resin for platen and cable entry sealing. This resin could crack due to shrinkage at cryogenic temperature. A proven adhesive was required for temperatures below -200°C which would both bond the polymide cable to metal and provide a metal to metal seal. A two component, solvent thinned, epoxy-phenolic adhesive with a temperature range down to -270°C and with low viscosity for flowability was chosen. This adhesive exhibits low creep and has elongation capabilities of 1% at -270°C, 3% at 24°C.

A3.2.3 COIL

One particular component which was carefully scrutinised was the coil. This features a nominal 100 ohms copper conductor coil wound on two acrylic plastic bobbins which are mounted on soft iron pole pieces. There were two principal considerations for suitability at cryogenic temperature:-

a)   With decreasing temperature the acrylic bobbins would exhibit
      shrinkage disproportional to the iron pole pieces. Should the
      bobbin to pole piece be initially a tight fit at ambient
      temperatures, fractures could occur which might damage the coil
      windings at -165°C. However, the manufacturers of the coils
      confirmed that there was adequate clearance to accommodate
      shrinkage and it was decided to retain the standard coil.

b)   The temperature change from ambient to -165°C would decrease
      the coil resistance considerably. The coefficient of
      resistivity for copper is 3.9×10^{-3} ohms per ohm per 1°C
      change and is non-linear, increasing significantly below
      -100°C.

      Assuming the coefficient to be linear, the calculated coil
      resistance change at -165°C would be:-

      Temperature change x coefficient x nominal coil resistance
      $185 \times 3.9 \times 10^{-3} \times 100$ ohms

      = 72.2 ohms resistance change

      At -165°C coil resistance would be less than 28.8 ohms.

In consideration of the above data, a change of ambient coil
resistance to 150 ohm was considered. However, positive gains would
be realised for the coil at cryogenic temperature by virtue of the
reduced resistance, as follows:-

(a)   Improvement in coil efficiency.
(b)   Increase in magnetic field strengths.

Hence, the original coil was maintained.

A3.3.   PRELIMINARY TESTS ON PROTOTYPE GAUGES

A3.3.1 GAUGE DETAILS

Two prototype embedment gauges were produced to the required specification in conjunction with Gauge Technique Ltd., a VWG manufacturer. The gauges were sealed and tensioned at different levels. On receipt the gauges had period readings of 06670 (1,494Hz) and 14785 (676Hz) providing an extreme range, and were designated P1 and P2 respectively.

Gauge P1 differed in two respects when compared to Gauge P2. Firstly, the coil housing was brass instead of mild steel, and secondly the distance between the platens was marginally greater, 5.531", compared to 5.468".

The relationship between strain and frequency in cycles per second for a vibrating wire 0.010 inches diameter is given approximately by the formula:-

Strain = $L^2 \times 10^{-10} f^2$, where L is the clear wire length
in inches between clamping pins

Gauge factors for the standard 5.5 inch gauge and the two prototypes and therefore:-

Standard	3.050×10^{-3}
Gauge P1	3.059×10^{-3}
Gauge P2	2.990×10^{-3}

The above factors represent theoretical values.

A3.3.2 TESTING

Initial tests involved cooling the gauges from ambient temperature down to -178°C and recording the gauge period for 100 cycles, the coil resistance and the temperature. The cabinet used for cooling

the gauges is described in Section 4.3.4.2 of the main text. Apparent strain changes were calculated using the above gauge factors. The results are summarised in Table A3.1.

A3.3.3 DISCUSSION

The recorded change in strain with decreasing temperature shown in Figure A3.1 is believed to be due to differential thermal contraction between the stainless steel tube and the high strength cold drawn vibrating wire. Stainless steel has a thermal expansion coefficient greater than that of high tensile steel. (At 20°C: stainless steel = 16 x 10^{-8}/°C, HT/steel = 12 x 10^{-6}/°C). Over a temperature change of about 200°C, the differential strain would, therefore, be of the order of 800 microstrain, this being similar to the recorded values.

The difference between the magnitude of the strain change for the two gauges was surprising, however. Assuming constant gauge factors down to cryogenic temperature, the calculated values of differential contraction between the tube and the wire were 3.18 microstrain/°C for Gauge P1 and 4.46 microstrain/°C for Gauge P2. The subsequent restoration of the initial ambient readings after cryogenic cycling discounted any possibility of mechanical slip of the wire. Furthermore, additional tests 2 and 3, confirmed the individual strain gauge characteristics as shown in Table A3.1 and Figure A3.1.

It would have been reasonable to expect a difference due to the use of a brass coil housing for Gauge P1, compared with a mild steel housing for Gauge P2. Brass at 20°C has a thermal expansion coefficient of about 18 microstrain/°C compared with a value of 12 microstrain/°C for mild steel. However, even if the housing totally influences the central gauge section in terms of its thermal response, this will have only made an overall difference of about 0.5 microstrain/°C in the indicated differential (tube/wire) contraction between the two gauges, compared with an observed difference of 1.28 microstrain/°C. Furthermore, Gauge P1 with the brass coil housing exhibits the lower microstrain/°C change which would mean that, ignoring the effect of the coil housing, the differential may have been greater.

T E S T 1

GAUGE 1						GAUGE 2					
TEMP °C	COIL OHMS	OUTPUT SIGNAL mV	PERIOD READING	STRAIN	STRAIN CHANGE	TEMP °C	COIL OHMS	OUTPUT SIGNAL mV	PERIOD READING	STRAIN	STRAIN CHANGE
20	99.9	4.0	06694	6818	—	20	101.1	3.0	14828	1360	—
-58	69.4	3.5	06792	6630	188	-62	68.7	12.0	16795	1060	300
-68	65.4	3.0	06830	6558		-73	64.2	7.0	17448	981	379
-94	55.3	1.5	06875	6444	374	-99	54.3	6.5	18760	849	511
-117	45.0	1.0	06920	6388	430	-120	44.5	12.0	19996	747	613
-138	36.6	1.0	06960	6315	503	-142	35.5	35.0	21421	651	709
-166	24.5	2.0	07000	6243	575	-169	23.7	15.0	23025	564	796
-178	19.3	2.0	07032	6187	631	-178	20.1	35.0	24589	494	866

AFTER CRYOGENIC CYCLE

| 20 | 99.9 | | 06694 | 6818 | 0 | 20 | 99.3 | | 14801 | 1370 | +50 |

AFTER ADDITIONAL 15 HOURS

| | | | | | | 20 | 101.0 | | 14820 | 1360 | 0 |

T E S T 2

GAUGE 1					GAUGE 2				
TEMP °C	COIL OHMS	PERIOD READING	STRAIN	STRAIN CHANGE	TEMP °C	COIL OHMS	PERIOD READING	STRAIN	STRAIN CHANGE
20	101.2	06686	6843	—	20	100.2	14760	1372	—
− 13	88.2	06746	6722	121	− 14	86.5	15705	1213	159
− 34	79.1	06775	6665	178	− 34	78.5	16280	1128	244
− 58	69.5	06822	6574	269	− 55	70.0	17163	1015	357
− 80	60.5	06860	6500	343	− 80	60.0	17842	939	433
−102	51.3	06899	6427	416	−103	50.9	19160	815	557
−122	42.5	06935	6361	482	−124	42.5	20115	739	633

T E S T 3

GAUGE 1				GAUGE 2		
TEMP °C	PERIOD READING	STRAIN	STRAIN CHANGE	PERIOD READING	STRAIN	STRAIN CHANGE
16	06692	6830	—	14780	1359	—
6	06715	6784	46	15088	1314	45
− 4	06732	6750	80	15377	1265	94
− 13	06748	6718	112	15622	1225	134
− 33	06782	6651	179	16211	1138	221
− 50	06814	6589	241	16867	1051	308
− 69	06847	6526	304	17568	969	390
− 88	06880	6463	367	18545	870	489
−108	06817	6394	436	19515	785	574

TABLE A 3.1   Results of preliminary tests on prototype gauges cooled to temperatures down to -178°C
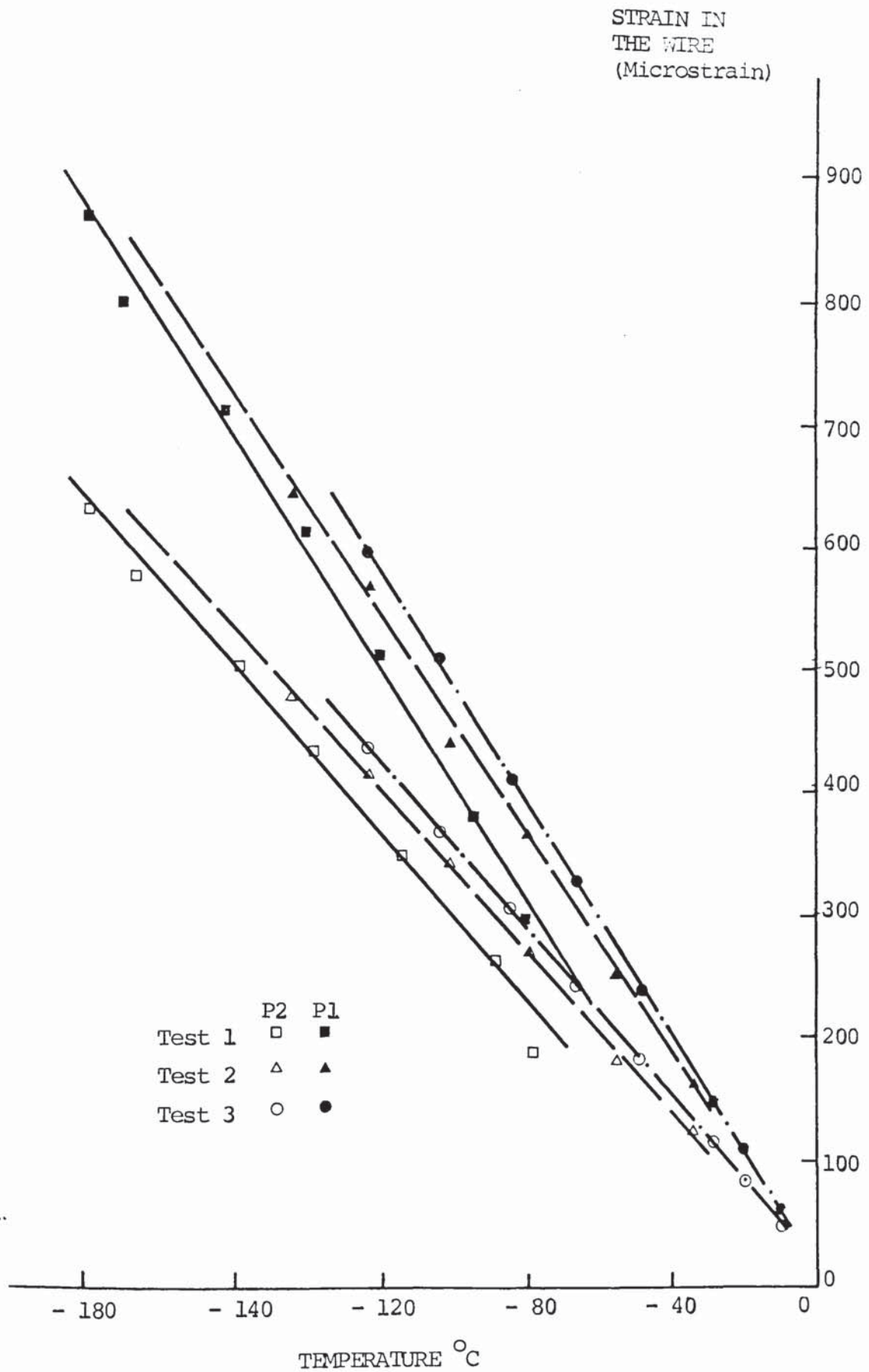
FIGURE A3.1 Results of preliminary cooling tests on two modified gauges

A possible reason for the difference in gauge performance may be encroachment of the end cap sealing adhesive on the vibrating wire which would affect the frequency change characteristic and hence the gauge factor.

No obvious explanation for the difference in performance of the gauges could be found at this stage and it was assumed that one of the gauges may have been defective in some way.

In relation to the performance of the coils, the recorded millivolt output signals indicated that there was a detectable level of signal amplitude down to -190°C. Gauge P1 results showed a decreasing amplitude of signal; however, no problem was experienced in obtaining a steady period measurement. For 100 cycles of count, a minimum output signal should not be less than 0.5 milli-volts. Test results for Gauge P2 show a large variation of signal amplitude, which suggests that the wire was touching the tube due to the low tension initially employed, which was considerably lower than the normal working range.

The insulation resistance measurements of the coils during and after each of the three tests showed no detectable deterioration. Whilst these results were related to short term and cryogenic cycling, expectations were that, in the long term, the coils would be satisfactory in a cryogenic environment.

A3.4. CALIBRATION

A3.4.1 INTRODUCTION

Having established that VWG's could be operated successfully at
cryogenic temperature, calibration tests were carried out to
establish the following:-

(1)   The gauge factor at ambient temperature.

(2)   The change in gauge factor of surface mounted gauges over
        the temperature range +20°C to -165°C.

(3)   The temperature correction factor for surface mounted gauges
        over the temperature range +20°C to -165°C.

(4)   The performance of embedded gauges with respect to both
        gauge factor and temperature correction factor.

A3.4.2 CALIBRATION OF SURFACE MOUNTED GAUGES AT AMBIENT TEMPERATURE

In order to determine the gauge factor of VWG's at -165°C, it was
first necessary to determine a consistent gauge factor at ambient
temperature.   Having determined a gauge factor for surface gauges
at ambient temperature, by comparison with dial gauges, these would
then be compared with surface gauges at -165°C. Embedded gauges in
concrete would then be calibrated against the surface gauges at
-165°C.

A calibration test rig was designed which would accommodate eight
surface gauges in groups of four at the top and bottom (Figure 5.2
p183).   To achieve sensitivity of movement, a differential screw
was used which gave 478.5 + 1%/-2% microstrain per revolution.
Movement of the differential screw caused an equal change in
distance between the top two plates and between the bottom two
plates. For the low temperature tests, the bottom two plates were
located in a cryogenic cabinet at -165°C, whilst the top two plates
were maintained at ambient temperature. The calibration test rig
was carefully tuned to give a smooth movement, particularly with
respect to bearing friction.

For calibration at ambient temperature, four 0.002mm dial gauges
were fixed on to the rig at 90° spacing, two at the top and two at

the bottom, and located between vertical pairs of gauges. Relative movement between the plates was monitored by both VWG's and dial gauges. The mean of the relevant pair of dial gauge readings was converted to change in microstrain over the VWG gauge length, and the change of frequency of the individual VWG's was divided into the appropriate microstrain value to obtain gauge factors.

Tables A3.2a and 2b and A3.3 give dial gauge and VWG readings together with calculated gauge factors for increments of compressive and tensile strain up to about 1,000 microstrain. Mean gauges factors from Tables A3.2a and 2b and A3.3 are as follows:-

Compressive Loading 2.922×10^{-3} per frequency^2
Compressive Loading 2.933×10^{-3} per frequency^2
Tensile loading 2.927×10^{-3} per frequency^2

The above values are lower than the theoretical gauge factor of 3.05×10^{-3} per frequency^2 for a 5.5" surface gauge. However, in computing a theoretical gauge factor, the square of the length of free wire is taken literally into account. The wire is fixed at either end by clamping, and this will reduce the effective length of actively free wire. Using a gauge factor of $2.927 \times 10^{-3}/f^2$, the effective length of free wire of 0.01" diameter would be 5.41", which suggests that $4\frac{1}{2}$ diameters of wire at either end should be discounted due to clamping influence.

A gauge factor of 2.927×10^{-3} has been used, therefore, for all subsequent 5.5" surfaced mounted VWG tests at ambient temperature.

A3.4.3   CALIBRATION OF SURFACED MOUNTED GAUGES AT CRYOGENIC TEMPERATURES

The calibration of 5.5" surfaced mounted VWG's at a cryogenic temperature of -165°C was undertaken using the previously mentioned calibration test rig.

The test rig was mounted with the bottom plates located in a cryogenic cabinet so that the top four gauges were at ambient temperature, and the lower four gauges in a controllable cryogenic environment.

a) COMPRESSION TEST AT AMBIENT

	Gauge 1	Gauge 2	Gauge 3	Gauge 4	Gauge 5	Gauge 6	Gauge 7	Gauge 8	Mean G.F.
Ref Period	10342	10316	10336	10468	10232	10251	10406	10238	
Period	11384	11321	11324	11512	11201	11233	11398	11198	
Dial Gauge µS	469	466	458	461	469	466	458	461	
Gauge Factor	2.871	2.923	2.931	2.916	2.866	2.929	2.978	2.942	2.932
Period	11687	11626	11612	11818	11503	11535	11708	11510	
Dial Gauge µS	584	587	578	576	584	587	578	576	
Gauge Factor	2.878	2.934	2.975	2.928	2.928	2.933	2.982	2.889	2.931
Period	12004	11925	11908	12122	11809	11853	12021	11816	
Dial Gauge µS	637	701	692	678	637	701	692	678	
Gauge Factor	2.849	2.964	2.998	2.920	2.884	2.922	2.989	2.849	2.922
Period	12242	12326	12278	12556	12196	12237	12394	12196	
Dial Gauge µS	819	827	819	811	819	827	819	811	
Gauge Factor	2.834	2.937	3.002	2.915	2.896	2.913	3.004	2.879	2.923
Period	-	12718	12707	-	12594	12642	12833	12621	
Dial Gauge µS	938	944	935	928	938	944	935	928	
Gauge Factor	-	2.938	2.951	-	2.888	2.897	2.955	2.843	2.912
Period	13348	13154	13146	13522	13026	13066	13242	13062	
Dial Gauge µS	1062	1060	1056	1058	1062	1060	1056	1058	
Gauge Factor	2.842	2.930	2.953	2.892	2.903	2.897	2.988	2.874	2.910
								TEST MEAN	2.922

b) COMPRESSION TEST AT AMBIENT

	Gauge 1	Gauge 2	Gauge 3	Gauge 4	Gauge 5	Gauge 6	Gauge 7	Gauge 8	Mean G.F.
Ref Period	09230	09248	09283	09379	09206	09216	09355	09214	
Period	09564	09567	09596	09702	09513	09535	09693	09534	
Dial Gauge µS	221	226	230	225	221	226	230	225	
Gauge Factor	2.921	2.945	3.090	3.020	2.943	2.915	2.939	2.892	2.959
Period	09763	09761	09778	09888	09694	09703	09848	09695	
Dial Gauge µS	340	349	350	342	340	349	350	342	
Gauge Factor	2.821	2.913	3.060	3.001	2.939	3.026	3.141	3.002	2.988
Period	09943	09913	09938	10078	09871	09877	10031	09885	
Dial Gauge µS	454	446	443	451	454	446	443	451	
Gauge Factor	2.884	2.939	2.993	2.960	2.952	2.926	2.975	2.917	2.943
Period	10176	10146	10158	10301	10088	10112	10234	10087	
Dial Gauge µS	573	576	569	566	573	576	569	566	
Gauge Factor	2.821	2.911	2.973	2.909	2.903	2.888	2.969	2.899	2.909
Period	10388	10337	10366	10309	10278	10294	10442	10282	
Dial Gauge µS	634	683	677	677	634	683	677	677	
Gauge Factor	2.824	2.882	2.944	2.927	2.930	2.922	3.000	2.919	2.919
Period	10591	10557	10583	10729	10475	10502	10673	10499	
Dial Gauge µS	791	796	792	787	791	796	792	787	
Gauge Factor	2.853	2.928	2.960	2.935	2.945	2.942	2.991	2.906	2.933
Period	10818	10769	10797	10974	10698	10761	10894	10725	
Dial Gauge µS	898	901	892	889	898	901	892	889	
Gauge Factor	2.859	2.936	2.947	2.901	2.934	2.960	2.973	2.882	2.922
Period	11121	11054	11100	11288	10978	11002	11174	10986	
Dial Gauge µS	1023	1021	1011	1013	1023	1021	1011	1013	
Gauge Factor	2.840	2.911	2.899	2.878	2.921	2.907	2.959	2.900	2.902
Period	11401	11321	11331	11361	11245	11263	11445	11279	
Dial Gauge µS	1182	1141	1128	1129	1142	1141	1128	1129	
Gauge Factor	2.860	2.933	2.957	2.906	2.935	2.933	2.975	2.882	2.923
								TEST MEAN	2.933

TABLE A3.2 Calibration tests in compression at ambient temperature.

	Gauge 1	Gauge 2	Gauge 3	Gauge 4	Gauge 5	Gauge 6	Gauge 7	Gauge 8	Mean G.F.
Ref Period	13786	13562	13562	13973	13421	13490	13704	13494	
Period	-	12715	-	-	12595	12635	12843	12614	
Dial Gauge μS	228	218	218	228	228	218	218	228	
Gauge Factor	-	2.918	-	-	3.037	2.871	2.954	2.875	2.931
Period	12423	12288	12275	12554	12186	12206	12392	12204	
Dial Gauge μS	352	347	351	356	352	347	351	356	
Gauge Factor	2.889	2.928	2.927	2.911	2.976	2.872	2.958	2.911	2.922
Period	12012	11918	11914	12131	11824	11856	12030	11826	
Dial Gauge μS	476	470	477	484	476	470	477	484	
Gauge Factor	2.885	2.929	2.964	2.889	2.976	2.915	3.008	2.915	2.931
Period	11703	11621	11606	11811	11516	11526	11687	11501	
Dial Gauge μS	583	587	595	591	583	587	595	591	
Gauge Factor	2.859	2.983	2.992	2.886	2.932	2.900	2.978	2.856	2.923
Period	11362	11295	11310	11497	11203	11222	11403	11211	
Dial Gauge μS	709	711	711	710	709	711	711	710	
Gauge Factor	2.855	2.959	2.986	2.905	2.936	2.915	3.004	2.880	2.932
Period	11016	10985	11003	11170	10894	10914	11104	10912	
Dial Gauge μS	840	836	837	840	840	836	837	840	
Gauge Factor	2.819	2.934	2.964	2.905	2.921	2.891	3.004	2.892	2.916
Period	10777	10757	10781	10911	10655	10673	10851	10661	
Dial Gauge μS	962	947	945	959	962	947	945	959	
Gauge Factor	2.872	2.955	2.983	2.926	2.953	2.891	2.981	2.901	2.933
Period	10641	10524	10541	10676	10437	10360	10624	10443	
Dial Gauge μS	1067	1061	1060	1066	1067	1061	1060	1066	
Gauge Factor	2.854	2.954	2.975	2.919	2.951	2.918	2.999	2.898	2.932
Period	10326	10300	10301	10437	10227	10244	10391	10220	
Dial Gauge μS	1177	1175	1175	1177	1177	1175	1175	1177	
Gauge Factor	2.859	2.947	2.946	2.899	2.936	2.919	2.984	2.882	2.922

TEST MEAN 2.927

TABLE A3.3 Calibration tests in tension at ambient temperature.

Successful calibration required careful tuning of the test rig bearings for smooth operation at low temperature. In addition, the bearings had to be free of moisture and were therefore dried out immediately prior to cool down. This operation and the time taken to achieve a stable temperature of -165°C permitted only one test run a day.

Four calibration runs were carried out in which tensile strains of up to 1,200 microstrain were imposed on the gauges. The results are given in Table A3.4 (a-d).

The gauge factor of 2.927 x 10^{-3} was applied to all eight gauges. Variations in the resultant strain values for gauges at ambient and cryogenic temperature were used to calculate the correct gauge factors.

The mean strain values for each set of four gauges at each strain increment did not show any significant change of gauge factor for gauges at -165°C, when compared with gauges at ambient temperature (Figure A3.2). The gauges at low temperature gave strain values which were marginally higher than the gauges at ambient temperature (by 3-4%) indicating that the gauge factor may be marginally lower.

A3.4.4 MEASUREMENT OF THERMAL CONTRACTION OF THE VIBRATING WIRE

The thermal contraction of the gauge wire was measured by clamping surface mounted gauges onto two different metals of known thermal expansion coefficients. The test metals chosen were copper (99.98% pure) and nickel (99% purity). These two materials have a greater thermal contraction than the high tensile steel gauge wire. When the temperature is decreased the wire tension of the gauges will therefore relax.

Four gauges were used on each test specimen, two at an ambient nominal frequency of 775 hz and two at 975 Hz. Period readings for all the gauges were taken at 20°C, -73°C and -173°C (Tables A3.5 and A3.6). From the known thermal contraction data for the two test metals the contraction of the wire was calculated and is shown in Fig. A3.3. Average values are given below:-

GAUGES AT AMBIENT / GAUGES AT -162°C (Table 1)

	1	2	3	4	MEAN	5	6	7	8	MEAN
Ref. Period	11135	11114	10808	10998		10274	10234	10353	09992	
Period	10966	10885	10575	10836		10138	10084	10127	09817	
Microstrain	73	112	112	73	92.5	75	84	123	105	96.8
Period	10729	10608	10325	10633		09893	09862	09955	09641	
Microstrain	182	243	240	169	208.5	218	215	223	217	218.3
Period	10452	10321	10009	10293		09611	09693	09806	09392	
Microstrain	319	389	416	343	366.8	396	321	313	387	354.3
Period	10308	10191	09932	10224		09496	09556	09688	09313	
Microstrain	394	460	461	380	423.8	473	411	388	443	428.8
Period	10034	10056	09826	10006		09404	09421	09521	09191	
Microstrain	546	536	526	504	528	537	503	498	533	517.8
Period	09892	09863	09622	09822		09221	09251	09336	09006	
Microstrain	631	650	656	614	637.8	669	625	627	677	649.5
Period	09726	09722	09476	09653		09081	09126	09190	08871	
Microstrain	734	738	754	721	736.8	776	720	735	788	754.8

GAUGES AT AMBIENT / GAUGES AT -162°C (Table 2)

	1	2	3	4	MEAN	5	6	7	8	MEAN
Ref. Period	10505	10176	10555	10628		09807	09453	10237	10433	
Period	10165	09768	10155	10354		09512	09127	09922	10181	
Microstrain	180	241	211	139	192.8	192	238	180	135	186.3
Period	09619	09205	09832	10127		09163	08606	09507	10044	
Microstrain	511	628	401	263	405.8	443	677	445	212	444.3
Period	09234	08964	09286	09421		08781	08446	08965	09224	
Microstrain	780	816	767	707	767.5	753	828	849	741	798.3
Period	08901	08567	08978	09254		08474	08115	08683	09011	
Microstrain	1042	1162	1004	827	1008.8	1033	1169	1089	916	1051.8
Period	08831	08357	08758	09174		08363	07896	08547	09021	
Microstrain	1101	1364	1189	886	1135	1142	1419	1214	908	1170.8

GAUGES AT AMBIENT / GAUGES AT -162°C (Table 3)

	1	2	3	4	MEAN	5	6	7	8	MEAN
Ref. Period	10367	10475	10263	10142		09903	09616	10652	10083	
Period	10168	10251	10052	09962		09726	09475	10426	09872	
Microstrain	108	118	118	104	112.0	110	95	113	124	110.5
Period	09992	10081	09788	09691		09506	09259	10187	09679	
Microstrain	208	213	276	271	242.0	255	249	241	245	247.5
Period	09757	09826	09617	09528		09332	09085	09925	09486	
Microstrain	351	364	386	379	370.0	376	381	392	374	380.8
Period	09515	09604	09428	09277		09099	08844	09768	09338	
Microstrain	511	506	514	555	521.5	551	577	488	478	523.5
Period	09334	09432	09266	09083		08968	08722	09554	09151	
Microstrain	636	623	630	702	647.8	655	682	627	616	645.0
Period	09121	09168	09036	08917		08764	08478	09216	08926	
Microstrain	795	815	806	836	813.0	826	907	867	795	848.8

GAUGES AT AMBIENT / GAUGES AT -162°C (Table 4)

	1	2	3	4	MEAN	5	6	7	8	MEAN
Ref. Period	10735	11147	10771	10624		10283	10383	10532	10887	
Period	10433	10751	10327	10233		10005	10214	10272	10528	
Microstrain	149	177	222	202	187.5	156	192	135	171	163.5
Period	10257	10511	10107	10078		09833	10056	10117	10325	
Microstrain	242	294	342	289	291.8	259	281	221	276	259.3
Period	09972	10337	09946	09793		09693	09753	09866	10205	
Microstrain	404	384	436	459	420.8	347	464	368	341	380.0
Period	09636	09948	09627	09545		09315	09398	09561	09835	
Microstrain	612	602	635	619	617.0	605	701	363	557	606.5
Period	09318	09646	09471	09357		09138	09180	09283	09569	
Microstrain	831	790	740	750	777.8	737	860	758	727	770.5
Period	09225	09532	09255	09144		09007	09022	09125	09428	
Microstrain	900	866	894	907	891.8	840	983	877	824	881.0
Period	09036	09292	09127	09036		08887	08876	08912	09211	
Microstrain	1045	1034	991	976	1011.5	938	1102	1047	980	1016.8

TABLE A3.4   Results obtained using the calibration rig with four gauges at ambient temperature and four gauges at -162°C.
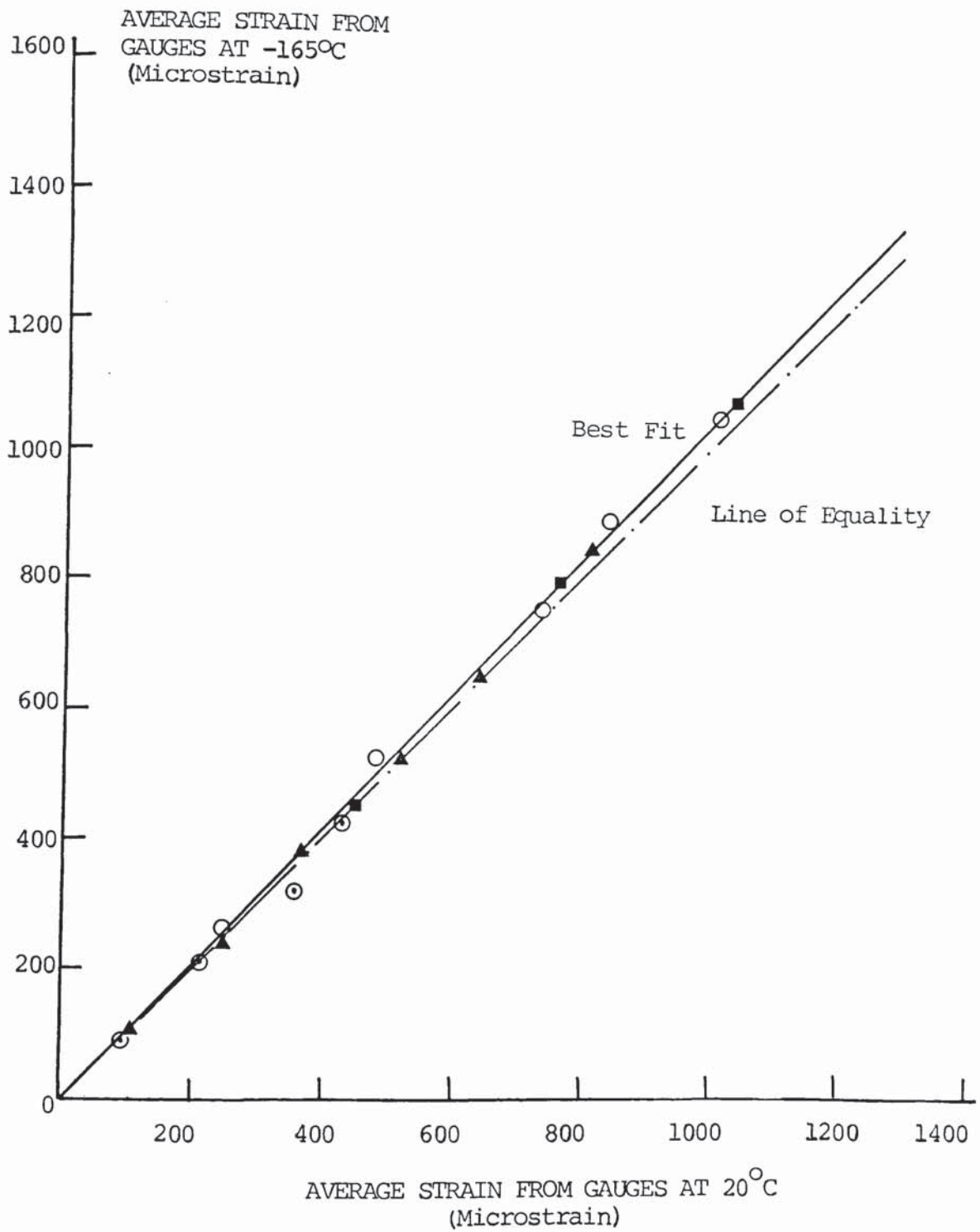
FIGURE A3.2 Gauge calibration at cryogenic temperature.
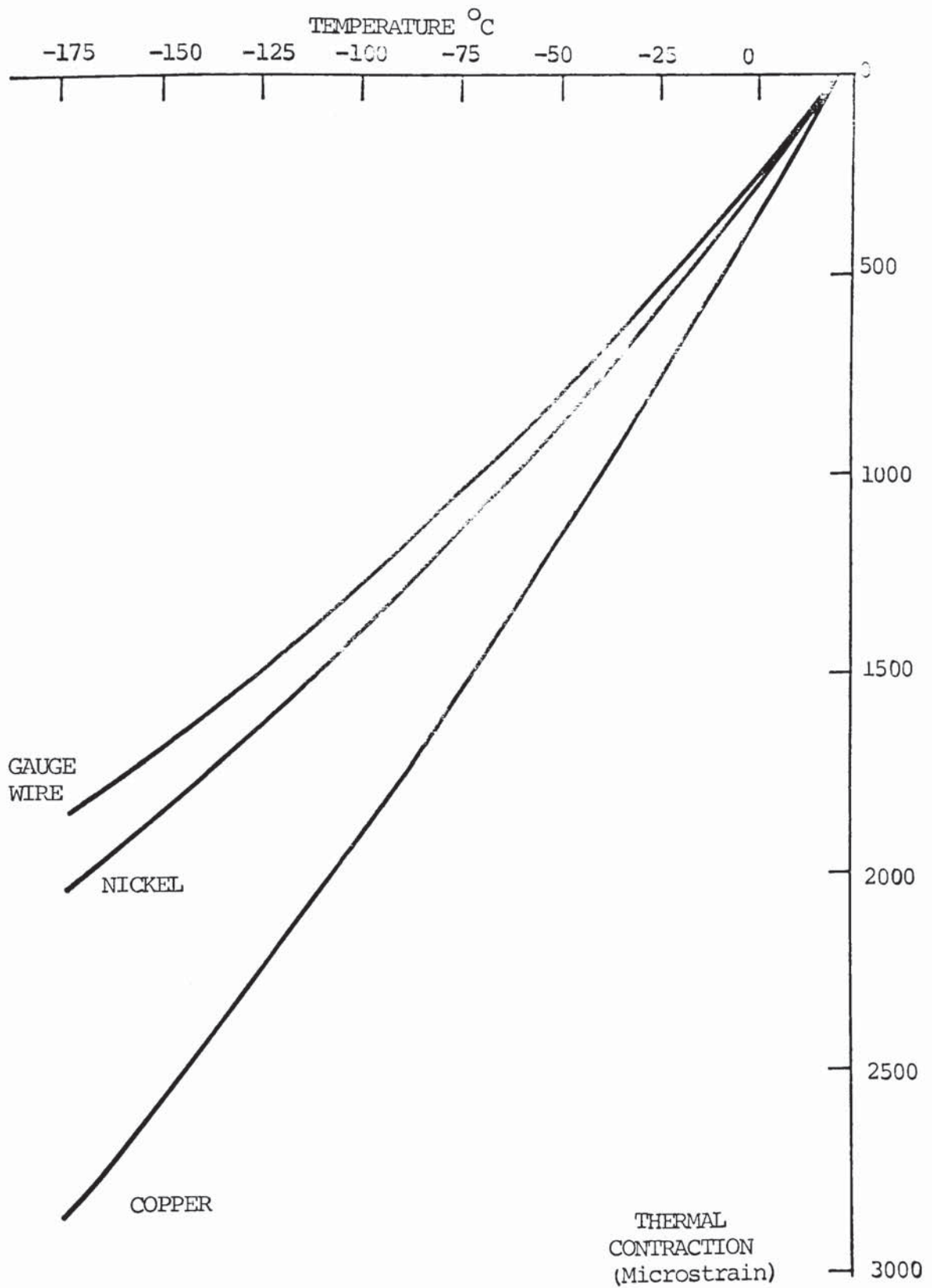
FIGURE A3.3 Results from tests to determine the thermal contraction
of the steel gauge wire.

	Copper	Nickel	Gauge Wire
20 to -73°C	149×10^{-5}	111×10^{-5}	102.6×10^{-5}
20 to -173°C	283×10^{-5}	201×10^{-5}	183.1×10^{-5}

The results from the thermal contraction tests are of additional interest with respect to gauge performance. The wire in the higher tensioned gauges, generally exhibited lower thermal contraction than the gauges tensioned at a lower frequency. This behaviour was similar to that observed during the tests on two prototype gauges and additional tests were therefore carried out to determine the influence of wire frequency on gauge response.

A3.4.5 DIFFERENTIAL THERMAL CONTRACTION AT DIFFERENT FREQUENCIES

To determine the influence of frequency on gauge response, a cryogenic test was initially carried out in which six surface mounted gauges, at different ambient wire frequencies, were mounted on a high tensile steel rod. The temperature of the rod and gauges were lowered to -10°C and period time readings of gauges were taken for datum reference. Further readings at -73°C, -100°C, -163°C and -173°C were taken and the resultant microstrain values, using a G.F. of $2.927 \times 10^{-3}/f^2$, were plotted (Figure A3.4).

Due to the similar contraction coefficients of the rod and wire, there was very little apparent strain change, particular in the gauges tensioned to low frequency (650 to 900 Hz). For gauges initially tensioned to higher frequencies the resultant thermal contractions show increasing wire tension. The indicated tension induced in the wire decreased with the initial frequency as shown in Figure A3.4.

Additional differential thermal contraction tests were undertaken using embedment gauges.

Four gauges with stainless steel tubes were tensioned at different frequencies in order to determine differential thermal contraction

GAUGE	1	2	3	4
+20 Period	977 HZ. 10239	989 HZ. 10111	788 HZ. 12685	762 HZ. 13125
-73 Period	896 HZ. 11157	906 HZ. 11039	684 HZ. 14622	645 HZ. 15500
$\Delta L \mu S$	-441	-461	-450	-481
-173 Period	793 HZ. 12610	798 HZ. 12527	541 HZ. 18479	482 HZ. 20744
$\Delta L \mu S$	-951	-998	-962	-1019

COPPER THERMAL CONTRACTION.
20°C to -73°C = 1490 microstrain.

Gauge 1 Wire Contraction = 1049 μS at 997 HZ.
Gauge 2 Wire Contraction = 1029 μS at 989 HZ.
Gauge 3 Wire Contraction = 1040 μS at 788 HZ.
Gauge 4 Wire Contraction = 1009 μS at 762 HZ.

COPPER THERMAL CONTRACTION.
20°C to -173°C = 2830 microstrain.

Gauge 1 Wire Contraction = 1879 μS at 997 HZ.
Gauge 2 Wire Contraction = 1832 μS at 989 HZ.
Gauge 3 Wire Contraction = 1868 μS at 788 HZ.
Gauge 4 Wire Contraction = 1811 μS at 762 HZ.

Mean for wire 20°C - -73°C = 1032 microstrain.
Mean for wire 20°C - -173°C = 1848 microstrain.

TABLE A3.5   Results of tests with surface mounted gauges attached to copper rods, and cooled to -173°C. (No adjustment has been made for different initial gauge frequencies)

GAUGE	1	2	3	4
+20	975 HZ	974 HZ	800 HZ	799 HZ
Period	10251	10270	12499	12519
-73	962 HZ	960 HZ	777 HZ	778 HZ
Period	10393	10418	12873	12857
$\Delta L \mu S$	-75.6	-78.3	-107.3	-96.9
-173	945 HZ	942 HZ	750 HZ	753 HZ
Period	10583	10614	13338	13276
$\Delta L \mu S$	-172	-177	-228.3	-206.9

NICKEL THERMAL CONTRACTION
20°C to -73°C = 1110 microstrain

Gauge 1 Wire Contraction = 1034.4 μS at 975 HZ.
Gauge 2 Wire Contraction = 1031.7 μS at 974 HZ.
Gauge 3 Wire Contraction = 1002.7 μS at 800 HZ.
Gauge 4 Wire Contraction = 1013.1 μS at 799 HZ.

NICKEL THERMAL CONTRACTION
20°C to -173°C = 2010 microstrain

Gauge 1 Wire Contraction = 1838 μS at 975 HZ.
Gauge 2 Wire Contraction = 1833 μS at 974 HZ.
Gauge 3 Wire Contraction = 1781.7 μS at 800 HZ.
Gauge 4 Wire Contraction = 1803.1 μS at 799 HZ.

Mean for wire 20°C - -73°C = 1020 microstrain.
Mean for wire 20°C - -173°C = 1814 microstrain.

TABLE A3.6   Results of tests with surface mounted gauges attached to nickel rods and cooled to -173°C.   (No adjustment has been made for different initial gauge frequencies).

FIGURE A3.4   Results obtained from surface gauges mounted on reinforcing steel and cooled to -173°C.

between the wire and the body of the gauge. The frequencies selected were representative of the likely range normally encountered when using 5.5" V.W. gauges.

Period time readings of the gauges were taken at -10°C, -73°C. -100°C, -165°C and -173°C. These readings were converted to microstrain, using a gauge factor of $2.927 \times 10^{-3}/f^2$, and are plotted in Figure A3.5.

The differential thermal contraction of wire and tube appears substantially linear, for a 5.5" gauge length, down to at least -173°C. The contraction of the tube is greater than that of the wire. From Figure A3.5 it can be seen that for a change of 1°C a gauge initially tensioned at 1500 Hz has an apparent differential thermal contraction of 3.275 microstrain. A gauge at an initial 600 Hz would indicate 4.72 microstrain per 1°C change. The wire frequencies used for this test were, 667 Hz, 833 Hz, 1123 Hz and 1423 Hz at ambient temperature.

The results obtained using both surface mounted and embedment gauges are shown in Figure A3.6 in which the apparent strain change is plotted against frequency^2. There is clearly a linear relationship between the frequency^2 and the change in thermal contraction, indicating that the thermal contraction of the wire is directly related to the initial strain imposed upon it. The higher the initial tension, the higher the thermal contraction. Hence, knowing the initial frequency of the wire the thermal contraction can be adjusted accordingly. Temperature correction curves for concretes with a range of initial frequencies are shown in Figure 6.1 (p 216).

A3.4.6 CALIBRATION OF EMBEDMENT GAUGES IN CONCRETE

To determine the gauge factor of VWGs embedded in concrete, three 150mm diameter by 450mm long concrete cylinders were cast each with a single embedment gauge cast centrally. After sealed curing for 28 days, three surface mounted gauges were fixed to the surface of each cylinder at 120° intervals. The three embedded gauges were tensioned to different frequencies from a high value of 1363 Hz to
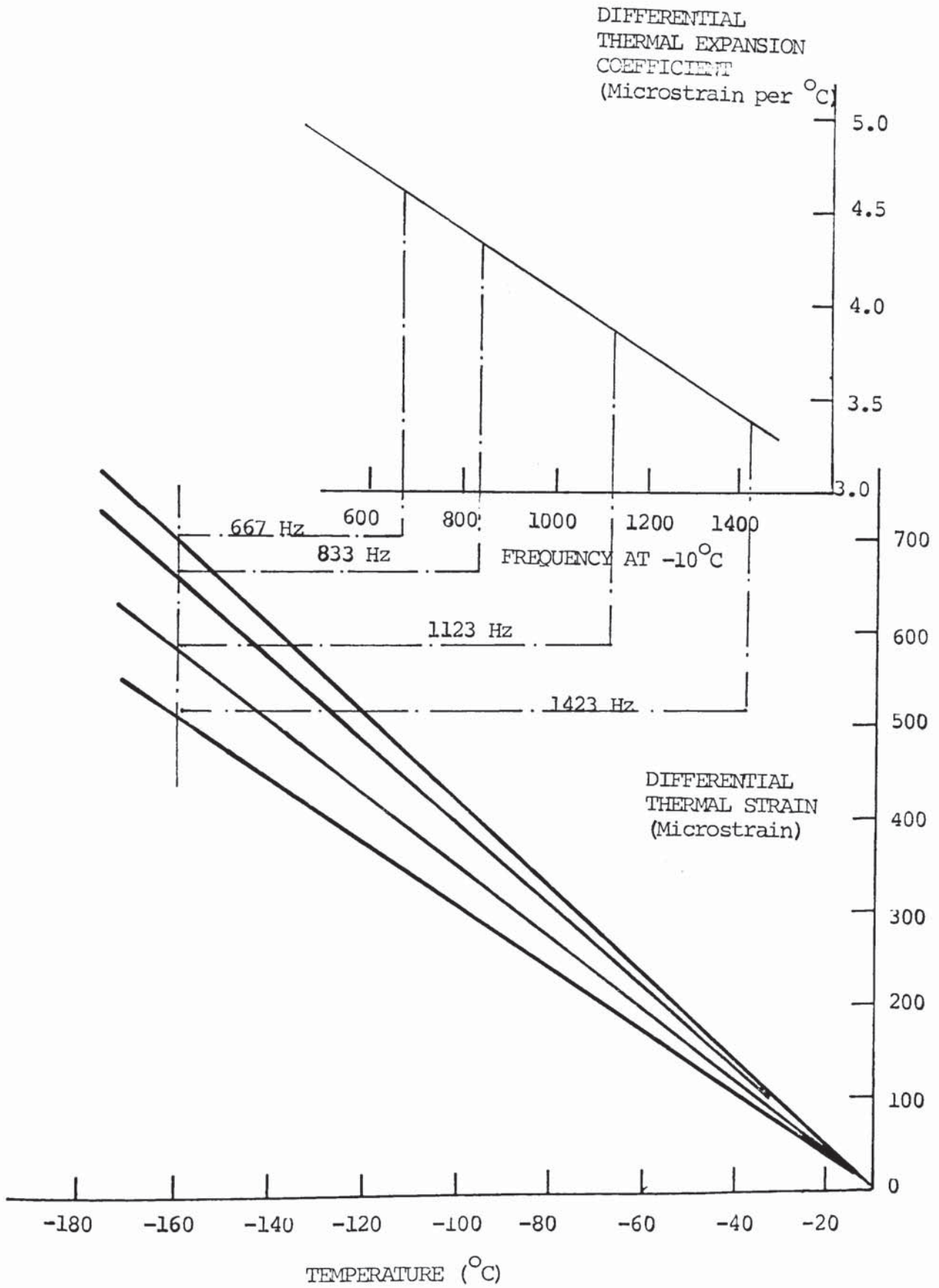
FIGURE A3.5 Results of tests on embedment gauges with different
initial frequencies, cooled to -173°C.

a low value of 779 Hz. The intermediate value was 973 Hz. The surface mounted gauges were tensioned to give a frequency with the range 1000 to 1300 Hz. As it was necessary to cool the specimens down to -165°C in order to carry out gauge factor tests, it was also possible to determine temperature correction factors.

The tests were carried out as follows. The specimens were located in their stainless steel loading rigs and placed into an insulated cryogenic cabinet. (Details are given in Sections 6.2.3 and 6.2.4 of the main text). Datum readings were then taken on each of the twelve gauges at ambient temperature prior to the application of a uniaxial compressive stress of 13.8 N/mm^2. The stress was maintained whilst readings were again taken on all twelve gauges. The stress was then relieved and a third set of gauge readings were taken. The temperature within the cabinet was then reduced at a rate of 4°C per hour to -20°C and maintained at this level for a period of not less than 6 hours before taken a further set of readings at no load, 13.8 N/mm^2 and after load release. This procedure was repeated at -70°C, -115°C and -165°C.

Individual gauge results are given in Table A3.7. Values of thermal correction have been derived from Figure 6.1, taking into account the specific gauge frequency (Additional tests using embedded gauges validated the use of the relationship between wire contraction and frequency[2] derived from surface mounted gauges - see Section A3.4.7). Correlation between the results for each specimen was generally very good with respect to both load induced and thermal strain.

Regarding the gauge factor there would appear to be a marginal reduction for the embedded gauges at temperatures down to about -20°C. At lower temperatures there was no significant difference between embedded and surfaced mounted gauges. With regard to thermal strains, however, there was a consistent difference between internal and external values, the former generally being about 10% higher. No specific reason for this difference has been identified, but the following hypotheses have been considered:-

		SPECIMEN 1				SPECIMEN 2				SPECIMEN 3			
TEMP (°C)		Embedded	Surface Gauges			Embedded	Surface Gauges			Embedded	Surface Gauges		
			1	2	3		1	2	3		1	2	3
	RUN 1												
17	No load	07335	09528	06100	09599	09463	08695	09966	09823	12833	09264	08844	07968
	Loaded	07650	10181	06272	10305	10181	09168	10473	10479	15071	10005	09520	08309
	ε_s	-439	-400	-426	-420	-445	-467	-278	-367	-489	-487	-517	-370
	No load	07347	09531	06153	09674	09543	08726	09912	09650	12967	09338	08954	07982
	ε_r	-18	-2	-90	-49	-55	-28	-32	-110	-37	-54	-91	-16
-20	No load	07268	09364	06075	09495	09419	08595	09727	09501	12632	09163	08793	07859
	ε_{tm}	+19	+116	+154	+118	+93	+127	+135	+145	+85	+118	+114	+99
	ε_{tc}	-505	-482	-525	-482	-491	-488	-480	-480	-483	-485	-487	-495
	ε_t	-386	-366	-371	-364	-398	-361	-345	-355	-398	-367	-373	-396
	Load	07603	10033	06244	10206	10139	09126	10320	10380	14880	09955	09489	08208
	ε_s	-478	-430	-424	-436	-452	-448	-345	-526	-513	-533	-535	-395
	No load	07280	09375	06078	09510	09422	08595	09732	09506	12677	09182	08804	07867
	ε_r	-18	-8	-8	-9	-2	0	-3	-4	-13	-14	-10	-10
-70	No load	07120	09032	05968	09150	09136	08328	09369	09184	12019	08861	08515	07641
	ε_{tm}	+251	+265	+295	+260	+223	+258	+244	+230	+218	+256	+260	+283
	ε_{tr}	-540	-513	-572	-513	-525	-521	-510	-512	-514	-515	-510	-530
	ε_t	-289	-248	-277	-247	-302	-263	-266	-276	-294	-259	-260	-247
	Load	07413	09615	06124	09772	09748	08792	09865	09942	13736	09551	09124	07956
	ε_s	-447	-422	-413	-431	-427	-434	-327	-509	-475	-591	-521	-389
	No load	07127	09034	05967	09159	09131	08321	09362	09170	12058	08880	08527	07650
	ε_r	-11	-2	+3	-7	+4	+7	+5	+11	-13	-16	-11	-12
-115	No load	07037	08854	05901	08966	08975	08175	09161	08998	11695	08698	08361	07522
	ε_{tm}	+148	+147	+185	+152	+123	+152	+148	+134	+127	+157	+161	+172
	ε_{tc}	-425	-402	-456	-402	-414	-410	-400	-401	-404	-405	-408	-420
	ε_t	-277	-255	-271	-250	-291	-258	-252	-267	-277	-248	-247	-248
	Load	07296	09376	06049	09512	09547	08595	09598	09688	13179	09309	08905	07805
	ε_s	-413	-404	-406	-406	-422	-417	-310	-495	-455	-491	-496	-368
	No load	07040	08832	05889	08952	08980	08145	09138	08967	11731	09697	08354	07514
	ε_r	-5	+19	+34	+11	-4	+32	+18	+25	-13	+1	+7	+11
-165	No load	06949	08654	05827	08754	08824	08012	08948	08792	11913	08744	08412	07502
	ε_{tm}	+155	+160	+180	+167	+130	+148	+150	+146	+134	+165	+159	+194
	ε_{tc}	-410	-383	-442	-383	-395	-391	-380	-382	-384	-385	-390	-400
	ε_t	-255	-223	-268	-216	-265	-243	-238	-236	-250	-220	-231	-206
	Loaded	07187	09127	05972	09273	09328	08401	09349	09420	12611	09062	08684	07651
	ε_s	-395	-395	-414	-416	-395	-413	-307	-488	-471	-471	-472	-378
	No load	06961	08654	05829	08757	08855	07981	08928	08770	11398	08527	08204	07381
	ε_r	-21	0	-6	-3	-27	+35	+16	+19	-8	-9	-4	-6
18 -173	RUN 2												
	No load	07047	07042	07171	07111	08878	09341	08959	08979	11611	11517	11516	11542
	No load	06720	06671	06778	06746	08337	08683	08272	08377	10622	10424	10360	10408
	ε_{tm}	+585	+675	+679	+643	+498	+527	+631	+541	+423	+487	+520	+505
	ε_{tc}	-1950	-1950	-1945	-1950	-1855	-1840	-1850	-1850	-1785	-1785	-1785	-1785
	ε_t	-1365	-1275	-1266	-1307	-1357	-1313	-1219	-1309	-1362	-1298	-1265	-1280

ε_s - Stress induced strain
ε_r - Residual strain after removal of load
ε_{tm} - Measured thermal strain
ε_{tc} - Temperature correction
ε_t - Thermal strain

TABLE A3.7 Period and strain readings during calibration of embedded gauges in concrete cylinders.

i)   As the specimen is cooled a temperature gradient develops, the surface being cooler than the centre. If moisture migrates down this gradient to the surface, this could result in a higher moisture content at the surface than at the centre. Hence when the water freezes within the concrete, with its associated expansion, this would tend to offset the contraction of the surface to a greater extent than the centre. The net effect would therefore be greater contraction at the location of the embedded gauge, as recorded. There is some evidence that moisture differentials may be, at least partially responsible for the differential contraction as the largest differences between internal and external contraction were generally recorded in the -20°C to -70°C range, when most of the ice is formed.

ii)   Temperature differentials is to induce stresses in the test specimen. If the surface is cooler it will be in tension, whilst the centre of the specimen will be in compression. The compression at the centre would cause additional contraction at this location whilst the tensile stresses on the surface would offset some of the thermal contraction. The net effect is again to increase the internal strain in relation to the surface.

A3.4.7 ADDITIONAL THERMAL CONTRACTION TESTS ON CAST-IN EMBEDDED GAUGES

A second series of tests were undertaken to obtain data for embedded gauges cast into concrete. Again, three 150mm diameter by 450mm long concrete cylinders were cast with an embedment gauge at the centre of each. Three surface mounted gauges were then fixed to the surface at 120° intervals after a 28 day sealed curing period. Frequencies for the embedded gauges were 861, 1126 and 1419 H2 and in each cast the respective surface gauges were tensioned to about the same level.

Datum readings were taken on all twelve gauges at an ambient temperature of 18.5°C and the specimens were then cooled to -165°C over a 24 hour period. The gauge readings were then taken at this temperature. Individual gauge results are given in Table A3.8.

- 356 -

Strains for the high and low frequency gauges, before thermal correction, differ by 162 microstrain, whether recorded internal or externally. These results are included in Figure A3.6, which demonstrates that the effect of initial frequency on thermal contraction of the steel wire is the same for both embedded and surface mounted gauges. Corrected thermal strains are included in Table A3.8.

Correlation between the three specimens was extremely good, whether assessed on the basis of internal or external strain. However, the difference between internal and external strain was again observed.
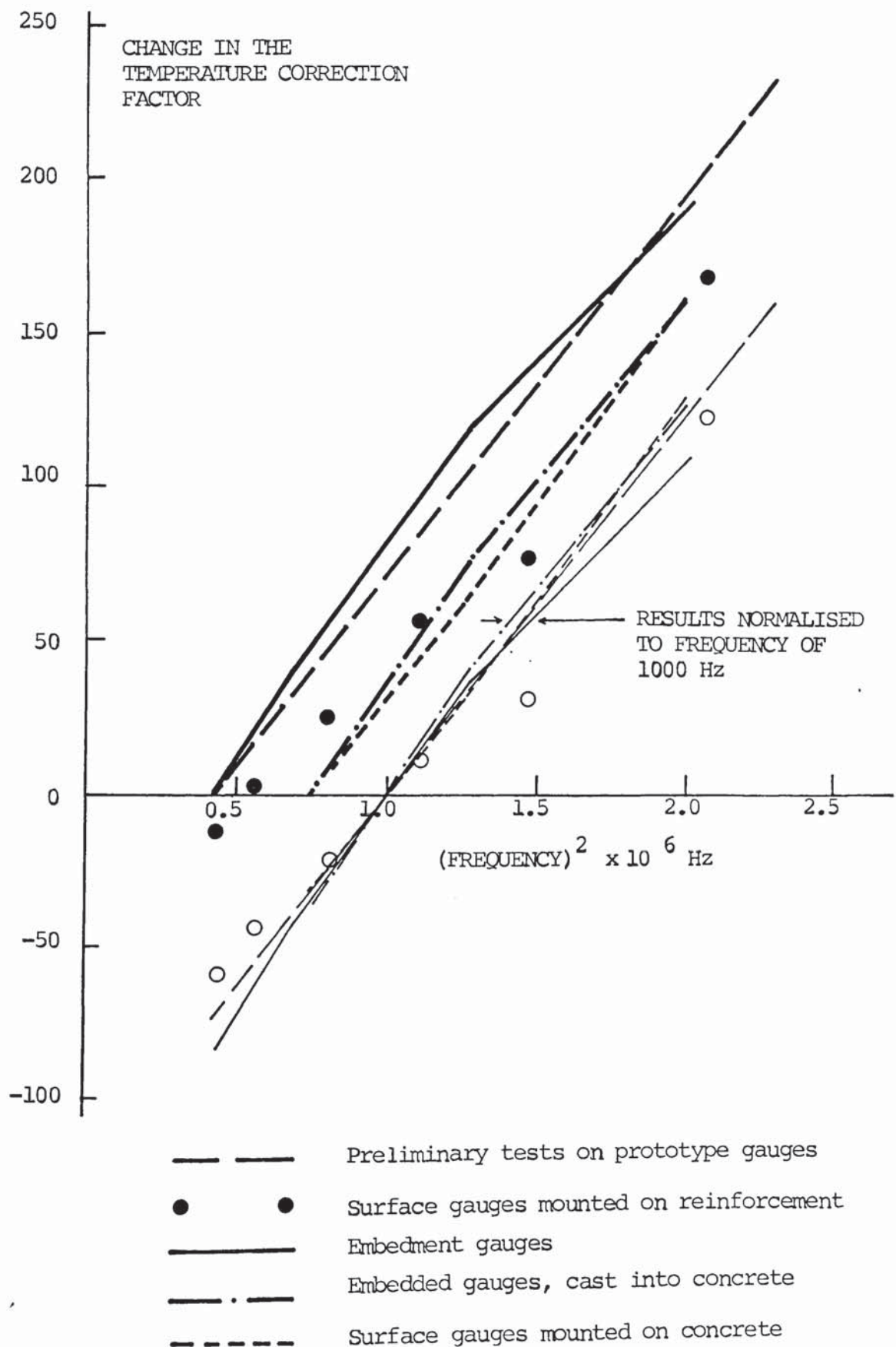
FIGURE A3.6 Summary of results from tests involving cooling gauges from ambient to cryogenic temperature.

Specimen 1	HZ	PERIOD	HZ	PERIOD	Er	TEMPERATURE CORRECTION	CORRECTED STRAIN
Gauge 1 Embedded	861	11611	941	10622	423	- 1785	- 1362
Gauge 2 Surface	868	11517	959	10424	487	- 1785	- 1298
Gauge 3 Surface	868	11516	965	10360	520	- 1785	- 1265
Gauge 4 Surface	866	11542	961	10408	505	- 1785	- 1280
Ave. Surface					504		- 1281
Specimen 2							
Gauge 1 Embedded	1126	08878	1199	08337	498	- 1855	- 1357
Gauge 2 Surface	1071	09341	1152	08683	527	- 1855	- 1313
Gauge 3 Surface	1116	08959	1209	08272	631	- 1855	- 1219
Gauge 4 Surface	1114	08979	1194	08377	541	- 1855	- 1309
Ave Surface					566		- 1280
Specimen 3							
Gauge 1 Embedded	1419	07047	1488	06720	585	- 1950	- 1365
Gauge 2 Surface	1420	07042	1499	06671	675	- 1950	- 1275
Gauge 3 Surface	1395	07171	1475	06778	679	- 1950	- 1266
Gauge 4 Surface	1406	07111	1482	06746	643	- 1950	- 1307
Ave. Surface					666		- 1282

TABLE A3.8 Results from embedded and surface mounted gauges when cooling 150 mm diameter by 450 mm concrete cylinders.

5. CONCLUSION AND RECOMMENDATIONS

Based on the results of calibration tests at both ambient and cryogenic temperature using both surface mounted and embedded gauges, a gauge factor of 2.927×10^{-3} microstrain per frequency^2 is recommended regardless of the initial gauge frequency. A small reduction in gauge factor (of the order of 5%)was identified for embedded gauges at temperatures down to -20^0C but at lower temperatures observed differences were marginal. There was a small reduction in the gauge factor of surface mounted gauges at -162^0C but this was only 3-4% and not considered to be significant.

With regard to temperature correction to compensate for contraction of the vibrating wire, this was found to vary with the initial frequency^2. The greater the initial tension in the wire, the higher the thermal correction. The need to adjust the thermal correction factor can be avoided, however, by ensuring that the initial gauge frequency is kept within acceptable limits. For example variations within a frequency range 950 to 1050 Hz would limit the variation of temperature correction to within a 30 microstrain range. For the anticipated strain change in the concrete, likely to be of the order of 1500 microstrain, the -1% variation associated with the temperature correction for an assumed initial frequency of 1000Hz would be acceptable, obviating the need to make adjustments for individual gauges.

REFERENCES

1. TURNER. F.H. - Concrete and cryogenics, Viewpoint Publications, Cement and Concrete Associations, 1979, London.

2. BRUGGELING. A.S.G. - Prestressed concrete for the storage of liquid gases, Viewpoint Publications, Cement and Concrete Association, 1981, London.

3. CLOSNER. J.J. - Developments in cryogenic concrete, 1st.Int.Conf.on Cryogenic Concrete, Concrete Society, March 1981, Newcastle.

4. CUPERUS. N.J. - Developments in cryogenic storage tanks, 6th.Int.Conf. on LNG, Kyoto Vol 1, Session 2, Paper 13, 1980.

5. CONCRETE SOCIETY, Assessment of fire damaged concrete structures and repair by Gunite, Concrete Society, Tech. Note No 15, Viewpoint Publications, 1978, London.

6. DAVIES. I.L. - A method for the determination of reaction forces and structural damage arising in ship collisions, Offshore Petroleum Conference, 1980. Published in 'Journal of Petroleum Technology', pp 2004-13, October 1981.

7. TURNER. F.H. Codes and hazards 1st.Int.Conf. on Cryogenic Concrete, Concrete Society, March 1981, Newcastle.

8. CEMENT ADMIXTURES ASSOCIATION AND THE CEMENT AND CONCRETE ASSOCIATION JOINT WORKING PARTY REPORT. Superplasticisers for concrete, Viewpoint Publications, 1976, London.

9. BAMFORTH. P.B. - Early age thermal cracking in concrete, Institute of Concrete Technology, Tech Note No 2 ITC, 1982, London.

10. COSTAZ. J.L. and PICAUT. J. - Multiple-barrier concrete containment without steel liner. Int.conf. on Experience of Design, Construction and Operation of Prestressed Concrete Pressure Vessels and Containments for Nuclear Pressure Vessels, Instn. of Civ Engrs, Intn of Mech. Engrs. Sept 1975, York.

11. YAMAME. S.,KASAMI. H., and OKUNO. T. Propeties of concrete at very low temperatures. Douglas McHenry Int. Symp. on Concrete and Concrete Structures, American Concrete Institute, SP-55, Paper 9, 1978.

12. TURNER. F.H. The interaction of concrete and ice at very low temperatures. Inst. of Conc.Tech,. Tech Note No 1, 1980, London.

13. TOGNON. G. Behaviour of mortars and concretes in the temperature range from + 20^{0}C to -196^{0}C. Proc. of 5th Int. Symp. on the chemistry of Cement. Part III, 1969.

14. WISCHERS. G. and DAHMS. J. The behaviour of concrete at very low temperature. Beton Herstellung Verwendung, Vol 20, No4, pp135-139, and Vol 20, No5, pp195-201, 1970 (In German).

15. MONFORE. G.E. and LENTZ. A.E. Physical properties of concrete at low temperatures. Journal of the Portland Cement Association, R and D Laboratories, 1962.

16. ROSTASY. F.S., SCHNEIDE. U. and WIESEMANN. G. Behaviour of mortar and concrete at extremely low temperatures, Cement and Concrete Research, Vol.9. pp365-376, 1979.

17. GOTO. Y. and MIURA. T. Mechanical properties of concrete at very low temperatures. Proc. of 21st Japanese Congress on Materials Research, pp 157-159, Oct. 1977, Tokyo.

18. GOTO Y. and MIURA, T. Mechanical properties of reinforced concrete members at very low temperatures. Transactions of the Japanese Society of Civ. Engrs. No. 285, pp 121-134, May 1979, (In Japanese).

19. OKADA. T., IMAI. M., NAGAZAWA. Y., ISHIKAWA. N. and KIMURA. Y. Bending characteristics of concrete blocks at low temperature. Concrete Journal, Japanese Concrete Institute, Vol.15, No11, Nov. 1977. (In Japanese).

20. OKADA. T. and IGURO. M.   Bending behaviour of prestressed concrete beams under low temperature.   Journal of Japanese Prestressed Concrete Engineering Association, Special Issue for 8th FIP Congress. Vol.20, pp17-35, 1978.

21. YOSHIWA. M. and IWATA. A. Performance characteristics of an apparatus based on the curve-fitting method for measuring thermal properties at cryogenic temperature. Cryogenics, pp273-282, May 1977.

22. IWATA. A., KEN. K., YOSHIHARA. T. and YASHIMA. M.   Properties of concrete at low temperatures. Transactions of Technical Symposium of Japanese Refridgeration Institute, November 1975, Tokoyo (In Japanese).

23. OSHIMA. M., OBOKATA. T., ASHIDA. H. and SAWAYANAGI. M.   Design and experiments of offshore LNG plants using prestressed concrete structures. Proceedings of 6th Int.Conf. on LNG, Session III, Paper 8, April 1980, Kyoto, Japan.

24. OKUMURA. T. Recommended practice for LNG inground storage. Proc. of 6th Int.Conf. on LNG, Session II, Paper 10, April 1980, Kyoto, Japan.

25. SAEMANN. T.C. and WASHA. G.W.   Variation of mortar and concrete properties with temperature. Proc. of Amer. Conc. Inst. Vol.54, pp385-395, 1957.

26. MOSKVIN. V.M., KAPKIN. M.M. and ANTONOV. L.I.   Effect of negative temperatures on the strengh and elastoplastic properties of concrete. Beton I Zhelezpberton, No.10, pp18-21, 1967.

27. MILOVANOV. A.F. and SAMOILGNKO. V.A.   Effects of low temperatures taken into account in calculating structures. The Scientific Research Institute for Concrete and Reinforced Concrete (In Russian).

28. NEVILLE. A.M.   Properties of concrete.   Pitman Paperbacks 1970, London, p28.

29. EAKING. B.E., BAIR. W.G., CLOSNER. J.J. and MAROTI. R. Below ground storage of liquefied natural gas in prestressed concrete tanks. Institute of Gas Technology, Technical Report No.8., American Gas Association, 1963.

30. SULLIVAN. P.J.E. Private correspondence with Taylor Woodrow International. Report on Permeability of concrete, Imperial College, London, 1976

31. HANOR. A. and SULLIVAN. J.E. Factors affecting concrete permeability to cryogenic fluids. Mag. of Conc. Res. Vol.35, No.124. September 1983.

32. GLANVILLE. W.H. The permeability of Portland cement concretes. Building Research Technical Paper No.3. HMSO, 1931, London.

33. MURATA. J. Studies on the permeability of concrete. RILEM Bulletin No.29, Dec 1965.

34. GOTO. S. and ROY. D.M. The effect of W/C ratio and curing temperature on the permeability of hardened cement paste. Cement and Concrete Research, Vol.11, pp575-579, Pergammon Press, 1981.

35. HUART. A. The permeability of concrete to gas. Chimie et Industrie, Vol.82, No.6, pp838-847, Dec 1959 (In French).

36. LOUGHBOROUGH. M.T. Permeability of concrete to air. Ontario Hydro Research Quarterly, 1st Quarter, 25, pp14-16, 1966.

37. GRAIFFER. A.G., SHCHEKANENKO. R.A. and MOSHCHANSKI. N.A. Effect of chemical additives on the gas pereability of concrete. Concrete and Reinforced Concrete, No.3, pp33-36, 1969 (In Russian).

38. BROWNE. R.D. and DOMONE. P.L. Permeability and fatigue properties of structural marine concrete at continental shelf depths. Conf. on Underwater Construction Technology, University College, 1975, Cardiff.

39. ELFERT. R.J. Bureau of Reclamation experiences with fly ash and other pozzolans in concrete. Proc. of 3rd Int. Ash Utilisation Symposium. U.S. Dept. of Interior, Bureau of Mines, pp80-93, March 1973.

40. GRUBE. H. Influence of concrete materials, mix design and construction techniques on permeability. One day meeting on Permeability of Concrete and its Control. Concrete Society, London. Dec 1985.

41. POWERS. T.C., COPELAND. L.E., HAYES. J.C. and MANN. H.M. Permeability of Portland cement paste. Journal of Amer. Conc. Inst. Vol.51, pp285-298, 1954.

42. DUNAGAN. W.M. and ERNST. G.C. A study of permeability of some integrally waterproofed concretes. Amer. Soc. of Testing and Materials, Vol.34, pp383-392, 1934.

43. REUTTGERS. A., VIDALAND. E.N. and WING. S.P. An investigation into the permeability of mass concrete with particular reference to the Boulder dam. Journal of Amer. Conc. Inst., Vol.31, pp382-416, March/April 1985.

44. TYLER. I.L. and ERLIN. B. A proposed simple test method for determining the permeability of concrete. Journal of the Portland Cement Association R and D Laboratory, Sept, 1961.

45. MATHER. B., CALLAN. E.J., McCOY. E.C. and CARLSON. R.W. Permeability and triaxial tests on lean mass concrete. U.S. Army Waterways Experiment Station, Vicksburg, Technical Memo 9-380, March 1954.

46. HAYNES. H.H. Permeability of concrete to seawater. Amer. Conc. Inst. Special Publication SP65-2.

47. TAYWOOD ENGINEERING LTD. Concrete in the Oceans, Phase II - Performance of uncracked cover in protecting reinforcement embedded in marine concrete against corrosion, Project 1b, CIRIA/UEG. June 1986.

48. TAYLOR WOODROW RESEARCH LABORATORY Marine Durability of the Tongue Sands Tower, Concrete in the Oceans, Tech. Report No. 5, CIRIA/UEG, C & CA, Dept. of Energy, Published by Cement and Concrete Association. Wexham Springs, 1980.

49. ELICES, M. and PLANAS J. Measurement of tensile strength of concrete at very low temperatures. Journal of ACI Proceedings V9, No. 3, May-June 1982.

50. BRITISH STANDARDS INSTITUTION. Testing concrete. Part 118, Method for determination of flexural strength, 1983. Part 121, Method for determination of static modulus of elasticity and compression 1983. BSI, Maylands Ave, Hemel Hempstead, Herts. HP2 4SQ.

51. MARACHEL, J.C. Thermal conductivity and thermal expansion coefficients of concrete as a function of temperature and humidity. Proc. of Amer. Conc. Inst. Int. Seminar, Paper SP34-49, 1970, Berlin.

52. ROSTASY, F.S., SCHNEIDER, U. and WIEDEMANN, G. Behaviour of mortar and concrete at extremely low temperatures. Cement and Concrete Research, Vol. 9, pp 365-376, 1979.

53. MONFORE, G.E. and LENTZ, A.E. Thermal conductivity of concrete at very low temperatures. Journal of the Portland Cement Association R and D Laboratories, May 1965.

54. MONFORE, G.E. and LENTZ, A.E. Thermal conductivities of Portland cement paste, aggregate and concrete down to very low temperatures. Journal of the Portland Cement Association R and D Laboratories, Sept. 1966.

55. MARACHEL, J.C. Variations in the modulus of elasticity and Poissons ratio with temperature. Amer. Conc. Inst. Special Publication SP35-27, 1972.

56. WOZNIAK, R.S., SALMON, M. and HUANG, W. Above ground concrete secondary containment for LNG. Cryogenic Engineering Conference, July 1975, Kingston, Ontario.

57. BRITISH STANDARDS INSTITUTION, British Standard Code of Practice for the structural use of concrete Part 1, Design, Materials and workmanship. CP110: Part 1: 1972: BSI, London.

58. BROWNE, R.D. and BURROW, R.E.D. An example of the utilization of complex multiphase material behaviour in engineering design. Proc. of Civ. Eng. Materials Conf. Structure, Solid Mechanics and Engineering Design, Southampton University, John Wiley and Sons Ltd, London, 1969.

59. MEHTA, P.K. Standard specifications for mineral admixtures - an overview. Proceedings of 2nd Int. Conf. on Fly Ash, Silica Fume, Slag and Natural Pozzolans in Concrete. Madrid ACI Special Publication SP-91, 1986.

60. CONCRETE SOCIETY Permeability testing of site concrete, Report of Conc. Soc. Working Party, Final Draft, Conf. on Permeability and its control, London, Dec. 1985.

61. BARRER, R.M. Diffusion in and through solids, Cambridge University Press, pp 60-61, 1951, Cambridge.

62. TAYLOR, D.W. Fundamentals of soil mechanics. Chapman and Hill Ltd. pp 192-199, London 1948.

63. CHEN, L.C. and KATZ, D.L. Diffusion of methane through concrete. Journal of the Amer. Conc. Inst., Proceedings, Vol. 75, No. 12, pp 673-679, Dec. 1978.

64. BUHNER, K., MAURER, G. and BENDER, E. Pressure-enthalpy diagrams for methane, ethane, propane, ethylene and propylene. Cryogenics Vol. 21, No. 3 pp 157-164, March 1981.

65. NYAME, B.K. and ILLSTON, J.M. Capillary pore structure and permeability of hardened cement paste, 7th Int. Symp. of Chemistry of Cement, pp VI, 181-186, 1980, Paris.

66. WINSLOW, D.N. and DIAMOND, S. A mercury porosimetry study of the evolution of porosity in Portland cement. Journal of Materials, JMLSA, Vol. 5, No. 3, pp 564-585, Sept. 1970.

67. DIAMOND, S. A critical comparison of mercury porosimetry and capillary condensation pore size distributions of Portland Cement pastes. Cement and Concrete Research, Vol. 1, pp 531-545, 1971.

68. OKPALA, D.C. Pore structure and oil flow through hardened cement paste, mortar and concrete. Ph.D. Thesis, University of Sheffield, October 1982.

69. MIDGELEY, H.A. and ILLSTON, J.M. Some comments on the microstructure of hardened cement pastes. Cement and Concrete Research, Vol. 13, pp 197-206, 1983.

70. MEHTA, P.K. and MANHOHAN, D. Pore Size distribution and permeability of hardened cement pastes. 7th Int. Symp. on Chemistry of Cement, VII 1-5, 1980, Paris.

71. BLUNDELL, R., DIMOND, C. and BROWNE, R. Thermal stresses in oil storage vessels. The properties of concrete for use in design. Construction Industry Research and Information Association, Tech. Note No. 9, London 1976.

72. Comite Euro-International du Beton (CEB)/Federation Internationale de la Precontrainte (FIP). Manual of lightweight aggregate concrete, design and technology. The Construction Press, London, 1977.

73. PLANAS, J., CORRESS, H., CHUECA, R., ELICES, M. and SANCHEZ-GALVEZ. The influence of load on thermal deformation of concrete during cooling. Proc. of 2nd Int. Conf. on Concrete and Cryogenics, Amsterdam. Concrete Society, Oct. 1983.

74. KLINKENBERG, L.J. The permeability of porous media to liquids and gases. Drilling and Production Practice, pp 200-14, American Petroleum Institute, New York, 1941.

75. AMERICAN PETROLEUM INSTITUTE, Recommended practice for determining permeability of porous media. Third Edition. API, RP27, p9, Sept. 1952.

76. FIGG, J.W. Method of measuring the air and water permeability of concrete, Mag. of Conc. Res. Vol. 25, No. 85, pp 213-19, December 1973.

77. MARTIN, G.R. A method for determining the relative permeability of concrete using gas. Mag. of Conc. Res. Vol. 38, No. 135, pp 90-94, June 1986.

78. BROWNE, R.D. Properties of concrete in reactor vessels. Conf. on Prestressed Concrete Pressure Vessels, Inst. of Civ. Engrs. London 1968.

79. BROWNE, R.D. and BAMFORTH, P.B. The use of concrete for cryogenic storage, a summary of research, past and present. Proc. of 1st Int. Conf. on Cryogenic Concrete, Concrete Society, Newcastle, March 1981.

80. KOMLOS, K. Determination of the tensile strength of concrete - 2. Indian Concrete Journal, pp 68-76, Feb. 1968.

81. CORNELISSEN, H.A.W. and REINHARDT, H.W. Uniaxial tensile fatigue failure of concrete under constant-amplitude and programme loading. Mag. of Conc. Res. Vol. 36, No. 129, Dec. 1984.

82. ZIELINKSI, A.J. and REINHARDT, H.W. Stress-strain behaviour of concrete and mortar at high rates of tensile loading. Cement and Concrete Research, Vol. 12, pp 309-319, Pergammon Press, 1982.

83. HUGHES, B.P. and CHAPMAN. The complete stress-strain curve for concrete in direct tension. RILEM Bulletin No. 30 pp 95-97, March 1966.

84. DOMONE, P.L. Uniaxial tensile creep and failure of concrete, Mag. of Conc. Res. Vol. 26, No. 88. September 1974.

85. LYDON, D. and BALENDRAN, R.V. Some properties of higher strength lightweight concrete under short term tensile stress. Int. Journal of Lightweight Concrete, Vol. 2, No. 3, September 1980.

86. BROWNE, R.D. Thermal movement of concrete, Current Practice Sheet No. 1, Concrete, November 1972.

87. BRITISH STANDARDS INSTITUTION, Code of Practice for the design and construction of reinforced concrete in buildings. CP114, 1957, Reprinted in 1965.

88. AMERICAN CONCRETE INSTITUTE. Cracking of concrete members in direct tension. Report by ACI Committee 224.2R-86, ACI Journal, Jan-Feb. 1986.

89. BRITISH STANDARDS INSTTUTION. Code of practice for the structural use of concrete for retaining aqueous liquids. BS 5337: 1976, BSI, London, 1976.